ON THE CHARACTERISTICS OF FAULT-INDUCED ROTOR-DYNAMIC BIFURCATIONS AND NONLINEAR RESPONSES

A Dissertation

by

BAOZHONG YANG

Submitted to the Office of Graduate Studies of
Texas A&M University
in partial fulfillment of the requirements for the degree of

DOCTOR OF PHILOSOPHY

August 2003

Major Subject: Mechanical Engineering

ON THE CHARACTERISTICS OF FAULT-INDUCED ROTOR-DYNAMIC BIFURCATIONS AND NONLINEAR RESPONSES

A Dissertation

by

BAOZHONG YANG

Submitted to Texas A&M University
in partial fulfillment of the requirements
for the degree of

DOCTOR OF PHILOSOPHY

Approved as to style and content by:

Chii-Der S. Suh (Co-Chair of Committee)	Andrew K. Chan (Co-Chair of Committee)
Suhada Jayasuriya (Member)	Alexander G. Parlos (Member)
Dennis L. O'Neal (Interim Department Head)	

August 2003

Major Subject: Mechanical Engineering

ABSTRACT

On the Characteristics of Fault-Induced Rotor-Dynamic Bifurcations
and Nonlinear Responses. (August 2003)

Baozhong Yang, B.S., Xi’an University of Technology, Xi’an, China;
M.S., Shanghai Jiao Tong University, Shanghai, China
Co-Chairs of Advisory Committee: Dr. Chii-Der S. Suh
Dr. Andrew K. Chan

Rotor-dynamic stability is a very important subject impacting the design, control, maintenance, and operating safety and reliability of rotary mechanical systems. As rotor-dynamic nonlinearities are significantly more prominent at higher rotary speeds, the demand for better and improved performance achievable through higher speeds has rendered the use of linear approaches for rotor-dynamic analysis both inadequate and ineffective. To establish the fundamental knowledge base necessary for addressing the need, it is essential that nonlinear rotor-dynamic responses indicative of the causes of nonlinearity, along with the bifurcated dynamic states of instability, be fully characterized. The objectives of the research are to study the various rotor-dynamic instabilities induced by crack breathing and bearing fluid film forces using a model rotor-bearing system and to investigate the applicability of the fundamental concept of instantaneous frequency for characterizing rotor-dynamic nonlinear responses. A comprehensive finite element model incorporating translational and rotational inertia, bending stiffness and gyroscopic moment is developed. The intrinsic modes extracted using the Empirical Mode Decomposition along with their instantaneous frequencies resolved using the Hilbert transform are applied to characterize the inception and progression of bifurcations suggestive of the changing rotor-dynamic state and impending instability.

The dissertation presents and demonstrates an effective approach that integrates nonlinear rotor-dynamics, instantaneous time-frequency analysis, advanced notions of dynamic system diagnostics and numerical modeling applied to the detection and identification of sensitive variations indicative of a bifurcated dynamic state. All presented studies on rotor response subjected to various system configurations and ranges of parameters show good agreement with published results. Under the influence of crack opening, the rotor-bearing model system displays transitional behaviors typical of a nonlinear dynamic system, going from periodic to period-doubling to chaotic to eventual failure. When film forces are also considered, the model system demonstrates very different behaviors and failures from different settings and ranges of control parameters. As a result, a dynamic failure curve differentiating zones of stability and bifurcated instability from zones of dynamic failure is constructed and proposed as an alternative to the traditional stability chart. Observations and results such as these have important practical implications on the design and safe operation of high performance rotary machinery.

ACKNOWLEDGEMENTS

I would like to dedicate the dissertation to my beloved mother, Mrs. Daizhi Wang, who raised my sister and me with sacrificial love and by whose fortitude we were kept in school. She and her feeble shoulders carried all the burdens, hardships, and many an adversity of life, so that I had to bear none. Her greatness is beyond words and no words of gratitude are worthy of her.

I would also like to express my deepest gratitude to my academic advisor, Dr. C. Steve Suh, who provided me with continuous support and guidance throughout my doctoral career at Texas A&M. His attitude of seriousness toward teaching and research and his sincerity greatly affected me as a graduate student. He is my life-long mentor. My thanks also go to Dr. Andrew K. Chan who co-chaired my dissertation committee and taught me knowledge of wavelets and time-frequency analysis. His constant encouragement and guidance shall always be with me.

Finally, I would like to express my sincere appreciation to Drs. Suhada Jayasuriya and Alexander Parlos for serving on my advisory committee and to Dr. Larry Yarak for being the most supportive Graduate Council Representative. If it were not for the kindness and generosity shown to me by James Steuber for allowing me to use his personal computer in the process of coding and debugging, I would not have been able to attain the level of quality required of a good dissertation work.

TABLE OF CONTENTS

Page

ABSTRACT ... iii

ACKNOWLEDGEMENTS ... v

TABLE OF CONTENTS ... vi

LIST OF FIGURES ... viii

LIST OF TABLES. ... xiii

CHAPTER

I INTRODUCTION ... 1

- 1.1 Overview ... 1
- 1.2 Literature Review ... 5
- 1.3 Objectives ... 12

II NONLINEAR ROTOR-DYNAMIC RESPONSES ... 13

- 2.1 Scope of Rotor-Dynamics ... 13
- 2.2 Nonlinearities in Rotor Dynamic Systems ... 17
- 2.3 Interpretation of Rotor-Dynamic Response ... 22
- 2.4 Summary ... 32

III ANALYTIC TOOLS FOR CHARACTERIZING ROTOR-DYNAMIC RESPONSES ... 33

- 3.1 Time Domain Approach ... 33
- 3.2 Fourier Analysis ... 46
- 3.3 Time Frequency Analysis ... 49
- 3.4 Summary ... 53

IV CONCEPTS AND APPLICATIONS OF INSTANTANEOUS FREQUENCY ... 55

- 4.1 Fundamental Notions of Instantaneous Frequency ... 55
- 4.2 Misinterpretation of Instantaneous Frequency ... 61
- 4.3 Decomposition of Multi-Mode Structure ... 70
- 4.4 Examples and Discussion of Instantaneous Frequency ... 76
- 4.5 Characteristics of Nonlinear Response Interpreted Using Instantaneous Frequency ... 80
- 4.6 Summary ... 84

CHAPTER Page

V NUMERICAL MODELING OF A SHAFT-ROTOR SYSTEM WITH NONLINEARITIES ... 86

5.1 Finite Element Model ... 86
5.2 Modeling of Local Nonlinearities ... 90
5.3 Solution Procedures ... 95
5.4 Shooting Method and Nonlinear Stability ... 98

VI RESULTS OF CRACKED ROTOR MODEL WITH ELASTIC SUPPORTS ... 102

6.1 Description of Results ... 102
6.2 Discussion ... 118

VII RESULTS OF ROTOR-JOURNAL BEARING MODEL WITH CRACKED SHAFT ... 120

7.1 Description of Results ... 120
7.2 Discussion ... 165

VIII RESULTS OF CRACKED ROTOR MODEL SUPPORTED BY JOURNAL BEARINGS WITH VARIOUS CLEARANCES ... 169

8.1 Description of Results ... 169
8.2 Discussion ... 213

IX CONCLUSIONS AND RECOMMENDATIONS ... 215

9.1 Conclusions ... 215
9.2 Contributions ... 218
9.3 Concepts and Design Guidelines for Instability-Free Rotary Machines ... 219

REFERENCES ... 223

VITA ... 232

LIST OF FIGURES

FIGURE Page

2.1 Orbit of journal center using linearized model when ω =100π 24

2.2 Orbit of journal center using linearized model when ω =200π 25

2.3 Orbit of journal center using linearized model when ω =300π 26

2.4 Orbit of journal center using nonlinear model when ω =100π 28

2.5 Orbit of journal center using nonlinear model when ω =200π 29

2.6 Orbit of journal center using nonlinear model when ω =250π 30

2.7 Orbit of journal center using nonlinear model when ω = 500π 31

3.1 Bifurcation diagram of the quadratic map 35

3.2 (a) Time history of a nonlinear model at driving frequency ω = 100π.
(b) Corresponding phase portrait and Poincare map of the response in (a) 36

3.3 (a) Time history of a nonlinear model at driving frequency ω = 200π.
(b) Corresponding phase portrait and Poincare map of the response in (a) 41

3.4 (a) Time history of a nonlinear time-delay model.
(b) Corresponding phase portrait and Poincare map of the response in (a) 42

3.5 Phase portrait and Poincare map of a fractal response....................................... 43

3.6 Phase portrait and Poincare map of a chaotic response 46

3.7 The spectrum of (a) a periodic response, (b) a period doubling response,
(c) a quasi-periodic response, and (d) a chaotic motion...................................... 47

3.8 Gabor wavelet transform of a signal undergoing period doubling....................... 51

3.9 Gabor wavelet transform of a signal experiencing milling chatter 52

4.1 (a) Time history of a simple sinusoidal signal initially starting with 1Hz and abruptly switching to 3Hz. (b) Instantaneous frequency determined using the traditional definition.. 57

4.2 A linear chirp signal (top) and its corresponding instantaneous frequency (middle)and fast Fourier transform (bottom) 58

FIGURE Page

4.3 (a) A two-component signal with equal amplitude. (b) Amplitude modulation of the signal. (c) Instantaneous frequency determined using Ville's definition, where dashed lines represent the two original frequencies 62

4.4 (a) A two-component signal with unequal amplitude. (b) Amplitude modulation of the signal. (c) Instantaneous frequency determined using Ville's definition, where dashed lines represent the two original frequencies 63

4.5 (a) A multicomponent signal (milling vibration data). (b) Amplitude modulation of the signal. (c) Instantaneous frequency determined using Ville's definition........ 64

4.6 (a) A time domain signal. (b)Original signal (——) with its maximum envelope and minimum envelope (-·-·-·-·-) and its local mean (━━) (c) *s1(t)*: result after one sifting process (d) the first Intrinsic Mode Function obtained........ 74

4.7 (a) A two-component signal with unequal amplitude and its two physical components obtained using the Empirical Mode Decomposition. (b) The two instantaneous frequencies determined using the two components of the signal........ 77

4.8 (a) Dynamic response and its decomposed intrinsic modes for $\beta_2 = 0.1$ and *k* being varied from 1.0 to 10.0. (b) Associated instantaneous frequencies corresponding to all resolved IMF C1-C2. 83

5.1 Configuration and coordinates for the presented rotor-bearing model system 88

5.2 Orbit of journal center of a rotor system obtained after three shooting processes 100

6.1 Rotor vibration time history for *hr* being varied from 0.0 to 0.06. The boxed portion is enlarged and shown again in Figure 6.2(a) for better visibility 104

6.2 (a) Time waveform and its IMFs, (b) Instantaneous frequencies, and (c) Marginal spectrum for h_r being varied from 0.0 to 0.06........ 105

6.3 (a) Time waveform and its IMFs, (b) Instantaneous frequencies, and (c) Marginal spectrum for *hr* being varied from 0.08 to 0.1035 107

6.4 (a) Time waveform and its IMFs, (b) Instantaneous frequencies, and (c) Marginal spectrum for *hr* being varied from 0.102 to 0.113 111

FIGURE Page

6.5 (a) Time waveform and its IMFs, (b) Instantaneous frequencies, and (c) Marginal spectrum for *hr* being varied from 0.113 to 0.1155 114

6.6 (a) Time waveform and its IMFs, (b) Instantaneous frequencies, and (c) Marginal spectrum for *hr* = 0.1155 116

7.1 (a) X-Y orbit of the journal center at $\omega = 30\pi$ and $h_r = 0.012$. (b) Spectrum of the response in (a) 123

7.2 (a) Time waveform and its IMFs, (b) Instantaneous frequencies, and (c) Marginal spectrum for $\omega = 30\pi$ and $h_r = 0.012$ 124

7.3 Changes of instantaneous frequency in response to crack opening and closing 126

7.4 Orbit of journal center at $\omega = 50\pi$ rad/s indicating a period doubling motion... 130

7.5 (a) Time waveform and its IMFs, (b) Instantaneous frequencies, and (c) Marginal spectrum for $\omega = 50\pi$ and $h_r = 0.0003$ to 0.001 131

7.6 (a) Orbit of journal center at $\omega = 50\pi$ and $h_r = 0.09$. (b) Spectrum of the vibration signal in (a) 133

7.7 Speed variation of the journal center in X-Y direction at $\omega = 50\pi$ and $h_r = 0.09$ 134

7.8 (a) Time waveform and its IMFs, (b) Instantaneous frequencies, and (c) Marginal spectrum for $\omega = 50\pi$ and $h_r = 0.06$ to 0.09 135

7.9 Orbit of journal center at $\omega = 50\pi$ and $h_r = 0.05$ 137

7.10 Orbit of journal center at $\omega = 100\pi$ rad/s indicating a period doubling motion 140

7.11 (a) Time waveform and its IMFs, (b) Instantaneous frequencies, and (c) Marginal spectrum for $\omega = 100\pi$ and $h_r = 0.0003$ to 0.001 141

7.12 (a) Time waveform and its IMFs, (b) Instantaneous frequencies, and (c) Marginal spectrum for $\omega = 100\pi$ and $h_r = 0.16$ to 0.205 143

7.13 (a) Orbit of journal center at $\omega = 100\pi$ and $h_r = 0.005$. (b) Orbit of journal center at $\omega = 100\pi$ and $h_r = 0.205$ 145

7.14 (a) Time waveform and its IMFs, (b) Instantaneous frequencies, and (c) Marginal spectrum for $\omega = 120\pi$ and $h_r = 0.0001$ to 0.0005 148

FIGURE Page

7.15 (a) Time waveform and its IMFs, (b) Instantaneous frequencies, and (c) Marginal spectrum for $\omega = 120\pi$ and $h_r = 0.10$ to 0.136 150

7.16 Orbit of journal center at $\omega = 120\pi$ and (a) $h_r = 0.00$. (b) $h_r = 0.01$. (c) $h_r = 0.10$. (d) $h_r = 0.136$ 152

7.17 Orbit of journal center at (a) $\omega = 150\pi$ and $h_r = 0.39$. (b) $\omega = 180\pi$ and $h_r = 0.49$ 154

7.18 Orbit of journal center at $\omega = 200\pi$ and (a) $h_r = 0.00$. (b) $h_r = 0.39$...................... 155

7.19 (a) Vibration signal of journal center at $\omega = 200\pi$ and $h_r = 0.39$. (b) The associated FFT.. 156

7.20 Orbit of journal center at $\omega = 900\pi$ and $h_r = 0.10$.. 159

7.21 (a) Time waveform and its IMFs, (b) Instantaneous frequencies, and (c) Marginal spectrum for $\omega = 900\pi$ and $h_r = 0.10$ 160

7.22 Orbit of journal center at (a) $\omega = 700\pi$ and $h_r = 0.10$. (b) $\omega = 500\pi$ and $h_r = 0.00$... 162

7.23 Tentative dynamic failure chart for the studied rotor-journal bearings system.. 163

8.1 (a) Time waveform and its IMFs, (b) Instantaneous frequencies, and (c) Marginal spectrum for $\omega = 100\pi$, Cr=0.0025r and $h_r = 0.05$........................ 170

8.2 (a) Time waveform and its IMFs, (b) Instantaneous frequencies, and (c) Marginal spectrum for $\omega = 100\pi$, Cr=0.002r and $h_r = 0.05$.......................... 172

8.3 (a) Time waveform and its IMFs, (b) Instantaneous frequencies, and (c) Marginal spectrum for $\omega = 100\pi$, Cr=0.001r and $h_r = 0.05$.......................... 174

8.4 (a) Time waveform and its IMFs, (b) Instantaneous frequencies, and (c) Marginal spectrum for $\omega = 100\pi$, Cr=0.002r and $h_r = 0.10$.......................... 176

8.5 (a) Time waveform and its IMFs, (b) Instantaneous frequencies, and (c) Marginal spectrum for $\omega = 100\pi$, Cr=0.001r and $h_r = 0.10$.......................... 178

8.6 (a) Time waveform and its IMFs, (b) Instantaneous frequencies, and (c) Marginal spectrum for $\omega = 100\pi$, Cr=0.0025r and $h_r = 0.20$........................ 180

8.7 (a) Time waveform and its IMFs, (b) Instantaneous frequencies, and (c) Marginal spectrum for $\omega = 100\pi$, Cr=0.002r and $h_r = 0.20$.......................... 182

FIGURE Page

8.8 (a) Time waveform and its IMFs, (b) Instantaneous frequencies, and (c) Marginal spectrum for $\omega = 100\pi$, Cr=0.001r and h_r =0.20 184

8.9 (a) Time waveform and its IMFs, (b) Instantaneous frequencies, and (c) Marginal spectrum for $\omega = 100\pi$, Cr=0.002r and h_r =0.30 186

8.10 (a) Time waveform and its IMFs, (b) Instantaneous frequencies, and (c) Marginal spectrum for $\omega = 100\pi$, Cr=0.001r and h_r =0.30 188

8.11 (a) Time waveform and its IMFs, (b) Instantaneous frequencies, and (c) Marginal spectrum for $\omega = 200\pi$, Cr=0.002r and h_r =0.05 190

8.12 (a) Time waveform and its IMFs, (b) Instantaneous frequencies, and (c) Marginal spectrum for $\omega = 200\pi$, Cr=0.001r and h_r =0.05 192

8.13 (a) Time waveform and its IMFs, (b) Instantaneous frequencies, and (c) Marginal spectrum for $\omega = 200\pi$, Cr=0.0025r and h_r =0.10 194

8.14 (a) Time waveform and its IMFs, (b) Instantaneous frequencies, and (c) Marginal spectrum for $\omega = 200\pi$, Cr=0.002r and h_r =0.10 196

8.15 (a) Time waveform and its IMFs, (b) Instantaneous frequencies, and (c) Marginal spectrum for $\omega = 200\pi$, Cr=0.001r and h_r =0.10 198

8.16 (a) Time waveform and its IMFs, (b) Instantaneous frequencies, and (c) Marginal spectrum for $\omega = 200\pi$, Cr=0.002r and h_r =0.20 200

8.17 (a) Time waveform and its IMFs, (b) Instantaneous frequencies, and (c) Marginal spectrum for $\omega = 200\pi$, Cr=0.001r and h_r =0.20 202

8.18 (a) Time waveform and its IMFs, (b) Instantaneous frequencies, and (c) Marginal spectrum for $\omega = 200\pi$, Cr=0.0025r and h_r =0.25 204

8.19 (a) Time waveform and its IMFs, (b) Instantaneous frequencies, and (c) Marginal spectrum for $\omega = 200\pi$, Cr=0.002r and h_r =0.30 206

8.20 (a) Time waveform and its IMFs, (b) Instantaneous frequencies, and (c) Marginal spectrum for $\omega = 200\pi$, Cr=0.001r and h_r =0.30 208

LIST OF TABLES

TABLE Page

5.1 Mass and inertia of disks..89

5.2 Element data of a flexible shaft..90

5.3 Relation between h_r and dt/R 94

CHAPTER I

INTRODUCTION

1.1 Overview

Well developed linearized methods including the linear stability analysis, eigenvalue analysis, waterfall plots and, in particular, determination of stiffness and damping coefficients [1] have been widely applied in industry to the investigation of dynamical response of rotary machines. While linear methods are considered adequate and thus dominating, however, it is now being understood that various responses of nonlinearity can have significant local and global effects on a rotor-dynamic system and that linearized methods are not viable for resolving nonlinearity. As the demand for high efficiency and performance calls for high rotating speeds and reliability design, nonlinear phenomena such as subharmonic bifurcation and jump phenomena are frequently observed [2].

Surface cracks, fluid-film bearings, squeeze-film dampers, nonlinear springs and clearances in rolling element bearings are just a few sources of strong nonlinearity in rotor-dynamic machines. For example the nonlinearity in fluid film bearings that are used in turbomachinery to support loads and reduce vibration and friction is attributable to the nonlinear film pressure [3] and local stiffness variation induced by surface crack breathing in a rotating shaft is now understood to be highly nonlinear [4]. These sources of nonlinearity create nonlinear reaction forces, which in turn could result in strong nonlinear responses including period-doubling bifurcation, quasi-periodic bifurcation, and even chaotic response [4,5].

Nonlinear dynamical states of quasi-periodic, fractal, and chaotic motions are characteristically non-periodic and broadband and of multi-mode structure. It is very difficult to

---

This dissertation follows the style and format of *Journal of Vibration and Acoustics*.

discern these dynamical states using their time waveforms and measurement and environmental noises could make the task even more difficult. Since physical interpretation of these dynamic responses would not only ensure reliable monitoring of machine operation, but also provide better understanding of the existence and progression of dynamic instability that could positively impact the design of instability-free machines, a large amount of research effort has been taken to analyze the measured waveforms. However, approaches and techniques developed to date for the analysis of nonlinear, non-stationary signals are either time domain based or Fourier-based [6, 7]. All time domain methods including the phase portrait and Poincare section are qualitative. They cannot be used to determine the extent of dynamic instability, and therefore not feasible for quantitatively establishing if an erratic response is in bifurcation or chaotic [8]. The disadvantage inherent to Fourier based analysis is that Fourier transform is a linear transformation, which makes it suitable only for analyzing linear stationary signals. In addition, a signal’s temporal information cannot be simultaneously separated from its spectral counterpart [9]. The analysis tool that can separate and characterize individual modes of the multi-mode responses in both time and frequency domains is thus highly desired. Such a tool would make it possible to observe the occurrence of bifurcation and the appearance/disappearance of modes (or frequencies), thus enabling the change of system state be instantaneously monitored. Although techniques such as the Wigner-Ville Distribution and Short Time Fourier Transform do provide simultaneous time-frequency distribution, they do not have wide applications in nonlinear system analysis due to their ineffectiveness in analyzing nonlinear, non-stationary signals.

These difficulties identify two coupled requirements necessary for investigating a nonlinear system. The first one is a practical theoretical model that can show the physical nature of the system and quantitatively correlate control parameters to the nonlinear response (a.k.a., input-output relations). The other is an effective tool for identifying and processing system responses and providing physical interpretation of the model. The first requirement demands an accurate modeling of the dynamic interaction between all rotary components involved and the stability-losing process of the system. The second requirement demands that the various modes of the multi-mode nonlinear response be separated and that the system transition from one dynamic state to another be simultaneously monitored in the joint time-frequency domain.

The research presented in this dissertation first establishes rotor-dynamic responses as function of control parameters and system configuration, which are obtained by an analytical model that describes the physical nature of the nonlinear mechanism within a rotor-bearing system. Because of its stability and capability in capturing the physical nature of a dynamical rotary system, the finite element method is employed over other methods for simulating system responses at different conditions. Specifically, the excitation is provided by the rotor unbalance and the nonlinearity is given by the inherent instability mechanism and nonlinear elements within the system. Thus, the set-in and progression of dynamic instability induced by nonlinearities in the rotary model is both theoretically and analytically investigated. The analysis tools used to process, analyze and interpret nonlinear, non-stationary vibratory signals are also developed. Through careful comparison of the results obtained using the new tools, the Fourier–based methods and other nonlinear analytical methods, the FEM model is verified and the nonlinear rotor-dynamic response is better understood. Knowledge base established through the research is believed to enable significant progress in monitoring the operation of rotary machinery and permit ultra-stable rotary machine design in the future.

A review of nonlinear phenomena in rotary machinery and the analysis tools commonly used for resolving nonlinear response is given in the following. Based on the review, research objectives for the dissertation are then identified and research scopes are summarized. The ever increasing demands for high performance and efficiency have rendered nonlinearity-induced rotor-dynamic instabilities a very important issue. This dissertation addresses the issue by first examining the inherent limitations of many popular linearized methods and identifying various possible pitfalls and drawbacks of these methods in revealing rotor-dynamic nonlinearity. It is concluded that a new analytical tool is needed for interpreting and understanding nonlinear rotor-dynamic responses in rotary machines.

In the past decade, efforts have been dedicated to studying and understanding the nonlinear phenomena in rotary machinery. Many practical analytical methods were developed to analyze and interpret the results. These methods are briefly introduced in Chapter III. Nonlinear analytical methods, such as phase portraits and Poincare Maps, are based on the geometric features in the phase plane. Because a dynamic response is uniquely determined by its frequency components, spectral analysis methods were introduced into the analysis of nonlinear time series. Time-frequency methods were also used to simultaneously resolve the information in time and frequency domains. Their advantages and disadvantages are summarized.

Instantaneous frequency is a very intuitive concept for describing the dependence of frequency on time for non-stationary signal [10]. The time sensitivity of instantaneous frequency is ideal for the detection of the initiation of instability and bifurcation. However, when the Hilbert transform based definition is applied to multicomponent signals, negative frequency and infinite amplitude are oftentimes obtained. These physically senseless results have inadvertently prevented the true nature of the signal and associated system from being understood. In Chapter IV, the fundamentals on which the concept was first defined are examined to check for the applicability of the definition. The problems with this definition and solutions to these problems are identified. How to analyze and characterize nonlinear responses using instantaneous frequency are then elaborated.

A high-order shaft-bearing system with high nonlinearity is modeled using the finite element method and presented in Chapter V. The model, which adopts the Timoshenko beam elements, considers translational and rotary inertia, bending stiffness, gyroscopic moments and shear forces. Breathing surface cracks and action of fluid-bearing force are the two nonlinear sources of practical concern and their effects on rotary instability are represented as nonlinear forces imposed on the model. Because the shaft-bearing model experiences numerical difficulties and instability, solution strategies for overcoming these difficulties are also discussed.

After the numerical vibratory response associated with each and every case is obtained, the concept of instantaneous frequency is then applied to the analysis of the nonlinear, non-stationary response in Chapter VI. In addition, results analyzed using nonlinear time series analysis techniques including phase portraits and Fourier Transform are compared to the ones using instantaneous frequency. Based on these analytical results, the various nonlinear responses due to crack breathing and fluid bearing forces are discussed in Chapters VII and VIII and the speed ranges for periodic, sub-harmonic, quasi-periodic and chaotic motions are determined for a set of system parameters of practical interest. The contributions of the research are summarized along with a proposed guideline feasible for the design of instability-free rotary machines in Chapter IX. The Chapter also discusses some important advancement in nonlinear time series analysis and prediction of nonlinear response in the context of instantaneous frequency.

1.2 Literature Review

Nonlinear phenomena were characterized as non-synchronous motions and have been widely observed since 1966 [11,12]. At a time when nonlinear phenomena were not fully understood, they were considered linear and analyzed using linearized methods. For example sub-harmonic response, which is a typical phenomenon of nonlinear, was once thought as linear in nature [2]. Linearized methods could misinterpret the response of a nonlinear dynamic system. According to the linearized stability criterion (established at a static equilibrium point), rotary machines should not be operated beyond the determined threshold speed of instability. However, there have been reports that machines do show virtually stable operation at speeds much beyond their threshold speeds of instability [13]. Nonlinear analysis of the rotor bearing system also shows that the amplitude of motion at above the threshold speed is not necessarily larger than motions at speeds below the threshold speed [14]. Linearized procedures could mask potentially dangerous bifurcations (for example, the Hopf bifurcation) that are fully described by the governing nonlinear equations of motion [15]. Such bifurcations that oftentimes lead to serious stability problems can only be predicted by retaining the high-order terms. It remains a question if stability criteria based linear coefficients would lead to meaningful results particularly when several interacting nonlinearities are present in the system, as is generally the case [16]. Since no suitable characterization tools were available, the area of nonlinear rotor-dynamics has not been adequately explored, especially for high order models that embody realistic designs. Effective characterization tools are essential for correctly interpreting rotor-dynamic responses and for guiding the development and analysis of physical models.

Many research efforts have been spent on developing methods viable for nonlinear time series analysis and on understanding various nonlinear phenomena. An explanation was given in [17] for the subharmonic response of a rotor in the presence of bearing clearances and side loads using perturbation techniques under the assumption of small nonlinearity. Myers [18] classified for long bearings the two possible types of bifurcation a static equilibrium point could undergo at the threshold speed: subcritical and supercritical. The nonlinear stability and bifurcation of the unbalance response of a squeeze film damper supported rigid rotor were investigated in [19]. Harmonic, subharmonic, quasi-periodic and chaotic responses were obtained numerically over a range of system parameters and different bifurcations were classified. In order to investigate the nonlinear response in a rotor-bearing system, Noah and his colleagues [5,15-16,20-27] introduced the harmonic method, along with the traditional nonlinear methods, such as the phase portrait, Poincare Map and bifurcation diagram, into the dynamic analysis of rotating machines. The various nonlinear responses due to different nonlinear sources ranging from nonlinear stiffness [20-21,25,27] to bearing clearances [22-24,26] to fluid-bearings [5,15-16] were investigated using nonlinear analytical methods, and periodic, period-doubling, quasi-periodic and chaotic response were numerically observed. While the simple Jeffcott model was mostly employed, models of high-order were also reported [15,24]. The harmonic method was applied by Choi and Noah [22] to a modified Jeffcott rotor with clearance at the supports. The relationship between the displacements and forces was used to correlate the coefficients expanded by the discrete Fourier and inverse Fourier transforms. The approach was further improved in [25]. The shooting method was used to obtain the periodic solution of a nonlinear system in [3,5,15] and the pseudo arc-length continuation scheme was applied to continue the solution branch through bifurcation points such as a saddle-node. The nonlinear response of a rotor-bearing system due to bearing clearances was studied in [28]. The nonlinear phenomena due to surface crack were analyzed in a turborotor and a state observer of an extended dynamical system was designed to estimate the nonlinear effect [29].

When the total number of degrees of freedom of a rotor-dynamic system is too large for even modern computers to compute its response economically, mode reduction methods such as the Component Mode Synthesis method, among others [30], would usually be adopted to simplify the system with low frequency modes to enable stability and nonlinear analyses [31,32]. The method was also applied to the transient dynamic analysis of a two-spool aircraft turbine engine with a squeeze film damper and the Space Shuttle Main Engine oxygen turbopump [33], fully demonstrating the capability and versatility of the method. In Refs. [34] and [35], a linear transformation of coordinates was employed to reduce the degrees of freedom of a high order rotor bearing system with the nonlinear mode remaining. After mode reduction, the nonlinear system was investigated using the phase portrait, Poincare Map, and Fourier Transform and its dynamic responses were numerically integrated using the Newmark Method.

Because a small perturbation is applied to perturb system equilibrium to allow for the linear or low-order terms being analyzed [6, 36], the Perturbation Method is a linearized method. A scheme widely applied in the study of chaos, the Poincare's qualitative topological approach gives an easy and clear way of understanding nonlinear dynamics and chaos in the state space. Such a representation is called a Poincare section [37] and it uses the geometrical characteristics of the trajectories of the system response to predict system behavior and stability. However, all these are qualitative approaches. It depends on the experience of the analyst to determine if a system is chaotic and how unstable the system is [8]. It is desired to specify quantitatively whether or not a system's apparent erratic behavior is chaotic. The changes of quantifiers may be linked to important changes in the development of faults and thus can be used for fault diagnosis and monitoring. Quantitative methods such as the Lyapunov exponents and fractal dimensions have been developed to quantify nonlinearity. However, these quantitative methods cannot show the occurrence or the type of bifurcation -- two very important requirements in nonlinear analysis and fault diagnosis. In addition, these methods may produce erroneous results, rendering that they are neither reliable, nor sufficient [6]. Because the change of system state is represented by its dynamic response, the change of dynamical response can be realized in its spectrum or power spectrum. Analyzing changes in frequency spectrum is an effective way to detect changes of system behavior. But FFT is a linear transformation. It uses basic spectral components commonly called harmonics of constant amplitude and frequency to approximate a time signal. As time domain information is totally lost and thus providing no temporal progression of the system, Fourier based methods are not suitable for nonlinear analysis [36,38]. Without time information the bifurcation of a dynamical system cannot be seen or interpreted at all. To observe bifurcations and the occurrence of bifurcation are essential to the detection of the presence and progression of faults in dynamical systems [8]. Therefore tools that can simultaneously resolve a vibratory signal in both the time and frequency domains are highly desirable.

Recently powerful time-frequency analytical techniques including the wavelet transform were introduced into the nonlinear analysis and detection of faults. Wavelets were used to determine underlying parameters and other characteristics in a nonlinear structural system in [39], showing that complicated nonlinear phenomena can be clarified using wavelets. Continuous Wavelet Analysis was used to process output data and extract information about structural nonlinearities in aeroelastic systems [40, 41], in which features and trends extracted from the wavelet transform maps of the response were used to characterize nonlinearities. Daubechies scaling functions were applied to discretize nonlinear governing differential equations of motion in [42] and through which the mechanical parameters were identified for zero-memory nonlinear discrete structural systems. Different vibration techniques for condition monitoring and fault diagnosis for mechanical systems were compared in [43-45] and it was concluded that because of the highly non-stationary nature of these vibration signals wavelet analysis is recommended. Harmonic Wavelets were developed to analyze non-stationary vibrations in [43]. Applications of wavelet transform to structural and mechanical system damage detection were reviewed in [46], in which how to use wavelets and wavelet maps to analyze nonlinear vibration signal is discussed. Wavelet packets, Gabor wavelets, multi-scale ridges and skeletons of wavelet transform, the amplitude and phase of wavelet maps were used to analyze nonlinear phenomena in various dynamic systems [47-51]. The energy of wavelet and scaling coefficients between double zero-crossing points in the time domain are used to detect crack-induced dynamic instability and to characterize milling chatters [4, 52-53].

Wavelet transform and other time-frequency methods can simultaneously localize a time event in the time-frequency domain and, therefore, they can process non-stationary signals and detect the changes of system behavior in real-time [54, 55]. Applying wavelets to monitor nonlinear responses is a significant achievement in that it points to the right direction. However, as wavelet time-frequency transformation is Fourier-based and thus linear, applications of wavelets are inevitably limited to linear systems only [36]. As discussed, misleading results can be generated if they were applied to nonlinear systems without careful discretion on the part of the user. In addition, their resolutions are poor as they evaluate the “energy” coefficients using the infinite integral in the average sense. This is also the reason why high resolution cannot be achieved in the join time-frequency domain. For example, even though the time-frequency window can be adjusted, two pulses within the same window cannot be discriminated [56]. If these two pulses are to be distinguished from each other, the required time window has to be narrow and, as a result, the frequency window has to be wide. Frequency resolution would thus be lost. High time resolution is obtained at the price of poor frequency resolution, and vice versa. In order to localize an event in time, a narrow time window has to be chosen. But, high frequency requires longer time window, thus is the inconsistency of Fourier-based time-frequency techniques. This drawback prevents some bifurcations in high frequency from being seen and could lead to the misinterpretation of nonlinearity and misunderstanding of the true physical nature of a dynamic system.

As discussed, traditional nonlinear analysis techniques are qualitative and not suitable for determining the extent of dynamic instability and for analyzing nonlinear responses.

Interpretation of nonlinear dynamics using these techniques is always subject to questions. For example, because Fourier transform uses harmonics to approximate time functions, fictitious frequency components could appear in the spectrum [36]. From the viewpoint of engineering, if a bifurcation could be detected, the development of the fault responsible for inducing this bifurcation could also be detected. Thus good strategies could be developed to ensure dynamic system stability, which in turn helps to improve operation safety and keep the maintenance cost down. Signal processing tools that can localize events in both the time and frequency domains with high resolution could detect small changes within the system response – an essentiality in detecting bifurcation and instability and in understanding nonlinearity. The Hilbert-based instantaneous frequency gives the dependence of frequency on time and has been shown to be a viable choice for nonlinear analysis [10,56]. Applications using instantaneous frequency to characterize various dynamical systems of strong nonlinearity can be found in [57-59]. The general applicability and interpretation of instantaneous frequency, as is realized through the use of the method of Empirical Mode Decomposition [10,36], to the analysis of nonlinear response is discussed in Chapter IV. The Empirical Mode Decomposition can separate a system response into its several intrinsic modes [36]. This definition of instantaneous frequency is based on the derivative of the phase and thus has good localization property in the time-frequency domain. This method is used in this research. Nonlinear techniques may provide characteristic indicators that discriminate an intact structure from one that is plagued with flaws [60]. Detecting the onset of nonlinear vibration behavior in rotating machines represents one of the most widely practiced forms of vibration-based fault identification [60,61]. This research addresses rotor-dynamic nonlinearity as a function of rotating speed, cracking breathing, and fluid bearing clearance and establishes the correlation of the three parameters with various dynamic responses of instability including bifurcation and chaos.

1.3 Objectives

It is demonstrated in Chapter II that nonlinear analysis is essential for understanding the behavior of a rotor-dynamic system. The present status of rotor-dynamic research is that nonlinear analytical methods for rotary machines are either impractical or unavailable and thus unsatisfactory. Effective algorithms for characterizing nonlinearities in rotor-dynamic systems are still being sought. Therefore, the major objectives of this research are to:

- Develop time-frequency tools proven suitable for nonlinear, non-stationary signal analysis.
- Model different nonlinearities and characterize the induced nonlinear dynamic behaviors, so that the underlying parameters and their ranges of stability operation can be found.
- Provide new understanding and interpretation of nonlinear rotor-dynamic phenomena using characterization tools of viability and effectiveness.
- Provide guidelines for the design, development and operation of instability-free rotary machines.

To provide effective solution to the detection of rotor-dynamic instability and to guide the design of new rotary machinery in the future, a rotor-bearing model is developed to investigate the complex nonlinear behaviors and nonlinearities induced by surface crack and fluid bearing forces [4, 29, 34-35].

CHAPTER II

NONLINEAR ROTOR-DYNAMIC RESPONSES

2.1 Scope of Rotor-Dynamics

Rotary machineries, such as gas turbines, steam turbines, internal combustion engines and electric motors, are the most widely used dynamical mechanical systems in engineering. Since the rotating parts in such machinery are oftentimes the main sources of vibration, full understanding of the vibration phenomena and sufficient knowledge of rotor-dynamics are necessary for finding ways to suppress or eliminate vibrations [2]. Initially the primary concern and effort were to predict the critical rotational speeds of resonance and afterwards to modify the design to achieve different critical speeds of resonance [62]. However, it has long been observed that when the running speed exceeds certain critical speeds, various kinds of undesirable problems of rotor-dynamic instability would occur. Henceforth, rotor-dynamics was developed to overcome these technical difficulties.

Rotor is the general term for the rotating part of a rotary machine, while stator means the stationary part of the machine. If the deformation of a rotating shaft is negligible in the operating speed range, it is called a rigid rotor. If the shaft deforms appreciably at some rotational speeds in the operating speed range, it is called a flexible rotor. In some models, disks are considered to be rigid and the distributed mass of an elastic shaft is concentrated at the disk position. Such a model is called a lumped-parameter system and it has been intensively investigated [15-16,19-23 and 25-27]. If a flexible rotor with distributed mass and stiffness is considered, the model is called a distributed-parameter system or continuous rotor system and this specific character of the model has allowed it to be explored using the finite element methods [34-35, 63-64].

Much fundamental knowledge of rotor-dynamics was established from a very simple model called the Jeffcott model, which consists of a massless elastic shaft and a rigid disk [30, 62]. It is believed that the key ideas provided by the model, including critical speed, gyroscopic moment, whirling motion, frequency diagrams, and balancing a rigid rotor, are common to all branches of rotor-dynamics. The model is helpful for understanding some phenomena in rotor-dynamics, but it is of no direct value in the development of models for real-world rotors [30].

The main purposes of rotor-dynamic analysis can be summarized as follows [2,30,62]:

1. To predict critical speeds. Speeds at which vibration due to rotor imbalance is maximum can be calculated from design data, so as to avoid them in normal operation of the machine.
2. To modify the design to alter the critical speed. When it is necessary to change the range of operating speed of a rotating machine, or the objective is not accomplished accurately, design modifications may be required to change the critical speed.
3. To predict the response due to rotor imbalance. Accurate response prediction depends on accurate modeling. However, accurate modeling is not easily achievable as many different machine parts could be involved and the dynamic interactions between them could be sophisticated, thus contributing to practical difficulties in predicting responses. In addition, the vibration of rotor also depends on two factors which are both very difficult to measure: the distribution of imbalance along the rotor and the rotor-bearing system damping.
4. To determine the limiting conditions for threshold speed or the power beyond which the motion of a rotor would be unstable. Since some destabilizing forces, for example from bearings and seals, are still not understood well enough for accurate mathematical modeling, this constitutes a very important and challenging objective for rotary machinery analysts.

5. To favorably modify the design to suppress dynamic instability in a rotor-bearing system. If the destabilizing forces and instability mechanisms are well understood, the design can be modified to suppress, or eliminate, problems of instability in a rotor system.
6. To calculate balance correction masses and locations from measured vibration data. This allows “in place” rotor balancing to be accomplished, thereby reducing the amplitude of synchronous vibrations.

As stated, many basic concepts of rotor-dynamics, including critical speed, bearing clearance and critical speed transition, were explained using very simple models such as the Jeffcott and Stodola-Green [30] models. But because these models are too simple to be used for real-world rotor-dynamic analysis, many new models were proposed and applied to turbomachinery analysis and design. These models include the Lumped-parameter model, Myklestad-Prohl transfer-matrix method, finite-element method for Euler beam model, and a slender beam model with rotary inertia and gyroscopic coupling [30]. Lumped-parameter structural dynamic models have traditionally been used to consider the distributed elastic and inertial properties of rotors, and rotors are modeled as a collection of many rigid bodies connected by massless elastic beam elements. Transfer-matrix formulations and general mass-stiffness matrix formulations were developed as a result of the lumped-parameter models, and they both have been employed to develop flexible-rotor models from the component rigid body equations. Subsequently finite element models were introduced for flexible rotors. Nelson *et al* [65-67] developed more general finite-element models that include rotary inertia, gyroscopic coupling, axial loads, shear deflections and the effect of axial torque -- a fairly complete model that has been employed in many relevant researches [34,35]. As compared with other areas of vibration analysis, the main analysis difficulty experienced in rotor-dynamics is the requirement for modeling forces induced by hydrodynamic bearings, squeeze film dampers, and seals, to name a few. As such, all above mentioned models represent the initial steps in the development of an adequate rotor-dynamic model.

Fluid-film bearings are commonly used in rotating machinery because they have various merits, such as large load capacity, damping and no life limit with good lubrication [2]. However, under special conditions, the fluid in a rotating field could cause self-excited vibrations, which could then lead tragically to unexpected accidents. Journal bearings, multilobe bearings, tilting pad bearings all belong to the fluid-film bearing category. Journal bearings and some of multilobe bearings with oil films have been investigated extensively as representative bearings of fluid-film bearings. Vibrations of rotors supported by these types of bearings have been much studied. Approximation formulations of fluid-film bearing forces obtained by integrating the Reynolds equation for short journal bearings, long journal bearings and finite-length bearings can be found in Refs. [30] and [68]. Once the equilibrium position of a rotor supported by these bearings is determined using the linearized procedures, coefficients of linear stiffness and damping for small motion about the equilibrium position of the journal can be calculated using the method developed by Lund [1,69-71]. Stiffness and damping coefficients are required for both synchronous response calculations and linear stability analysis. In fact, the development of stiffness and damping coefficients and the method for computing damped critical speeds [72] have resulted in vast research interest in the linear stability analysis of rotor bearings.

The forces from liquid and gas seals, impellers and turbines, along with their effects on the rotor systems supported by them, have also been studied using similar linear stability methods [30]. The fluid trapped in a hollow rotor works as unbalance and affects the rotor system response [2,73]. Ball bearings, bearing pedestals, universal joints and couplings are also widely used in rotating machinery and may cause vibrations, and research in understanding the characteristics of these machine elements was also reported [2].

Approach adopted in the literature for determining critical speeds making use of eigenvalue analysis, fast Fourier transform and the linearized damping and stiffness coefficients obtained near the (linear) equilibrium point are all linear methods. Thus, regardless of if a model is of intrinsically nonlinear or not, as long as linearized approach is applied, the behavior of a rotor-dynamic system cannot be correctly described simply because of the fact that linear stability analyses are not sufficient for a rotor system of characteristically nonlinear.

2.2 Nonlinearities in Rotor Dynamic Systems

When the running speed of rotating machinery is increased, nonlinear phenomena are frequently encountered. With the requirement for high performance design, high operating speeds and high reliability in compact configuration has become essential in the design of rotating machines, thus rendering understanding the nonlinear phenomena in rotary machines an important issue.

As discussed in Introduction, restoring and/or damping forces realized by clearances in ball bearings and squeeze film dampers, oil films in journal bearings, seals, magnetic forces, friction, or stiffening effects in the elongation of a shaft are possible sources of rotor-dynamic nonlinearity. Local nonlinearity within rotor systems could have significant local and global effects on rotary behavior that contribute as a result to different nonlinear phenomena. For example, changes in the shape of resonance curves, jump phenomena, subharmonic resonance, combination resonance, chaotic vibration, self-excited oscillations and entrainment phenomena are nonlinear behaviors that have been widely observed [74]. The commonly seen sources of nonlinearity and their associated responses are briefly presented in the following paragraphs.

1. Bearing clearances

Ball bearings with clearances [2,11] that have been broadly studied in [17,20-25,28] are among the earliest that were investigated for nonlinear rotor-dynamic phenomena. The equations of motion of a lumped-parameter rotor model with radial clearance have the form [2],

$$\begin{aligned} m\ddot{x} + c\dot{x} + F_r \frac{x}{\sqrt{x^2 + y^2}} &= m e \omega^2 \cos \omega t \\ m\ddot{y} + c\dot{y} + F_r \frac{y}{\sqrt{x^2 + y^2}} &= m e \omega^2 \cos \omega t - m g \end{aligned} \tag{2.1}$$

where

$$\begin{aligned} F_r &= \begin{cases} k_1 r & r \le R_0 \\ k_1 R_0 + k_2 (r - R_0) & r \ge R_0 \end{cases} \\ r &= \sqrt{x^2 + y^2} \end{aligned} \tag{2.2}$$

with x, y denoting the coordinates of the rotor center, and m, c, e, ω representing, respectively the mass, damping coefficient, imbalance and running speed. When the deflection r from the bearing centerline is small, the stiffness is determined by the stiffness of the shaft. When the deflection becomes large and the radial clearance disappears, the overall stiffness increases. Eq. 2.1 can be integrated using the Runge-Kutta or Newmark method. Using this model, harmonic resonance, subharmonic resonance, harmonic response and subharmonic response of 1/2 and 1/3 order, and even chaotic motion were reported [75]. The bifurcation involved in this model is period-doubling and, through a series of bifurcations, the model demonstrates chaotic characteristics.

2. Internal damping

Frictions generated between two rotating parts are attributed as internal damping. Internal damping is further classified into hysteresis damping and structural damping [2]. The former is an internal friction that is due to the friction in the shaft material; while the latter one is due to the sliding between the shaft and mounted elements such as bearings and gears. In real world applications, the effect of the former is very small while the self-excited oscillation due to the second one is often observed. The internal damping forces were derived in [2,74], which can be further simplified to Coulomb damping. Ishida [74] studied a rotor system with nonlinearity in internal damping and found the entrainment phenomenon at the critical speed of a subharmonic resonance of order 1/2 of a forward whirl mode. Other than the above, no more phenomena of rotor-dynamic instability were otherwise reported.

3. Fluid-film bearing forces

Oil film in a journal bearing is a well-known source of nonlinearity simply because fluid film bearings and dampers produce reaction forces that are nonlinear functions of journal displacement and velocity. The nonlinear phenomena and stability problem due to multilobe journal bearings, especially the plain journal bearings and elliptical bearings, have received much attention [3, 15-16, 34-35]. The nonlinear reaction forces are calculated from solving the Reynolds Equation in Eq. 2.3.

$$\frac{\partial}{\partial x}\left(h^3\frac{\partial p}{\partial x}\right)+\frac{\partial}{\partial z}\left(h^3\frac{\partial p}{\partial z}\right)=6U\mu\frac{\partial h}{\partial x}+12\mu\frac{\partial h}{\partial t} \tag{2.3}$$

where μ is the fluid viscosity, $p(x, z)$ is the pressure distribution around the bearing, and U is the fluid velocity near the bearing. Oil-film thickness, h, is given by

$$h = Cr - x\cos\theta - y\sin\theta \tag{2.4}$$

where Cr is the bearing clearance. The Reynolds Equation can be converted into to its polar coordinates form using

$$U = R\omega,\ x = R\theta,\ \partial x = R\partial\theta$$

where R is the journal radius and ω is the journal angular speed. Note that $p = p(\theta, z)$ and the Reynolds Equation is now

$$\frac{1}{R^2}\frac{\partial}{\partial\theta}\left(h^3\frac{\partial p}{\partial\theta}\right)+\frac{\partial}{\partial z}\left(h^3\frac{\partial p}{\partial z}\right)=6\mu\omega\frac{\partial h}{\partial\theta}+12\mu\frac{\partial h}{\partial t} \tag{2.5}$$

From Eqs. 2.4 and 2.5, it is evident that the pressure is a nonlinear function of journal position and velocity. Once the pressure is available, the components of the fluid bearing force can be calculated using the two integrals as follow

$$\begin{aligned} f_x &= -\int_{-\frac{L}{2}}^{\frac{L}{2}}\int_0^{2\pi} p(\theta,z)\,R\cos\theta\,d\theta\,dz \\ f_y &= -\int_{-\frac{L}{2}}^{\frac{L}{2}}\int_0^{2\pi} p(\theta,z)\,R\sin\theta\,d\theta\,dz \end{aligned} \tag{2.6}$$

where L is the bearing length. These forces are to be incorporated into the equations of motion of the rotor-bearing system to predict system time responses. One simple example is given in the next section. The nonlinear responses induced by this kind of nonlinearity can generate period doubling, quasi-periodic, subharmonic (of many orders) and chaotic responses. Some demonstrative results will be presented in chapters that follow.

4. Surface crack

Surface fatigue cracking is one of the most serious causes of rotary accident. In order to detect the existence and progression of crack and develop a monitoring methodology, its vibration characteristics have to be investigated [4]. The state of opening or closing of a crack depends on the angular direction of shaft deflection relative to the crack. The opening condition of the crack can be formulated approximately by the displacement near the crack as

$$\xi_i - \frac{\xi_{i-4}+\xi_{i+4}}{2} > 0 \tag{2.7}$$

where ξ is the direction that is perpendicular to the crack. Using the transformation matrix

$$T = \begin{bmatrix} \cos(\omega t) & \sin(\omega t) \\ -\sin(\omega t) & \cos(\omega t) \end{bmatrix} \tag{2.8}$$

with ω denoting the spinning velocity. The element-stiffness-matrix, K_{crack}, for a discrete model in the inertial coordinate system has the form

$$K_{crack} = \frac{h_r}{h(1+h_r)} \begin{bmatrix} \sin^2(\omega t) & \sin(\omega t)\cos(\omega t) \\ \sin(\omega t)\cos(\omega t) & \cos^2(\omega t) \end{bmatrix} \tag{2.9}$$

Here, h is the compliance in the ξ direction and h_r is the relative crack depth. The relation between h_r and crack depth was experimentally established by Mayes and Davis [77]. In addition, the values of K_{crack} depend on the opening condition. If the condition is satisfied, the values of K_{crack} are determined using the above equation; otherwise the values of K_{crack} are 0. It is obvious that the cracked rotor-bearing system as described by the model is a nonlinear, dynamical problem with the relative flexibility, h_r, as the control parameter. Thus, the shaft stiffness and crack breathing vary as the direction of deflection varies, and the induced response becomes highly nonlinear. Resonances of harmonic, subharmonic and super-harmonic, along with the combination of them, were modeled and thoroughly analyzed in [2]. The nonlinear phenomena of a cracked rotor-bearing system were studied in [4,29] in which the effects of nonlinear stiffness were realized as nonlinear forces and different nonlinear dynamic states were simulated through employing the Runge-Kutta algorithm. In addition, a highly effective real-time wavelet-based crack detection algorithm was developed to enable the determination of crack characteristic frequency, period-doubling bifurcation, fractal and chaotic motions. This kind of nonlinearity is also to be discussed in later chapters. There are also many other nonlinear phenomena that were observed or investigated as results of other types of nonlinear sources attributable to, for example, rolling element bearings, rotors partially filled with liquid, or other nonlinear spring characteristics. For more detailed nonlinear phenomena and explanations for weak and strong nonlinear sources, the works by Ishida and Ehrich [2,74,76] are referred.

2.3 Interpretation of Rotor-Dynamic Response

Once the rotor system and nonlinear sources are accurately modeled, rotor-dynamic time responses can be obtained using methods of direct integration or the model can be linearized in the neighborhood of equilibrium points to determine linear stability. These two interpretations of a given rotor-bearing system have fundamental differences impacting the understanding of the dynamics and operation of the system being modeled. To make a point, a rigid rotor model supported by journal bearings is used to demonstrate the differences in interpretation put forth by the two approaches. The rotor is of mass *2m*, thus being acted on by its gravity force, 2*mg*, and supported by two identical plain journal bearings. The constant speed differential equations of motion for this rotor are

$$\begin{aligned} m\ddot{x} &= f_x + me\omega^2 \cos\omega t \\ m\ddot{y} &= f_y + me\omega^2 \sin\omega t - mg \end{aligned} \qquad (2.10)$$

where *m* and *e* are the rotor's mass and imbalance-vector, respectively, *x*, *y* are the coordinates of the journal center, and f_x, f_y are the bearing reaction force components. The journal bearing is assumed to be short. First, the equations are linearizd near the equilibrium point, (x_0, y_0). By giving the point a small perturbation,

$$x = x_0 + p_x, \quad y = y_0 + p_y \qquad (2.11)$$

and using the stiffness and damping coefficients representation

$$\begin{Bmatrix} f_x \\ f_y \end{Bmatrix} = -[k_{I,J}]\begin{Bmatrix} p_x \\ p_y \end{Bmatrix} - [c_{I,J}]\begin{Bmatrix} \dot{p}_x \\ \dot{p}_y \end{Bmatrix} \qquad (2.12)$$

Substituting Eqs. 2.11 and 2.12 into Eq. 2.10, we have

$$m\begin{Bmatrix}\ddot{p}_x\\ \ddot{p}_y\end{Bmatrix}+[c_{I,J}]\begin{Bmatrix}\dot{p}_x\\ \dot{p}_y\end{Bmatrix}+[k_{I,J}]\begin{Bmatrix}p_x\\ p_y\end{Bmatrix}=me\omega^2\begin{Bmatrix}\cos(\omega t)\\ \sin(\omega t)\end{Bmatrix} \tag{2.13}$$

Normalize the two equations using

$$X=\frac{p_x}{Cr},\quad Y=\frac{p_y}{Cr},\quad \ddot{X}=\frac{\ddot{p}_x}{Cr\omega^2},\quad \ddot{Y}=\frac{\ddot{p}_y}{Cr\omega^2},\quad \tau=\omega t$$

and then divide all terms by the side load *mg*, Eq. 2.13 becomes

$$\frac{Cr\omega^2}{g}\begin{Bmatrix}\ddot{X}\\ \ddot{Y}\end{Bmatrix}+[C_{I,J}]\begin{Bmatrix}\dot{X}\\ \dot{Y}\end{Bmatrix}+[K_{I,J}]\begin{Bmatrix}X\\ Y\end{Bmatrix}=\frac{e\omega^2}{g}\begin{Bmatrix}\cos\tau\\ \sin\tau\end{Bmatrix} \tag{2.14}$$

Note that x_0, y_0 are obtained when $f_x = 0$, and $f_y = mg$ and that *Cr* is the journal bearing clearance. A simplified formula for short plain journal bearings can be found in [30]. $K_{I,J}, C_{I,J}$ are non-dimensional rotor-dynamic coefficients, which can be derived following [68].

Linear stability analysis can be performed on Eq. 2.14 using the eigenvalue analysis by first obtaining the characteristic equation and then checking the real parts of the roots of the equation to determine stability. Using the linearized procedure, only two cases can be determined; that is, stable and unstable, and the critical case can rarely be found. Here the responses of Eq. 2.14 are numerically integrated using the Newmark method. The parameters used are $m = 300kg$, $R = 0.05m$, $Cr = 0.003*R$, $e = 0.3*Cr$, and viscosity $\mu=0.022\ N.sec/m^2$. When the rotating speed ω = 100π rad/sec, the corresponding equilibrium point is (x_0, y_0) = (0.373, -0.561) and the induced response is stable, as is evident from Figure 2.1 where the orbit converges very quickly to the equilibrium point. Figure 2.2 shows that when ω = 200π rad/sec and (x_0, y_0) = (0.382, -0.414), though the trajectory doesn't converge as fast, the corresponding response demonstrates a motion of stability. After an extended amount of time, the orbit trajectory is seen to settle down into the equilibrium point. As shown in Figure 2.3, when ω

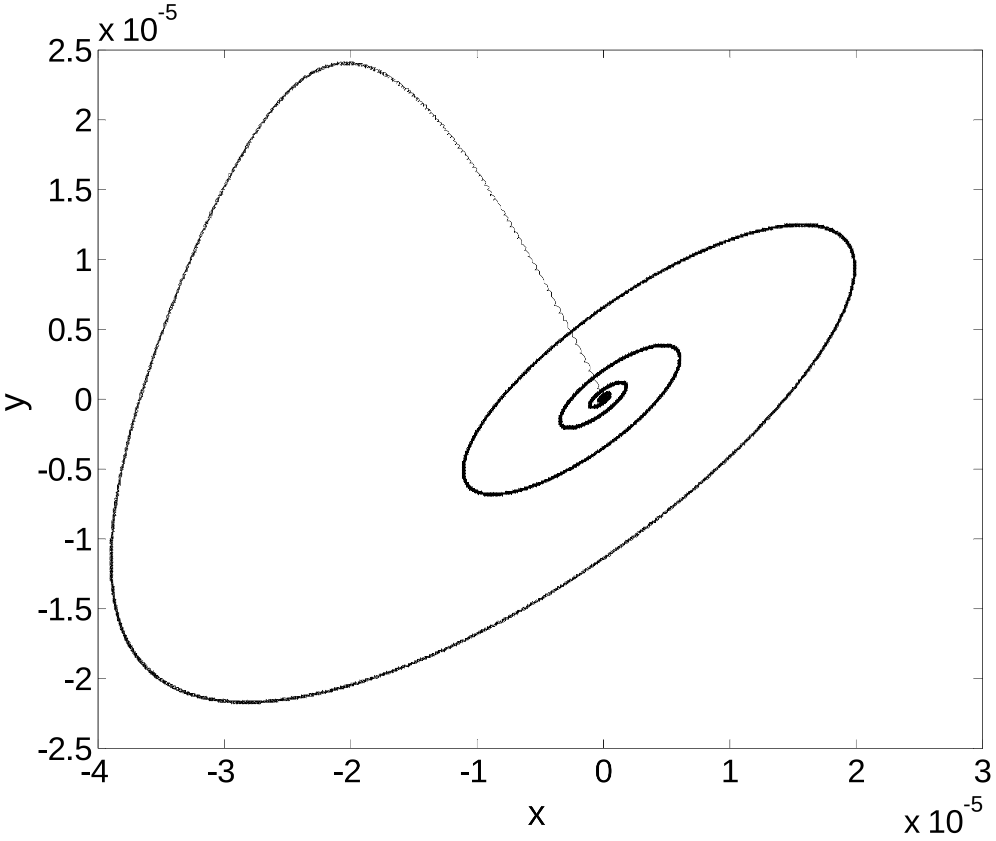

Figure 2.1 Orbit of journal center using linearized model when $\omega = 100\pi$

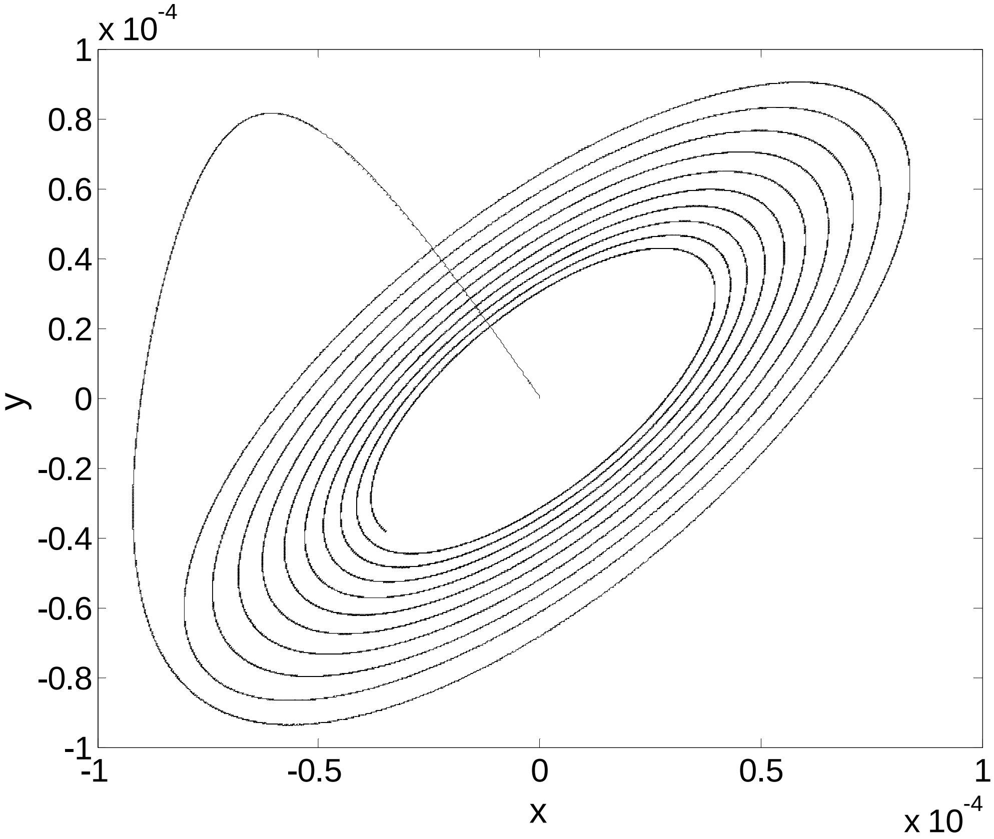

Figure 2.2 Orbit of journal center using linearized model when $\omega = 200\pi$

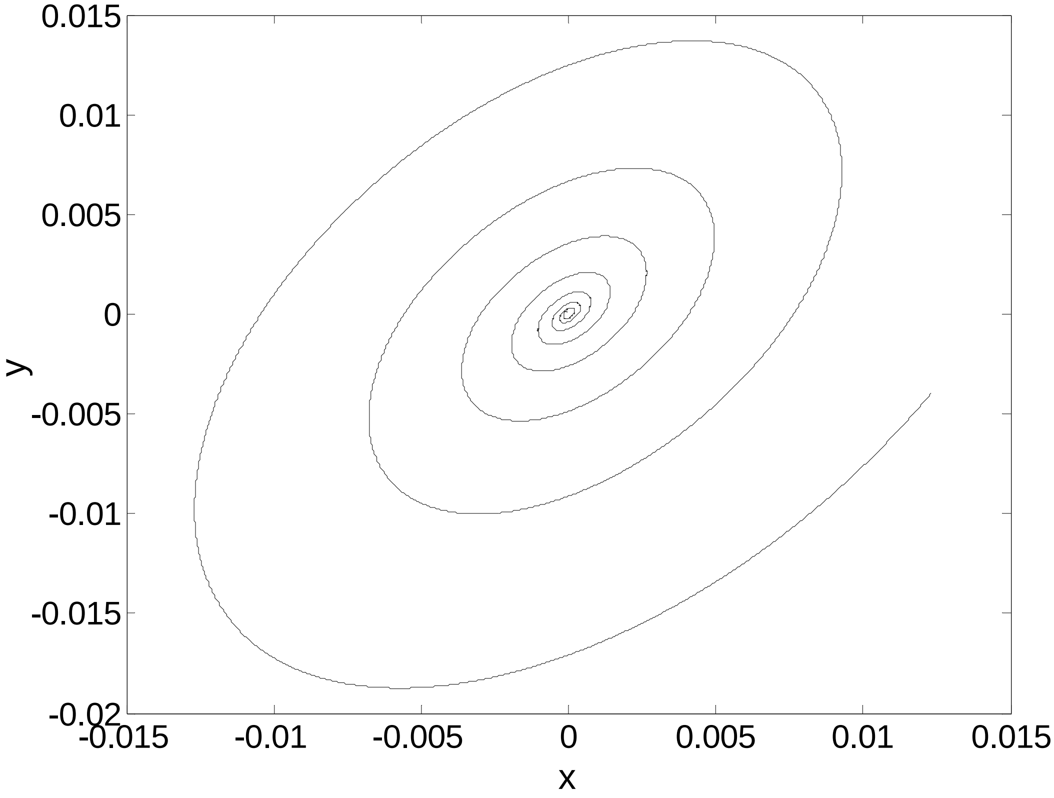

Figure 2.3 Orbit of journal center using linearized model when ω = 300π

reaches 300π and (x_0, y_0) = (0.362, -0.295), the system becomes unstable and the orbit of the journal center fast diverges.

The linear procedure and synchronous-response procedures are commonly used in the design and production of rotary machines. Nonlinear dynamical model for the same rigid rotor is analyzed to compare the results obtained using the linearized model. First the model equation, Eq. 2.10, is normalized using

$$X = \frac{x}{Cr}, \quad Y = \frac{y}{Cr}, \quad \ddot{X} = \frac{\ddot{x}}{Cr\omega^2}, \quad \ddot{Y} = \frac{\ddot{y}}{Cr\omega^2},$$
$$F_x = \frac{f_x}{mCr\omega^2}, \quad F_y = \frac{f_y}{mCr\omega^2}, \quad \tau = \omega t, \quad u = \frac{e}{Cr}$$

The following equations are acquired

$$\begin{aligned} \ddot{X} &= F_x + u\cos\tau \\ \ddot{Y} &= F_y + u\sin\tau - \frac{g}{Cr\omega^2} \end{aligned} \tag{2.15}$$

The same system parameters are used in this nonlinear model and the system responses are determined by integrating Eq. 2.15 using the Runge-Kutta method.

When the rotor runs at 100π rad/sec, the system is stable. However, Figure 2.4 shows that the center response is not an equilibrium point, but rather a limit cycle, thus a periodic solution representing a stable motion at the speed considered. Continuing to increase the angular speed to 200π results in an unstable motion that is characterized in Figure 2.5 as a period doubling bifurcation. The center trajectory will never converge to an equilibrium point as the linearized model predicts. If the speed reaches 250π, more periodic doubling bifurcations would occur. The close orbits in the orbit diagram Figure 2.6, though would never go out of bound, the dynamic state is becoming more unstable. The same dynamic state of periodic doubling bifurcations is seen to persist even when the speed is further increased to 300π-400π.

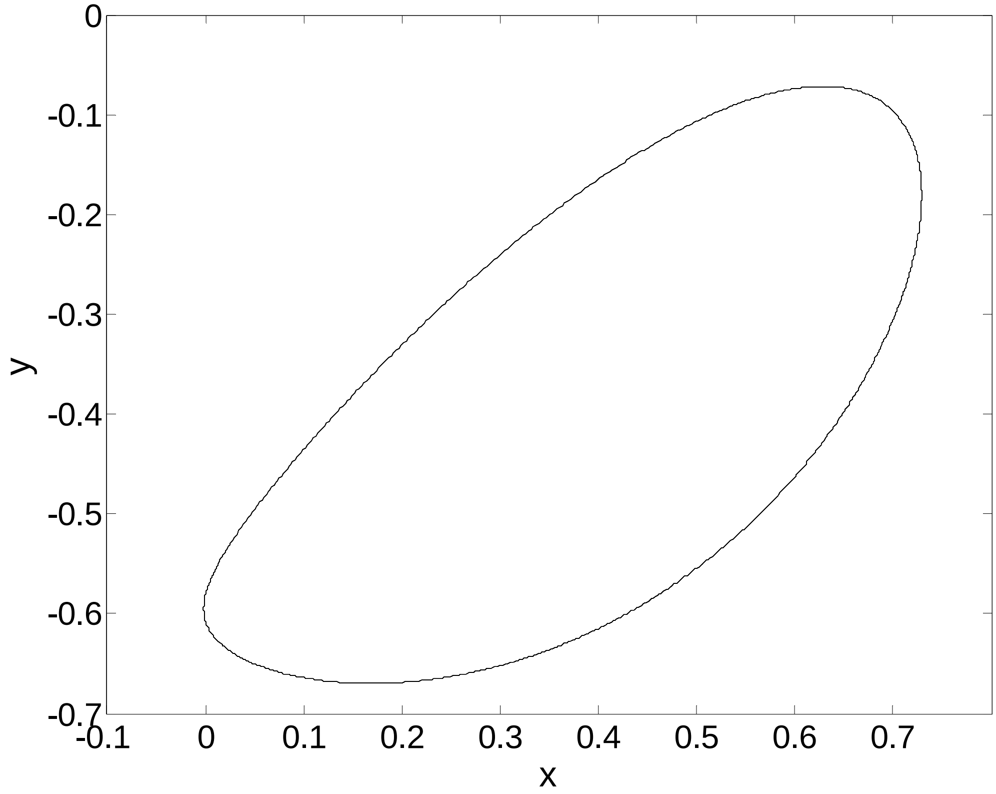

Figure 2.4 Orbit of journal center using nonlinear model when ω = 100π

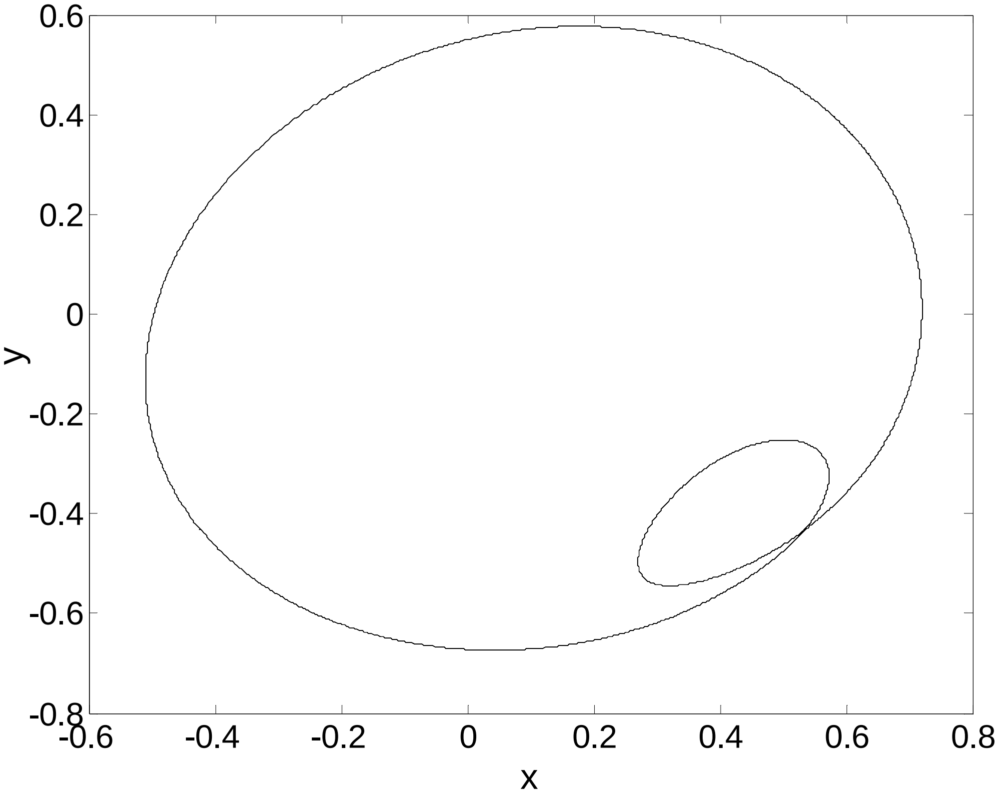

Figure 2.5 Orbit of journal center using nonlinear model when ω = 200π

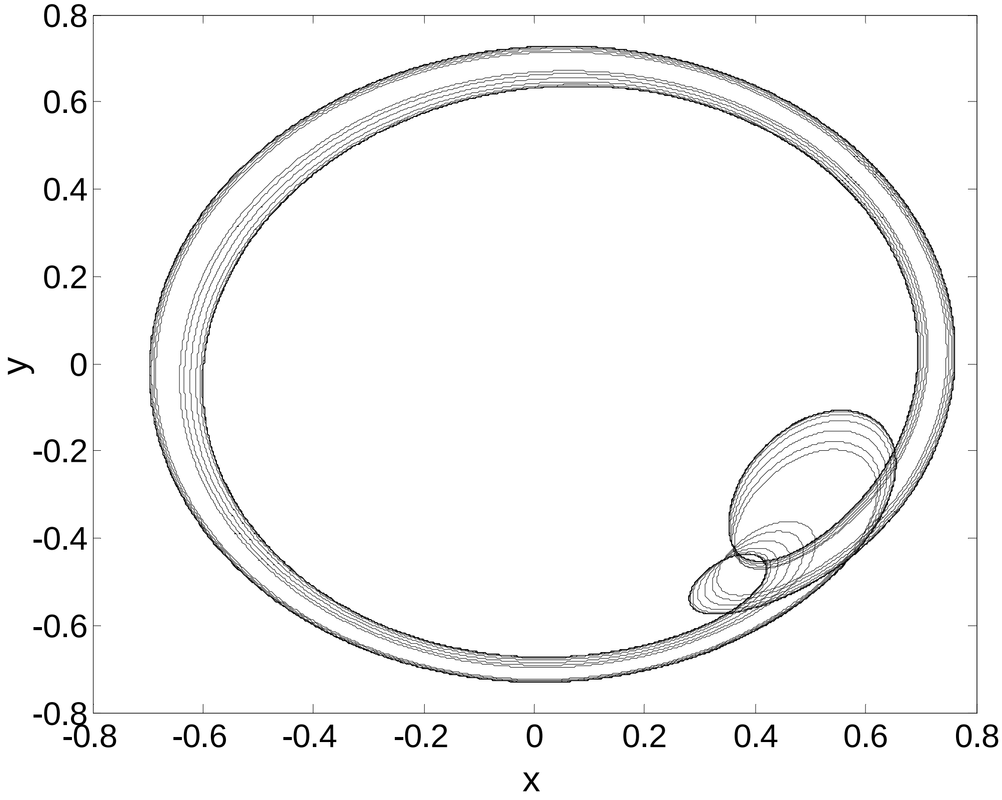

Figure 2.6 Orbit of journal center using nonlinear model when ω = 250π

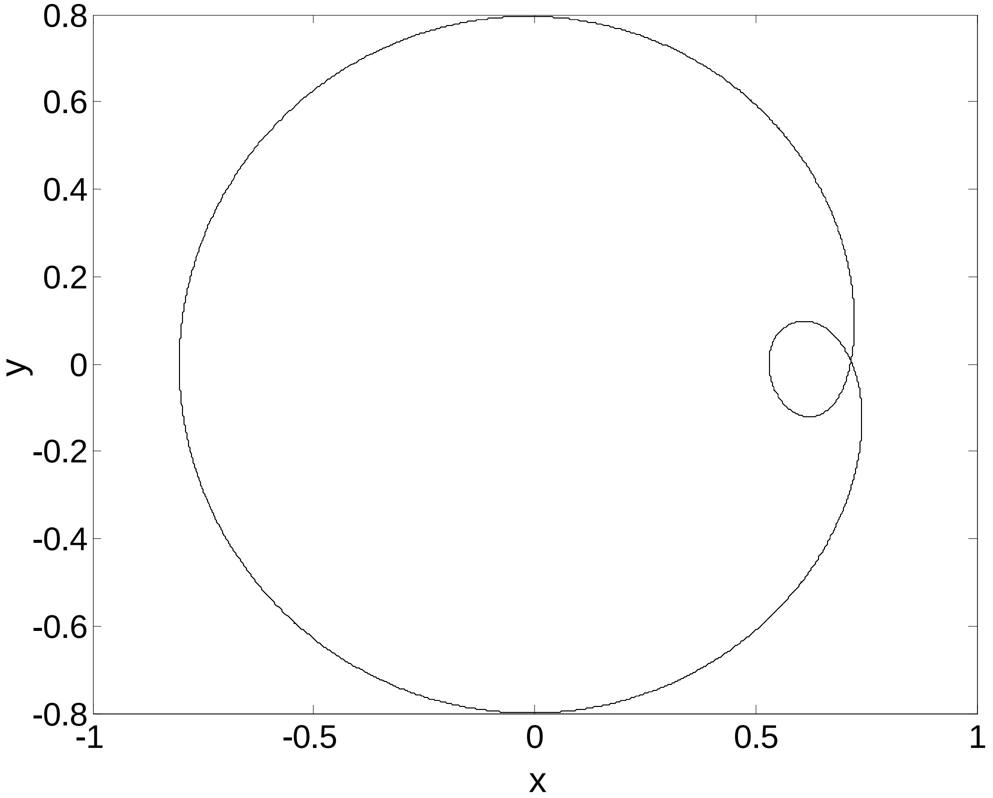

Figure 2.7 Orbit of journal center using nonlinear model when ω = 500π

Interestingly, when ω = 500π, the dynamic state found in Figure 2.7 is of subharmonic type. The linearized model can never predict this kind of dynamic behavior in a simple rotor. Thus results using nonlinear models can be compared to those obtained with linearized methods. Linearized models dictate that, when control parameters exceed what the stability limit is allowed, the rotor would become unstable with exponentially diverging and unbounded vibration amplitudes. On the other hand, as oppose to the linearized models, a nonlinear model would describe responses as nonlinear and bounded.

2.4 Summary

In this chapter, the research scopes of rotor-dynamics were reviewed. It is summarized that the knowledge regarding the various rotor-dynamic behaviors are more often than not established using linearized rotor models and notions such as critical speeds, stability charts, stiffness and damping parameters. The nonlinearity in rotor dynamic systems was discussed in reasonable detail. A simple rigid rotor model supported by plain journal bearings was comparatively analyzed using nonlinear and linearized procedures. The linearized model showed that the system is either uniformly stable or unstable while the nonlinear analysis described complicated nonlinear phenomena including periodic motion, period doubling and subharmonic motion. The presented comparative study showed that linearized methods could misinterpret a bifurcated response as a stable motion and an almost stable motion as one of unstable, thus severely risking misreading the dynamics of a rotor system and also missing the important stability information about the system as a result. With the increasing realization that rotor-dynamic nonlinearity cannot be neglected, advanced nonlinear analysis tools will need to be developed and applied to the analysis of rotary response in order to fully investigate and understand the physical nature of rotor-dynamic systems.

CHAPTER III

ANALYTIC TOOLS FOR CHARACTERIZING ROTOR-DYNAMIC RESPONSES

3.1 Time Domain Approach

As discussed in the last chapter, the indiscretionary use of linearized models or linear approach to the study of nonlinear rotor-dynamic systems could result in erroneous results and false physical interpretation, thus risking misreading system response and missing out critical information indicative of imminent instability or failure. Henceforth, the need for being able to characterize nonlinearity and chaos has resulted in broad effort and progress in the area of nonlinear dynamics [4, 37, 78-79]. In this section, a few time domain nonlinear analytical methods are reviewed, along with some illustrative examples on employing them to interpret nonlinear responses.

The response of a dynamic system in general could be a fixed point, a periodic solution, or a non-periodic solution. A stable linear or almost linear system would have an equilibrium point or a fixed point as its response. The Hartmen-Grobman theorem states that the dynamic characteristics of a perturbed system are qualitatively similar to its linear counterpart in the neighborhood of the equilibrium point [7] and that the stability near the equilibrium point can thus be determined by slightly perturbing this point. If the system restores back to the original point, the system near the point is stable. Otherwise, if the system diverges away from the point, it is unstable. This is exactly the area in which linearized model and linear analysis can be applied. Figures 2.1 and 2.2 show the linearly stable case, while Figure 2.3 shows the linearly unstable case.

By studying the geometric characteristics and flow paths of the solution trajectory in the state space, the stability near the trajectory can be determined using phase portraits. Powerful graphical tools that aid in identifying the dynamic state of a system include also the Poincare maps and bifurcation diagrams. A Poincare map is a collection of sequential points in the state space generated by the penetration of a continuous evolution trajectory through a generalized surface or plane in the space [79]. For a periodically forced, second-order nonlinear oscillator, a Poincare map can be obtained by stroboscopically observing the position and velocity at a particular phase of the forcing function. For a nonlinear rotor-dynamic system, its Poincare map is generally obtained this way. Bifurcation diagram is used to plot the transition of a motion from stability to chaos as some parameters are varied. Such diagrams can be obtained by time sampling the motion as in a Poincare map and displaying the output against the control parameter. The bifurcation diagram of the Quadratic map shown in Figure 3.1 is given as an example, in which f_μ is plotted against the control parameter μ using the iterative scheme defined in Eq. 3.1

$$\begin{aligned} &f_\mu(x) = \mu x(1-x) \quad x \in [0,1] \\ &y = f_\mu^n(x) = f_\mu(f_\mu(f_\mu...(x))) \end{aligned} \tag{3.1}$$

It can be seen that period doubling bifurcation occurs at $\mu = 3$ and another bifurcation takes place at approximately $\mu = 3.47$. Through a cascade of period doubling bifurcation, the map becomes chaotic at $\mu = 4$.

For a trajectory that follows a close orbit in the phase portrait and returns precisely to where it first started after one period, T, the motion is periodic and the closed orbit is called a limit cycle. The trajectory of a periodic motion, starting initially either close to or away from the origin, always converges to a limit cycle in the phase space when this periodic solution is stable. Periodic solution will locate at the same position in the corresponding Poincare map. Poincare map is a qualitative topological approach widely applied to the prediction of chaos and study of stability in the state space through exploring the geometric features of the sequence of points on

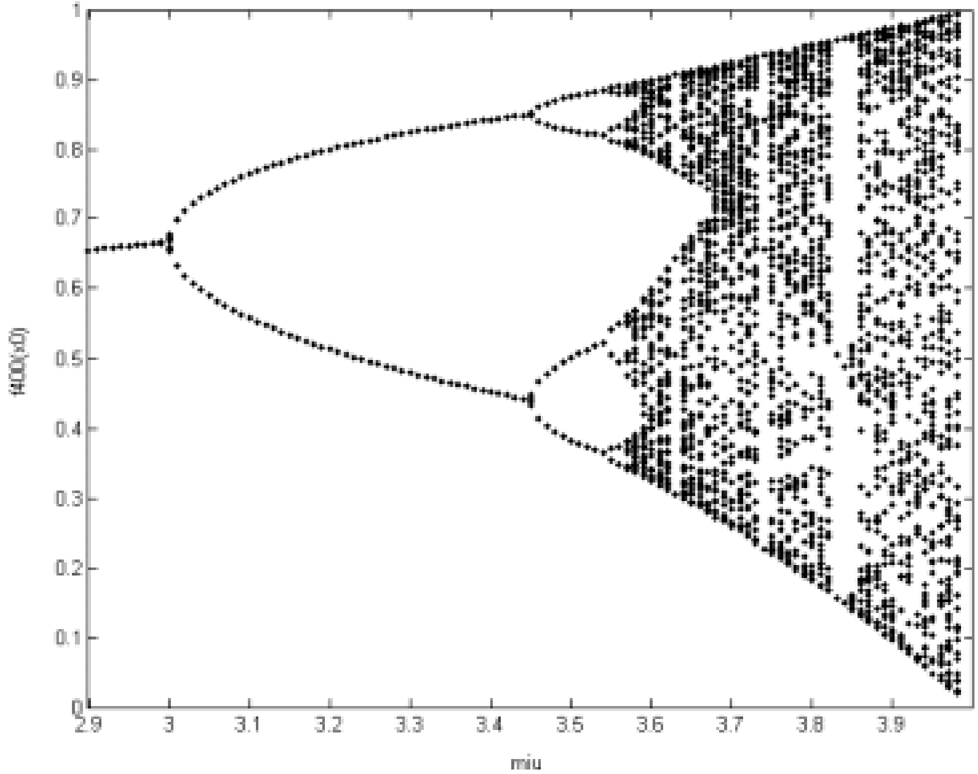

Figure 3.1 Bifurcation diagram of the quadratic map

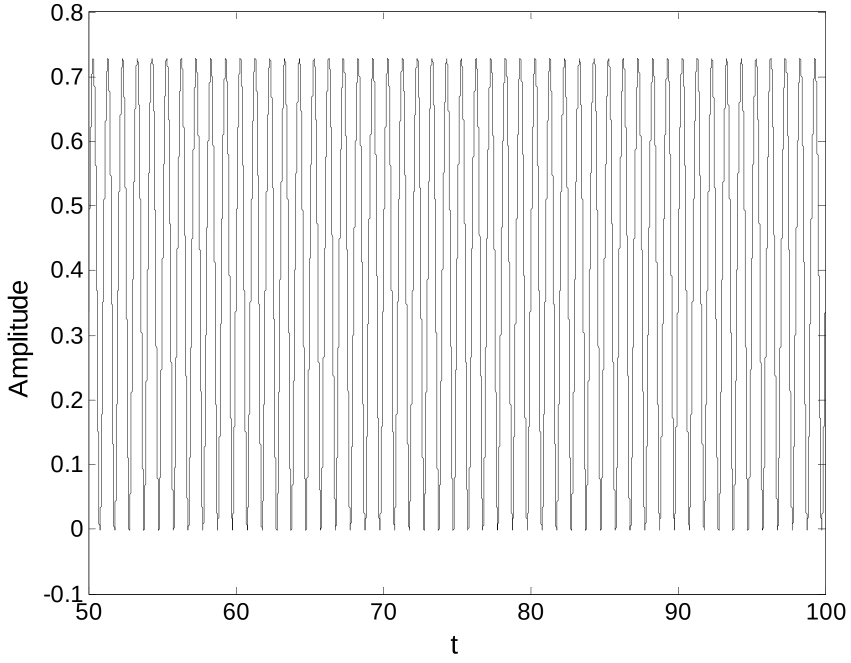

(a)

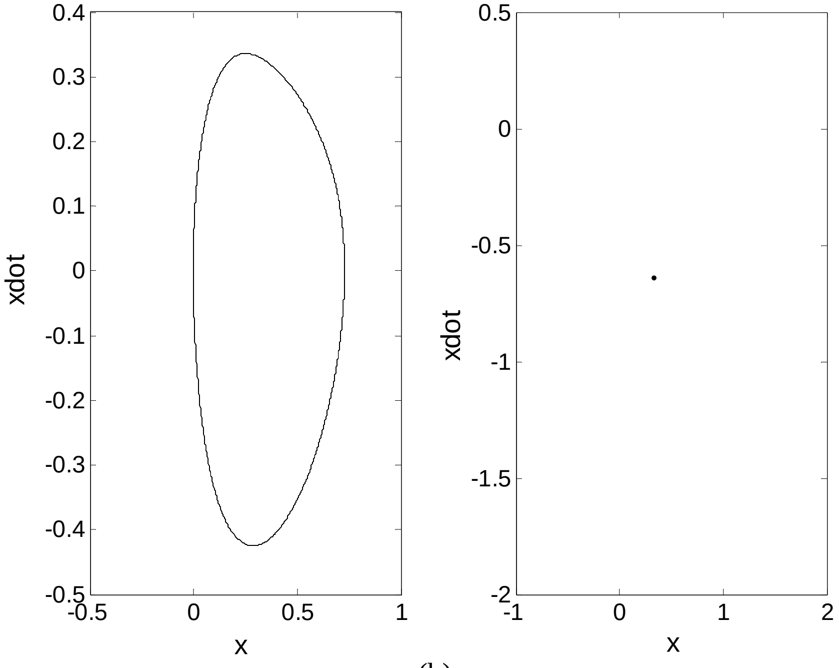

(b)

Figure 3.2 (a) Time history of a nonlinear model at driving frequency ω = 100π. (b) Corresponding phase portrait and Poincare map of the response in (a) the Poincare section. This Poincare mapping has the same general stability as the flow in the state space [78]. When a system undergoing chaotic motion, its associated Poincare map will show specific shapes and features indicating the state and extent of bifurcation. Figure3.2 shows the time history, phase portrait and Poincare Map of the response in Figure 2.1. Figure 3.2(b) shows that there is one close orbit in the phase portrait and one point in the Poincare map.

Consider the autonomous system below

$$\dot{\vec{x}} = \vec{f}(\vec{x}, \lambda) \tag{3.2}$$

Let $\vec{x}_0(t)$, function of a minimal period *T*, be the periodic solution to Eq. 3.2. Imposing a perturbation $\vec{y}$ on $\vec{x}_0(t)$

$$\vec{x}(t) = \vec{x}_0(t) + \vec{y}(t) \tag{3.3}$$

and substitute Eq. 3.3 into Eq. 3.2, the Taylor series expansion of the resulted equation about $\vec{x}_0(t)$ is thus

$$\dot{\vec{y}}(t) = D_x F(\vec{x}_0(t), \lambda)\vec{y}(t) + o(\| \vec{y}(t) \|) \tag{3.4}$$

When *n* perturbations are applied to $\vec{x}_0(t)$, the *n*-dimensional linear system represented by Eq. 3.4 has *n* linearly independent solutions, $\vec{y}_i(t)$. These *n* solutions can be expressed as a $n \times n$ matrix

$$\vec{Y}(t) = [\vec{y}_1(t), \vec{y}_2(t), ..., \vec{y}_n(t)] \tag{3.5}$$

From Eq. 3.4, the following relation is satisfied

$$\dot{\vec{Y}} = D_x F(\vec{x}_0(t), \lambda)\vec{Y} \tag{3.6}$$

Because $\vec{x}_0(t) = \vec{x}_0(t+T)$, it can be derived that

$$D_x F(\vec{x}_0(t), \lambda) = D_x F(\vec{x}_0(t+T), \lambda) \tag{3.7}$$

If $\vec{Y}(t) = [\vec{y}_1(t), \vec{y}_2(t), ..., \vec{y}_n(t)]$, then $\vec{Y}(t+T) = [\vec{y}_1(t+T), \vec{y}_2(t+T), ..., \vec{y}_n(t+T)]$. Because Eq. 3.4 has at most n linearly independent solutions, and $\vec{Y}(t)$ are such n linearly independent solutions, then $\vec{Y}(t+T)$ must be the linear combination of $\vec{y}_1(t), \vec{y}_2(t), ..., \vec{y}_n(t)$, thus meaning that

$$\vec{Y}(t+T) = \vec{Y}(t)\Phi \tag{3.8}$$

The matrix Φ is a transformation from an n-dimensional vector at $t = 0$ to another vector at $t = T$. Assuming the initial condition $\vec{Y}(0) = I$, where I is an identity matrix, and $t = 0$ in Eq. 3.8, we have

$$\vec{\phi} = \vec{Y}(T) \tag{3.9}$$

The matrix Φ is called monodromy matrix. The reason for $\vec{Y}(0) = I$ is because the differentiation of the solution at $t = 0$ with respect to the initial condition $\vec{x}_0$ is an identity matrix. Differentiate Eq. 3.2, we have

$$\frac{d}{dt}\left(\frac{\partial \vec{x}}{\partial \vec{x}_0}\right) = D_x F(\vec{x}(t), \lambda) \frac{\partial \vec{x}}{\partial \vec{x}_0} \tag{3.10}$$

And differentiate the initial condition $\vec{x}(0) = \vec{x}_0$, with respect to $\vec{x}_0$, we have

$$\frac{\partial \vec{x}(0)}{\partial \vec{x}_0} = I \tag{3.11}$$

Eq. 3.10 is an initial value problem with the initial condition Eq. 3.11 that $\frac{\partial \vec{x}(0)}{\partial \vec{x}_0} = \vec{Y}(0) = I$ and $\frac{\partial \vec{x}(T)}{\partial \vec{x}_0} = \vec{Y}(T) = \Phi$ is the monodromy matrix. Differentiating Eq. 3.2 with respect to t, we have

$$\ddot{\vec{x}} = D_x F(\vec{x}(t), \lambda)\dot{\vec{x}} \tag{3.12}$$

If $\vec{x}(t)$ is a solution of Eq. 3.2, then $\dot{\vec{x}}(t)$ is a solution of Eq. 3.12, thus also of Eq. 3.4. In addition, because

$$\vec{x}_0(t) = \vec{x}_0(t+T) \Rightarrow \dot{\vec{x}}_0(t) = \dot{\vec{x}}_0(t+T) \tag{3.13}$$

When $t = 0$, we have

$$\dot{\vec{x}}(0) = \dot{\vec{x}}_0(T) \tag{3.14}$$

Because $\dot{\vec{x}}_0(t)$ is a solution of Eq. 3.4, therefore it is a linear combination of $\vec{y}_1(t), \vec{y}_2(t), \ldots, \vec{y}_n(t)$.

$$\dot{\vec{x}}_0(t) = \vec{Y}(t)\vec{c} \tag{3.15}$$

where $\vec{c}$ is a constant vector. Evaluating Eq. 3.15 at $t = 0$ and $t = T$, we obtained

$$\dot{\vec{x}}_0(0) = \vec{Y}(0)\vec{c} \quad \text{and} \quad \dot{\vec{x}}_0(T) = \vec{Y}(T)\vec{c} \tag{3.16}$$

Because of Eq. 3.14, then

$$\vec{Y}(0)\vec{c} = \vec{Y}(T)\vec{c} \tag{3.17}$$

From $\vec{Y}(0) = I$ and also Eq. 3.9, Eq. 3.17 can be written as

$$\Phi\vec{c} = \vec{c} \tag{3.18}$$

Therefore, Eq. 3.18 shows that 1 is an eigenvalue of the monodromy matrix Φ corresponding to the eigenvector $\vec{c} = \vec{x}_0(0)$. Thus the stability of periodic solution can be determined by other eigenvalues of the monodromy matrix Φ. These eigenvalues are commonly called the Floquet multipliers. According to the Floquet theory, if all the magnitudes of these eigenvalues are less than 1, the periodic solution is stable. If one or more than one of their magnitude are greater than 1, the periodic solution is not stable and bifurcations would occur. The type of bifurcation can be determined by the way the eigenvalue(s) behaves outside of the unit circle.

A periodic motion may become unstable if the control parameters are allowed to vary, a scenario signifying dynamic deterioration of stability that could lead to eventual chaos. Period doubling, secondary Hopf bifurcation, intermittence, and crises are several possible routes to chaos. Period doubling is a commonly observed route through which a dynamic system becomes chaotic [2,4]. When the control parameter slowly varies, period doubling bifurcation will occur when one of the Floquet multipliers goes out of the unit circle from –1. This is depicted in the Poincare section as two points. In addition, this frequency-halving bifurcation would occur at smaller and smaller intervals of the control parameter and chaos would occur beyond a critical value as shown in Figure 3.1. Figure 3.3 shows the waveform, phase portrait and Poincare map of the signal given in Figure 2.5. Figure 3.3(b) shows that there are two closed orbits and there are two points in its corresponding Poincare map.

A quasi-periodic motion is a dynamic solution characterized by two or more incommensurate frequency components; that is, when the ratio of two frequencies is an irrational number. Quasi-periodic motions come from the secondary Hopf bifurcation. In terms of Floquet multipliers, the Hopf bifurcation is marked by having two complex-conjugate multiplier crossing the unit circle simultaneously. Again, if the control parameter were further varied, the motion would become chaotic. Appearance of quasi-periodic motion indicates the set-in of dynamics instability. Although the presence of many incommensurate frequencies in the motion inevitably complicates the time waveform and phase portrait of a quasi-periodic motion; however, this kind of response can be determined using Poincare maps and Fourier Transform. The corresponding phase portrait will show complex closed orbits and the Poincare map will contain one or more closed-orbit-like point group. Figure 3.4 shows the waveform, phase

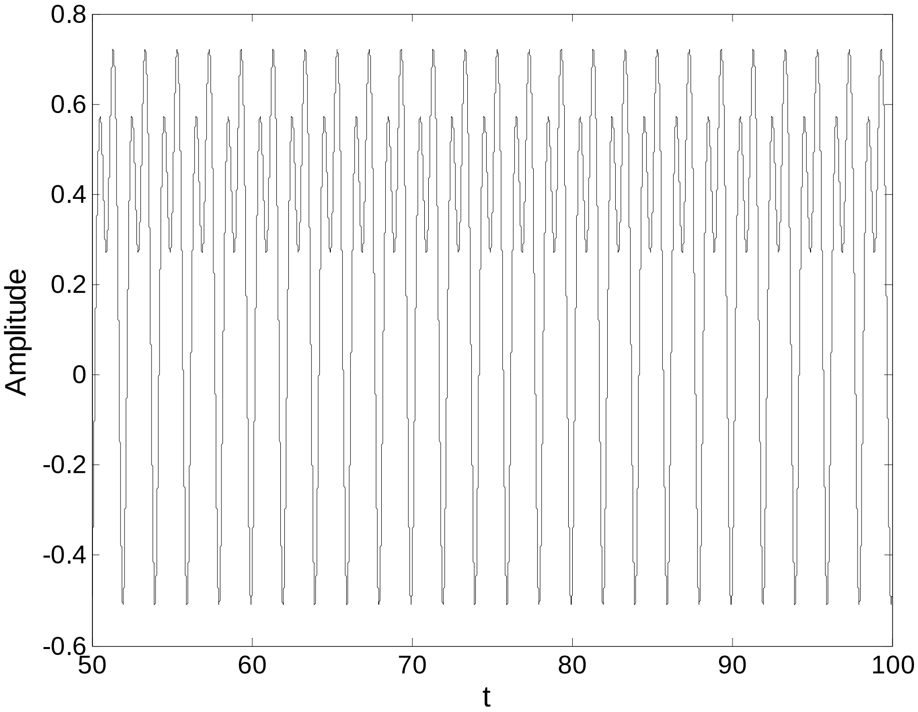

(a)

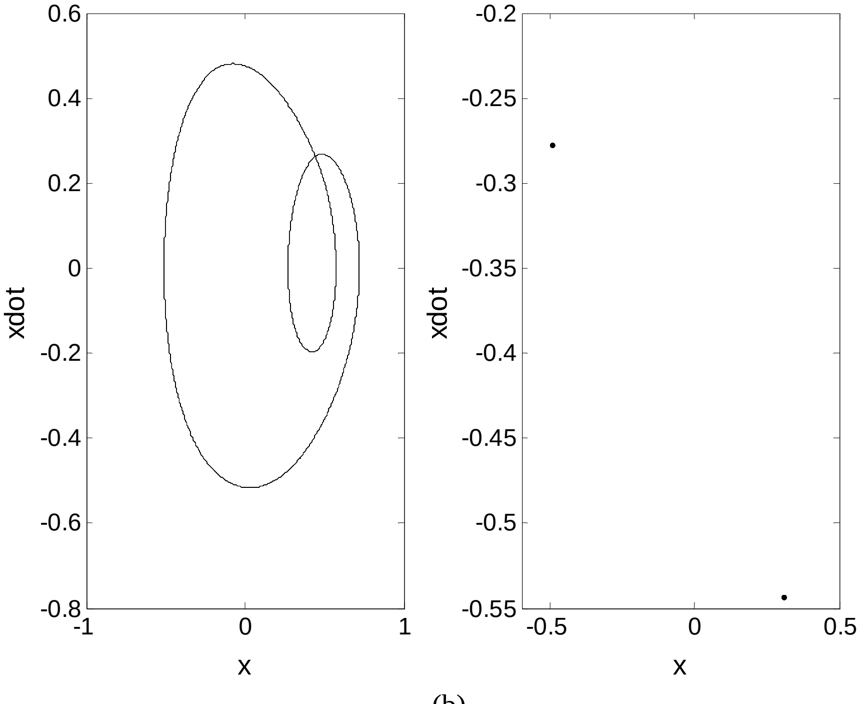

(b)

Figure 3.3 (a) Time history of a nonlinear model at driving frequency ω = 200π. (b) Corresponding phase portrait and Poincare map of the response in (a)

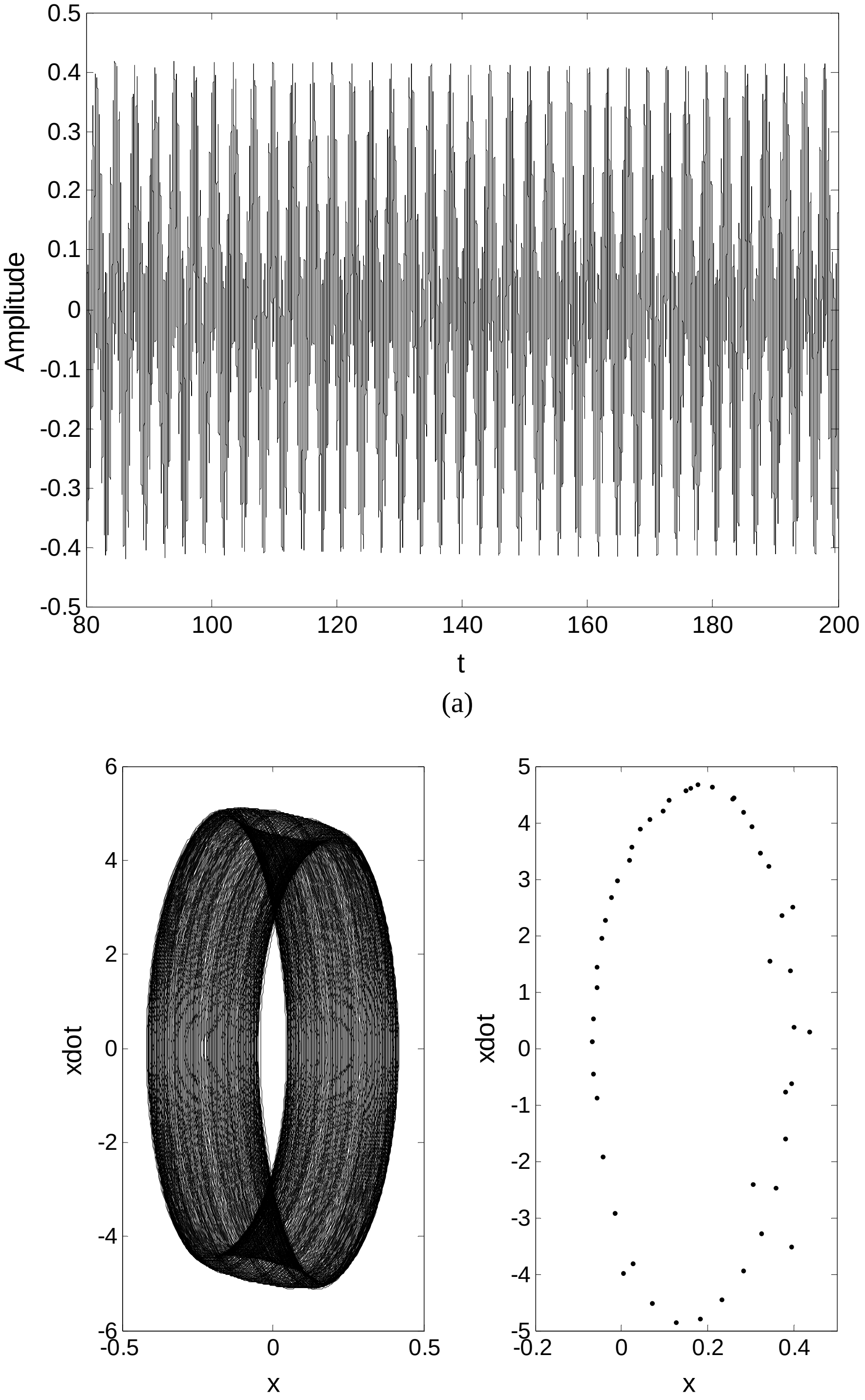

(a)

(b)

Figure 3.4 (a) Time history of a nonlinear time-delay model. (b) Corresponding phase portrait and Poincare map of the response in (a)

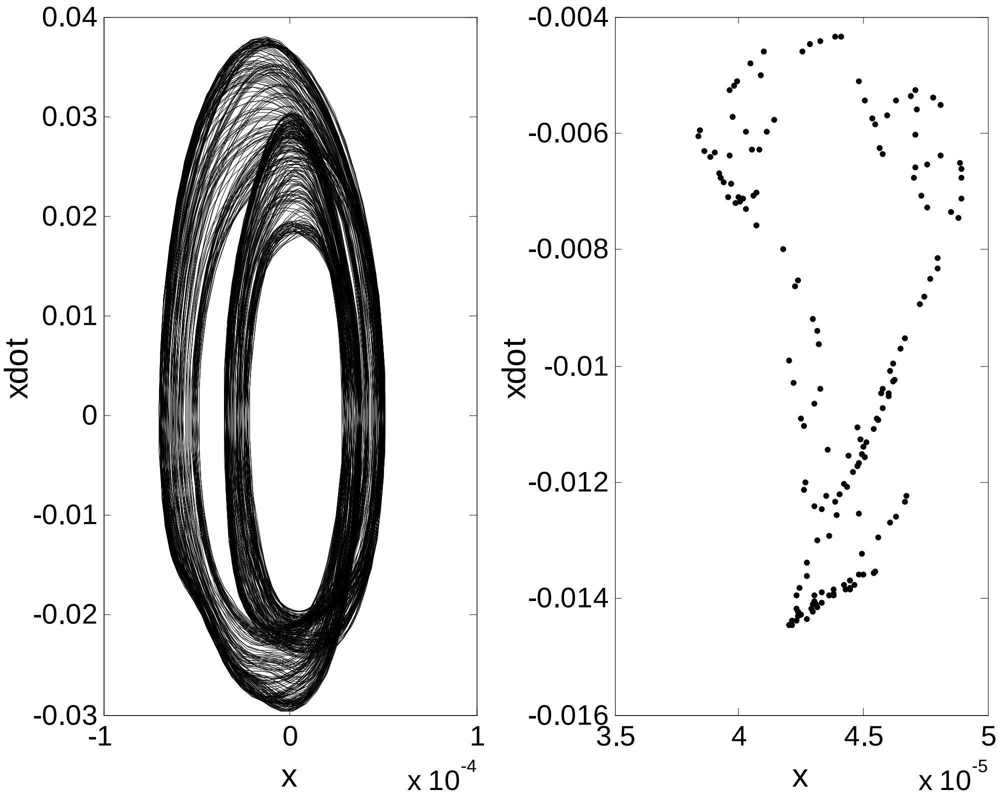

Figure 3.5 Phase portrait and Poincare map of a fractal response

portrait and Poicare map of a quasi-periodic response. This response is obtained from a time-delayed model in [80]. It can be seen in Figure 3.4(b) that the phase plot of the quasi-periodic response is heavily intertwined and its Poincare map shows a closed point sequence.

These graphical tools are powerful in providing qualitative measures and therefore not feasible for quantitatively establishing whether an erratic response is indeed chaotic or not. As a quantitative measure, the Lyapunov exponents and fractal dimensions were developed to determine if a motion is in the state of full-fledge or weak chaos. Some systems could eventually display certain fractal features in its Poincare section subjected to continual dynamic deterioration. A fractal state is the transition from a quasi-periodic motion or period doubling to a chaotic motion. A fractal or fractal set has fine details at all possible scales and the quality of self-similarity at different scales; however, there is not a universal definition for fractal. Fractal dimension is a quantitative property of a set of points in an n-dimensional space that measures the extent to which the points fill a sub-space, as the number of points becoming very large [81]. The fractal dimension of an infinite fractal set of points is generally non-integer and less than n. The phase portrait of a fractal response is characterized by many tightly linked and hard to discern closed orbits. Poincare maps are generally considered a better alternative to the phase portrait in revealing the physical essence of a fractal response. Figure 3.5 shows the phase portrait and Poincare map of a fractal response acquired from [4], in which crack-induced rotor-dynamic nonlinearities were investigated. The fractal structure is clearly seen.

Because they are both non-periodic and spectrally broadband, it is difficult to distinguish a fractal motion from a chaotic motion. Chaos is completely irregular and unpredictable, and can be thought as a bounded non-periodic behavior whose attractors are geometrical objects that possess fractal dimensions. Because of its relatively broadband spectrum characterized by spikes indicating the dominant frequencies, a chaotic response can also be considered as the superposition of a very large number of unstable motions. Chaotic systems are also characterized by their sensitivity to perturbations to the initial condition; that is, a tiny variation in the input can be quickly amplified to create overwhelmingly disproportional output. As expected, it is difficult to make out a chaotic motion from among many fractal-like using the phase portraits. However, as chaos can sometimes be readily identified with the forming of certain geometric shapes such as a horseshoe or a spoon in the Poincare space, the Poincare map is one of the alternatives for positively identifying a chaotic response. Figure 3.6 shows the phase portrait and Poincare map of a chaotic response also from [4], where a strange geometric shape appears in the Poincare map.

A powerful tool for the same objective, the Lyapunov exponents is a quantitative measure of the exponential attraction or repulsion in time of two adjacent trajectories in the state space with different initial conditions. Chaos can be distinguished from noisy behavior due to random external influences and its degree evaluated using Lyapunov exponents. A positive Lyapunov exponent would thus indicate a chaotic motion with a bounded trajectory. However, as different attractors can have the same exponents or dimensions, descriptions of chaotic response using the Lyapunov exponents or fractal dimensions are oftentimes insufficient [6]. As such, these time-domain methods, which are initial condition dependent and also require that all data be available for analysis, rely on the expertise and subjective discretion of an experienced person for sound judgment calls.

3.2 Fourier Analysis

Bifurcation is the transition of a motion from one state to another accompanied by the appearance of new modes, the disappearance of old modes, or both. Thus, different states of periodic, period-doubling, quasi-periodic, and chaotic motions can be readily identified by their respective spectrum. This is one of the reasons that Fourier-based methods are often used for the

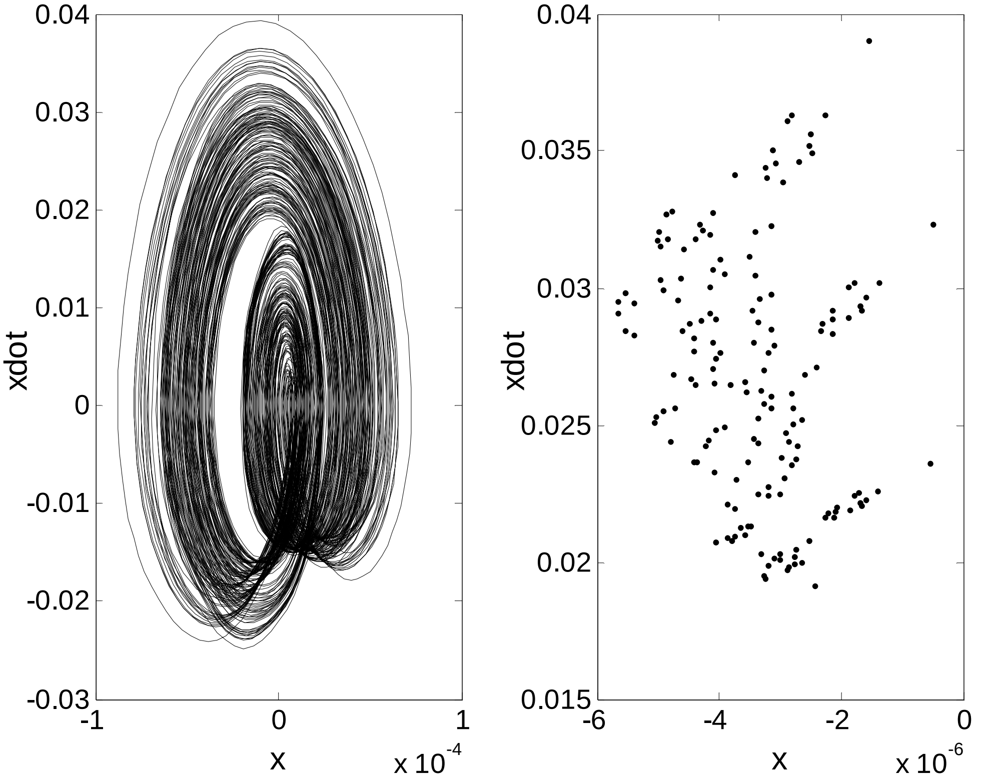

Figure 3.6 Phase portrait and Poincare map of a chaotic response

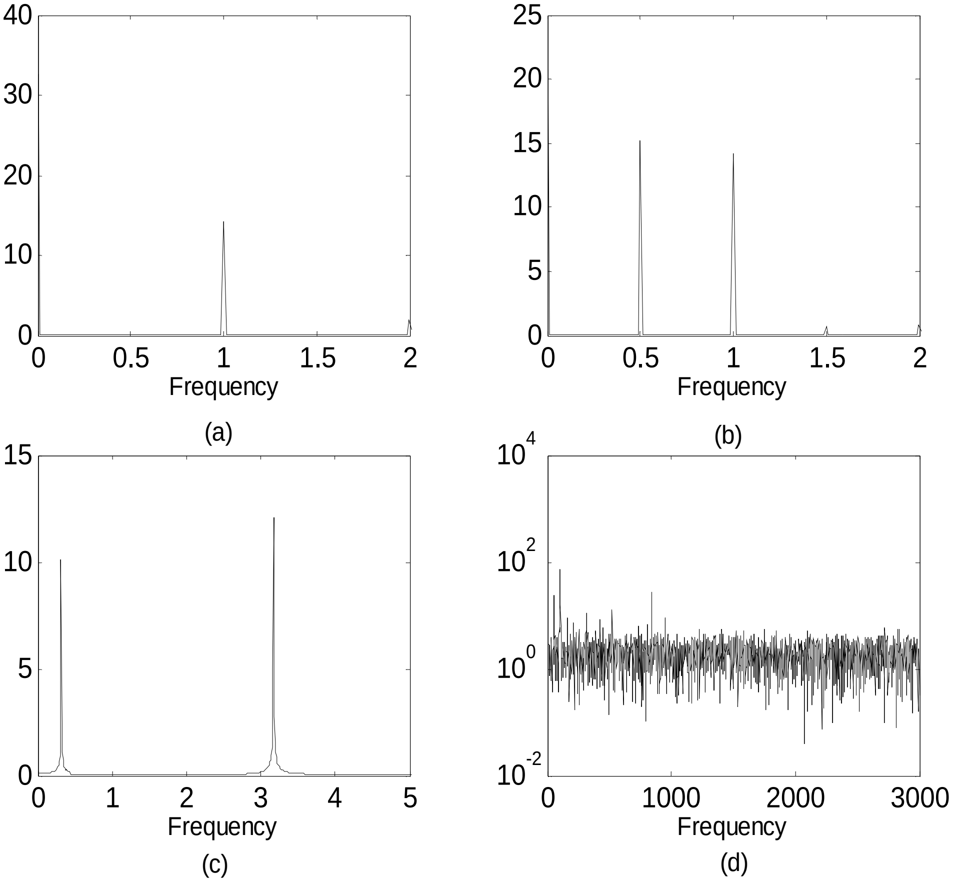

Figure 3.7 The spectrum of (a) a periodic response, (b) a 4period doubling response, (c) a quasi-periodic response, and (d) a chaotic motion

identification of bifurcations. The assumption made in the method is that a periodic or non-periodic signal can be represented as a synthesis of sine or cosine signals

$$x(t) = \frac{1}{2\pi}\int_{\Gamma} F(\omega)e^{i\omega t}\,d\omega = \sum_{j=1}^{\infty} a_j \exp(i\omega_j t) \tag{3.19}$$

where $e^{i\omega t} = \cos(\omega t) + i\sin(\omega t)$.

Since $F(\omega)$ is often complex, the absolute value $|F(\omega)|$ is used in graphical displays. When the motion is periodic or quasi-periodic, $|F(\omega)|$ shows a set of narrow spikes or lines indicating that the signal can be represented by a discrete set of harmonic functions. Near the onset of chaos, however, a continuous distribution appears, and in the fully chaotic regime, the continuous spectrum may dominate the discrete spikes. Figure 3.7 shows the spectra of the periodic motion given in Figure 3.2, the period doubling response in Figure 3.3, the quasi-periodic motion in Figure 3.4 and the chaotic motion in [53] (for a milling data at 2700 rpm spindle speed). In Figure 3.7(a), there is only one frequency component for the periodic solution. There is a frequency-halving phenomenon for period doubling bifurcation in Figure 3.7 (b). There are two incommensurate frequencies in the spectrum of the quasi-periodic motion in Figure 3.7(c). The chaotic motion has a broadband spectrum as shown in Figure 3.7 (d) in which continuous frequency distribution is seen occuring.

However, the Fourier transform in Eq. 3.19 uses a set of linear periodic harmonic functions with constant amplitude and constant frequency to represent nonlinear and non-periodic signals, which is clearly against our understanding about nonlinear nonstationary signals. For the obvious arguments that the Fourier transform is linear and that its analyzing harmonic functions are stationary, spectral domain methods are not feasible for time-varying series demonstrating nonlinearity [36]. What, then, are the fundamental attributes required of a viable approach effective for characterizing nonlinear states of motion and for identifying bifurcations as they occur and as they are in transition? Because this frequency domain method totally loses the time domain information, which is essential to the detection of the occurrence of bifurcation and state change in real time, many research efforts were dedicated to developing approach that can simultaneously detect small variations in both the time and frequency domains.

3.3 Time Frequency Analysis

A good way of detecting and identifying changes in dynamic state and bifurcations is to monitor spectral variations in time, thus implying characterizing a signal in both the time and frequency domains. The objective of time-frequency analysis is to describe how the spectral content of a signal evolves and to establish the physical and mathematical essences needed for understanding a time-varying spectrum. Among the various time frequency analysis methods applied to dynamical nonlinear analyses and fault detection [4,43-44, and 47-48] are the Short-Time Fourier Transform (STFT), wavelet analysis, Wigner-Ville Distribution (WVD), Choi-Williams Methods and Born-Jordan Distribution [82-83]. Since the cross items of bilinear methods, such as the WVD, can obscure the resolution of the time-frequency distribution, and thus the physical nature of the studied system, linear mathematical transformations including the wavelet transform have been widely adopted for the time-frequency analysis of nonlinearity [82-83]. The continuous wavelet transform of a function *f(t)* with respect to some analyzing wavelet *ψ(t)* is defined as

$$W_\psi f(a,b) = \frac{1}{\sqrt{a}} \int_{-\infty}^{\infty} f(t) \overline{\psi}\left(\frac{t-b}{a} \right) dt \tag{3.20}$$

The parameters *a* and *b* are called the dilation and translation parameters, respectively. In the equation below, the Gabor wavelet is given. It is a complex sinusoid multiplied by a windowing Gaussian function

$$\psi(t) = \frac{1}{\sqrt{\gamma}} \exp(-\frac{t^2}{2\gamma^2})(\cos t + i \sin t) \tag{3.21}$$

where γ is a positive constant. The Gabor wavelet function has been shown to offer the smallest f time-frequency window than any other wavelets [85], and therefore provides very high resolution in the joint time-frequency domain. The Gaussian part of this function provides a smooth, finite time window for the scalable sinusoidal function. It is also important to note that the Gabor wavelet function does not satisfy the continuous wavelet admissibility condition in a strict sense, but can be assumed satisfactory if γ is large [86]. If period doubling occurred in a dynamic system, a new frequency at half of the forcing frequency would appear in the time-frequency domain. If the system continues to deteriorate, more period-doublings would occur and more low-order subharmonic frequency components would appear in the time-frequency domain. Similar situations would also happen to the secondary Hopf bifurcation where a frequency component incommensurate to the forcing frequency would appear afterwards. Figure 3.8 shows the period doubling case, again, from [8], in which case the forcing frequency is 50 Hz and the 25 Hz frequency component corresponding to the period doubling bifurcation appears at 1.8 sec.

Even though time-frequency distribution does work for some simple cases, however, it cannot provide the needed resolution required for analyzing nonlinear non-stationary signals and identifying bifurcation and system dynamic states. To localize an event in time, the time window width has to be narrow, thus inevitably resulting in the dilemma of poor frequency resolution. The dilemma is inherent of all Fourier-based time-frequency distribution. Although their time windows can be adjusted, nevertheless, wavelets in general provide uniformly unsatisfactory resolution [36]. In summary, all Fourier-base time-frequency methods are of poor time resolution in low frequency. Since all time events within the time window are averaged

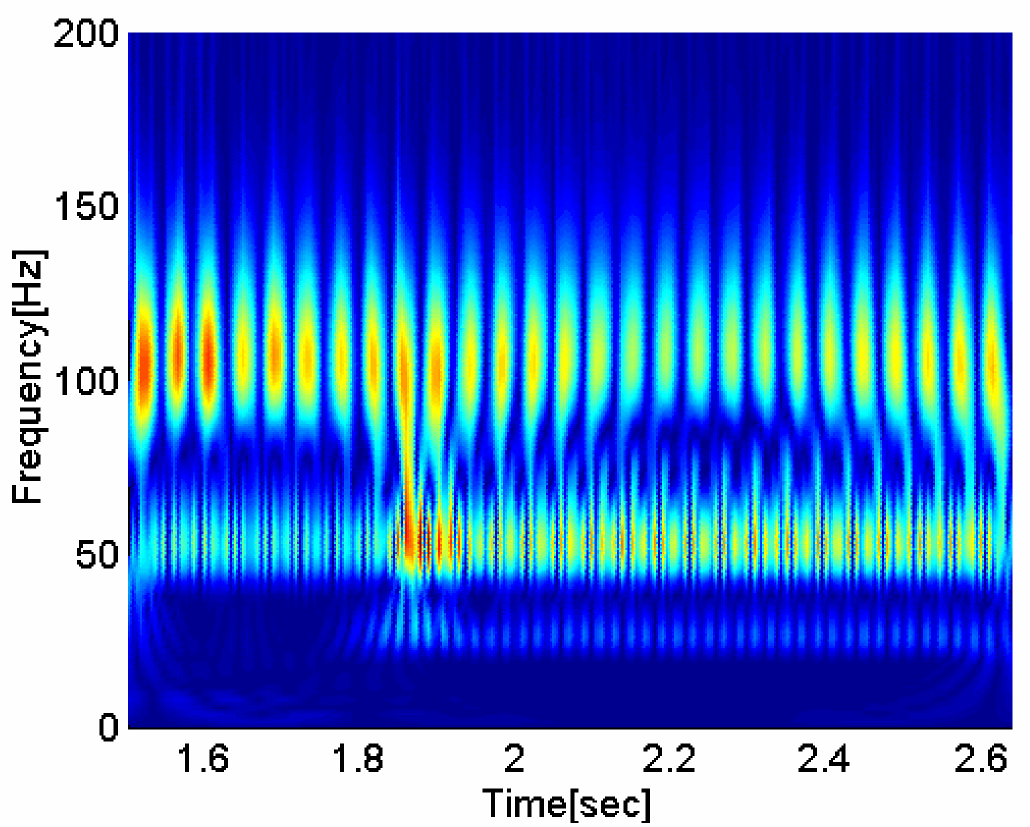

Figure 3.8 Gabor wavelet transform of a signal undergoing period doubling

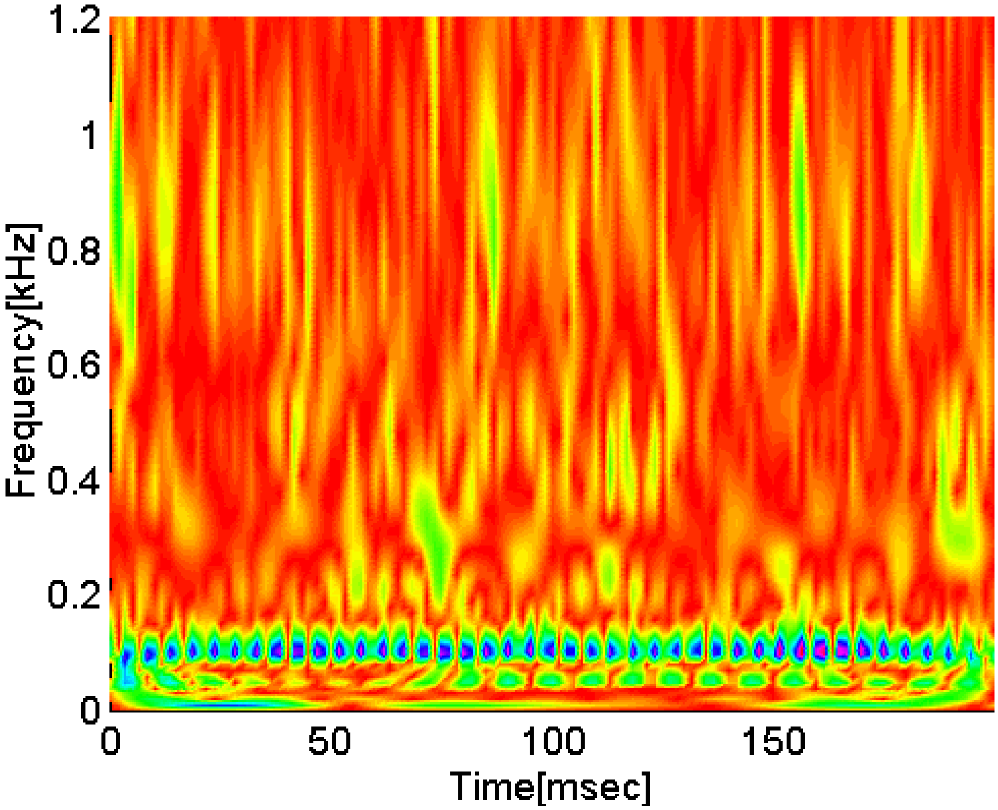

Figure 3.9 Gabor wavelet transform of a signal experiencing milling chatter

over the entire window, for example, Fourier method cannot distinguish two pulses from each other [56]. To define a local change using the wavelet analysis, since the higher the frequency the more localized the basic wavelet will have to be, one must find the result in the high frequency range. Even if a local event happens only in the low frequency range, one would still be forced to find its effects in the high frequency range, thus making the task of interpreting nonlinear non-stationary signals more difficult. In addition, as they are all Fourier-based and thus effective for analyzing linear stationary signals, the above mentioned time-frequency methods are unsuitable for nonlinear non-stationary signal analysis. Using the example in Figure 3.8, should the bifurcation occur in the frequency range higher than 150 Hz, the newborn frequency would be obscured with the forcing frequency and other frequencies, thus falsifying the detection and identification of the bifurcation. Due to its low time-frequency resolution in resolving chaotic responses of characteristically non-periodic and broadband in spectrum, and in locating the time location in which bifurcation occurs, result is at best non-conclusive for this case. Figure 3.9 shows the time-frequency distribution of a milling chatter response obtained at 2700 rpm spindle speed [53]. Since all the modes are mixed together due to the averaging effect inherent of the Fourier-based time window, only the forcing frequency is unambiguously visible. All other frequencies cannot be discerned and no bifurcation can be detected or identified.

3.4 Summary

In this chapter, commonly used nonlinear analytical methods were reviewed, along with examples illustrating their ineffectiveness and disadvantages. Phase portraits and Poincare maps are qualitative measures for the analysis of nonlinear time series and they are not viable for quantifying bifurcated or chaotic motions. Fractal dimensions and Lyapunov exponents can give the same numbers for physically different attractors. More importantly, they are incapable of detecting bifurcations or differentiating as to the types of bifurcations. Spectral methods were introduced to detect the changes in system behavior through analyzing the variations of its frequency components. Though some progresses and applications have been made, however, due to the loss of all time information, the methods have been shown to be ineffective in detecting the occurrence of bifurcation. In order to show the time-dependent spectrum, several time-frequency analysis methods have been developed to try to resolve nonlinear non-stationary signals in the time and frequency domain simultaneously. But all these methods are Fourier-based and this inherent nature imparts to them all the disadvantages of the Fourier Transform. As there are many conflicting requirements and dilemma for reaching high resolution in the time-frequency domain if they were used to analyze nonlinear non-stationary signals, these time-frequency methods are shown to be suitable for linear and stationary signal analysis only. A feasible solution to these problems is thus one that can resolve signals of nonlinearity and non-stationarity with satisfactory resolution in the time and frequency domain and void of all the identified drawbacks inherent of the Fourier analysis.

CHAPTER IV

CONCEPTS AND APPLICATIONS OF INSTANTANEOUS FREQUENCY

As discussed in the previous chapters, because the Fourier transform is mathematically linear and the spectral characteristics of a nonlinear non-stationary signal vary with time, conventional Fourier-based analyses are insufficient in resolving the temporal progression of all individual spectral components in these signals. A new approach has to be developed to resolve the predicaments identified and discussed in the last chapter. As an alternative to methods of Fourier in characteristic, the fundamental notion of instantaneous frequency is presented in the chapter whose effectiveness in resolving the dilemmas are demonstrated using non-stationary responses obtained from several nonlinear dynamic systems.

4.1 Fundamental Notions of Instantaneous Frequency

The frequency of a stationary signal is well defined following the Fourier approach. Generally, the frequency is defined as the number of oscillations per unit time of a physical field parameter such as displacement, current or voltage. But for non-stationary signals commonly encountered in communications, seismic, radar, medicine, sonar, and ultrasonic wave applications, this definition becomes ambiguous [87] and loses its effectiveness over the fact that the spectral characteristics of the signals vary with time. Concepts that are viable and complete in describing this specific time-varying nature are thus needed. This is the practical motivation behind the notion of instantaneous frequency. Because instantaneous frequency is an intuitively sound and physically useful concept for describing signals of time-dependent spectral characteristics, efforts over the years have been focused on establishing a feasible definition for instantaneous frequency that is applicable to non-stationary signals of both monocomponent and multicomponent. Gabor [88] was the first to introduce a complex analytic signal, which was later employed to define instantaneous frequency as the time derivative of the phase of a signal by Ville [89]. The definition works well for monocomponent signals. However, it fails to produce physically reasonable results for multicomponent signals. Unfortunately, this failure not only hinders the progress on developing a universally accepted definition of instantaneous frequency but oftentimes leads to doubts and questioning of the necessity and existence of instantaneous frequency [90]. The fundamental concept of instantaneous frequency will be introduced in this section, and the problems with this definition will be analyzed using a few examples in sections that follow.

A time-varying signal $x(t)$ having both Amplitude Modulation (AM) and Frequency Modulation (FM) can be expressed as

$$x(t) = a(t)\cos(\varphi(t)) \tag{4.1}$$

with $a(t)$ the instantaneous amplitude and $\varphi(t)$ the instantaneous phase. The corresponding complex form of the signal is then

$$z(t) = a(t)\exp(i\varphi(t)) \tag{4.2}$$

where $z(t)$ is simply called the analytic signal. The time derivative of $\varphi(t)$ is defined as the Instantaneous Frequency. However, there are infinite numbers of possible combinations of AM and FM for any given signal using this representation. The lack of uniqueness thus imparts no physical sense to the representation in Eq. 4.2. To circumvent the problem and be able to obtain unique complex signals, Gabor [88] proposed an approach to “suppress the amplitudes belonging to negative frequencies and multiply the amplitudes of positive frequencies by two.” Following this approach, the Gabor’s time domain complex signal, which is also an analytic signal by definition, can be determined using a slightly different definition as follows

$$\begin{aligned} z(t) &= x(t) + iy(t) = x(t) + iH[x(t)] \\ &= a(t)\exp(i\varphi(t)) \end{aligned} \tag{4.3}$$

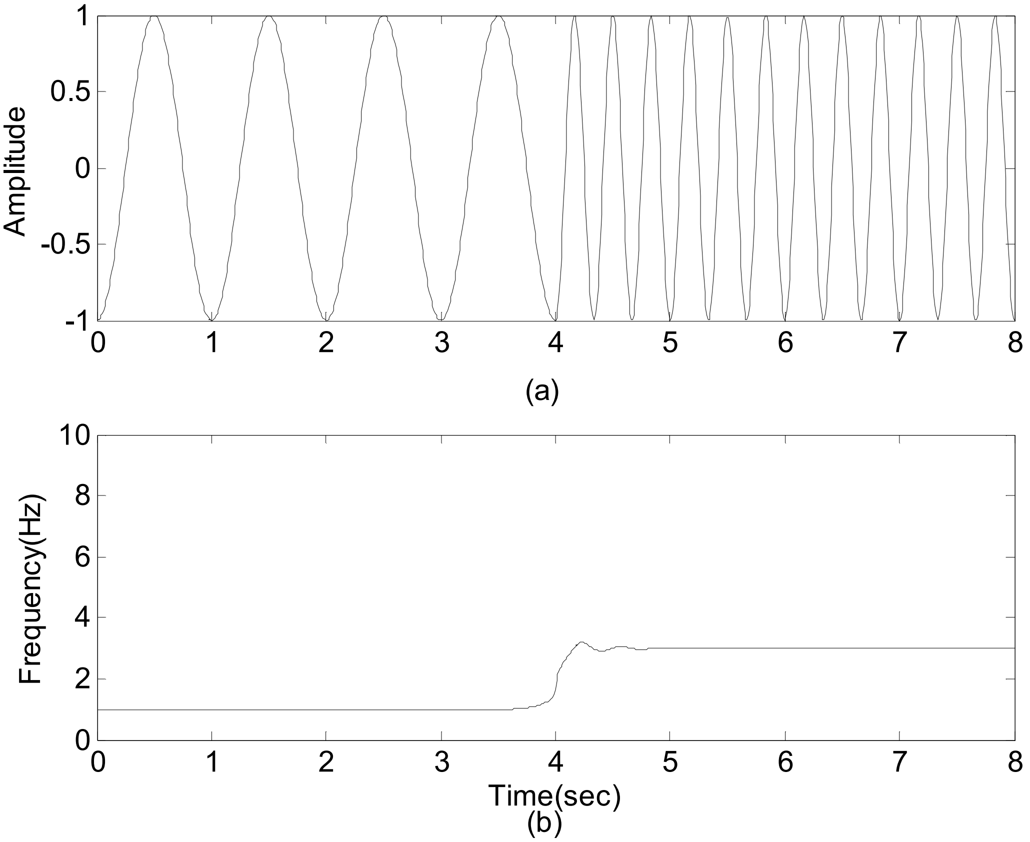

Figure 4.1 (a) Time history of a simple sinusoidal signal initially starting with 1Hz and abruptly switching to 3Hz. (b) Instantaneous frequency determined using the traditional definition

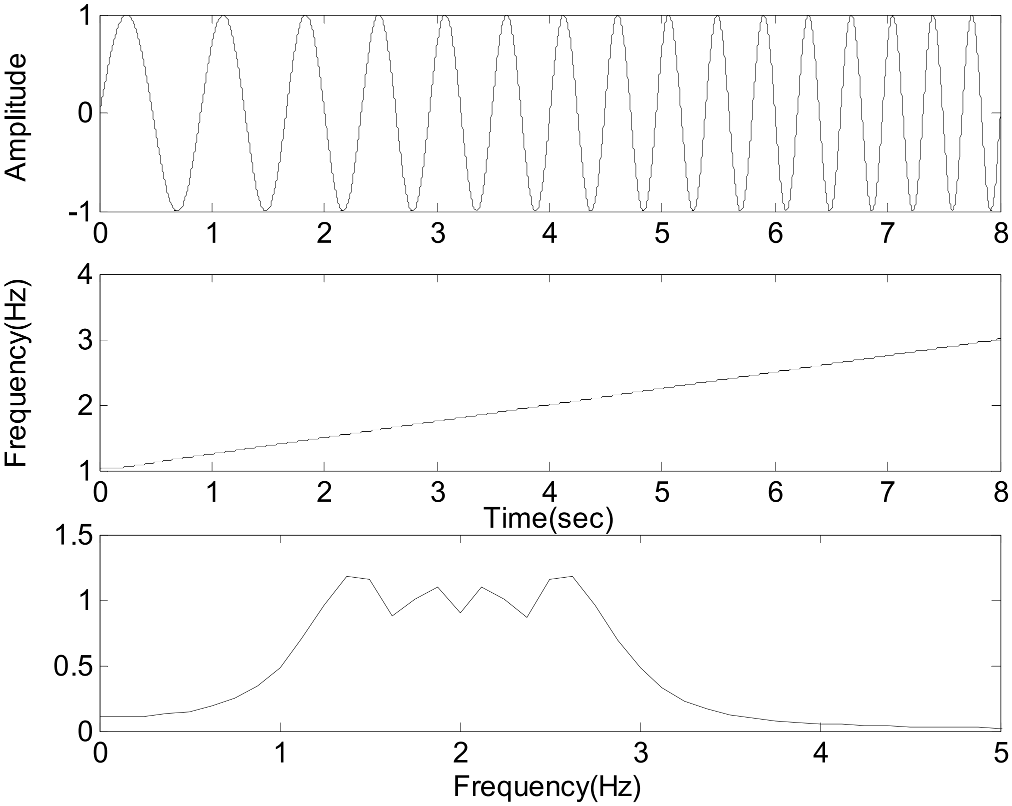

Figure 4.2 A linear chirp signal (top) and its corresponding instantaneous frequency (middle) and fast Fourier transform (bottom)

In Eq. 4.3 *z*(*t*), *a*(*t*) and $\varphi(t)$ are used in the same sense as before for convenience and $y(t)$ is the imaginary part of the analytic signal. H[*x*(*t*)] is the Hilbert Transform of the time-varying signal *x*(*t*) defined as

$$y(t) = H[x(t)] = \frac{p}{\pi}\int_{-\infty}^{\infty}\frac{x(\tau)}{t-\tau}d\tau = x(t) * ({}^{p}\!/_{\pi t}) \tag{4.4}$$

where *p* is the Cauchy principle value. In theory *x*(*t*) and *y*(*t*) are out of phase by $\pi/2$. The instantaneous amplitude and phase are thus defined uniquely as

$$a(t) = \sqrt{x^2(t) + y^2(t)} \tag{4.5}$$

$$\varphi(t) = \arctan(y(t)/x(t)) \tag{4.6}$$

Building upon Eqs. 4.5 and 4.6, Ville [89] went further and defined the time derivative of the instantaneous phase as the instantaneous frequency

$$f(t) = \frac{1}{2\pi}\frac{d\varphi(t)}{dt} = \frac{1}{2\pi}\frac{d}{dt}(\arctan(y(t)/x(t))) \tag{4.7}$$

The above definition captures the notion of instaneity in nature and fits our intuitive expectation of the instantaneous frequency concept. It is encouraging that when the definition is applied to a sinusoidal signal, the obtained instantaneous frequency is exactly the frequency of the signal. As an illustration, Figure 4.1 shows the waveform of a sinusoidal signal and its corresponding instantaneous frequency determined using Eq. 4.7. The frequency of this signal is initially 1 Hz and then it abruptly switches to 3 Hz. The instantaneous frequency depicted in Figure 4.1(b) also shows this change. Figure 4.2 shows the waveform of a linear chirp signal, along with its corresponding instantaneous frequency and Fourier transform. The instantaneous frequency is seen to change from 1 Hz to 3 Hz linearly in Figure 4.2. This linear increase in frequency is not realized in the Fourier spectrum that also erratically displaying fictitious frequency components outside the 1-3 Hz range.

There are also other reasons for supporting this definition [82, 91]. From the following definition for the frequency spread associated with the complex analytic signal, $a(t)\exp(i\varphi(t))$ [82],

$$\sigma_{\omega}^{2} = \int_{-\infty}^{\infty} (a'(t))^{2} dt + \int_{-\infty}^{\infty} (\varphi'(t) - <\omega>^{f})^{2} a^{2}(t) dt \tag{4.8}$$

where $<\cdot>^{f}$ is the average over frequency domain, it is clear that the first integral represents the frequency spread from the Amplitude Modulation and the second term is due to the deviation of $\varphi'(t)$ from the average frequency indicating explicitly that $\varphi'(t)$ is closely related to the instantaneous frequency. In addition, the average frequency defined as follows [82],

$$<\omega>^{f} = \int_{-\infty}^{\infty} \omega \,|\, X(\omega) \,|^{2}\; d\omega = \int_{-\infty}^{\infty} \varphi'(t) \,|\, x(t) \,|^{2}\; dt = <\varphi'(t)>^{t} \tag{4.9}$$

where $X(\omega)$ is the Fourier transform of $x(t)$ and $<\cdot>^{t}$ is the average over the time domain, suggests that the average frequency may be obtained by integrating the derivative of the phase with density over the time axis. It is thus considered appropriately suitable to call the derivative of the phase the instantaneous frequency.

Because of these supporting reasons, the concept of instantaneous frequency has been intimately combined with the analytic signal and Hilbert Transform. However, the definition fails to work in cases involving multicomponent signals. This inevitably presents a constant difficulty for signal analysts because in the simple case of monocomponent signals the instantaneous frequency is oftentimes not necessary or required [91]. The dilemma between the seemly theoretically sound and physically appealing definition and the impracticality of the same definition to multicomponent signals has motivated a very long line of research aiming to remove the predicament of Ville’s definition [82,91-100]. A historical review of the successive attempts performed to define instantaneous frequency was presented in [87]. The relationship between instantaneous frequency and analytic signal, group delay, and bandwidth-time product were also reviewed along with a thorough discussion on the relationship with time-frequency distribution. Cohen [82] also reviewed the development of Ville's definition and reported some doubts on the definition. Additionally, he studied the relationship of instantaneous frequency with group delay [92] and the ambiguity in the definition of instantaneous frequency and amplitude [93]. The proper use of Ville's definition, Cohen concluded, requires a choice be made between the nonnegative amplitude but an instantaneous frequency with infinite spikes and a bounded instantaneous frequency but an instantaneous amplitude with negative values. Oliveira *et al*. [91] analyzed the advantages and shortcomings of Ville's definition and determined when and why the definition fails. Two alternative definitions were given by them: instantaneous frequency as an average frequency and instantaneous frequency as a heterodyning law. Loughlin *et al.* [94] proposed four conditions that the definition of instantaneous frequency should satisfy in order for the definition to have sound physical meanings. They also presented a method using the positive time frequency distribution and time-varying coherent demodulation of the signal to find the instantaneous frequency. Also tackling along the same line, Barkat and Boashash [95-96] recently demonstrated that the accuracy for estimating instantaneous frequency could be further enhanced using time-frequency distributions of better resolution.

4.2 Misinterpretation of Instantaneous Frequency

In the following, a few example signals are considered to analyze the cause of failure of Ville's definition. Figure 4.3 presents an example two-component signal with equal amplitude

$$x(t) = a_0(\cos(\omega_1 t) + \cos(\omega_2 t)), \text{ where } a_0 \text{ is constant} \tag{4.10}$$

and Figure 4.4 gives also an example two-component signal but with unequal amplitude,

$$x(t) = a_1 \cos(\omega_1 t) + a_2 \cos(\omega_2 t), \text{ where both } a_1 \text{ and } a_0 \text{ are constant} \tag{4.11}$$

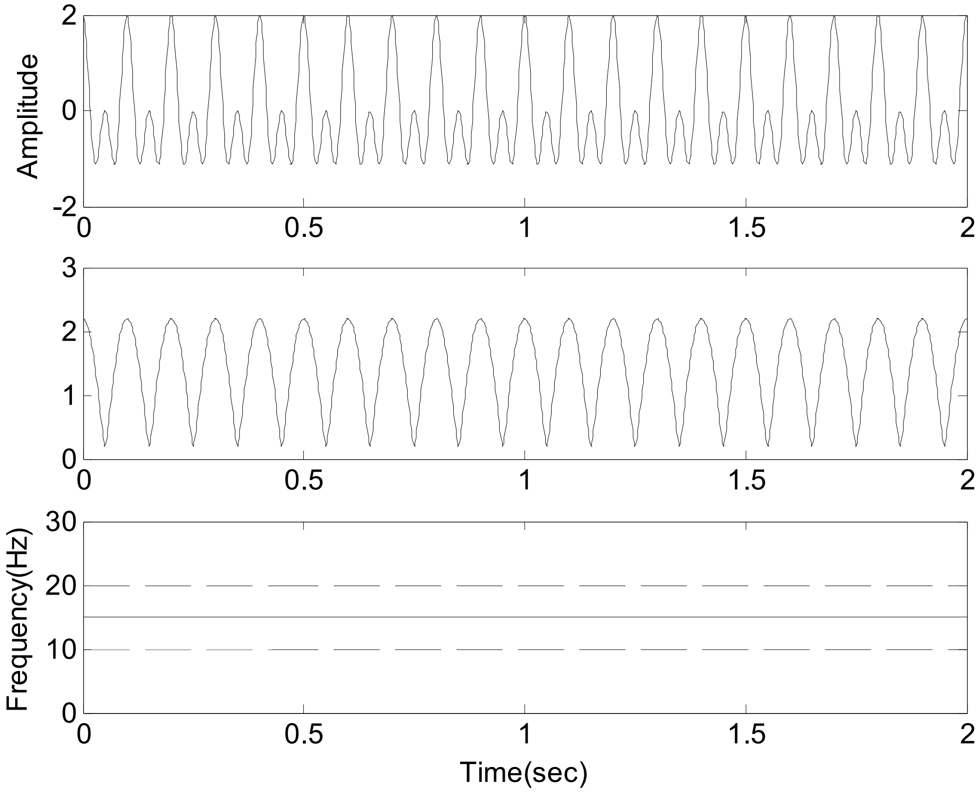

Figure 4.3 (a) A two-component signal with equal amplitude. (b) Amplitude modulation of the signal. (c) Instantaneous frequency determined using Ville's definition, where dashed lines represent the two original frequencies

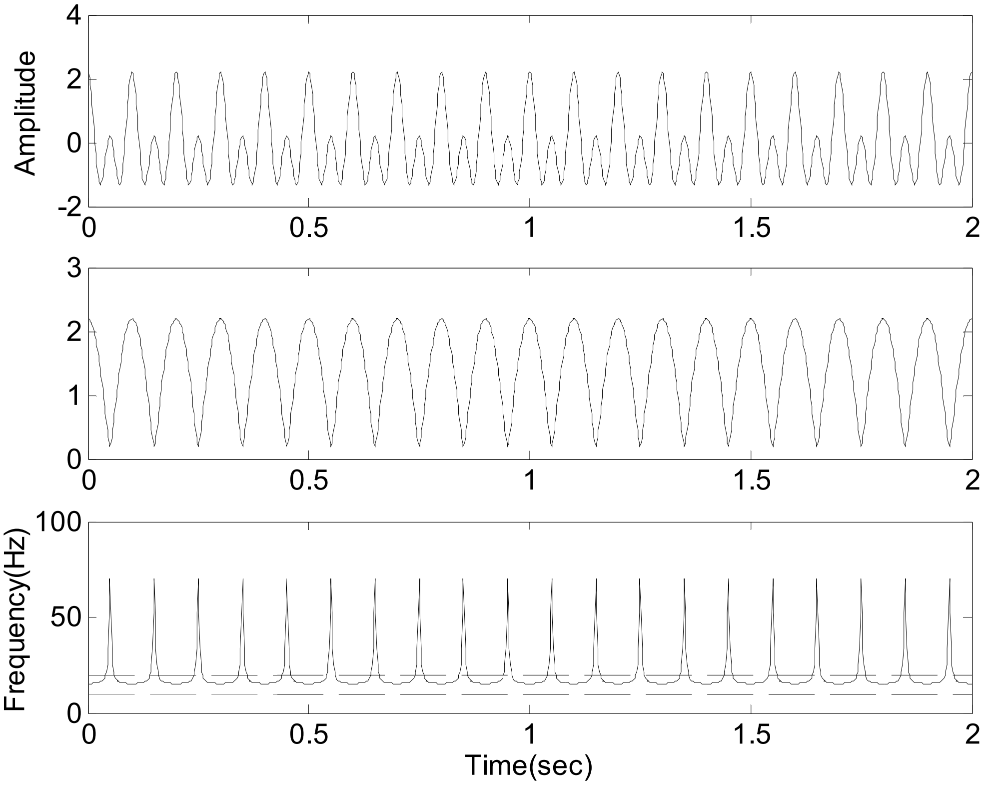

Figure 4.4 (a) A two-component signal with unequal amplitude. (b) Amplitude modulation of the signal. (c) Instantaneous frequency determined using Ville's definition, where dashed lines represent the two original frequencies

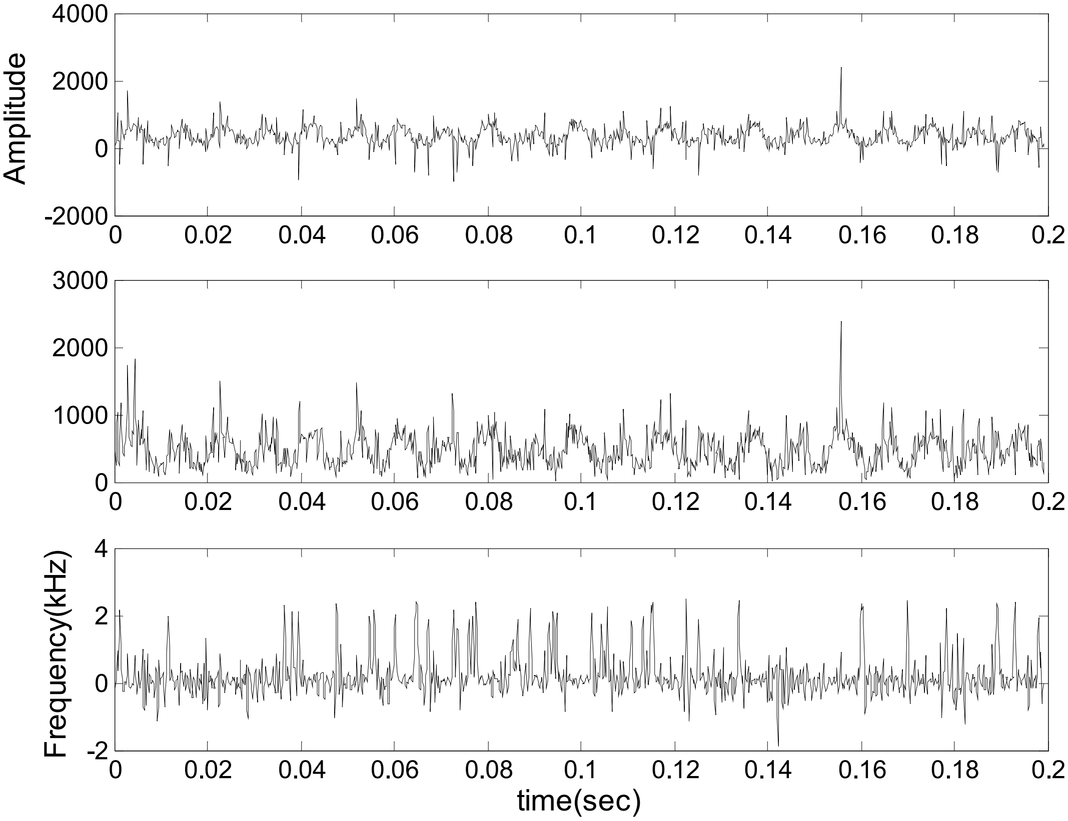

Figure 4.5 (a) A multicomponent signal (milling vibration data). (b) Amplitude modulation of the signal. (c) Instantaneous frequency determined using Ville's definition

The multicomponent signal shown in Figure 4.5 is a type of dynamic instability response that was recorded from a milling machine [53]. In all three figures, (a) plots the time history of the signal and (b) and (c), respectively, shows their associated amplitude modulation and frequency modulation using Ville's definition. In Figure 4.3(c) and Figure 4.4(c), the dashed lines are the frequencies of the two components (ω_1 and ω_2) and the solid lines are the obtained instantaneous frequencies using Ville's definition.

Figure 4.4 is a typical example for illustrating the various questions raised regarding the ambiguity of the definition of instantaneous frequency. Some of them are:

- The signal $x(t)$ consists of two constant amplitude and frequency signals. It is thus a stationary signal. However, its amplitude modulation and frequency modulation (instantaneous frequency) both demonstrate time-varying characteristics.
- There are only two frequencies, ω_1 and ω_2, in the signal but the obtained instantaneous frequency is severely obscured by becoming negative at times.
- Notwithstanding, why is there only one instantaneous frequency while the two frequencies ω_1 and ω_2 are physically present at all time?

Other questions raised regarding4 this definition can also be found in [82]. A meticulous examination of the amplitude and frequency modulations in Figure 4.5 concludes that the instantaneous frequency as is interpreted by Ville's does not in any way conform to the underlying characteristics of the milling process as we understand it so well. In other words, although instantaneous frequency is a well-founded physical concept, the instantaneous frequency in Figure 4.4(c) makes no physical sense. Is the case with the traditional definition of instantaneous frequency yet another example demonstrating that mathematical elegance does not always ensure or deliver sound physical interpretation?

The questions on what properties must the instantaneous frequency have and if these properties reveal the nature of the signal under investigation were widely reported [82,87,91,94]. Four physical conditions were proposed for calculating the AM and FM of a signal in [94]:

i) If the signal, $x(t)$, is bounded in magnitude, then the magnitude of its amplitude modulation, $A(t)$, should also be bounded; that is, $|x(t)| < \infty \quad implies \quad |A(t)| < \infty$.

ii) The instantaneous frequency, $f(t)$, should be limited to the range of frequencies occupied by the signal; that is, $|X(\omega)|^2 = 0, \omega \notin (\omega_{\min} < \omega < \omega_{\max}) \Rightarrow \omega_{\min} < f(t) < \omega_{\max}$.

iii) For a pure sinusoidal signal $x(t) = A_0 \cos(\omega_0 t + \phi_0)$, it is always true that $|A(t)| = |A_0| \quad and \quad f(t) = \omega_0$.

iv) If the signal is scaled in amplitude by a constant *c*, then the value of the instantaneous frequency should not be changed; that is, if *x(t)* implies *A(t)* and *f(t)*, then *cx(t)* implies *cA(t)* and *f(t)*.

Furthermore, for a multicomponent signal having individual constant amplitude and time independent spectral contents, the instantaneous frequency should also be time independent; that is,

$$x(t) = \sum_{i=1}^{N} a_i e^{j(\omega_i t + \phi_i)} \quad implies \quad \frac{d}{dt} f(t) = 0 \; .$$

The above condition was added at a later date by Oliverira and Barroso as the condition v [91].

The signal in Figure 4.3 is also stationary. Its amplitude modulation is non-stationary, but its instantaneous frequency is both the average of the two frequencies and stationary, a case which made many researchers embrace Ville's definition with acceptance. The average frequency at any one moment was even considered by some as one type of definition for instantaneous frequency [91,94]. However, this perspective is not satisfactory. To demonstrate, consider a non-stationary signal defined below.

$$x(t) = a_0(\cos(\omega_0 t + bt^2) + \cos(\omega_0 t - bt^2)),\ \text{where } a_0 \text{ and } b \text{ are constant} \tag{4.12}$$

The signal is time dependent, but using Ville's definition the instantaneous frequency is determined to be ω_0. That is, the non-stationary signal was interpreted as having single stationary instantaneous frequency. Thus the frequency cannot tell us anything about the temporal evolution of all the frequencies in the signal. Therefore, it is unacceptable that the average frequency is defined as the instantaneous frequency even if the average frequency satisfies all the formerly listed five physical conditions. These five conditions are insufficient for completely defining instantaneous frequency.

It is obvious that the concept of instantaneous frequency defined following Ville's definition is in the average sense. Eqs. 4.8 and 4.9 are infinite integrals evaluated along time and thus are each an average in the infinite integral sense. The following definition using the time-frequency distribution also determines the average frequency at every time instances, instead of the true instantaneous frequency,

$$f(t) = \frac{\int_{-\infty}^{\infty} f\rho(t,f)df}{\int_{-\infty}^{\infty} \rho(t,f)df} \tag{4.13}$$

where $\rho(t,f)$ is the Fourier Transform of the time dependent autocorrelation function defined in [101]. There should be exactly two instantaneous frequencies, ω_1 and ω_2, in Figure 4.4 at each and every time moment. The averaging effect inherent of the definition not only averages the two frequencies in the stationary signal but also erroneously and erratically interprets the signal as non-stationary with negative instantaneous frequencies! It is beyond any argument that average frequency and instantaneous frequency are two different concepts. There can be only one average frequency at any one time, but instantaneous frequency can be many. Ville's definition would work well for monocomponent signals and would understandably fall short on resolving multicomponent signals because it would make no discretion and henceforth interpret the average (in the infinite integral sense) of all presenting frequencies as the instantaneous frequency. Oliveira and Barroso [91] argued that "… the difficulties encountered in the previous example [i.e., Figure 4.4] are not intrinsic problems of traditional definition of Instantaneous Frequency, but instead a mere consequence of misuse of the concept." Since the studied signal has two components, and there is no point in asking what the instantaneous frequency of a multicomponent signal is. The rationale is that a multicomponent signal does not have one instantaneous frequency; by construction, it has several, at each moment. Furthermore, they considered that separating a signal into a set of different components remains an arbitrary human activity and, as such, the number of "components" can never be the key to the physical acceptability of the definition. These arguments are insightful but unfortunately misleading. The key to eliminate the various difficulties and ambiguities experienced in the previous examples ought to be finding a viable decomposition scheme. Seeking to develop or formulate another definition for instantaneous frequency from the notion of average frequency would be missing the point. Boashash [87] also concluded the same that Ville's definition has physical meaning only for monocomponent signals, where there is only one frequency or a narrow range of frequencies varying as a function of time. For multicomponent signals, the notion of a single-valued instantaneous frequency becomes meaningless, and a breakdown into its components is needed. Thus a decomposition method effective for decomposing a multicomponent signal into its associated monocomponent subsets and not obscuring or obliterating the physical essentials of the signal would allow the traditional definition of instantaneous frequency to be complete and applicable to signals of both mono- and multi-component.

According to [36], it is indicated that the traditional definition of instantaneous frequency is not applicable to data that are not symmetric. Multicomponent signals are necessarily not symmetric but, by definition and also by requirement, a monocomponent subset is symmetric in time. Recall that the analytic signal in Eq. 4.3, which has the form $a(t)\exp(i\varphi(t))$, indicates that the physical meaning of the signal is implicitly carried by $a(t)$ and $\varphi(t)$, the amplitude and frequency modulation, respectively. If the spectra of $a(t)$ and $\varphi(t)$ are not separated in frequency, it can be shown that the Hilbert transform of the signal will be phase-distorted [87]. A multicomponent signal is generally broadband and more often than not the spectra of $a(t)$ and $\varphi(t)$ would overlap. This is one of the reasons why the traditional definition of instantaneous frequency does not work for multicomponent signals. Because the Hilbert Transform based analytical formulation provides better approximation to signals of relatively narrow bandwidth, the more closely a signal approaches the narrowband condition, the better in general the traditional definition would be in estimating the instantaneous frequency [87]. Therefore, in order to find the true frequency progression within a multicomponent signal, it is necessary to break down the many, coupled components of the signal into its individual intrinsic components.

Thus, the instantaneous frequency for a multicomponent signal is defined as a global characteristic collectively described by the instantaneous frequencies associated with all the individual components in the signal, and the instantaneous frequency of each component can be uniquely determined using the traditional definition. The number of instantaneous frequency is the same as the number of monocomponents in the signal. As an illustration, the signal $x(t) = \cos(\omega_1 t)\cos(\omega_2 t)$, where $\omega_2 > \omega_1$, can be decomposed into two distinct parts: $\frac{1}{2}\cos(\frac{\omega_1 + \omega_2}{2})$ and $\frac{1}{2}\cos(\frac{\omega_1 - \omega_2}{2})$. Applying Ville's definition to the individually decomposed parts and the two instantaneous frequencies, $\frac{\omega_1 + \omega_2}{2}$ and $\frac{\omega_2 - \omega_1}{2}$, within this signal would be readily resolved.

Contingent upon the availability of an effective decomposition scheme, Ville's definition would be a powerful tool allowing the temporal development of all frequency components to be represented by the corresponding instantaneous frequency at any time instance and thus enabling signals of monocomponent and multicomponent alike to be fully characterized. In the next section an effective decomposition method will be introduced and the feasibility of the scheme in decoupling a signal into its monocomponent subsets will be demonstrated using two of the examples previously considered in Figures 4.3(a) and 4.4(a).

4.3 Decomposition of Multi-Mode Structure

As stated, the traditional definition of instantaneous frequency is meaningful only for monocomponent signals. In order to study the time-dependent characteristics of a multicomponent signal, the signal has to be decomposed into its monocomponent subsets, so that the instantaneous frequency of all the intrinsic components can be subsequently determined following the traditional definition. To answer the questions as to how to extract these components and simultaneously avoid turning the decomposition process into a mere “arbitrary” human activity, it is imperative that one provides sound answers to the following: How are the intrinsic components of a multicomponent signal defined and why do they individually have physical meanings?

It is appropriate to first examine what properties a physically meaningful component should have. From the perspective of amplitude and frequency modulation, a monocomponent signal should have one and only one instantaneous frequency at any time and that its amplitude modulation and frequency modulations are completely separated meaning that their individual spectra are not overlapped. However, from the spectrum alone a signal cannot be discerned as one of monocomponent or multicomponent. As such, for all components, the associated analytic signal defined using the Hilbert transform is therefore needed. To ensure a good estimation of the instantaneous frequency using the Hilbert Transform approach, the frequency modulation must be demodulated from the amplitude modulation. In other words, the spectra of $a(t)$ and $\varphi(t)$ of the resulted analytic signal $a(t)\exp(i\varphi(t))$ would need to be well separated. The relationship between the amplitude modulation and the frequency modulation is dependent upon the covariance defined as follows [82],

$$Cov_{t\omega} = < t\varphi'(t) > - < t >< \omega > \tag{4.14}$$

where

$$< t\varphi'(t) >= \int t\varphi'(t) \, | \, s(t) \, |^2 dt \, , \; < t >= \int t \, | \, s(t) \, |^2 \; dt \, , < \omega >= \int \omega \, | \, S(\omega) \, |^2 \; d\omega$$

and $< t\varphi'(t) >$ is the average (again, in the infinite integral sense) of the product of time with instantaneous frequency. Since $< t\varphi'(t) >$ equals to $< t >< \varphi'(t) >=< t >< \omega >$, if time and frequency are not mutually dependent then the covariance $Cov_{t\omega} = 0$. For a symmetric signal, the covariance between the amplitude and frequency modulation is zero [82] implying that the amplitude and frequency modulations are completely demodulated. Hence symmetry seems desirable for the intrinsic component of a multicomponent signal.

An intrinsic component can be expressed as an analytic signal as $z_j(t) = a_j(t)\exp(i\varphi_j(t))$, where the subscript j denotes the individual components so that $z(t) = \sum_{j=1}^{n} z_j(t)$. It should have only one frequency at any time instance and both of its frequency and amplitude may change with time. Consider the following four possible physical scenarios for the component:

1) without amplitude and frequency modulation, the analytic component signal is a sinusoidal signal

$$z_j(t) = a_j \exp(i\omega_j t), \quad \text{where} \quad a_j \text{ and } \omega_j \text{ are constant.} \tag{4.15}$$

2) without amplitude modulation but with frequency modulation, the analytic component is

$$z_j(t) = a_j \exp(i\varphi_j(t)), \quad \text{where} \quad a_j \text{ is constant.} \tag{4.16}$$

3) with amplitude modulation but without frequency modulation, the analytic component is

$$z_j(t) = a_j(t) \exp(i\omega_j t), \quad \text{where} \quad \omega_j \text{ is constant.} \tag{4.17}$$

4) with amplitude and frequency modulation, the analytic component signal can be written as

$$z_j(t) = a_j(t) \exp(i\varphi_j(t)) \tag{4.18}$$

For the simple cases 1) and 2), by definition, the real part of the analytic signal has to be symmetric in time. As long as the spectrum of $a_j(t)$ is well separated from (or much lower than) ω_j, the same can be concluded for case 3) that the real part of the analytic signal is symmetric. Following the same token, it is reasonable to say that, if the spectrum of $a_j(t)$ is well separated from (much lower than) the spectrum of $\varphi_j(t)$, the real part of the analytic signal in the complicated case 4) is also symmetric. It should be noted that by definition if the real part of the analytic signal is symmetric, then its corresponding imaginary part is also symmetric in time. Because the time frequency covariance of a symmetric signal is zero, well separation of the spectra of $a_j(t)$ and $\varphi_j(t)$ can always be maintained. In summary, satisfying the symmetric condition is thus a natural and meaningful requirement for the construction of the intrinsic components of a multicomponent signal.

Huang *et al.* [36] presented a decomposition scheme capable of breaking a multicomponent signal down into its intrinsic components. The method, referred to as the Empirical Mode Decomposition (EMD), was developed from the simple assumption that any signal consists of many simple intrinsic modes of oscillation. Each mode has the same numbers of extrema and zero-crossings, and the inherent oscillation is symmetric with respect to a local mean. The local mean is defined by the maximum envelope and minimum envelope without resorting to time scales. Given this local mean, modes of different time scales can be separated. Once separated, each mode is independent of one another and all modes would have no multiple extrema between successive zero-crossings. As such, each separated mode can be designated as an Intrinsic Mode Function (IMF) by the following conditions: (a) the number of extrema and the number of zero-crossings must be either equal or different at most by one in the entire data set, and (b) the mean value of the envelope defined by the local maxima and the envelope defined by local minima is zero at every point. The two conditions fit perfectly our understanding of what are required of an intrinsic component.

An IMF represents a simple oscillatory mode. Given the two conditions required of an IMF, the first IMF can be extracted using the following steps:

Step 1. Identify and then connect all the local maxima of the signal $x(t)$ using a smooth function to obtain the maximum envelope function $max(t)$. Identify and connect all the local minima of $x(t)$ using a smooth function to obtain the minimum envelope function $min(t)$. Finally, set $mean1(t)=(max(t)+min(t))/2$.

Step 2. Subtract $mean1(t)$ from the original signal, $x(t)$, so that $s1(t)= x(t) - mean1(t)$.

Step 3. Repeat Step 1 and 2 on $s1(t)$ to obtain $mean2(t)$ and $s2(t)$ and afterwards, on $s2(t)$ to obtain $mean3(t)$ and $s3(t)$. Keep recursively repeating Step 1 and 2 until $sn(t)$ is obtained that satisfies the two conditions of an IMF. Denote $C1(t)=sn(t)$ and the difference between the original signal $x(t)$ and the first IMF as $d1(t)= x(t)- C1(t)$. This sifting process is shown in Figure 4.6 using an example signal.

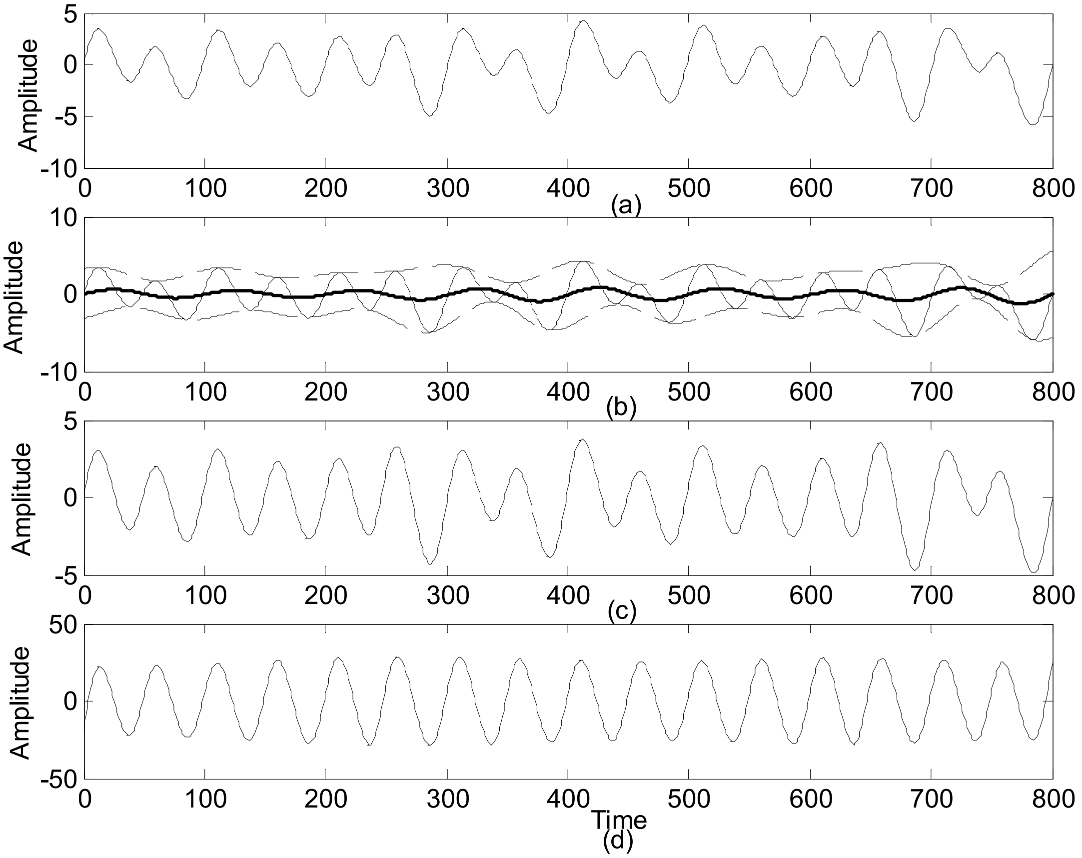

Figure 4.6 (a) A time domain signal. (b) Original signal (———) with its maximum envelope and minimum envelope (- · - · - · -) and its local mean (━━━). (c) *s1(t)*: result after one sifting process. (d) The first Intrinsic Mode Function obtained

Repeat the above procedures to get *C2(t)* and *d2(t)*, *C3(t)* and *d3(t)*,…, and *Cn(t)* and *dn(t)*, until *dn(t)* has less than two extrema or no IMF can be extracted from it. Denote *R(t)=dn(t)*, which is called the residue. Thus the collection of all the IMFs *C1(t)*, *C2(t)*,…, and *Cn(t)* and the residue *R(t)* restores back the original signal $x(t)$:

$$x(t) = \sum_{j=1}^{n} Ci(t) + R(t) \tag{4.19}$$

The sifting process has two objectives: removing riding waves and making the signal profile more symmetric [36]. It can be seen from the following analysis that the first mode has the smallest time scale indicating that it includes the highest frequency components. As the decomposition goes on, the frequency components included in the IMF become lower. The residue should include almost no frequency components at all. Simply put, the decomposition is based on the local characteristic time scale of the data to produce an adaptive basis and it thus does not resort to a set of fixed time scales. Understandably the EMD is highly feasible for the analysis of nonlinear and non-stationary signals.

When all the intrinsic components are available, the corresponding monocomponent analytic signals can be constructed using the Hilbert Transform and the obtained analytic signals can then be used to determine the signal's instantaneous frequencies and amplitude modulations using Eqs. (4.5) and (4.7). The original signal, $x(t)$, can now be expressed as

$$x(t) = \sum_{j=1}^{n} a_j(t) \exp(i \int \omega_j(t) dt) \tag{4.20}$$

Alternatively, the signal can also be expressed using its Fourier representation as

$$x(t) = \sum_{j=1}^{\infty} a_j \exp(i \omega_j t) \tag{4.21}$$

The Hilbert Transform in Eq. 4.4 can be appropriately interpreted as the convolution of $x(t)$ with $1/t$, thus clearly emphasizing the property of temporal locality of $x(t)$. The polar coordinate representation in Eq. 4.18 further clarifies the local nature of the expression. It can be readily seen from Eqs. 4.20 and 4.21 that the Hilbert transform expression reveals the nature of an amplitude-varying and phase-varying trigonometric function of $x(t)$, while the Fourier transform expression does not show the property of amplitude variation.

It is evident from Eq. 4.19 that the decomposition is mathematically complete. However, since the local mean acquired using the maximal and minimal envelopes is not exactly a mathematical mean, the IMF's obtained sequentially through the repetitive shifting process listed above are therefore not mutually orthogonal in the strict mathematical sense. Nevertheless, the two conditions of IMF, namely, symmetric in time and having no multiple extrema between zero-crossings, ensure that IMF's can be made almost orthogonal if certain conditions are met. It can be shown that the inner products of $c_i(t)$ with $c_j(t)$, and of $c_i(t)$ with $x(t) - c_j(t)$, where $i \neq j$, are almost zero. Therefore, although the local mean is not a true mean, the decomposition is both complete and orthogonal. In addition, Eq. 4.19 shows that a multicomponent signal can be represented by its individual amplitude-varying and frequency-varying monocomponent whose amplitude modulation and frequency modulation are completely separated. The equation also makes it possible to represent the instantaneous frequency along with the corresponding amplitude as a function of time in a 3D-plot. For example, the amplitude can be plotted on the instantaneous time-frequency plane and this time-frequency distribution of amplitude is properly named as the Hilbert Amplitude Spectrum, $H(\omega,t)$, to note and differentiate from the more accustomed to Fourier spectrum [10].

4.4 Examples and Discussion of Instantaneous Frequency

A demonstrative example is considered in this section. Figure 4.7(a) is a repetition of the same two-component signal as in Figure 4.4(a). Following the shifting procedures defined previously, the two intrinsic components were resolved and there was almost no residue, thus

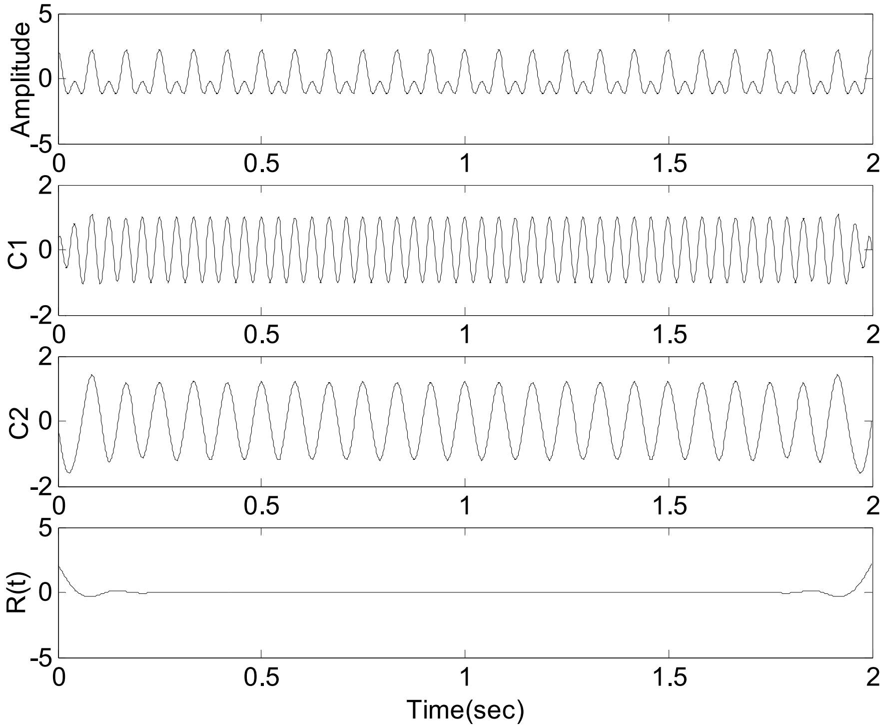

(a)

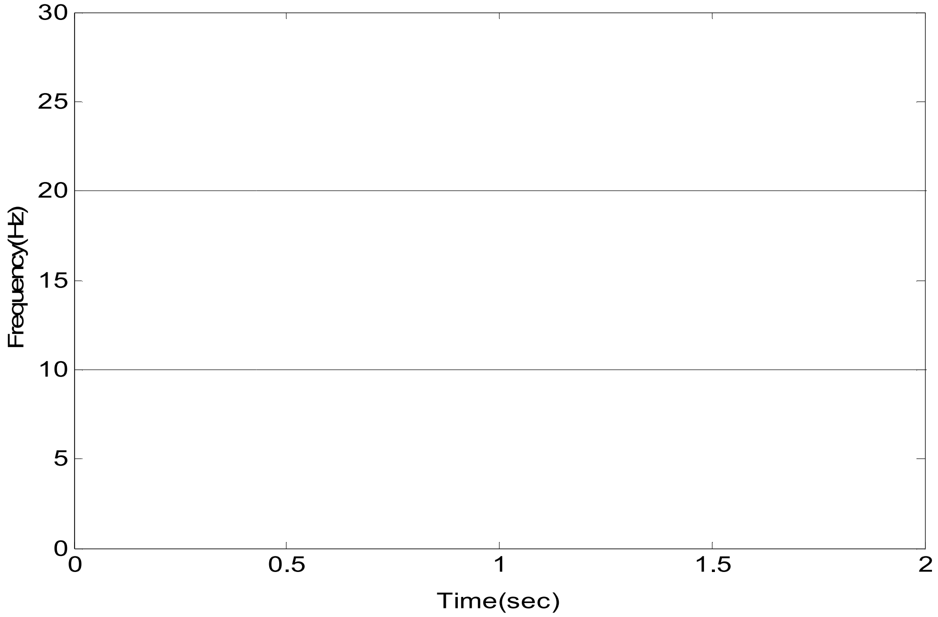

(b)

Figure 4.7 (a) A two-component signal with unequal amplitude and its two physical components obtained using the Empirical Mode Decomposition. (b) The two instantaneous frequencies determined using the two components of the signal indicating a null signal. Note that the two obtained components C1 and C2 are the two sinusoids comprised of the signal. The traditional definition of instantaneous frequency was then applied to the two resolved intrinsic modes to obtain the two instantaneous frequencies plotted in Figure 4.7(b). The two instantaneous frequencies are exactly what were expected without being averaged or obscured. The EMD enables multiple components (or modes) to be separated using the intrinsic time scales that are inherent to the signal (Eq. 4.19). It also fits one's intuitive well that a component is uniquely characterized by its intrinsic time scale. Because the Hilbert transform temporally localizes and extracts the phase information pertaining to only one mode at a time, the phase velocity of the mode is then evaluated as the instantaneous frequency of the mode.

The instantaneous frequency and its amplitude modulation thus defined clearly demonstrate the development of all the frequency components within the two example systems and allowed the physical characteristics of the systems to be studied. The four conditions given in [94], along with the one given in [91], can be applied to check and prove that this definition of instantaneous frequency on each and every separated intrinsic component surely satisfies all the conditions. The definition imparts concrete physical meanings to all intrinsic components and, henceforth, all the corresponding instantaneous frequencies!

Cohen [82] summarized the five paradoxes regarding the concept of instantaneous frequency defined as the time derivative of the phase of the analytic signal. Using two-component signals similar to those presented in Figures 4.3 and 4.4 as illustration, Cohen expressed his concerns over the observations made to the two-component signals that 1) The calculated instantaneous frequency is not one of the frequencies in the spectrum. 2) The line of spectrum consists of only a few sharp frequencies and the instantaneous frequency is continuous and ranges over an infinite number of values. 3) Although the frequency response of the analytic signal is zero for negative frequencies, the instantaneous frequency occasionally becomes negative. 4) The signal is bandlimited, however, the evaluated instantaneous frequency is seen to go outside the band. The difficulties summarized by Cohen have their roots in the fact that the notion of instantaneous frequency, which is physically applicable to only mono-component signals, was inadvertently applied to signals of multicomponent. Because by definition instantaneous frequency is a conditional average frequency, the instantaneous frequencies associated with all inherent components of the signal were "averaged" and misrepresented as one obscured frequency with periodic sharp spikes and going occasionally out of bandwidth into the negative range as a result. From the presented examples in which multicomponent signals were properly decomposed into their monocomponent intrinsic subsets and then instantaneous frequencies were successfully extracted by applying Ville's definition to the individual subset, it is clear that an effective mode decomposition method would ultimately resolve all the paradoxes listed above. By having the long-standing ambiguities and difficulties removed, the Empirical Mode Decomposition is one such powerful decomposition method enabling Ville's notion of instantaneous frequency to be generally, if not universally, applicable to signals of both mono- and multi-component. However, a few questions remain. For example, Can instantaneous frequency thus defined be related to the frequency defined in the Fourier sense? Or are they two totally different notions? Because the instantaneous frequency for a sinusoidal signal is the same as the frequency defined in the Fourier sense, the idea is preferred that the two concepts are related. If so, how exactly the energy of instantaneous frequency is or to be defined and how to relate it to the energy of Fourier frequency? Huang, *et al.* [36] indicated that the energy of instantaneous frequency is related to the amplitude modulation. However, more specifics in this regard are needed.

4.5 Characteristics of Nonlinear Response Interpreted Using Instantaneous Frequency

Bifurcation is the transition of a motion from one dynamic state to another accompanied by the appearance of new modes, the disappearance of old modes, or both. More specifically, a periodic motion contains only one frequency component (along with its harmonics), a quasi-periodic motion has at least two incommensurate frequencies (along with their harmonics), and a chaotic motion has a broadband spectrum. Thus, different states of periodic, period-doubling, quasi-periodic, or chaotic motions can be readily identified by their respective spectrum. This is one of the reasons that Fourier-based methods are often used in conjunction with time domain methods for the identification of bifurcations. However, for the obvious arguments that the Fourier transform is linear and that its analyzing harmonic functions are stationary, spectral domain methods are not feasible for time-varying signals demonstrating nonlinearity. Because instantaneous frequency displays frequency variation with time, changes of dynamic states indicative of bifurcation and instability can be identified through monitoring the instantaneous frequencies and the corresponding amplitudes. By comparing the instantaneous frequencies of the old mode to that of the new mode, the type of bifurcation can be determined. For example, if the instantaneous frequency of a new mode is about half of the frequency of the old mode, period-doubling occurs. If the instantaneous frequency of the new mode is incommensurate with the old mode, quasi-periodic bifurcation occurs. Similarly, intermittence, crises and chaotic motion can be thus determined.

How does one quantify bifurcation and chaotic response of a dynamic nonlinear motion using instantaneous frequency? The idea is that a dynamic state can be determined simultaneously by observing the changes in time of the instantaneous frequency components and their corresponding energy. Because time information is essential for positively localizing aberrations, it is required that instantaneous frequency components occurring at the present moment be compared with those components that occurred one instance before. To prevent this qualitative comparison, an understandably enormous task, the cumulated weights of all instantaneous frequency components between a starting moment, t_0, and a selected ending moment, t_1, can be calculated as a function of the frequency as follows

$$h_{01}(\omega) = \int_{t_0}^{t_1} H(\omega,t)\, dt \tag{4.22}$$

Thus $h_{12}(\omega), h_{23}(\omega), \ldots$ can be similarly computed at moments between t_1 and t_2, and t_2 and t_3, … ., respectively. The idea behind Eq. 4.22 is borrowed from the Fourier transform in which the weights of all the harmonic components are evaluated over the whole time span. However, it should be noted that the marginal spectrum defined in Eq. 4.22 describes and interprets the meaning of the frequency completely differently from the Fourier spectrum does. In the Fourier transform, presence of energy at a harmonic is interpreted as if the specific sinusoidal component is present throughout the entire duration of the time event. On the other hand, the marginal spectrum only gives the cumulated weights of all instantaneous frequency components over some selected time span in a probabilistic sense [9], thus indicating the occurrence probability of the frequency components being considered.

If the motion is periodic before instance t_1, $h_{01}(\omega)$ will then have only one peak. If bifurcation occurs between t_1 and t_2, appearance of new modes will be registered as new frequency components in $h_{12}(\omega)$. This can be readily realized in the simultaneous instantaneous time-frequency plane as the secondary frequency component appears and its amplitude becomes larger. If dynamic stability is allowed to further deteriorate beyond t_2 to eventual chaotic states, more frequency components will exist in the marginal spectrum, $h_{23}(\omega)$, where broadband characteristics will be prominent. In addition, the amplitude variations of all the frequency components can be easily resolved either on the time-frequency plane or from the marginal spectrum at any instance t. The cumulated values of different frequency components can therefore be used to characterize a nonlinear system and to also quantify bifurcation and chaotic response of the system. In summary, the exact moment of bifurcation occurrence can be pinpointed using more refined marginal spectra. As an alternative demanding less computing requirement, the same task can be equally achieved in the instantaneous time-frequency domain.

In the immediate following an example is given to illustrate the use of instantaneous frequency to the detection and identification of bifurcation and nonlinear response. The example, which was investigated in [80], is a time-delay oscillator that displays pitchfork bifurcation and other types of bifurcation as results of nonlinear feedback. The time-delayed equation is given by

$$\ddot{x}+\omega_0^2\, x-\alpha_1\,\dot{x}+\alpha_2\,\dot{x}^3 = k\cos(\Omega t)+\beta_1\,[\dot{x}(t-\tau)-\dot{x}(t)\,]+\beta_2\,[\dot{x}(t-\tau)-\dot{x}(t)\,]^3 \tag{4.23}$$

where all system parameters α's, β's, and k are assumed to be positive and Ω is the external driving frequency. Given ω_0^2 = 10.0, α_1 = 12.2, α_2 = 0.3, β_1 = 6.5, and Ω =2.0, different sets of periodic forcing (k's) and nonlinear feedback (β_2's) are studied in [80].

In the case presented in Figure 4.8 where β_2 is set to equal 0.1 and k is linearly increased from 1 to 10, a time step Δt = 0.001 sec is used to increment the response history, $x(t)$, and k and β_2 are each kept constant in the first 25,000 time steps. Starting at t = 25 sec the periodic forcing parameters are then linearly increased for the next 20 seconds (20,000 time steps) to its final values. Only the portion of the entire time response enclosing t = 25 sec and beyond is considered. As is evident from Figure 4.8(b), when k is relatively small, the driving frequency (f = 1/π) is not exactly prominent to begin with. The two IMFs resolved using EMD are seen in

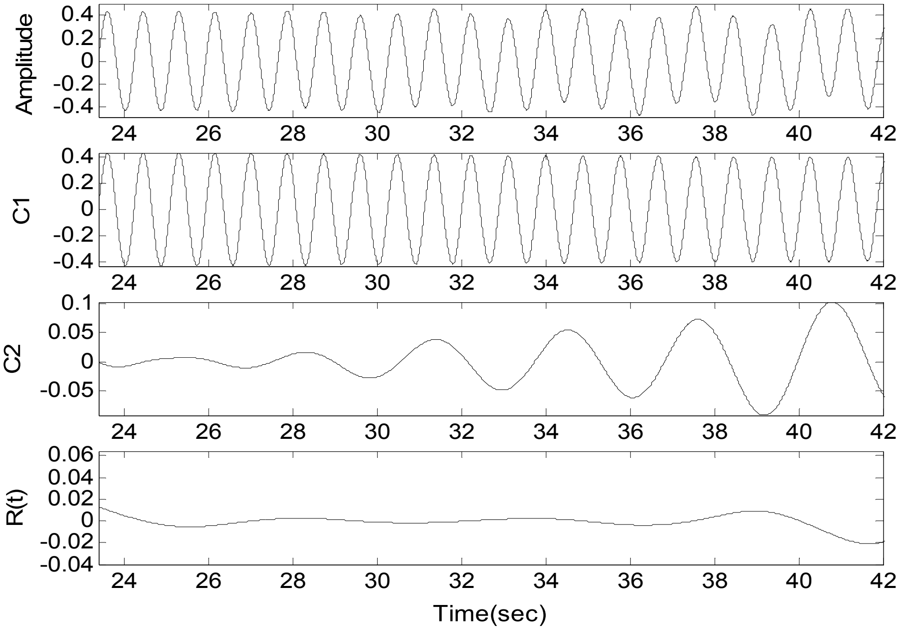

(a)

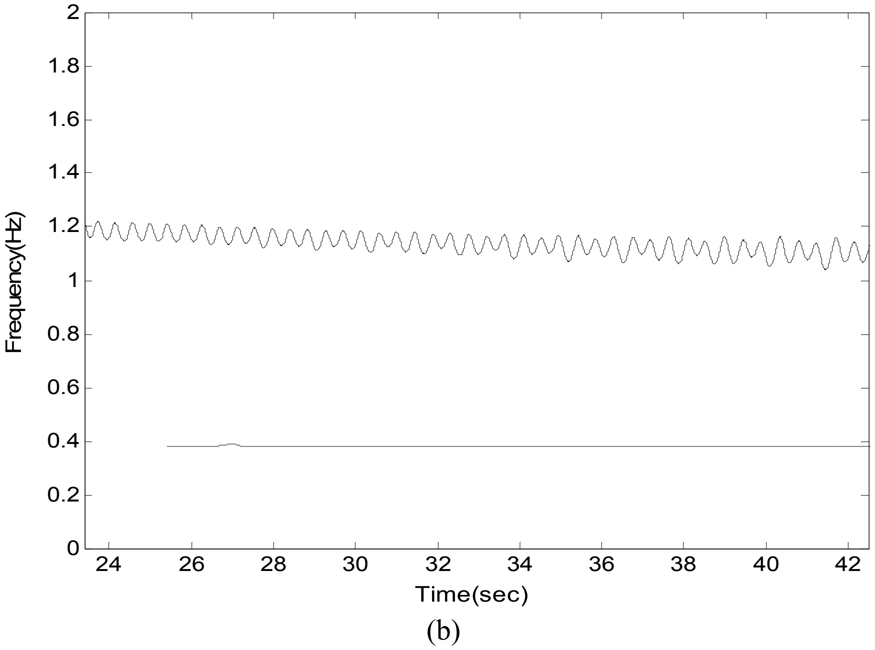

(b)

Figure 4.8 (a) Dynamic response and its decomposed intrinsic modes for $\beta_2 = 0.1$ and *k* being varied from 1.0 to 10.0. (b) Associated instantaneous frequencies corresponding to all resolved IMF C1-C2

Figure 4.8(b) as two incommensurate modes demonstrating the attribute of a quasi-periodic motion. It is noted that only one of the modes in the figure displays temporal-modal structure with an oscillation period of approximately 0.4sec. As no aberration is observed with either mode within the 19-second window, no bifurcation or further change of dynamic state occurs for increasing the periodic forcing amplitude from 1.0 to 10.0. In addition, it can be shown that the accumulated effect from the forcing frequency becomes more prominent while the effect from the natural frequency remains the same on the marginal spectrum, $h_{i,i+1}(\omega)$.

4.6 Summary

The concept of instantaneous frequency is of high practical significance for the analysis of nonlinear non-stationary signals. Because their spectral characteristics vary with time, conventional Fourier-based analyses are insufficient in resolving the temporal progression of all individual spectral components in multicomponent signals. Ville's definition of instantaneous frequency works well for monocomponent signals; however, the definition falls short on providing a unified interpretation applicable also to signals of multicomponent. The definition realizes infinite instantaneous frequency or negative amplitude in multicomponent signals; both of which are against our intuitive understanding of instantaneous frequency. As signals subject to daily investigation are mostly non-stationary and of multiple components in nature, it is essential that the definition of instantaneous frequency be re-examined and physically established to enable wider application. In this chapter, problems associated with the use of Ville's definition for instantaneous frequency were analyzed using a few simple examples and a viable solution to the problems were identified. A decomposition method was employed to separate multicomponent signals into their associated monocomponent signal subsets. Ville's notion was then applied to the subsets to successfully extract signal instantaneous frequencies. The presented approach resolves the predicament commonly experienced in applying the definition of instantaneous frequency and thus is significant and essential to the analysis and study of nonlinear rotor-dynamic systems.

CHAPTER V

NUMERICAL MODELING OF A SHAFT-ROTOR SYSTEM WITH NONLINEARITIES

5.1 Finite Element Model

Time domain and spectral domain methods for investigating nonlinear dynamic systems and for characterizing nonlinear, non-stationary responses were reviewed. Analysis tools developed based on these methods, along with the fundamental notion of instantaneous frequency, have provided many options for understanding the governing physics of a wide range of nonlinear systems readily found in dynamic, economics, chemistry and psychology. The respective advantages and disadvantages were examined in depth. In the current chapter, a shaft-rotor model of practicality and significance in engineering is developed. The various effects of nonlinearity induced by varying the underlying parameters are quantitatively established using the model. In the followings, the numerical procedures developed and employed for acquiring system time histories in response to changing parameters is also discussed.

As summarized in Chapter II, the dynamic characteristics of linear rotor systems have been successfully identified using a variety of schemes including the lumped parameter method, Myklestad-Prohl transfer-matrix method, direct stiffness approach [102], and finite element method. Beginning in 1970s, the finite element method has seen applications in modeling rotor-dynamic responses. The finite elements used by Ruhl [103] included translational inertia and bending stiffness but neglected rotary inertia and gyroscopic moments. In addition to translational and rotary inertia, bending stiffness and gyroscopic moments, the finite elements developed by Gasch [104] also incorporated the effect of distribution eccentricity. A comprehensive finite element model presented by Nelson and colleagues [65-67] embodied not just all the above but also shear deformation, axial load, axial torque and internal damping.

Many books employ this model in the introductory treatment on modeling rotor-dynamics using finite elements [2,30]. However, Nelson's is a linear model and it does include no elements such as fluid-film bearing support and bearing clearances that would contribute to rotor-dynamic nonlinearity. Due to the inherent complexity and high overhead of time needed for simulating high-order finite element models, they [31-32] also introduced the Component Mode Synthesis method into their investigation of rotor systems to substantially reduce the size of the overall system equations while still retaining the essential dynamic characteristics. Nevertheless, only a handful of research was dedicated to addressing the dynamic responses of high order nonlinear systems. Among them are Sundararajan and Noah [15] who studied an isotropic bearing supported rotor system and observed certain nonlinear phenomena and Shiau and Jean [63] applied the generalized polynomial expansion method to a flexible rotor system with nonlinear bearing support. It is also worth mentioning that Fey [64] and Zheng and Hasebe [34-35] were among the first to investigate the long-term behaviors of rotor-dynamic systems with local nonlinearities using the component Mode Synthesis techniques.

The finite element method is a proven approach for analyzing dynamic systems. Thus the rotor-bearing system developed for the research are formulated using finite elements to enable the true physical representations of rotor-dynamic responses subjected to the actions of various sources of nonlinearity. The model is developed based on the pioneering work found in [4,29,34-35] to investigate the nonlinearity induced by the individual and combined actions of surface cracks and bearing forces. Figure 5.1 is the schematic representation of the rotor-bearing model of four disks. Values of disk parameters are provided in Table 5.1 below.

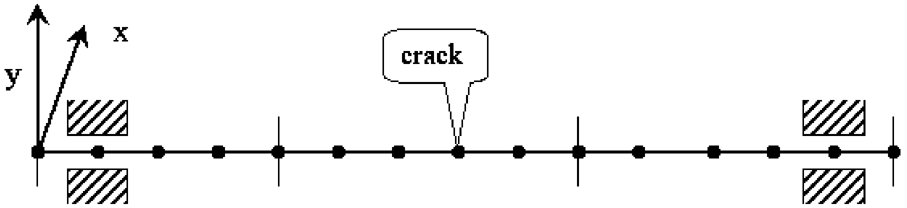

Figure 5.1 Configuration and coordinates for the presented rotor-bearing model system

Table 5.1: Mass and Inertia of Disks

Disk No.	1	2	3	4
Mass (Kg)	52	54	58	50
Inertia (kg.m^2)	1.2	1.4	2.2	1

The equation of motion for a rigid disk can be expressed by [65]

$$([M_T^d]+[M_R^d])\left\{\ddot{q}^d\right\}-w[G^d]\left\{\dot{q}^d\right\}=\left\{Q^d\right\} \tag{5.1}$$

where $\left\{q^d\right\}^T=\{x,y,q_x,q_y\}$, w is the rotating speed, G^d is the gyroscopic matrix, $\{Q^d\}$ is the external force vector incorporating gravity and imbalance, and

$$[M_T^d]=\begin{bmatrix} m_d & 0 & 0 & 0 \\ 0 & m_d & 0 & 0 \\ 0 & 0 & 0 & 0 \\ 0 & 0 & 0 & 0 \end{bmatrix},\quad [M_R^d]=\begin{bmatrix} 0 & 0 & 0 & 0 \\ 0 & 0 & 0 & 0 \\ 0 & 0 & I_d & 0 \\ 0 & 0 & 0 & I_d \end{bmatrix},\quad [G^d]=\begin{bmatrix} 0 & 0 & 0 & 0 \\ 0 & 0 & 0 & 0 \\ 0 & 0 & 0 & -I_p \\ 0 & 0 & I_p & 0 \end{bmatrix} \tag{5.2}$$

with m_d, I_d the mass and inertia of the disk, respectively, and $I_p=2I_d$. Note that the derivation of $[G^d]$ can be found in [2].

The system equation of motion of a rotor-bearing system composed of rigid disks, flexible shaft and bearings can be expressed using finite elements as

$$M\ddot{z}+(D+G)\dot{z}+Kz=g(t)+f(z,\dot{z}) \tag{5.3}$$

where $\ddot{z},\dot{z},z$ are, respectively, the acceleration, velocity and displacement vector. g(t) is the imbalance and gravity force vector and M, G, K are the mass, gyroscopic and stiffness matrix, respectively, whose detail formulation can be found in [67]. For a rotor modeled using the Timoshenko beam element and having b nodes, the displacement vector has the following format

$$z^T=\{x_1,y_1,q_{x1},q_{y1},x_2,y_2,q_{x2},q_{y2},\ldots,x_b,y_b,q_{xb},q_{yb}\} \tag{5.4}$$

Once the finite element for the shaft and bearing are available, the equations of motion for the rigid disks can be readily assembled into Eq. 5.3 and afterwards be ready for system rotor-dynamic analysis including determining the steady state and transient responses. The element data are given in Table 5.2.

Table 5.2: Element data of a flexible shaft

Segment	1	2	3	4	5	6	7	8	9
Length (m)	0.16	0.10	0.32	0.36	0.34	0.30	0.12	0.08	0.08
Radius (m)	0.07	0.07	0.08	0.09	0.10	0.09	0.08	0.07	0.07
Element	1	1	2	3	2	2	1	1	1

In the model there are 14 (Timoshenko) beam elements for the flexible shaft, thus having 15 nodes in total. Each node has 4 degrees of freedom. Therefore, the rotor-bearing model is a 60 degrees of freedom system.

5.2 Modeling of Local Nonlinearities

Mechanisms of instability such as fluid-film bearings and internal damping are sources of nonlinearity in rotary machines. Surface cracks and auxiliary bearings are other sources of nonlinear rotor-dynamic responses. Fluid-film bearing force and surface crack propagation are two factors that, if unhindered and uncontrolled, are commonly credited for rotor-dynamic instability of various degrees in rotating machinery. As such, the effects due to the individual as well as combined actions of the two common sources of nonlinearity are investigated in the research. The modeling of the two is detailed in the following.

1. Fluid-film bearing forces

There are two plain journal bearings applied at node 2 and node 14 in the rotor-bearing model system. The fluid-film bearing force can be obtained by integrating the pressure distribution of the journal bearings in lieu of solving the Reynolds equation

$$\frac{\partial}{\partial x}\left(h^3\frac{\partial p}{\partial x}\right)+\frac{\partial}{\partial z}\left(h^3\frac{\partial p}{\partial z}\right)=6U\mu\frac{\partial h}{\partial x}+12\mu\frac{\partial h}{\partial t} \tag{5.5}$$

where, μ is the viscosity of the fluid, p(x, z) is the pressure distribution around the bearing, U is the fluid velocity near the bearing, and h , the oil-film thickness, is given by

$$h=Cr-x\cos\theta-y\sin\theta \tag{5.6}$$

with Cr representing the bearing clearance. Reynolds equation can be recast into its polar coordinate representation by using

$$U=R\omega, x=R\theta, \partial x=R\partial\theta$$

where R is journal radius and ω is journal angular speed. As the pressure distribution is a function of θ and z, that is $p=p(\theta, z)$, the resulted Reynolds equation now has the form

$$\frac{1}{R^2}\frac{\partial}{\partial\theta}\left(h^3\frac{\partial p}{\partial\theta}\right)+\frac{\partial}{\partial z}\left(h^3\frac{\partial p}{\partial z}\right)=6\mu\omega\frac{\partial h}{\partial\theta}+12\mu\frac{\partial h}{\partial t} \tag{5.7}$$

From Eq. 5.6 and 5.7, it is seen that the pressure is a nonlinear function of journal position and velocity. When the ratio of the rotor span, L, to rotor diameter, D is less than 0.5, it is believed that the pressure in bearing length z-direction is significantly larger than that in the x-direction ($\frac{\partial p}{\partial z}>>\frac{\partial p}{\partial x}$). Thus, in short bearing analysis where L/D < 0.5, the first term on the left-hand side of Eq. 5.7 is often neglected, resulting a simplified Reynolds equation

$$\frac{\partial}{\partial z}\left(h^3\frac{\partial p}{\partial z}\right)=6\mu\omega\frac{\partial h}{\partial\theta}+12\mu\frac{\partial h}{\partial t} \tag{5.8}$$

Integrating Eq. 5.8 using the boundary conditions that oil-film pressure distributions in the z-direction are $\frac{\partial p}{\partial z}=0$ at z = 0 and p = 0 at $z=\pm\frac{L}{2}$, the resulted pressure distribution is

$$p(q, z) = \frac{3m}{h^3}\left(w\frac{\partial h}{\partial q} + 2\frac{\partial h}{\partial t}\right)\left(z^2 - \frac{l^2}{4}\right) \tag{5.9}$$

For the long bearing approximation analysis (L/D>1), it is assumed that the pressure does not change in the z-direction, that is, $\frac{\partial p}{\partial z} \approx 0$. This allows the second term on the left-hand side of Eq. 5.7 to be dropped and the Reynolds equation is simplified to be

$$\frac{1}{R^2}\frac{\partial}{\partial q}\left(h^3\frac{\partial p}{\partial q}\right) = 6mw\frac{\partial h}{\partial q} + 12m\frac{\partial h}{\partial t} \tag{5.10}$$

Using this simplified equation, Childs developed a pressure distribution approximation in the x-direction [30, 68] as follows

$$p(q) = 6mR^2V_s(\cos a \, \cos q - b\sin a \, \sin q)(2 + e\cos q)/(C_r^3h^2) \tag{5.11}$$

Here $q = 0$ at the opposite direction of eccentricity,

$$e = \sqrt{x^2 + y^2}, e = \frac{e}{Cr}, h = 1 + \cos q, b = \frac{2}{2 + e^2},$$

and

$$V_s = \sqrt{(\dot{x} + 0.5wy)^2 + (\dot{y} - 0.5wx)^2} \tag{5.12}$$

$$a = \tan^{-1}\left(\frac{y(\dot{x} + 0.5wy) - x(\dot{y} - 0.5wx)}{x(\dot{x} + 0.5wy + y(\dot{y} - 0.5wx)}\right) \tag{5.13}$$

$x, y, \dot{x}, \dot{y}$ are the displacement and velocity of the journal center. For the finite-length bearing analysis that 0.5<L/D<1 is satisfied, the pressure distribution and bearing forces are given in [30,68]. Once the pressure distribution is known or determined, the fluid bearing force can be calculated by integration its two components using Eq. 5.14,

$$\begin{aligned} f_x &= -\int_{-\frac{L}{2}}^{\frac{L}{2}}\int_0^{2p} p(q,z)R\cos q\,dq\,dz \\ f_y &= -\int_{-\frac{L}{2}}^{\frac{L}{2}}\int_0^{2p} p(q,z)R\sin q\,dq\,dz \end{aligned} \tag{5.14}$$

f_x, f_y thus evaluated are then applied to nodes 2 and 14 as external excitations.

2. Surface crack propagation

The presence of surface crack in a rotating machine introduces a local flexibility that affects the overall vibration response. Dimarogonas [105] and Wauer [106] reviewed and concluded that fatigue cracks play a prominent role in affecting the structural dynamic response of a rotating machine. Gasch [107] developed a spring-hinge model to approximate the behavior of a cracked shaft and reviewed the long line of investigation on the dynamics induced by transverse surface cracks in rotor-bearing systems [108]. Because it approximates the true dynamic behavior of a cracked rotor system and the validity of it is supported by much experimental verification, many works that followed [4,29,77,109] were based on Gasch's model to a large extent. The opening and closing of a surface fatigue crack depends on the rotation and vibration amplitude and also the direction of the shaft deflection relative to the crack [105]. A cracked rotor system is therefore nonlinear. Furthermore, if the general motion of the whole system is considered, the local stiffness matrix description of the cracked section of the shaft would lead to a coupled system, while for an uncracked shaft the system is a one of decoupled. The opening-condition of the crack can be formulated approximately by the displacement near the crack using Eq. 2.7. As a result, the element-stiffness-matrix, K_{crack}, for a discrete model in the inertial coordinate system has the form of Eq. 2.9, which is duplicated below

$$
\begin{aligned}
K_{crack} &= \frac{h_r}{h(1+h_r)} \begin{bmatrix} \cos^2(\omega t) & \sin(\omega t)\cos(\omega t) \\ \sin(\omega t)\cos(\omega t) & \sin^2(\omega t) \end{bmatrix} \\
&= \frac{h_r}{2h(1+h_r)} \begin{bmatrix} 1+\cos(2\omega t) & \sin(2\omega t) \\ \sin(2\omega t) & 1-\cos(2\omega t) \end{bmatrix}
\end{aligned}
\tag{5.15}
$$

Here, ω denotes the spinning velocity, h is the compliance in the ξ direction, h_r is the relative compliance. The relation between h_r and the crack depth was experimentally established by Mayes and Davis [77]. Table 5.3 provides a list of mapping h_r to the ratio of the physical crack depth, dt, with the rotor radius, R.

Table 5.3 Relation between h_r and dt/R

h_r	0.012	0.09	0.205	0.164	0.46	0.49	0.56
dt/R	NA	near 20%	27%	23%	39%	41%	43%

As discussed before, the values of K_{crack} depend on the opening condition. If the condition is satisfied, the values of K_{crack} are determined using the above equation; otherwise the values of K_{crack} are 0. The crack-induced effects realized in the model as nonlinear (external) forces. It is obvious that the cracked rotor-bearing system as described by the model is nonlinear, with the relative flexibility, h_r, as the control parameter. Thus, shaft stiffness and crack breathing all vary depending upon the direction of deflection and the spring characteristics of shaft. Understandably responses of the model system are thus highly nonlinear.

A crack is implemented at node 8. The opening condition is determined by the positions of nodes 7, 8 and 9 using the following

$$
x_8\cos(\omega t) + y_8\sin(\omega t) > ((x_7 + x_9)\cos(\omega t) + (y_7 + y_9)\sin(\omega t))/2 \tag{5.16}
$$

If Eq. 5.16 is not satisfied, the crack is closed and thus f_{x10}, f_{y10} = 0. If Eq. 5.16 is satisfied, the crack is open and the force components at node 10 are

$$\begin{aligned} f_{x8} &= [x_8 \cos^2(\omega t) + y_8 \sin(\omega t)\cos(\omega t)]\frac{kh_r}{1+h_r} \\ f_{y8} &= [y_8 \sin^2(\omega t) + x_8 \sin(\omega t)\cos(\omega t)]\frac{kh_r}{1+h_r} \end{aligned} \tag{5.17}$$

where, $k = \dfrac{192EJ}{l^3}$, $J = \dfrac{\pi d^4}{64}$, l is the length between two bearings. Forces f_{x8}, f_{y8} are then applied at node 8 to determine the nonlinear respon4se using the equations of motion.

5.3 Solution Procedures

The transient responses of the system require step by step numerical integration. In order to ensure unconditional numerical stability and stable converged numerical solution, the Newmark method was modified and employed in this research. For specifics regarding the Newmark numerical scheme, see Refs. 110 and 111. Integrating from time t to $t+\Delta t$, the following relations can be obtained using the Newmark method

$$\begin{aligned} \ddot{u}^{t+\Delta t} &= \frac{1}{\alpha \Delta t^2}(u^{t+\Delta t} - u^t) - \frac{1}{\alpha \Delta t}\dot{u} - (\frac{1}{2\alpha} - 1)\ddot{u}^t \\ \dot{u}^{t+\Delta t} &= \dot{u}^t + \Delta t(1-\delta)\ddot{u}^t + \delta \Delta t \ddot{u}^{t+\Delta t} \end{aligned} \tag{5.18}$$

where *α, δ* are parameters that the Newmark method is unconditionally stable if $0.5 \le \delta \le 1, \alpha \ge 0.25(0.5+\delta)^2$ are satisfied. In the research, $\alpha = 0.25, \delta = 0.5$ were chosen, which corresponds to the unconditionally stable constant-average acceleration method [111]. Substitute the first equation of Eq. 5.18 into the second, the followings are obtained

$$\begin{aligned} \ddot{u}^{t+\Delta t} &= au^{t+\Delta t} + \ddot{\tilde{u}}^t \\ \dot{u}^{t+\Delta t} &= bu^{t+\Delta t} + \dot{\tilde{u}}^t \end{aligned} \tag{5.19}$$

where $a = \dfrac{1}{\alpha \Delta t^2}$, $b = \dfrac{\delta}{\alpha \Delta t}$ and

$$\begin{aligned}
\ddot{\tilde{u}}^t &= -\frac{1}{\alpha \Delta t^2} u^t - \frac{1}{\alpha \Delta t} \dot{u}^t - (\frac{1}{2\alpha} - 1)\ddot{u}^t \\
\dot{\tilde{u}}^t &= -\frac{1}{\alpha \Delta t} u^t - (\frac{\delta}{\alpha} - 1)\dot{u}^t + (1 - \frac{\delta}{2\alpha})\ddot{u}^t
\end{aligned} \tag{5.20}$$

Rewrite Eq. 5.3 as

$$M_1\ddot{x} + C_1\dot{x} + K_1 x = g_1(\tau) \ + f_1(x,\dot{x}) \tag{5.21}$$

Note that τ is time. To simply the formulation and also to ensure computational stability, Eq. 5.21 is normalized using $X = \dfrac{x}{Cr};\ \dot{X} = \dfrac{\dot{x}}{Cr\omega};\ddot{X} = \dfrac{\ddot{x}}{Cr\omega^2};t = \dfrac{\omega\tau}{2\pi}$, in which t is the normalized time. The equation in the normalized variables is now

$$M\ddot{X} + C\dot{X} + KX = g(t) \ + f(X,\dot{X}) \tag{5.22}$$

Rearrange the equation and express it using components and matrices

$$\begin{bmatrix} M_{11} & M_{12} \\ M_{21} & M_{22} \end{bmatrix} \begin{Bmatrix} \ddot{X}_1 \\ \ddot{X}_2 \end{Bmatrix} + \begin{bmatrix} C_{11} & C_{12} \\ C_{21} & C_{22} \end{bmatrix} \begin{Bmatrix} \dot{X}_1 \\ \dot{X}_2 \end{Bmatrix} + \begin{bmatrix} K_{11} & K_{12} \\ K_{21} & K_{22} \end{bmatrix} \begin{Bmatrix} X_1 \\ X_2 \end{Bmatrix} = \begin{Bmatrix} g_1(t) \\ g_2(t) \end{Bmatrix} + \begin{Bmatrix} f(X_1,\dot{X}_1) \\ 0 \end{Bmatrix} \tag{5.23}$$

Substitute Eq. 5.19 into Eq. 5.23 and the resulted equations are

$$\begin{bmatrix} A_{11} & A_{12} \\ A_{21} & A_{22} \end{bmatrix} \begin{Bmatrix} X_1^{t+\Delta t} \\ X_2^{t+\Delta t} \end{Bmatrix} = \begin{Bmatrix} q_1(t) \\ q_2(t) \end{Bmatrix} + \begin{Bmatrix} \tilde{f}(X_1^{t+\Delta t}) \\ 0 \end{Bmatrix} \tag{5.24}$$

where

$$\begin{aligned} A_{11}X_1^{t+\Delta t} &= q_1(t) + \tilde{f}(X_1^{t+\Delta t}) - A_{12}X_2^{t+\Delta t} \\ A_{22}X_2^{t+\Delta t} &= q_2(t) - A_{21}X_1^{t+\Delta t} \end{aligned} \tag{5.25}$$

Substitute $X_2^{t+\Delta t}$ from the second equation of Eq. 5.25, the equation is simply

$$K_{nm}X_1^{t+\Delta t} = F_{nm} \tag{5.26}$$

Here $K_{nm} = A_{11} - A_{12}A_{22}^{-1}A_{21}, \quad F_{nm} = q_1(t) + \tilde{f}(X_1^{t+\Delta t}) - A_{12}A_{22}^{-1}q_2(t)$.

As F_{nm} includes nonlinear terms, therefore, Eq. 5.26 is an nonlinear system and iteration scheme is needed to get its dynamic response. Because only the first several equations include nonlinear forces, iterations can be executed on the first several modes. Through this way, not only the number of computation required for each iteration is significantly lower, the iteration steps needed for achieving convergence are also greatly reduced. Numerical iteration was performed using the Newton-Raphson method and the procedure followed is

$$X_{1,k+1}^{t+\Delta t} = X_{1,k}^{t+\Delta t} - [D_{X_1}\tilde{f}(X_{1,k}^{t+\Delta t}) - K_{nm}]^{-1}(F_{nm} - K_{nm}X_{1,k}^{t+\Delta t}) \tag{5.27}$$

here,

$$D_{X_1}\tilde{f}(X_{1,k}^{t+\Delta t}) = \frac{\partial f(X_1, \dot{X}_1)}{\partial X_1} + b\frac{\partial f(X_1, \dot{X}_1)}{\partial \dot{X}_1} \tag{5.28}$$

Eq. 5.28 is the Jacobian matirx for Eq. 5.26. Iteration would stop when

$$\frac{< \Delta X_1^{t+\Delta t}, \Delta X_1^{t+\Delta t} >}{< X_1^{t+\Delta t}, X_1^{t+\Delta t} >} \le 10^{-12} \tag{5.29}$$

Once converged $X_1^{t+\Delta t}$ is obtained, $X_2^{t+\Delta t}$ is computed using

$$X_2^{t+\Delta t} = A_{22}^{-1}(q_2(t) - A_{21}X_1^{t+\Delta t}) \tag{5.30}$$

5.4 Shooting Method and Nonlinear Stability

Normally, the system responses are integrated by direct integration as discussed in the last section to locate fixed points or to determine periodic, quasi-periodic, or chaotic solution. But there is no guarantee that the integration will converge to the desired attractors. Therefore, some approaches have been proposed to overcome this problem. The shooting method is introduced below to demonstrate how these approaches work to quickly find the periodic solution. The one other reason for selecting the shooting method is that the monodromy matrix inherent of the method can be readily used to determine the stability of periodic solution.

Define

$$z(t,z_0)=\begin{Bmatrix} X(t,X_0) \\ \dot{X}(t,X_0) \end{Bmatrix} \quad z_0=\begin{Bmatrix} X_0 \\ \dot{X}_0 \end{Bmatrix} \tag{5.31}$$

rewrite the system equations of motion as

$$\dot{z}=F(t,z,l) \tag{5.32}$$

Eq. 5.32 is an initial value problem with the initial conditions given in Eq. 5.31. In this study, the excitation is periodic, so the periods for all periodic solutions are the same as the excitation period, *T*. The following relation holds for any periodic motion

$$z(T,z_0)-z_0=0 \tag{5.33}$$

Therefore, to find the periodic solution is equivalent to solving a boundary value problem, which requires the guessing of the initial conditions, z_0. The shooting method recasts the boundary value problem associated with solving Eq. 5.33 using Newton-Ralphson method. The procedure is

$$z_0^{k+1}=z_0^k-[D_{z_0}(T,z_0^k)-I]^{-1}(z(T,z_0^k)-z_0^k) \quad k=1,2,... \tag{5.34}$$

where $D_{z_0}(T, z_0^k)$ is the so-called monodromy matrix. The computation of monodromy matrix is given as follows. Differntiate Eq. 5.32 with respect to the initial condition, z_0,

$$\frac{d}{dt}\left(\frac{\partial z}{\partial z_0}\right) = D_{Z_0} F(t, z, M) \frac{\partial z}{\partial z_0} \tag{5.35}$$

The initial condition for Eq. 5.35 is $\frac{\partial z(0)}{\partial z_0} = I$, because $\frac{\partial z(0)}{\partial z_0} = \frac{\partial z_0}{\partial z_0} = I$. It can be seen that both Eqs. 5.32 and 5.35 are initial value problems and can be integrated simultaneously. Thus it is not necessary to have to first integrate Eq. 5.32 and then Eq. 5.35. The procedures for the shooting method are: (1) specify an initial guess for z_0, (2) integrate Eq. 5.32 and 5.35 to get $z(T, z_0)$ and $D_{z_0}(T, z_0^k)$, (3) use Eq. 5.34 to get another z_0 with correction, (4) repeat the steps above until

$$\frac{< \Delta z_0, \Delta z_0 >}{< z_0, z_0 >} \le 10^{-10} \tag{5.36}$$

Then $z(t, z_0)$ is the obtained perioidc solution and $D_{z_0}(T, z_0^k)$ is the monodromy matrix. Figure 5.2 shows the shooting process of a rotor system supported by a pair of plain journal bearings. It can be seen from the figure that only three shootings are required to find the periodic solution.

The stability of periodic solution can be determined using the eigenvalues (Floquet multipliers) of the monodromy matrix, $D_{z_0}(T, z_0^k)$. As proved in Chapter II, there is always one eigenvalue of value of 1. If all others are within the unit circle, the periodic solution is stable and if one or more of them is out of the unit circle, the solution is unstable. As stated in Chapter III, the type of bifurcation can be determined by the way through which the eigenvalue(s) goes out of the unit circle. When one of the Floquet multipliers leaves the unit circle through (+1,0), then the periodic solution loses stability by a symmetry-breaking bifurcation, a pitchfork

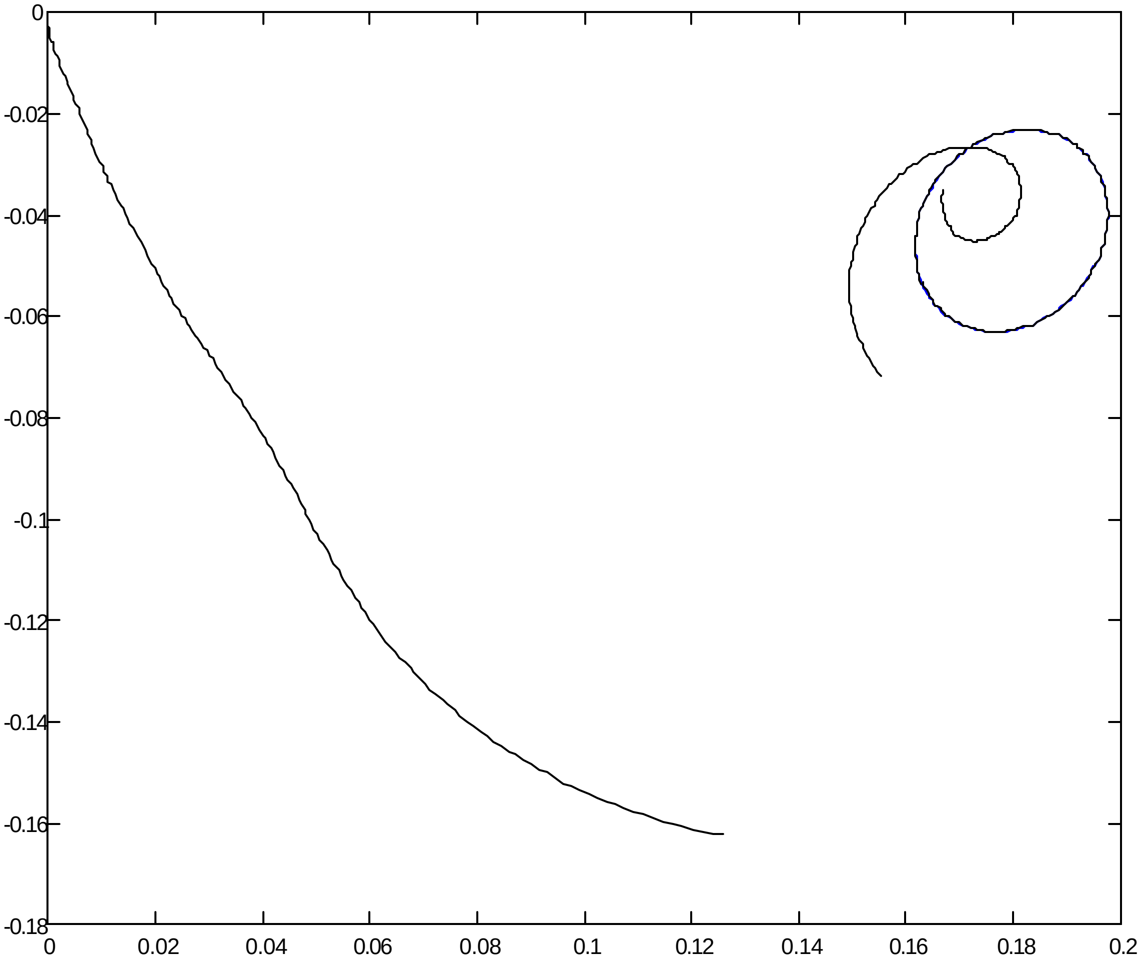

Fig 5.2 Orbit of journal center of a rotor system obtained after three shooting processes

bifurcation, or a saddle node bifurcation [5]. Of these three, the saddle-node bifurcation is structurally stable and is more common in problems of single parameter. When the leading Floquet multiplier leaves the unit circles at (-1,0), a period-doubling bifurcation would occur. A period-1 solution would become a period-2 solution and a cascade of period doubling bifurcation can eventually lead to chaos. When the leading pair of Floquet multipliers cross the unit circle as complex conjugate, a secondary Hopf bifurcation would occur. This type of bifurcation leads to a quasi-periodic motion that can further bifurcate to chaotic motion. Some of these bifurcations and different dynamic behaviors will be studied in the next chapter.

CHAPTER VI

RESULTS OF CRACKED ROTOR MODEL WITH ELASTIC SUPPORTS

6.1 Description of Results

In previous chapters, the commonly applied methods for investigating nonlinear dynamic systems were reviewed and a new analytical approach based on the concept of instantaneous frequency was developed and applied to nonlinear time series analysis. In this chapter, the nonlinear responses induced by two specific sources of nonlinearity, namely, transverse fatigue crack and oil-film bearing force, are explored using all these nonlinear methodologies. First, the various nonlinear responses induced by crack breathing are studied using the instantaneous frequency. Specifics regarding the dynamic model developed and employed, along with the all associated parameters, can be found in [8].

The physical bases employed to model the crack and the configuration particular of the rotor are briefly given in the following. The breathing of a crack is modeled as a physical effect equivalent to the localized changing of elastic stiffness of the rotor shaft and this change of shaft stiffness induces rotor imbalances and nonlinearity. These effects are incorporated into the governing equations of motion as imbalance vectors, *f(t)*, and externally caused forces, [N_n $H(z,t)$], as

$$M\,\ddot{z} + (D+G)\,\dot{z} + K\,z = f(t) + N_n\,H(z(t),t) \tag{6.1}$$

where $z, \dot{z}, \ddot{z}$ denote the rotor displacement, velocity, and acceleration vectors, which correspond, respectively, to matrices *M*, *D*, and *K* to constitute the effects contributed by mass, damping, and stiffness. Note that to cover the gyroscopic effect attributable to the conservation of angular momentum, a matrix *G* is included in the equation. Note also that the crack-induced nonlinearity is governed by the input matrix of nonlinearity, N_n, and the vector of nonlinearity,

$H(z(t),t)$, whose definitions can be found in [4,29,108]. One of the basic assumptions regarding the local stiffness is that in the case of an open crack, the shaft flexibility, h, in the crack direction is increased with an additional compliance, Δh, which is dependent on the crack depth. The relative crack flexibility or compliance, h_r, defined as $h_r = \Delta h / h$, is the control parameter of the nonlinear, dynamical cracked rotor model described in Eq. 6.1 [4]. In the following analysis, continual increasing of h_r along time is exploited to realize the vibration response of the rotor subject to the opening and closing of a propagating surface crack. The rotor, which is a lumped-mass model, has seven beam elements. The crack is located at the fourth joint and a mass eccentricity is placed at the sixth joint. All relevant system parameters are provided as follow: rotor density = 7860 kg/m^3; rotor stiffness = 210kN/mm^2; rotor length = 600 mm; rotor weight = 19920.67N; shaft radius = 140 mm; rotation frequency = 100π rad/s; mass eccentricity = 0.02 mm; bearing spring constant = 750 kN/mm; damping defined as $D = \alpha_{\text{mod}} M + \beta_{\text{mod}} K,\ \alpha_{\text{mod}} = 0,\ \beta_{\text{mod}} = 0.00001$; number of degrees of freedom for the model = 16.

Due to the variation of the crack configuration, facilitated through varying the relative flexibility, h_r, the rotor model would experience periodic motion and dynamic instabilities including period-doubling, fractals and chaotic responses. In all cases considered in the section, h_r is allowed to linearly, while slowly, extend from an initial value to a selected final value over a 5.0-sec time window and a time step of $\Delta t = 0.00025$ sec is used to increment rotor vibration response from 0-sec. Figure 6.1 presents the amplitude (displacement time history) of the rotor when h_r is varied from 0.0 to eventual 0.06 at t = 5-sec and afterwards is kept constant for another 1-sec. It is seen that the initial transient covers approximately 0.4-sec and between t = 0.4-sec and t = 5.0-sec the vibration amplitude steadily increases in response to the crack growth. For better visibility, the portion of the time response between 1.6-sec and 2.7-sec is isolated and placed in Figure 6.2(a), along with its corresponding IMFs C1-C3 obtained through the scheme

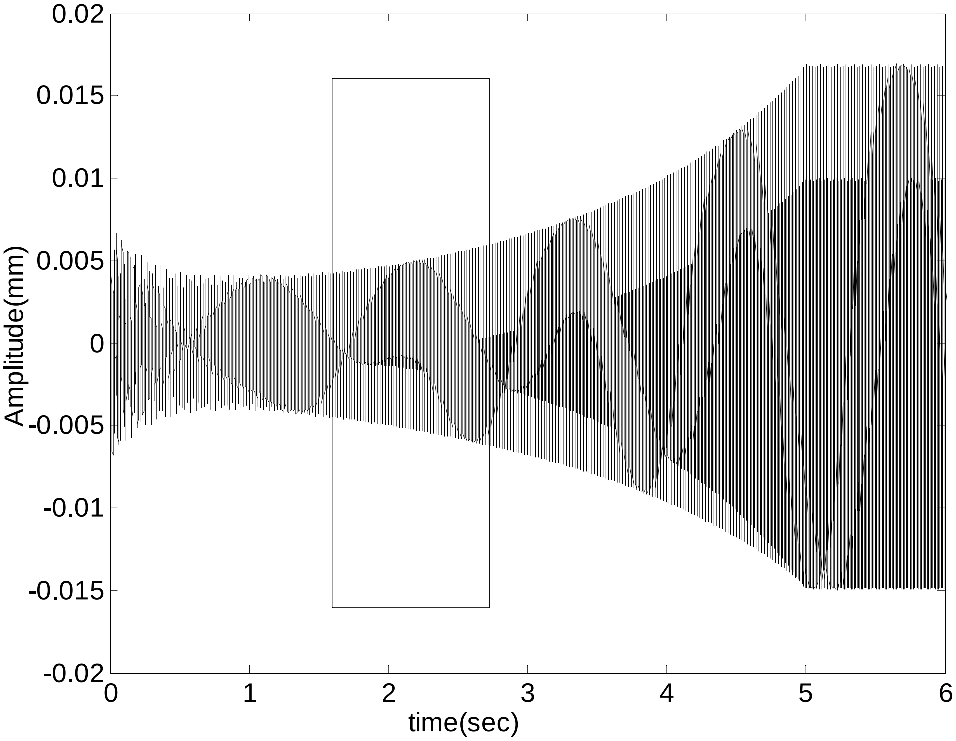

Figure 6.1 Rotor vibration time history for *hr* being varied from 0.0 to 0.06. The boxed portion is enlarged and shown again in Figure 6.2(a) for better visibility

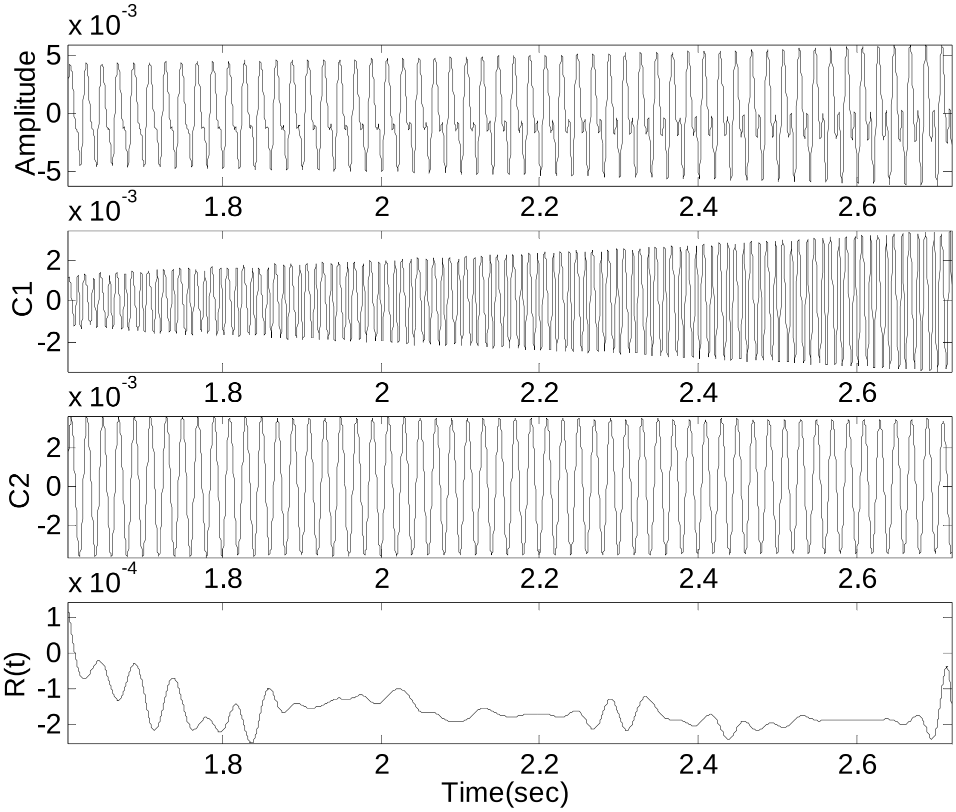

(a)

Figure 6.2 (a) Time waveform and its IMFs, (b) Instantaneous frequencies, and (c) Marginal spectrum for h_r being varied from 0.0 to 0.06

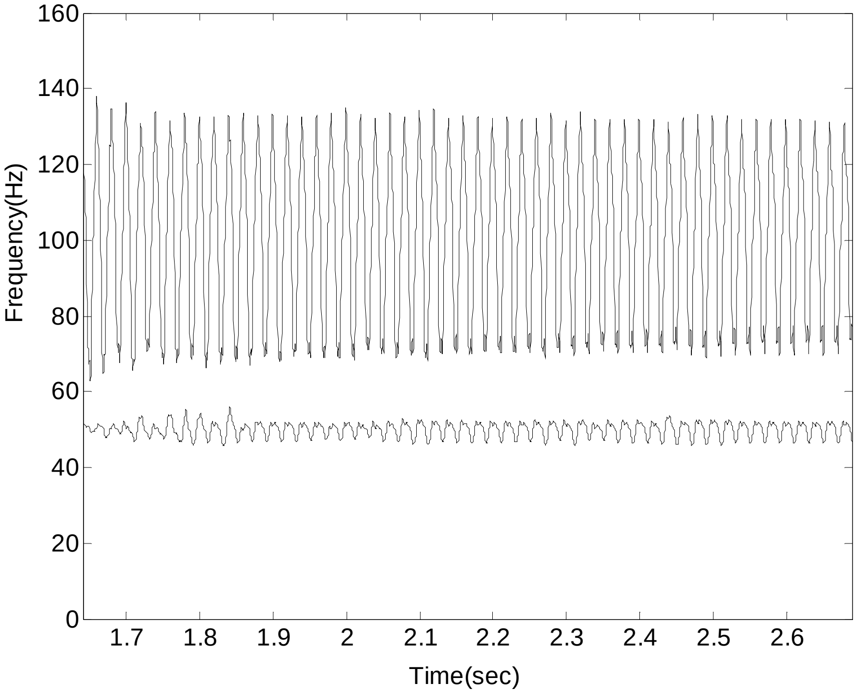

(b)

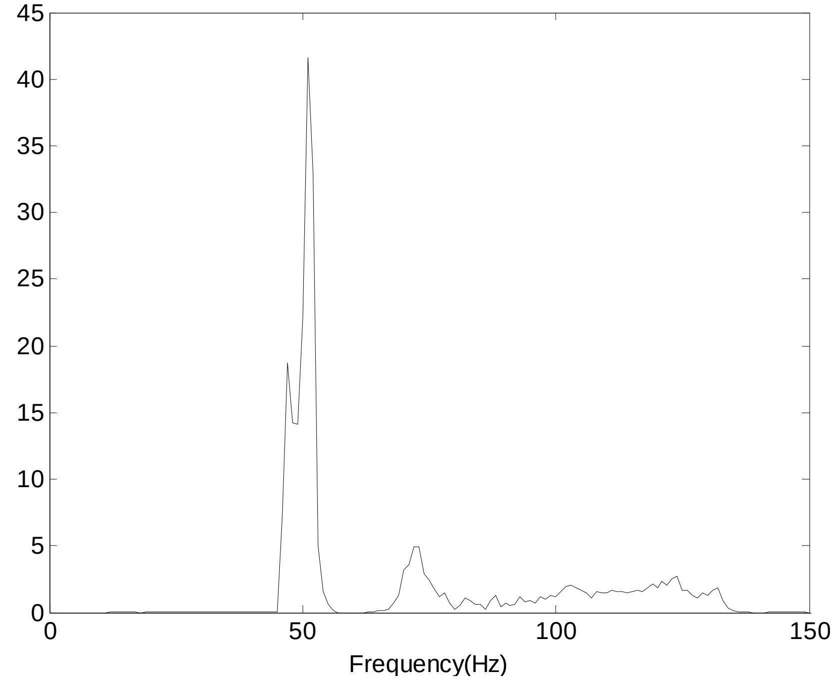

(c)

Figure 6.2 Continued

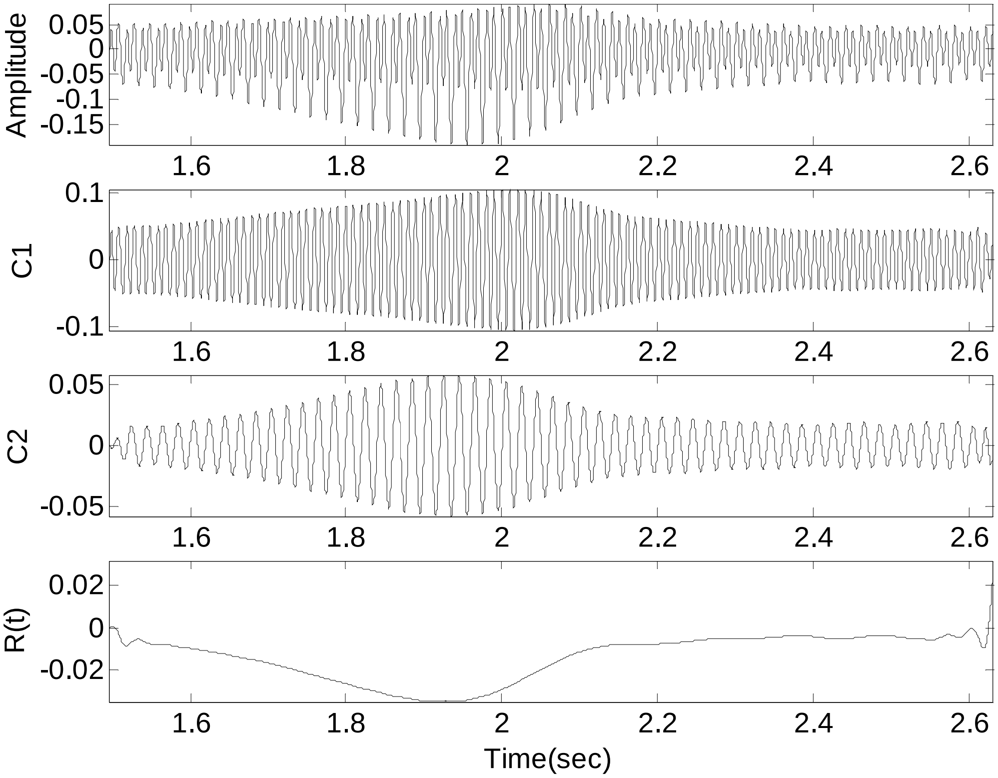

(a)

Figure 6.3 (a) Time waveform and its IMFs, (b) Instantaneous frequencies, and (c) Marginal spectrum for *hr* being varied from 0.08 to 0.1035

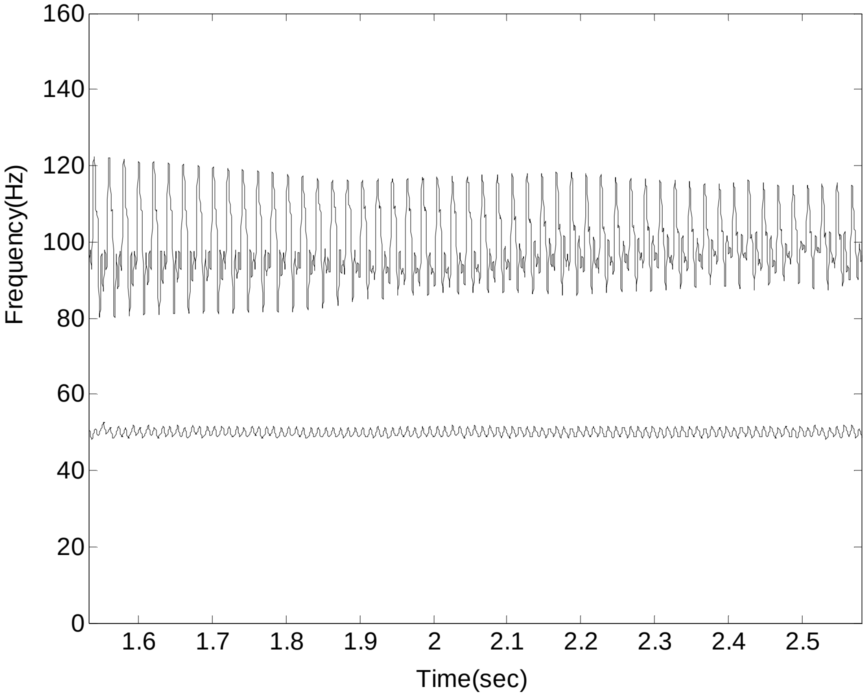

(b)

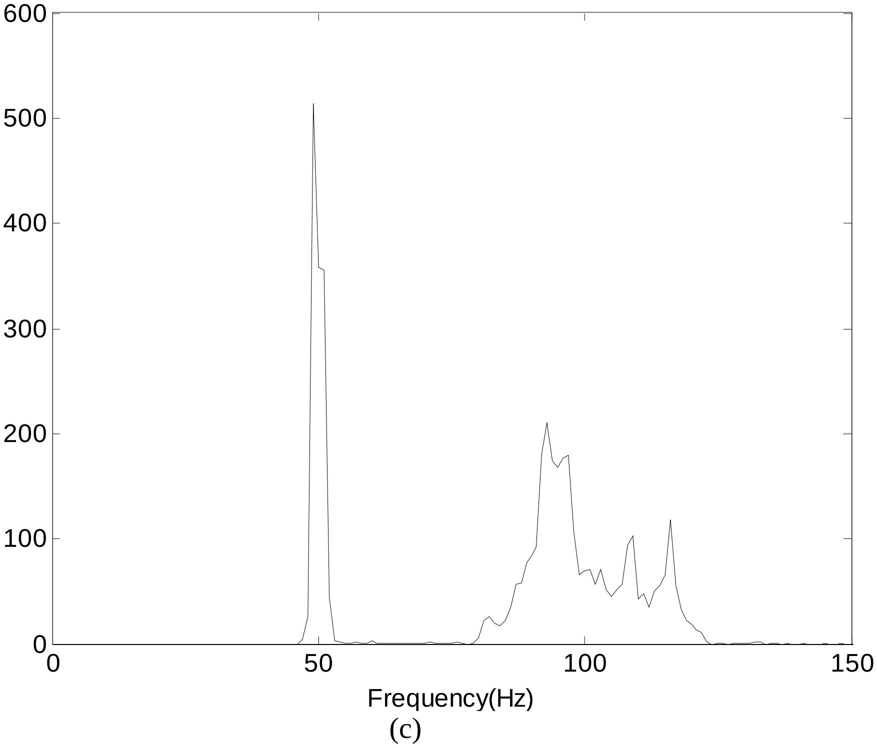

(c)

Figure 6.3 Continued

of empirical mode decomposition detailed in Chapter IV. While IMF C2 strongly suggests a harmonic motion and IMF C3 contains almost no frequency components, IMF C1 is comparatively more complex. Instantaneous frequencies resolved using C1 and C2 as plotted in Fig 6.2(b) show two modes that are fundamentally periodic and, thus, characteristic of a stable motion. The one mode at around 50Hz is evidently related to the driving frequency of the rotor and the one that oscillates rather noticeably about 100Hz in approximate is due to the nonlinear dissimilarity of the local flexibility as was proven the same by Dimarogonas [105] (see Eq. 5.15). However, as oppose to the observation made by Dimarogonas as the higher harmonic at twice the rotating frequency, instantaneous frequency interprets that the second mode is not a harmonic, but rather it demonstrates a temporal modal behavior oscillating periodically back and forth between 70 and 130 Hz. Similar interpretation is also made to the 50Hz mode, though whose modal oscillation is not as prominent. Because the continuous opening and closing of the transverse crack effectively affects both the stiffness and the effective cross-sectional area of the rotor -- the two primary parameters of which frequency is a function, thus, intuitively as well as physically the equivalent frequency ought to be varying from one rotary angle (or time instance) to the next. Indeed this physical essence is factually retained and revealed in the instantaneous time-frequency plane in Figure 6.2(b). The associated marginal spectrum depicted in Figure 6.2(c), which conveys the occurrence probability of the two instantaneous modal components within the 1.1-sec time window, shows that the 50-Hz mode is the dominant mode and that the 70-Hz frequency component in the 100-Hz mode is probabilistically more likely to be registered. This is the second inherent characteristic particular to this type of rotor response subject to small crack induced nonlinearity.

With the continual development of the crack, the rotor becomes increasingly unstable. Indications of incipient instability that precede the state of bifurcation can be seen in Figure 6.3

in which h_r is ranged from 0.08 to 0.1035. Again, the instantaneous frequencies resolved using the intrinsic modes shown in Figure 6.3(a) reveal two modal components, with one at 50-Hz and the other approximately at 100-Hz. Figure 6.3(b) shows that while the 50-Hz mode remains of the same characteristics as observed in the previous case, however, the higher mode does not. In spite of that the mode is still basically periodic with the period being measured to be approximately 0.02-sec, as the crack slowly opens further, a spurring feature accompanied by a gradual reducing of the oscillation amplitude is seen to appear and reappear at each rotor revolution. This particular feature can be seen to become indistinct in the neighborhood of t = 2.5 sec. As is evident from Figures 6.4(a) and 6.4(b) in which the case for h_r being varied from 0.102 to 0.113 is considered, the higher mode is now so obscured that within the initial 1.9-sec not just the specific spurring feature is gone but the definitive periodic structure is also lost. However, this brief display of aberration of the higher mode is seen to be accompanied at approximately t = 1.85 sec by the birth of a new mode at 25-Hz, which is half of the driving frequency. The corresponding IMF in Figure 6.4(a) (C3 to be exact) confirms that the mode is null before t = 1.85 sec. The presence of the third mode signifies the staging of the bifurcated state of period-doubling. Once period-doubling is brought about with the presence of the 25-Hz mode, it can be seen from both the IMF and instantaneous frequency plots that the higher mode abruptly regains a distinct periodic and modal structure at and beyond t = 2.0 sec and that, in the mean time, the driving 50-Hz mode migrates into a different modal structure. Thus, inception of the crack-induced bifurcation is not immediate, but rather is a progressive process indicated by the abnormal periodic-modal behavior of one of the modes and the simultaneous introduction of a new mode. In addition, hints of initiation of instability can also be collected through monitoring the marginal spectrum. A comparison of Figures 6.2(c), 6.3(c) and 6.4(c) shows that

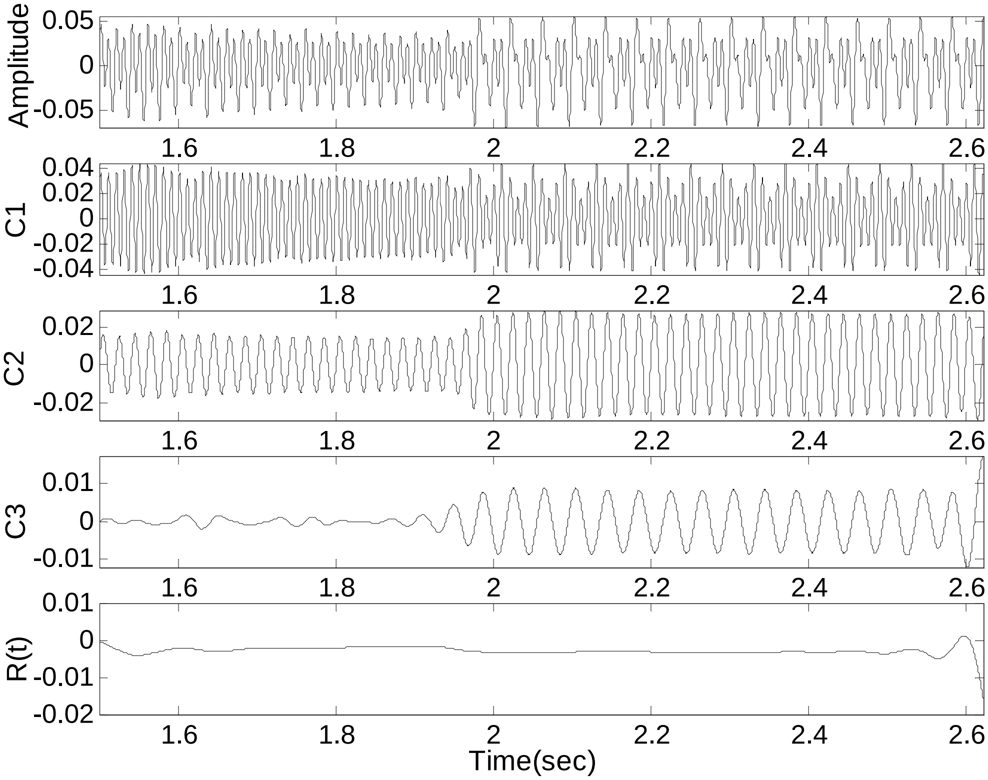

(a)

Figure 6.4 (a) Time waveform and its IMFs, (b) Instantaneous frequencies, and (c) Marginal spectrum for *hr* being varied from 0.102 to 0.113

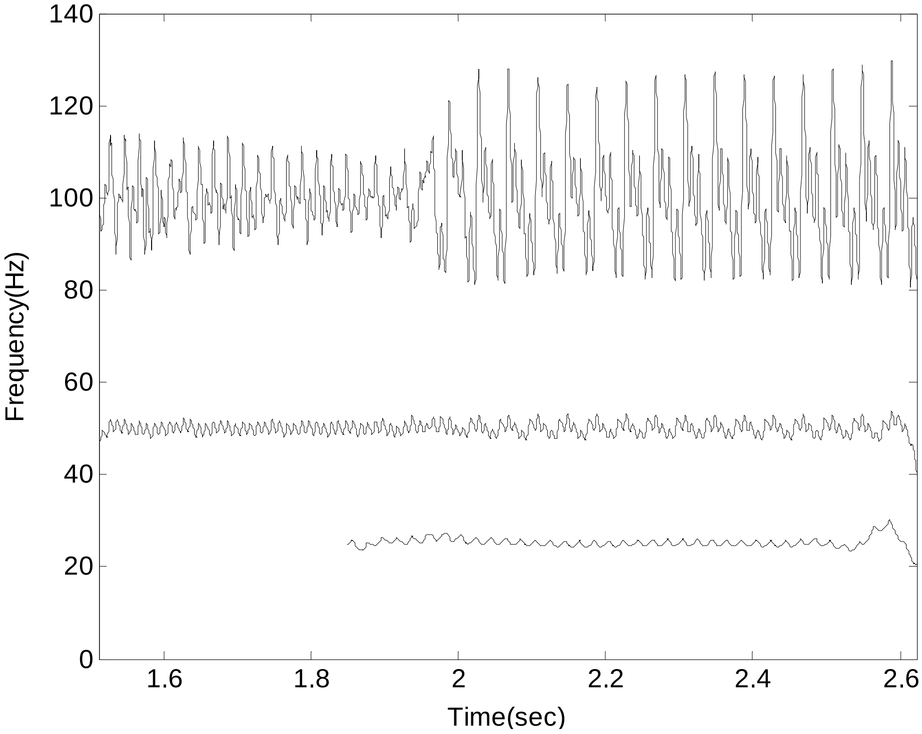

(b)

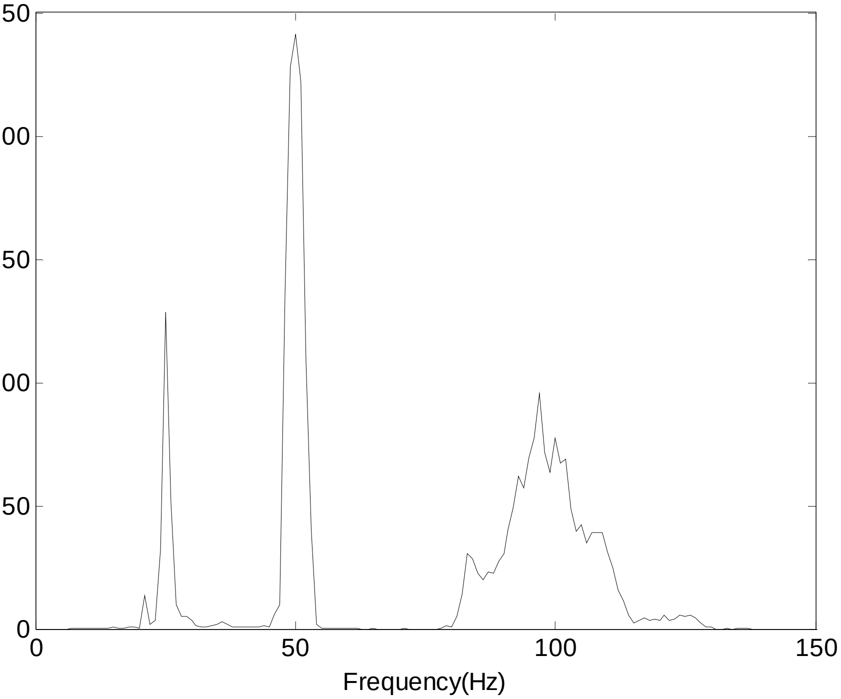

(c)

Figure 6.4 Continued

the probabilistically more dominant frequency component in the higher mode shifts with increasing weight from the initial 70-Hz to the eventual 99-Hz in Figure 6.4(c).

As h_r is further changed from 0.113 to 0.1155, rotor dynamic stability is seen to deteriorate and bifurcate further with more period-doubled modes. The waveform in Figure 6.5(a) now has one additional decomposed intrinsic function, C4, which contributes to the 12.5-Hz mode as seen in Figure 6.5(b). Unlike the previous case where the first period-doubled mode was seen born, the delivery of the second period-doubled mode is not preceded by aberrant simultaneous periodic-modal behaviors of one of the higher modes. Instead, the modal structures of all the three existing modes are seen to exhibit various degree of variation before t = 2.15 sec. In addition, a closer examination of Figure 6.5(b) reveals the followings: 1) the respective periodic structure of the three modes is relatively unchanging, and 2) the periods of the two higher modes are approximately twice the revolution period (0.02-sec). In Figures 6.2(c) and 6.3(c) the periods of the 100-Hz mode are both 0.02-sec, meaning the modal structures reappear at every rotor revolution. Starting at the birth of the third mode, however, the reappearing period of the 100-Hz mode, along with the driving 50-Hz mode as seen in Figure 6.4(b), becomes a noticeable 0.04-sec. That is, the presence of the frequency-halving new mode goes concurrently along with the period-doubled old modes. Sure enough, the periods of modes 100-Hz, 50-Hz, and 25-Hz are all doubled upon the introduction of the 12.5-Hz mode in Figure 6.5(b). Additionally, the lower three modes are noted in the marginal spectrum found Figure 6.5(c) to demonstrate vigorous modal association with their immediate neighboring modes beyond t = 2.2 sec. Modal association necessarily eclipses identifying the dominant modes and frequency components and therefore, if all individual modes were not properly disassociated, would obscure the true dynamic characteristics of the nonlinear motion. Such an association bespeaks the extent to which the bifurcated state of dynamic instability has reached, thus

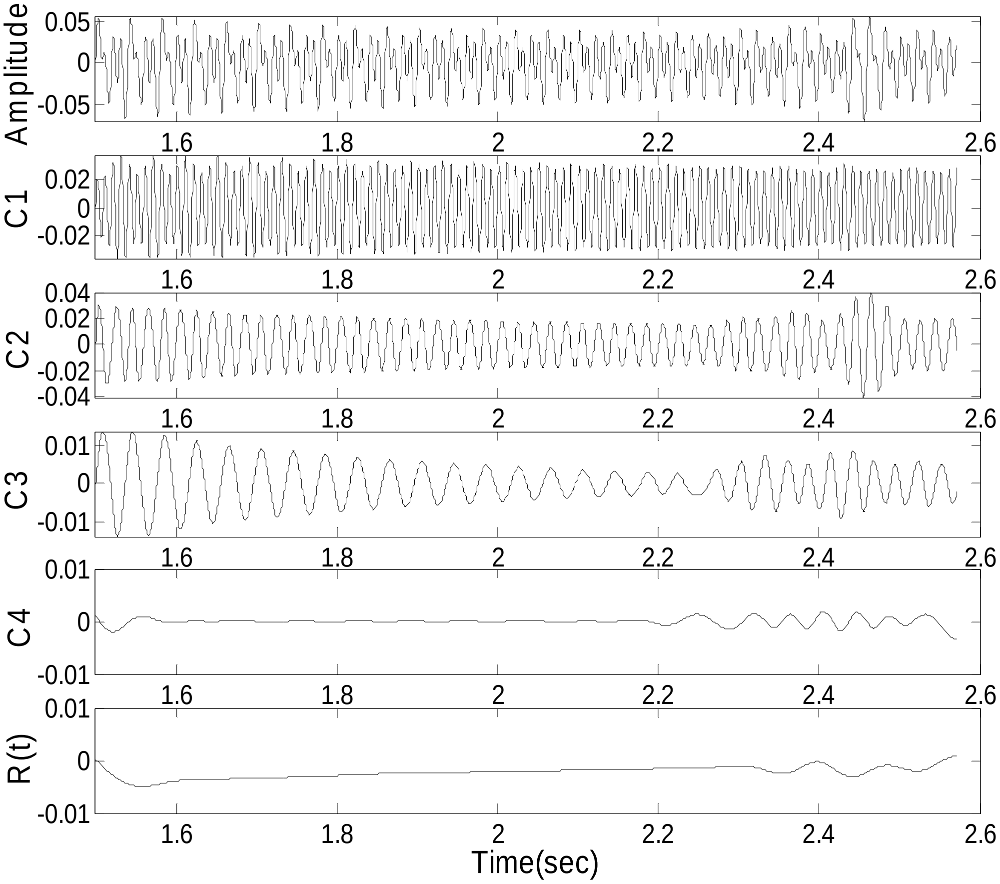

(a)

Figure 6.5 (a) Time waveform and its IMFs, (b) Instantaneous frequencies, and (c) Marginal spectrum for *hr* being varied from 0.113 to 0.1155

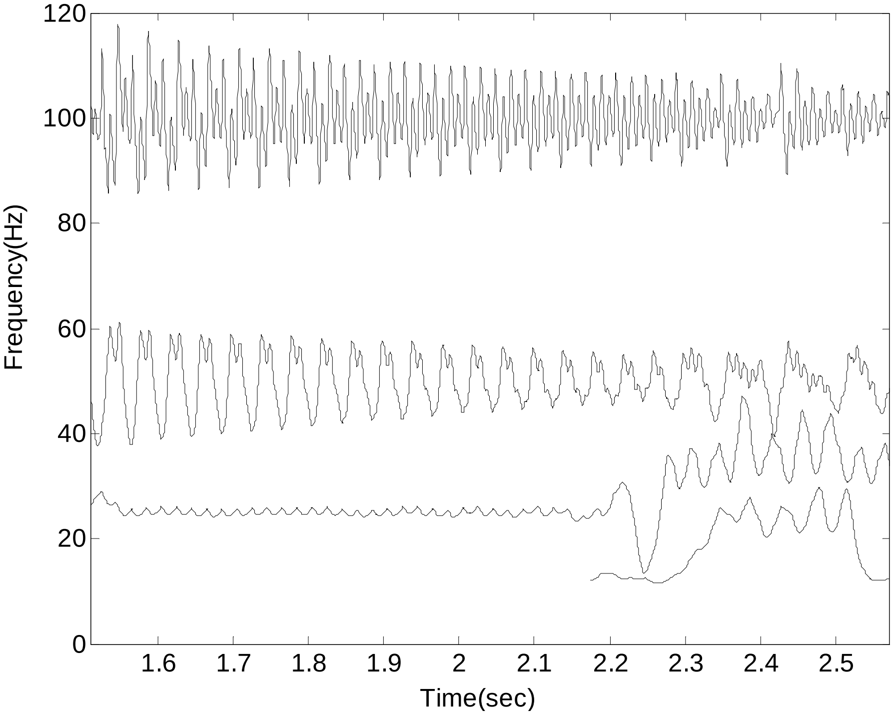

(b)

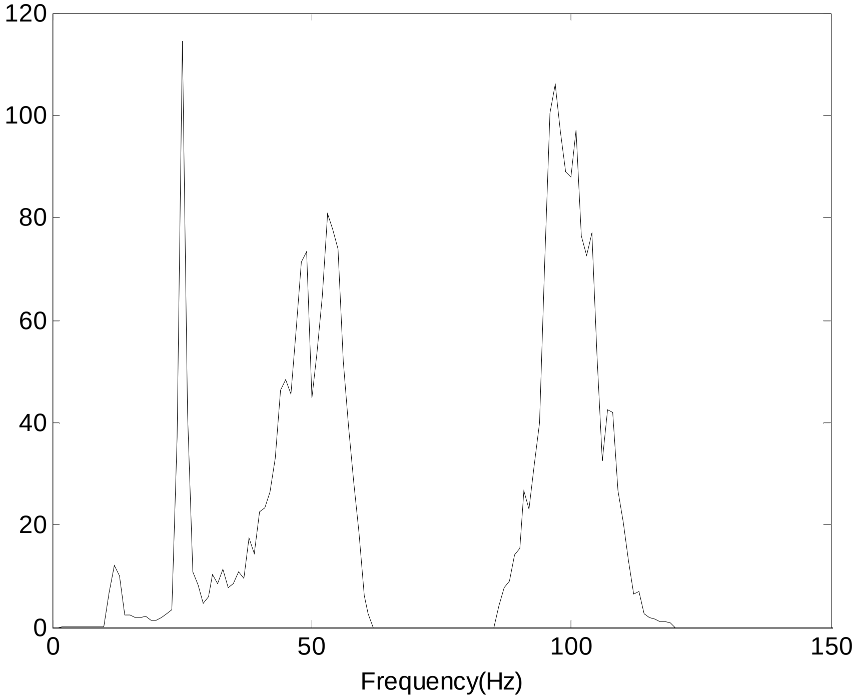

(c)

Figure 6.5 Continued

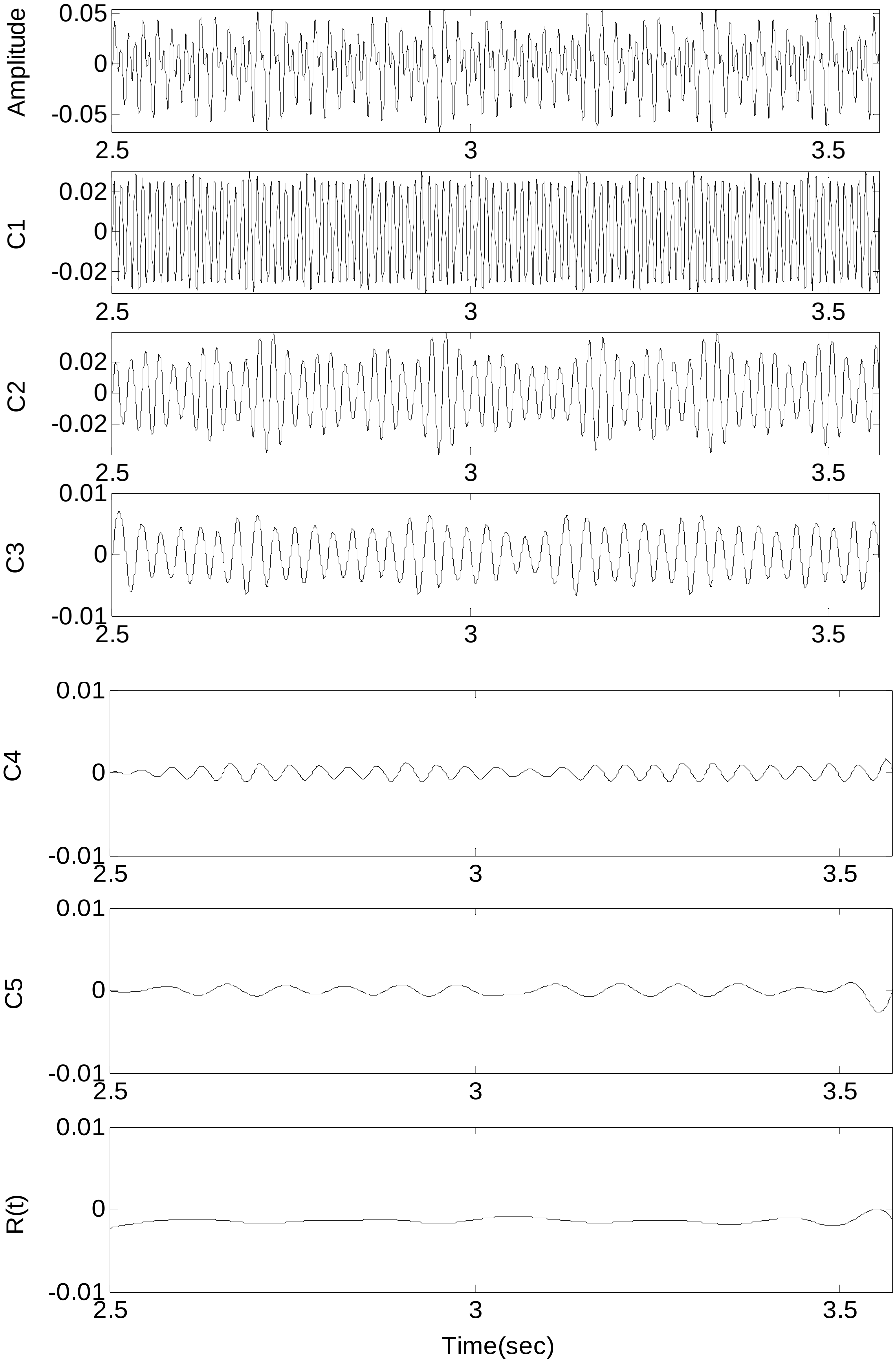

(a)

Figure 6.6 (a) Time waveform and its IMFs, (b) Instantaneous frequencies, and (c) Marginal spectrum for *hr* = 0.1155

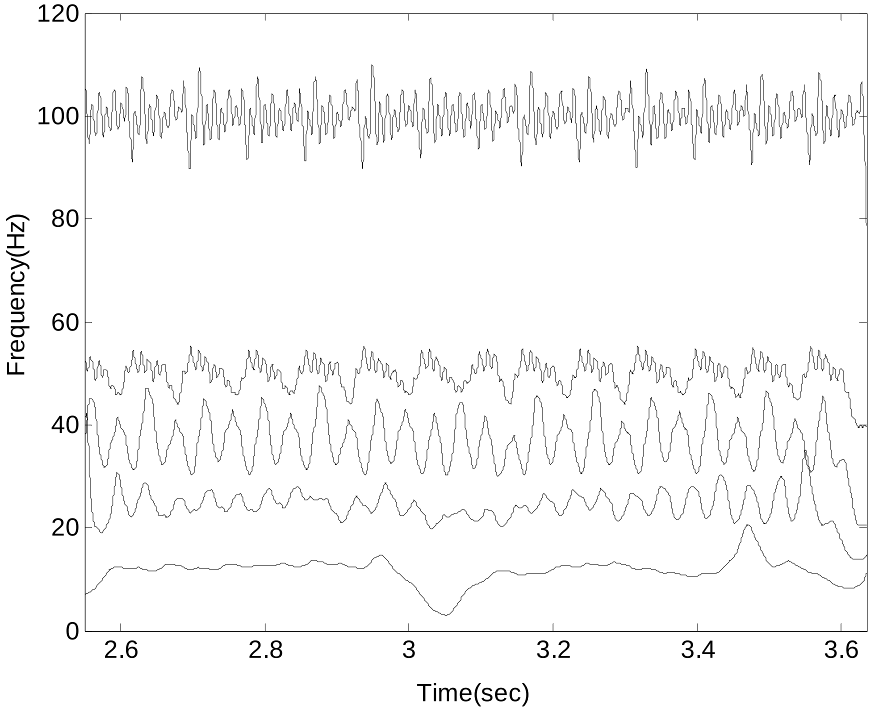

(b)

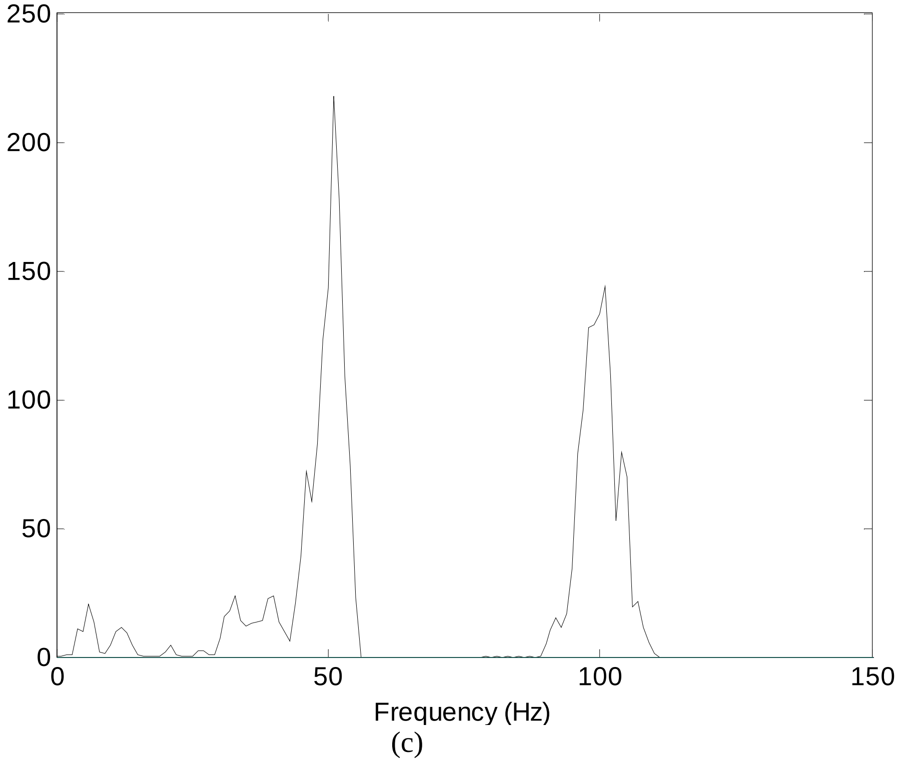

(c)

Figure 6.6 Continued

indicating the imminence of the chaotic state and eventual failure that is to follow.

When h_r is allowed to stay unchanged at 0.1155, the rotor response bifurcates further with the appearance of a fourth mode at 37.5-Hz, which corresponds to the IMF C3 in Figure 6.6(a). All the characteristics previously identified associated with period-doubling bifurcation are again observed in Figures 6.6(b) and 6.6(c). However, the new mode is not a further frequency-halving of the 12.5-Mz mode, but a mode at approximately 37.5-Hz. With the bearing of the new mode, the modal association as realized in the marginal spectrum in Figure 6.6(c) now carries a broadband feature whose probabilistically dominant modes are even more obscured with sufficiently less energy as compared to Figure 6.5(c). Strong modal association as seen in this very example had presented a challenge in disassociating the multitude modes of period-doubling with satisfactory temporal and modal resolution. Specifically, as the lowest (12.5-Hz/C3) mode carries relatively less energy (i.e., small amplitude in time and low cumulated weight in marginal spectrum) and also due to the inherent oscillation of instantaneous frequencies, it was difficult to be separated using the presented methods. Nevertheless, as the rotor responds chaotically at a slightly longer c4rack length at $h_r = 0.1156$ [4], further bifurcation is not anticipated and therefore not studied. Finally, it should be commented that since the Hilbert transform of all the IMFs considered in the presented example were implemented using the same algorithm developed for the Fast Fourier Transform (FFT), it is then inevitable to have the Gibbs end effects as seen in Figures 6.2(c)-6.6(c).

6.2 Discussion

The rotor model considered in the chapter, which is elastically supported and subjected to the breathing and slow propagation a transverse surface crack, has seen to generate many elegant nonlinear responses and bifurcations. They include super-harmonic bifurcations resulted from crack-induced dissimilar flexibility and period-doubling bifurcations borne out of the propagation of the crack. The Empirical Mode Decomposition (EMD) scheme was utilized to separate a multi-component vibration signal into its orthogonal mono-component subsets called the Intrinsic Mode Function (IMF) and then the Hilbert transform was applied to each IMF to obtain instantaneous amplitudes and frequencies. It was demonstrated that the fundamental concepts of instantaneous frequency and amplitude are viable for the effective interpretation of non-stationarity and nonlinearity. In addition, all obtained results using the instantaneous frequency were shown to be highly intuitive and physically reasonable. As the amplitude of the super-harmonic mode increases continuously with the continual development of a transverse crack, it is potentially probable to achieve crack detection through monitoring the crack-induced super-harmonic modes. As was demonstrated in Fig 6.2 (a), the very moment when a bifurcation occurs can be identified using the IMFs. Being able to do this is a significant advancement in the study of nonlinear dynamics and nonlinear time series analysis. When the cracked rotor model underwent transition from one dynamic state to another, the corresponding instantaneous frequencies demonstrated periodicity-mode aberrations. After the transition, all modes involved became periodic functions of time, thus complying with the physical nature inherent of the crack-induced dissimilar flexibility defined to accommodate shaft stiffness as a function of rotating angle and time. In characterizing chaotic motions, IMFs were shown to faithfully resolve all the modes inherent in the original signal and their associated instantaneous frequencies revealed the aperiodic nature characteristic of a chaotic motion. In addition, the marginal spectrum was shown to be another powerful tool for quantifying the nonlinearity within the rotor system and for monitoring the occurrence of bifurcation.

CHAPTER VII

RESULTS OF ROTOR-JOURNAL BEARING MODEL WITH CRACKED SHAFT

7.1 Description of Results

All rotor systems have certain degrees of mass imbalance that could induce excitations at the running speed and other nonlinear responses. Therefore, it is important to be able to predict such responses of a multi-degree of freedom rotor system subject to different rotating speeds and parameter ranges of interest. In this section, the nonlinear response of a rotor system with disk imbalance and supported by two plain journal bearings is investigated. The transition from one dynamic state to another is identified using the instantaneous frequency. Shaft and disk parameters were given in Chapter V and parameters associated with the journal bearings are that r = 0.07m, Cr(clearance) = 0.0025r and bearing length, BL = (1.0)D = (1.0)(2r) = 0.14m. As stated previously, displacement, velocity and acceleration are normalized using

$$X = \frac{x}{Cr}; \quad \dot{X} = \frac{\dot{x}}{Cr\omega}; \quad \ddot{X} = \frac{\ddot{x}}{Cr\omega^2}; \quad t = \frac{\omega\tau}{2\pi} \tag{7.1}$$

Note that the variable time is normalized using $\frac{\omega}{2\pi}$ and thus the frequency is also normalized. Specifically, as the un-normalized period ranges from 0 to $\frac{2\pi}{\omega}$, the normalized frequency of value 1 thus corresponds to $\frac{\omega}{2\pi}$ Hz in un-normalized frequency. Following the same token, normalized frequency of value 2 is thus $\frac{\omega}{\pi}$ Hz in physical frequency. In addition, normalized frequency 1 is the forcing frequency, normalized frequency 2 is a super-harmonic frequency and normalized frequency 0.5 is a subharmonic frequency, with the latter representing the case of a period-doubling bifurcation.

When rotor speed is low, the system response is stable if subject to no cracks in this system. Without the presence of fatigue crack in the rotor, however, if the rotor is supported by fluid-film bearings, the entire rotor-bearing system could still become unstable when the rotating speed exceeds certain critical value. This critical value can be determined using methods of linearization. Beyond this threshold/critical value the system would become exponentially unstable according to linearized methods. As demonstrated in Chapter II contrasting the result obtained using a linearized model with that of a nonlinear dynamic model, significant nonlinear phenomena including chaos can occur if the critical value is exceeded. As reported in [5], violation of the critical value could result in either catastrophic dynamic failure or restoration of stability – two nonlinear phenomena of significant implication that cannot be realized using linearized methods. Although fluid bearings induced nonlinearity and nonlinear responses have been much investigated [5,15,19, 34-35], no report on the study of crack-induced nonlinear responses in a rotor-bearing system supported by fluid bearings has ever been presented. In the section that follows, crack and film pressure induced nonlinear responses are explored using, again, the concept of instantaneous frequency. As will be shown later, the presence and continual development of cracks greatly impact the dynamics of the rotor-bearing system at, especially, low rotating speeds.

At a given speed, increasing the relative flexibility, h_r, would first bring about periodic motion and subsequently nonlinear rotor-dynamic responses of instability including period-doubling, quasi-periodic motion and eventual chaos. Because there were no discernible differences in the rotor-dynamic responses corresponding to the range of crack depth considered, certain selected cases presented in the following assume constant crack depth; that is, constant

h_r. In all other cases, h_r is increased linearly from an initial value to a final value over 4000 time steps. A normalized time step $\Delta t = 0.02$ is used to integrate the rotor vibration response from 0, thus meaning that every rotating cycle has 50 points, a sampling rate that is sufficient to resolve the highest frequency at $\frac{25\omega}{2\pi}$. The relative flexibility is varied between t = 240 and t = 320 (4000 time steps as stated above) and is kept constant afterwards. For the sake of visualization, only the portion of data registered between t = 240 and t = 400 (8000 time steps) are analyzed and presented, to show the transition as experienced by the rotor subject to crack opening. The (normalized) *Y*-direction response components of the left bearing are considered in the following analysis.

First consider the case of low rotating speed at 900 rpm ($\omega = 30\pi$). When there is no crack, the system displays characteristics indicative of stable periodic motion. When the crack is allowed to develop to a fairly small depth, the crack opening is seen to prominently affect the dynamics of the system and a super-harmonic bifurcation occurs. Figure7.1 shows the orbit of the journal center of and the FFT of the response at $\omega = 30\pi$ and $h_r = 0.012$. The plot of orbit is conceptually identical to the phase portrait. As it also shows the position of the journal center, so the orbit of the journal center is thus used in the study. Closed orbits in the normalized X-Y plane as seen in Figure 7.1(a) indicate that either super- or sub-harmonic bifurcation has happened. From the spectrum in Figure 7.1 (b), in addition to the forcing frequency at 1, there are also super-harmonic frequency components at 2, 3 and 7. Figure 7.2(a) gives the time history of the response, along with its decomposed intrinsic modes C1 and C2 obtained using the Empirical Mode Decomposition (EMD). The C2 mode is the forcing frequency and has large amplitudes, while the C1 mode shows high frequency with low amplitude. The residue contains almost no frequency components. (Note that the slight wiggling at its two ends is attributable to

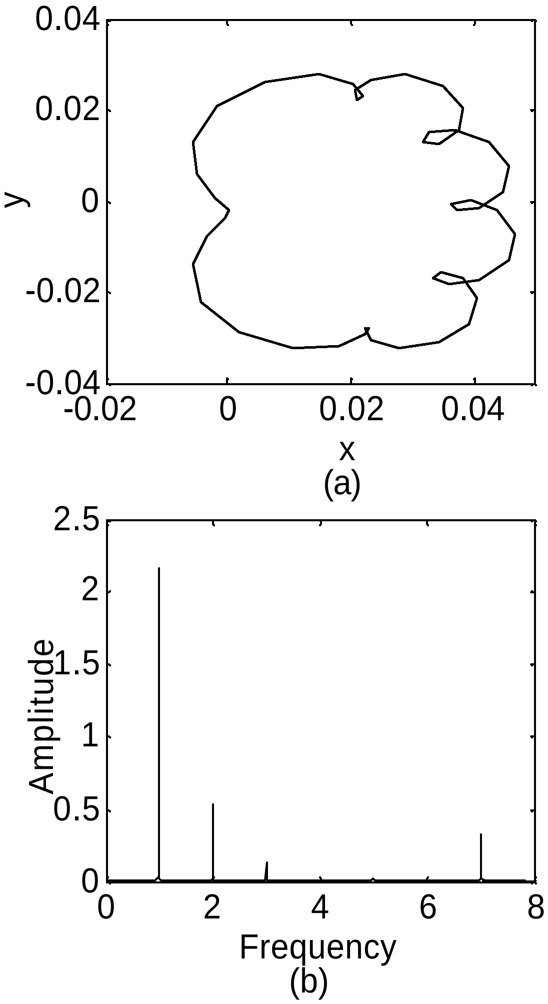

Figure 7.1 (a) X-Y orbit of the journal center at $w = 30\pi$ and $h_r = 0.012$. (b) Spectrum of the response in (a)

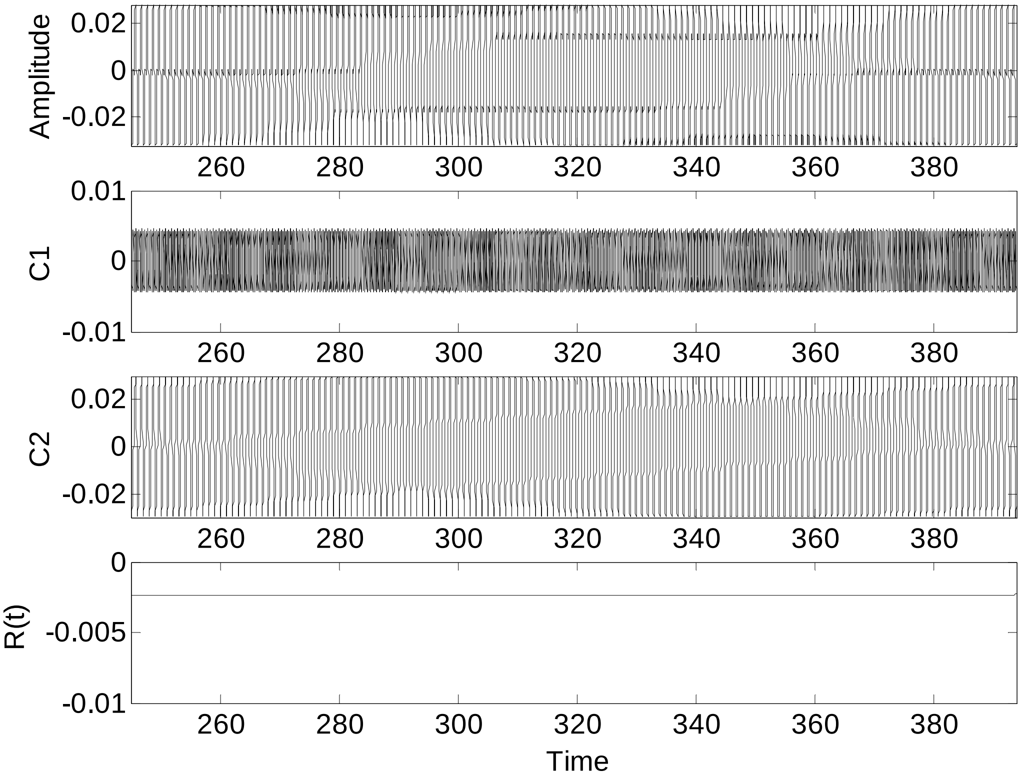

(a)

Figure 7.2 (a) Time waveform and its IMFs, (b) Instantaneous frequencies, and (c) Marginal spectrum for $\omega = 30\pi$ and $h_r = 0.012$

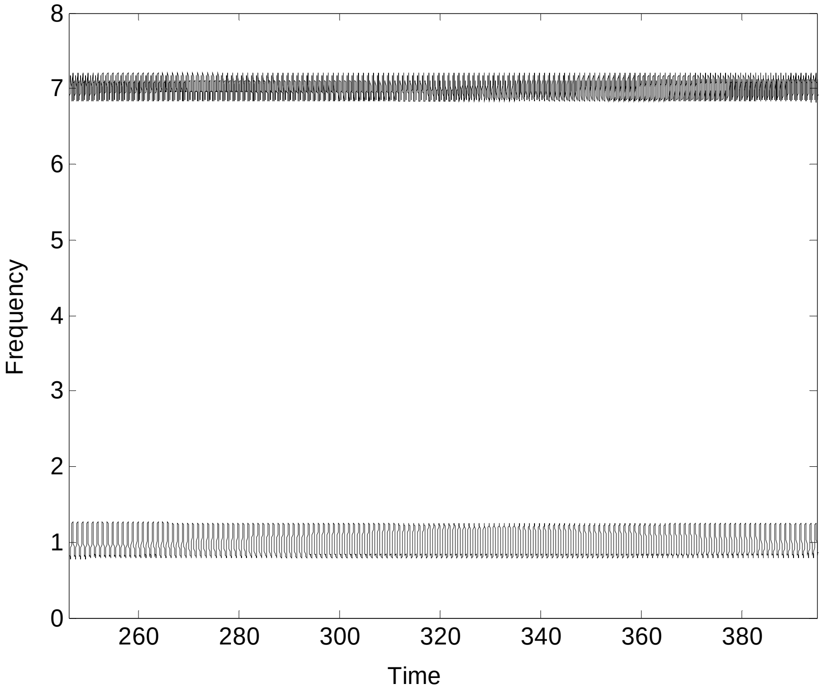

(b)

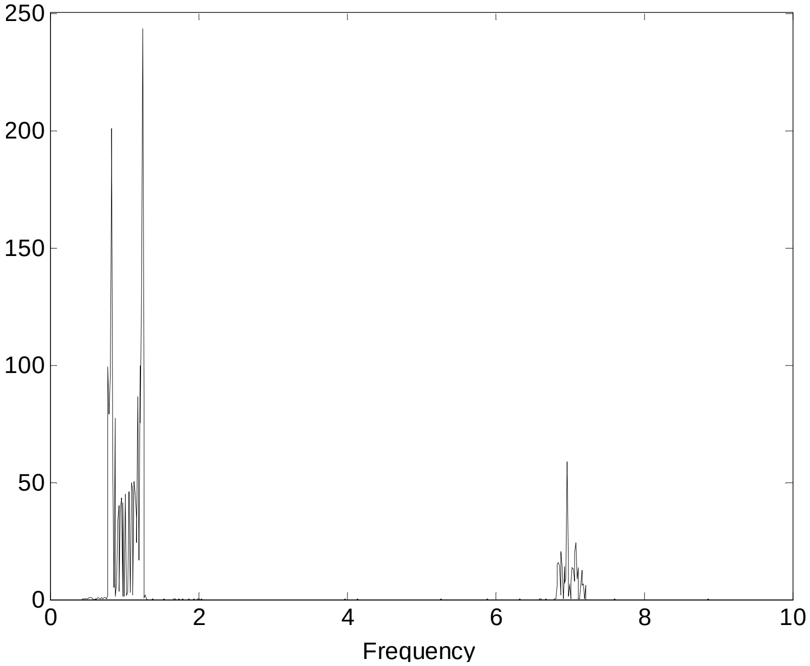

(c)

Figure 7.2 Continued

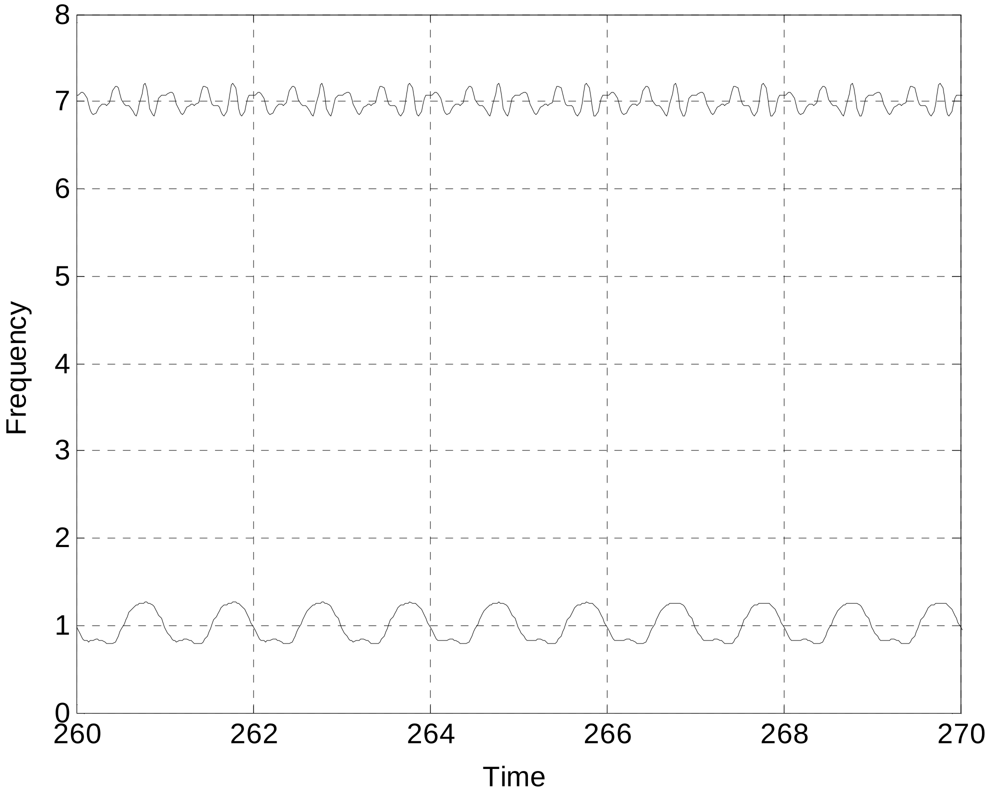

Figure 7.3 Changes of instantaneous frequency in response to crack opening and closing

the end effect of the EMD.) Instantaneous frequency computed using C1 and C2 as plotted in Figure 7.2 (b) indicate two modes that are fundamentally periodic. The mode at about 1 is clearly the forcing frequency and the one around 7 is the new mode corresponding to the super-harmonic bifurcation. Instead of constant-amplitude, constant-frequency as is interpreted by the Fourier transform, the instantaneous frequency interprets that both modes are not simple harmonics, but rather they demonstrate oscillations between 6.9 and 7.1, and 0.8 and 1.2, respectively. As discussed in the previous section, the continuous opening and closing of the transverse crack physically, though locally, alters the effective cross-sectional area, and thus the stiffness, of the shaft. Therefore the breathing behavior of the crack would impact the spectral response in the way that the frequency spectrum is no longer invariant respect to time. Figure 7.2 (b) shows exactly this variation in time (at each angular position). Again, instantaneous frequencies determined for the case at hand does reveal the physical essence of this subtle variation. Figure 7.2 (c) shows the accumulative effect of the instantaneous frequency components in a probabilistic sense. By monitoring these components, changes in dynamic states and initiation of bifurcation can be detected. As a brief example, suppose the 7 component appears in the marginal spectrum and increases continuously, then it can be concluded that a super-harmonic bifurcation is occurring.

In addition, instantaneous frequency offers a powerful tool to study the frequency modulation within a period. A period is defined as the time duration for an oscillation starting from an equilibrium point to a maximum point, then to a minimal point and eventually returning back to the same equilibrium point. And the reciprocal of the defined period is frequency [87]. According to this definition, the frequency variation within this period can never be detected at all. However, the concept of instantaneous frequency can readily deal with this variation, thus signifying a long-waited while important breakthrough for the study of nonlinear, non-stationary time series. To demonstrate, Figure 7.3 shows a clear view of the variation of instantaneous frequencies within one period of the signal in Figure 7.2. At the beginning, the crack starts to open and the stiffness local to the crack position decreases accordingly. This is fully realized as the decreasing instantaneous frequency. After ¼ period, the local stiffness is restored as the crack closes and thus the corresponding instantaneous frequency is seen also restored. The instantaneous frequency variation in the other half period is the result of the interaction between the rotary angle and system inertia. The change of instantaneous frequency at approximately frequency 7 is highly involved and the interpretation of it will require further research.

Comparing the Fourier-based spectrum to the instantaneous frequency show that there are four frequency components 1,2,3 and 7 resolved in the Fourier spectrum, while there are only two modes in the instantaneous time-frequency domain. In order to explain this disparity, a sample monocomponent signal of small frequency change is adopted from [36] as follows

$$x(t) = \cos(\omega t + \varepsilon \sin(\omega t)), \varepsilon > 0 \tag{7.2}$$

Here ε is a very small positive number, the amplitude *a* = 1. The corresponding phase is

$$\phi(t) = \omega t + \varepsilon \sin(\omega t) \tag{7.3}$$

and the instantaneous frequency is

$$\omega(t) = \frac{d\phi(t)}{dt} = \omega(1 + \varepsilon \cos(\omega t)) \tag{7.4}$$

Using Eq. 7.2, the following process is derived

$$\begin{aligned} x(t) &= \cos(\omega t + \varepsilon \sin \omega t) \\ &= \cos \omega t \cos(\varepsilon \sin \omega t) - \sin \omega t \sin(\varepsilon \sin \omega t) \\ &\approx \cos \omega t - \varepsilon \sin^2 \omega t \qquad [\sin^2 \omega t = \frac{1}{2}(1 - \cos(2\omega t))] \\ &= -\frac{1}{2}\varepsilon + \cos \omega t + \frac{1}{2}\varepsilon \cos(2\omega t) \end{aligned} \tag{7.5}$$

From Eq. 7.4, the true frequency ought to be oscillating about ω; however, the Fourier transform gives a frequency that is 2ω in value. Where does this doubled frequency come from? The explanation is simply that the Fourier transform employs harmonics to approximate physical signals in the infinite integral sense. Should the use of one harmonic is insufficient, two or more harmonics would be taken on to achieve maximal approximation. The fact that the mathematical soundness of the Fourier transform necessarily obscures the true characteristics inherent of physical system speaks in volume that mathematical success does not always guarantee its physical admissibility and reasonability [36]. In summary, though some resolved Fourier components may not be physically admissible and outright fictitious, but because the mathematical transform needs them to approximate the physical signal, these components appear.

When the rotating speed is increased to 1500 rpm ($\omega = 50\pi$), even without the presence of cracks, a period-doubling bifurcation is seen to occur in the system response of very small vibration amplitude. The orbit of the journal center given in Figure 7.4 is clearly evident of a period doubling bifurcation. The system is then subjected to crack propagation facilitated through linearly increasing h_r from 0.0003 to 0.001. Figure 7.5(a) shows that there are only two extracted intrinsic modes and the corresponding instantaneous frequency plot in Figure 7.5(b) displays one mode at frequency 1 and the other at frequency 0.5. Furthermore, while the frequency 1 mode demonstrates similar characteristics as observed in the case previously considered, the ½ order subharmonic mode appears in the frequency, thus bespeaking a birfurcated state of period doubling. From the C2 intrinsic mode in Figure 7.5(a), it is clear that the period doubling bifurcation gradually disappears with the further development of the crack. At the end of the data window, the mode is seen decreasing to almost zero amplitude. With the amplitude becoming small, the instantaneous frequency becomes broadband as shown in Figure

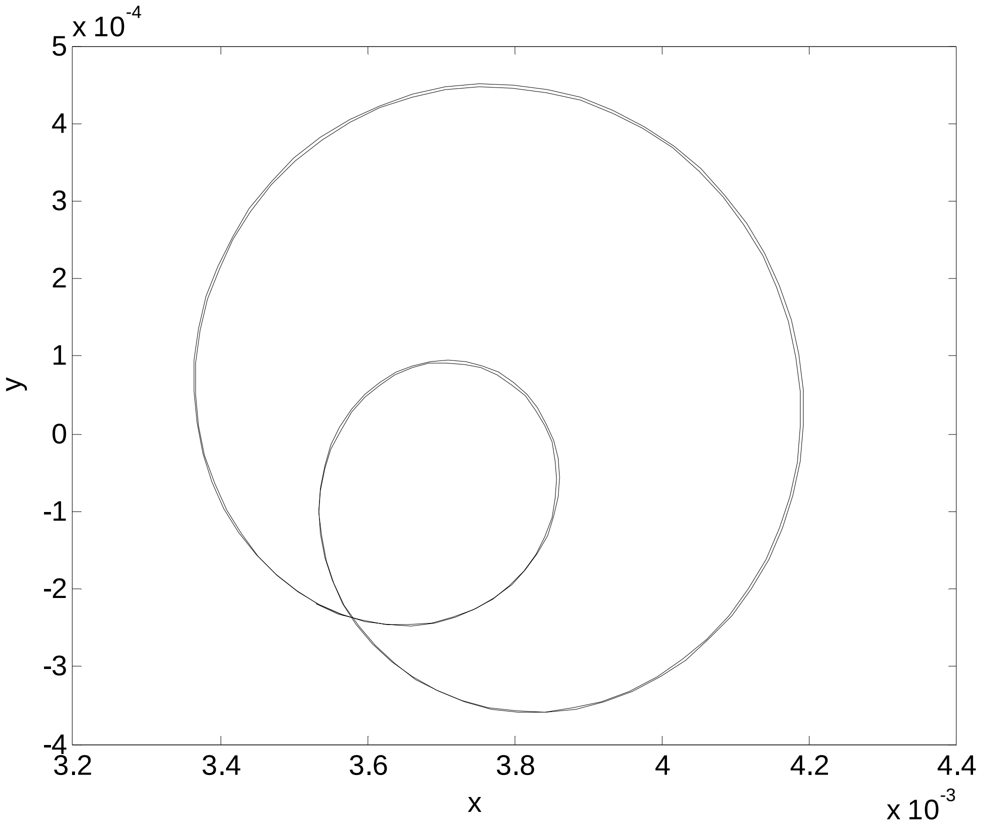

Figure 7.4 Orbit of journal center at $\omega = 50\pi$ rad/s indicating a period doubling motion

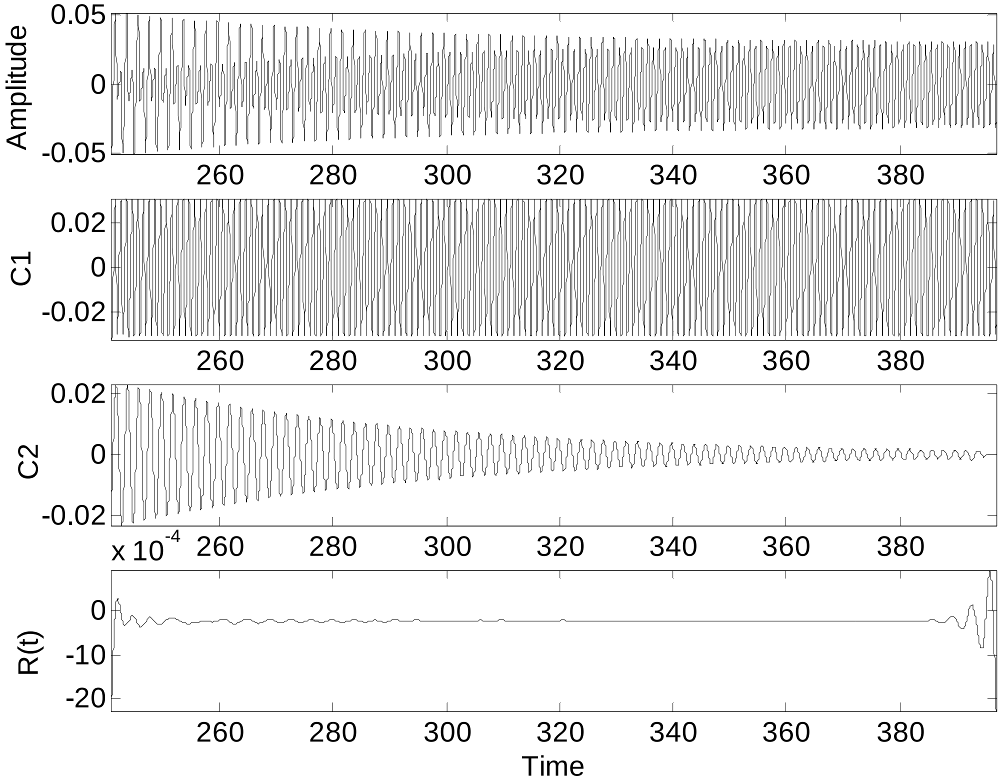

(a)

Figure 7.5 (a) Time waveform and its IMFs, (b) Instantaneous frequencies, and (c) Marginal spectrum for $\omega = 50\pi$ and h_r =0.0003 to 0.001

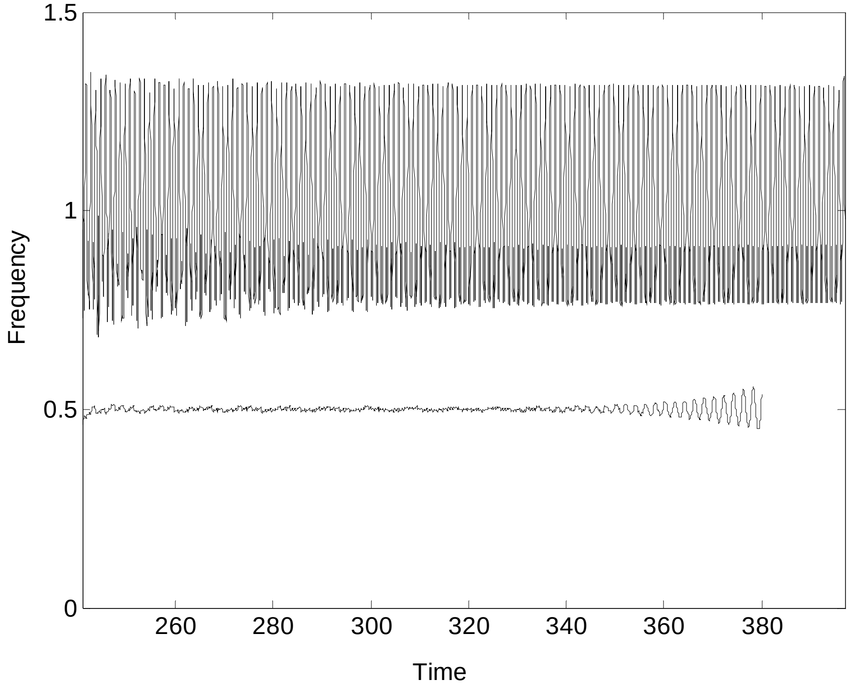

(b)

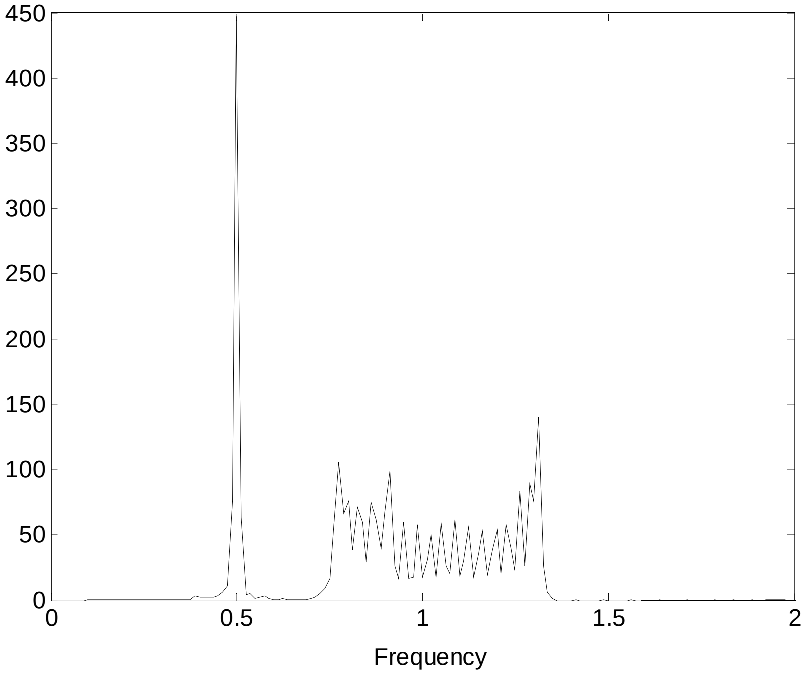

(c)

Figure 7.5 Continued

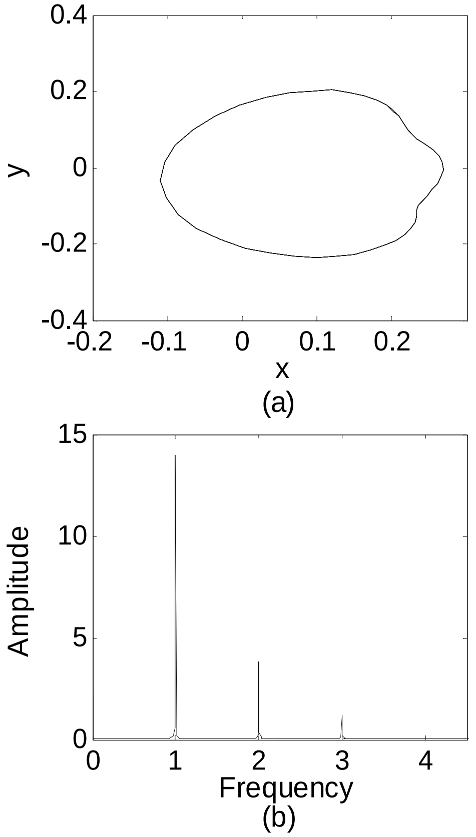

Figure 7.6 (a) Orbit of journal center at $\omega = 50\pi$ and $h_r = 0.09$. (b) Spectrum of the vibration signal in (a)

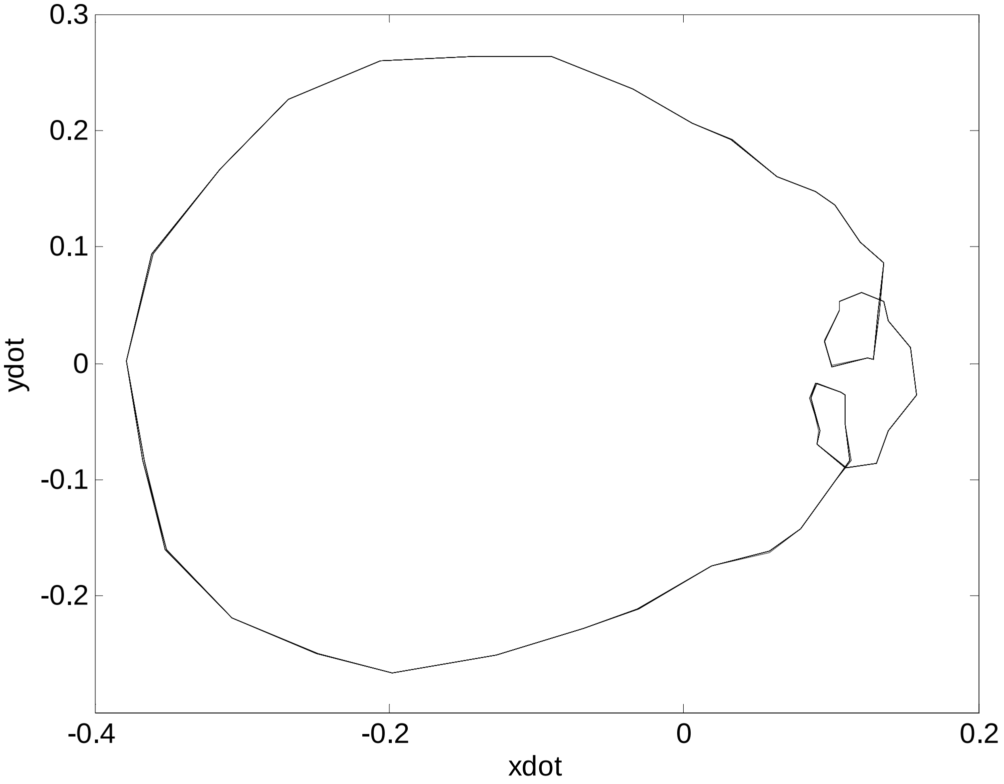

Figure 7.7 Speed variation of the journal center in X-Y direction at $\omega = 50\pi$ and $h_r = 0.09$

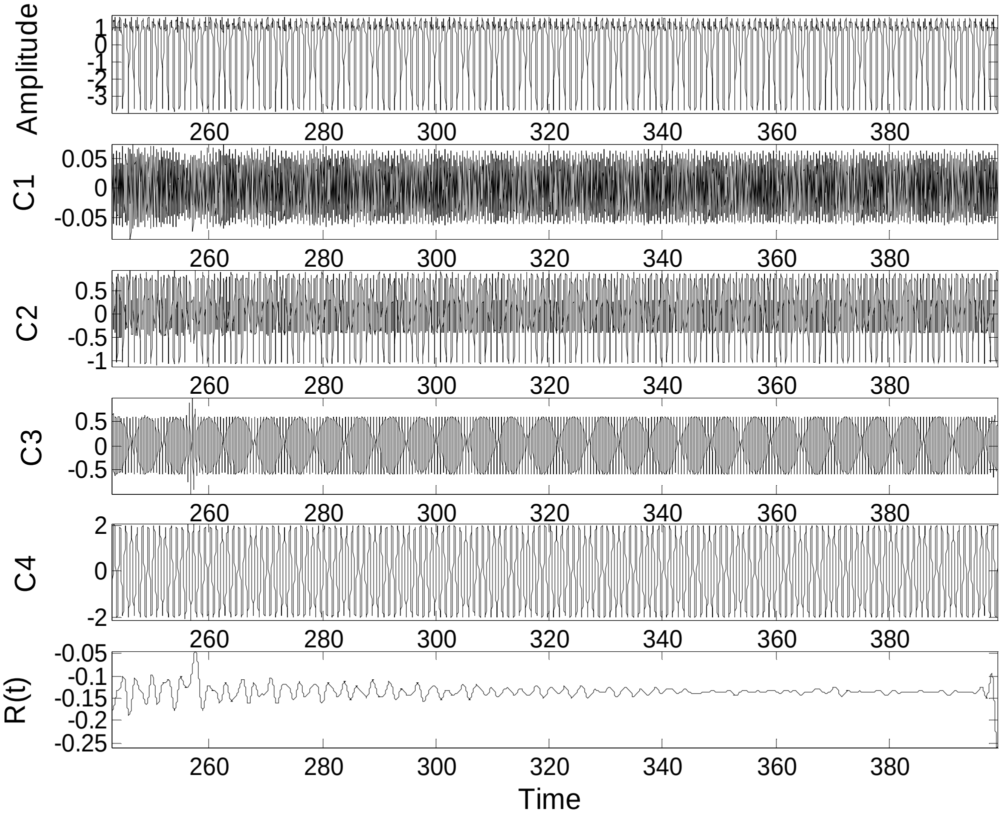

(a)

Figure 7.8 (a) Time waveform and its IMFs, (b) Instantaneous frequencies, and (c) Marginal spectrum for $\omega = 50\pi$ and $h_r = 0.06$ to 0.09

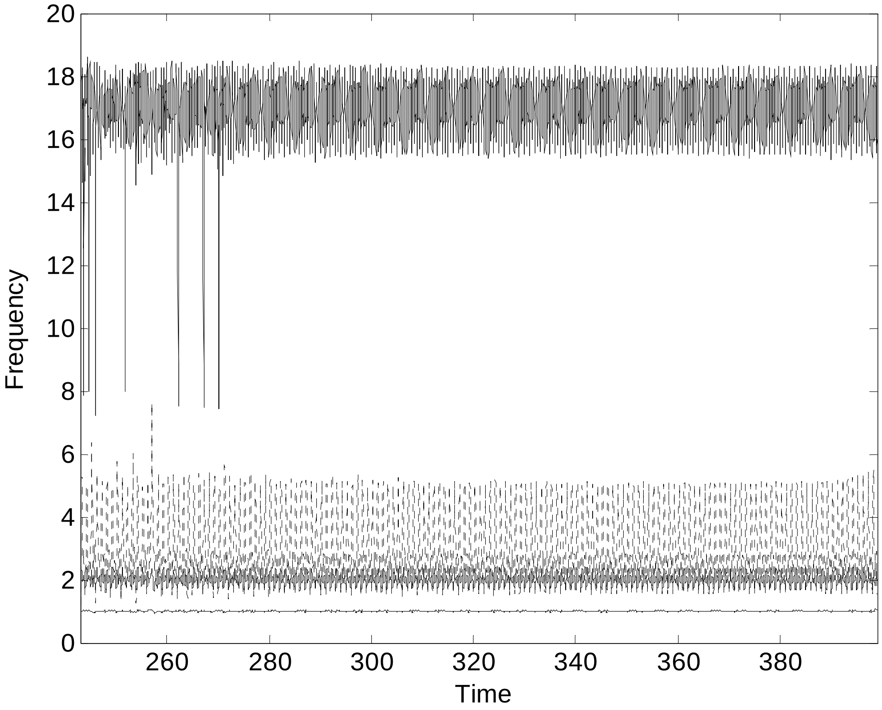

(b)

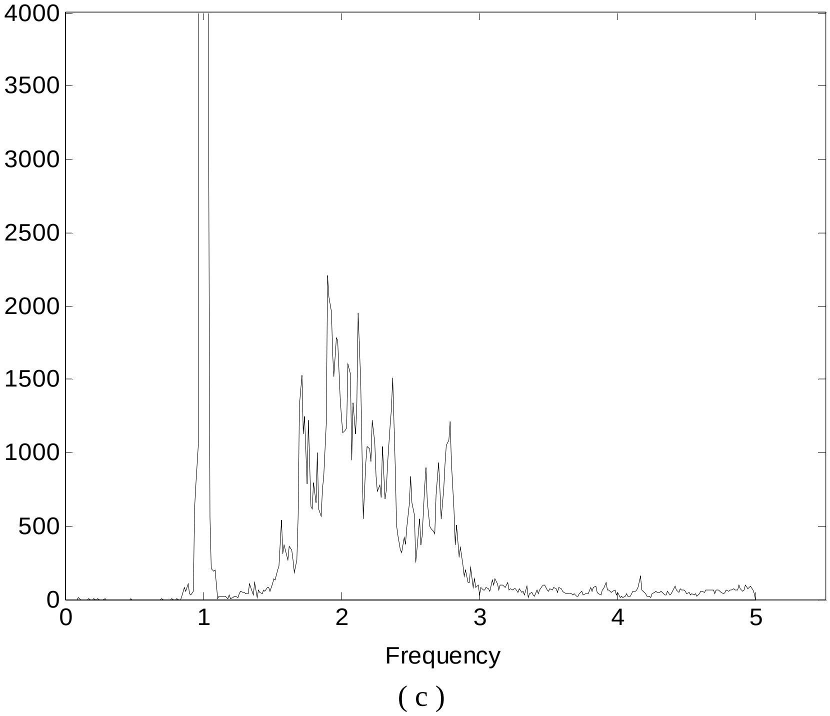

(c)

Figure 7.8 Continued

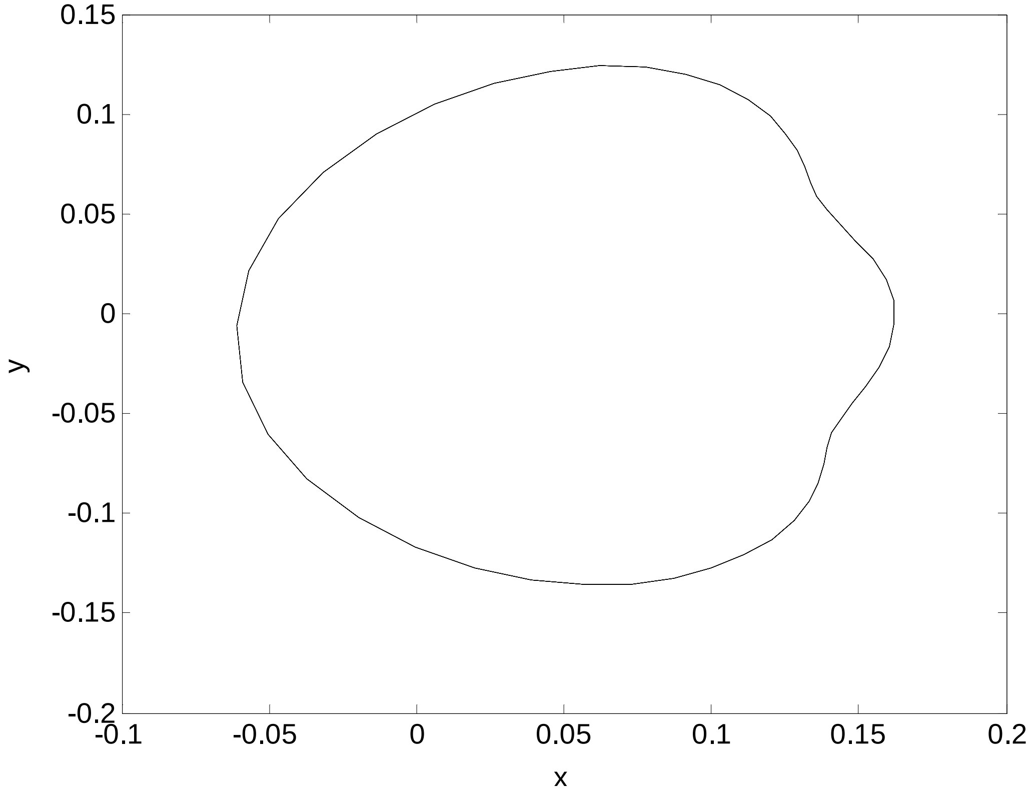

Figure 7.9 Orbit of journal center at $\omega = 50\pi$ and $h_r = 0.05$

7.5 (b). The disappearing of a mode as seen in Figure 7.5(a) and (b), along with the birth of a new mode as seen, for example, in Figure 6.4(b), has never been observed in the history of nonlinear dynamic analysis. These phenomena can only be observed and investigated using the EMD and instantaneous frequency, which together provide a new way of perceiving, interpreting and understanding nonlinear dynamic response. Once the crack development starts to exert the 0.5 frequency mode, it can be seen from both the IMFs and instantaneous frequencies show oscillations of relatively large amplitudes. Also note that, with the disappearing of the 0.5 frequency mode, the forcing frequency mode displays no discernible changes in its waveform and the associated instantaneous frequency. In addition, hints of changes of dynamic state can also be detected by monitoring the corresponding marginal spectrum found in Figure 7.5 (c). If the accumulative effect from the mode with frequency 0.5 increases slowly or simply stops, it is understood that the mode of interest is in the process of disappearing, while the forcing frequency mode is being enhanced.

When the crack is further developed, the system exhibits more complicated dynamic responses. Figure 7.6 (a) shows the orbit of the journal center for the case when $\omega = 50\pi$ and $h_r = 0.09$. The orbit looks like one of periodic motion, but its instantaneous frequency in Figure 7.6 (b) shows that there are three different frequency components 1,2 and 3. As the orbit is of a symmetric signal in time, the EMD scheme cannot be applied to signals as such to properly resolve all underlying intrinsic mode functions. This difficulty is overcome by considering instead the velocity orbit of the center. The velocity profile of the journal center plotted in Figure 7.7 is not symmetric with non-uniform maximum and minimum points. Figure 7.8 (a) shows a selected portion of the center velocity time history at $\omega = 50\pi$ and $h_r = 0.06$ to 0.09. The amplitude of this velocity signal does not change much with the development of crack, but the amplitude of the displacement signal becomes larger with the change of crack depth. Figure 7.9

shows the journal center orbit at $\omega = 50\pi$ and $h_r = 0.05$. If h_r exceeds 0.09, the system would fail without any further bifurcations. Four modes are extracted from the vibration signal and they are given in Figure 7.8(a). Figure 7.8 (b) shows the instantaneous frequencies corresponding to each intrinsic mode. It can be seen that the C4 mode with frequency 1 is the mode of the driving frequency and it has large amplitude. Though C4 is the dominant mode, the oscillation amplitude of its instantaneous frequency, however, is small. The C3 mode oscillating about frequency 2 is due to the nonlinear dissimilarity of the local flexibility [105]. A surface crack on a shaft introduces dissimilar flexibilities in the direction of the crack tip and the one perpendicular to it. As the shaft rotates, the stiffness in a fixed direction will change with time or more precisely it will be a periodic function of time. As expressed in Eq. 5.15, these nonlinear dissimilar flexibilities are modeled as nonlinear forces having the frequency component 2ω, thus having been regarded as an effective indicator for crack detection [105]. However, as versus the constant 2ω harmonic in the Fourier spectrum, the mode realized by the instantaneous frequency is not a harmonic, but rather demonstrating variation with time. Similar interpretations can also be applied to the C2 mode, which oscillates noticeably about frequency 3 and is induced by super-harmonic bifurcation. Because velocity signals have higher frequencies due to its sensitivity to changes in acceleration, one additional component is seen oscillating about frequency 17. From the instantaneous frequencies of all the intrinsic modes, it can be concluded that the breathing of the surface crack will affect every mode. The marginal spectrum found in Figure 7.8 (c) shows that the system response becomes broadband. Thus by monitoring the variation of frequency energy from 1.5 to 3, crack propagation can be detected.

The dynamic response at 3000 rpm rotor speed ($\omega = 100\pi$ rad/sec) is considered next. When there is no crack present in the shaft, the system exhibits a period-2, period doubling bifurcation as is evident from the orbit plotted in Figure 7.10. Figure 7.11(a) shows the transient

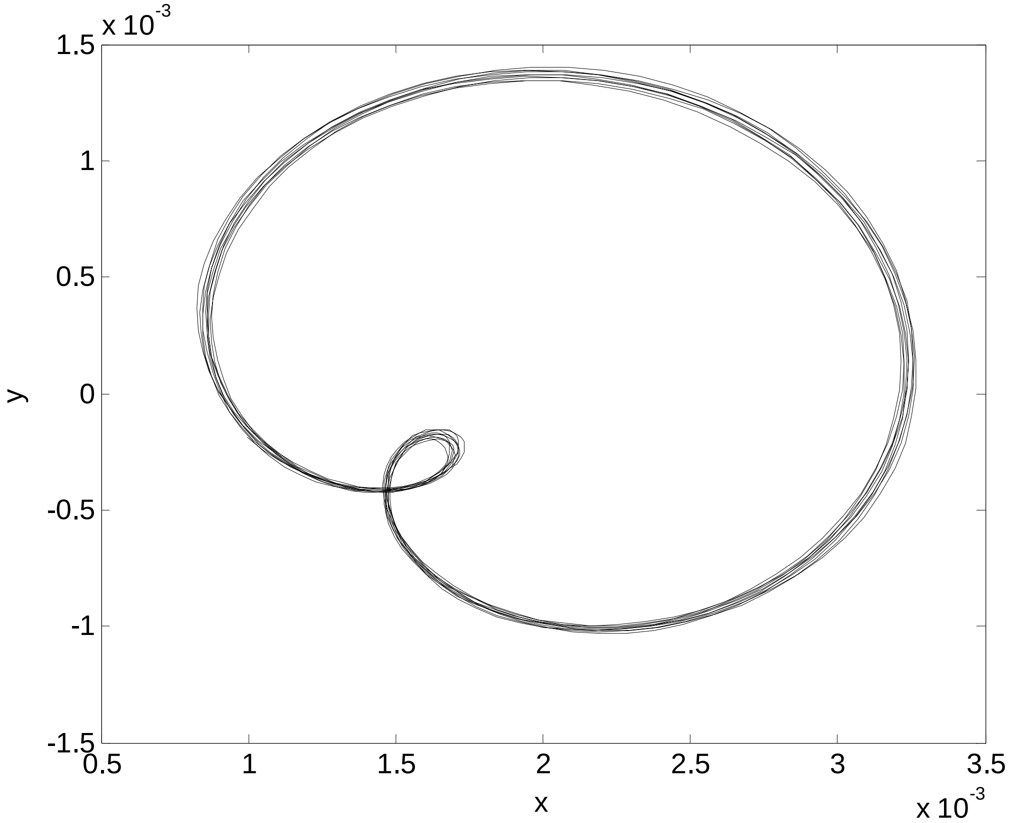

Figure 7.10 Orbit of journal center at $\omega = 100\pi$ rad/s indicating a period doubling motion

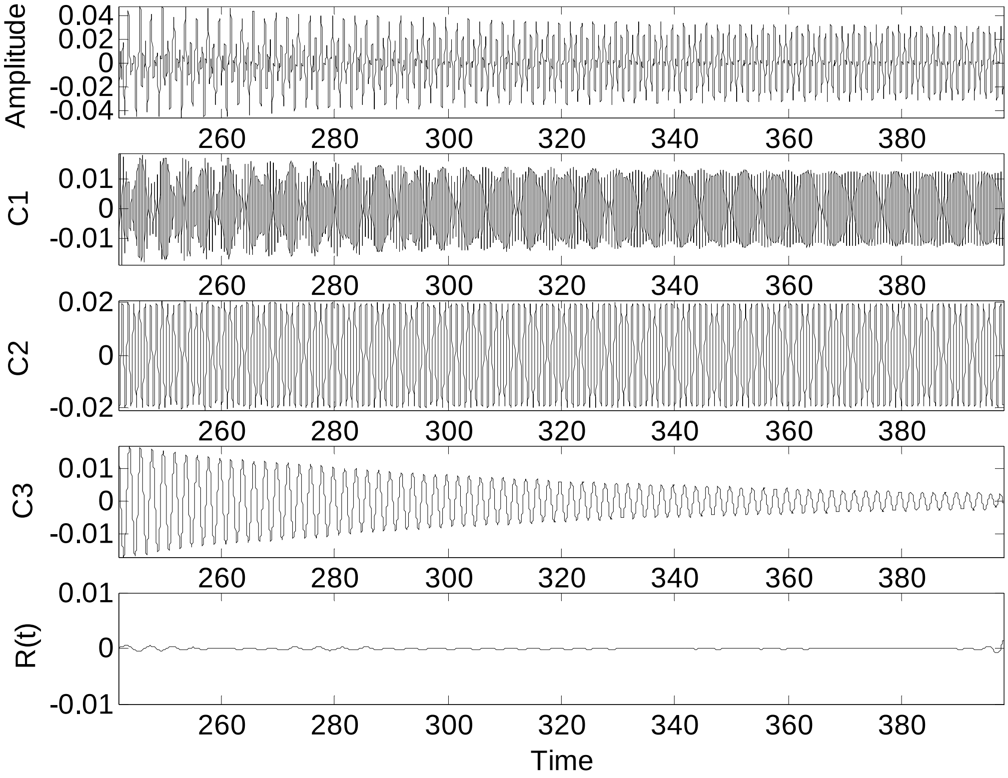

(a)

Figure 7.11 (a) Time waveform and its IMFs, (b) Instantaneous frequencies, and (c) Marginal spectrum for $\omega = 100\pi$ and $h_r = 0.0003$ to 0.001

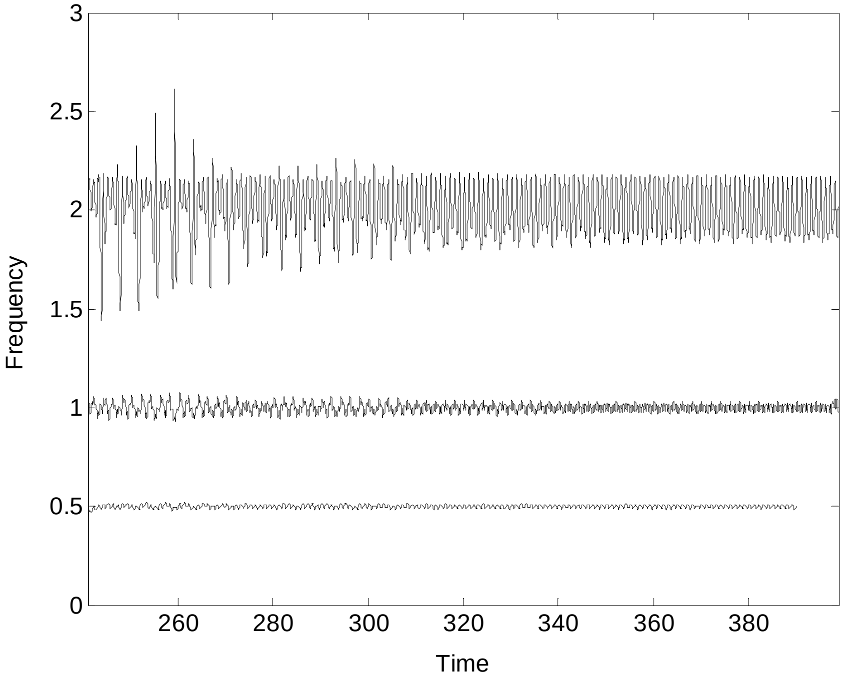

(b)

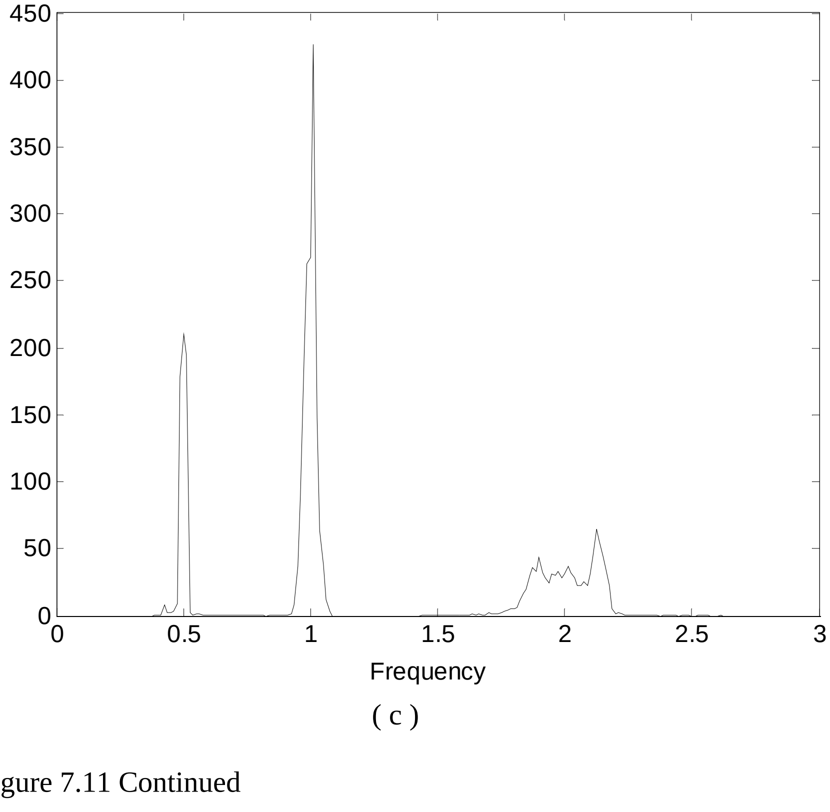

(c)

Figure 7.11 Continued

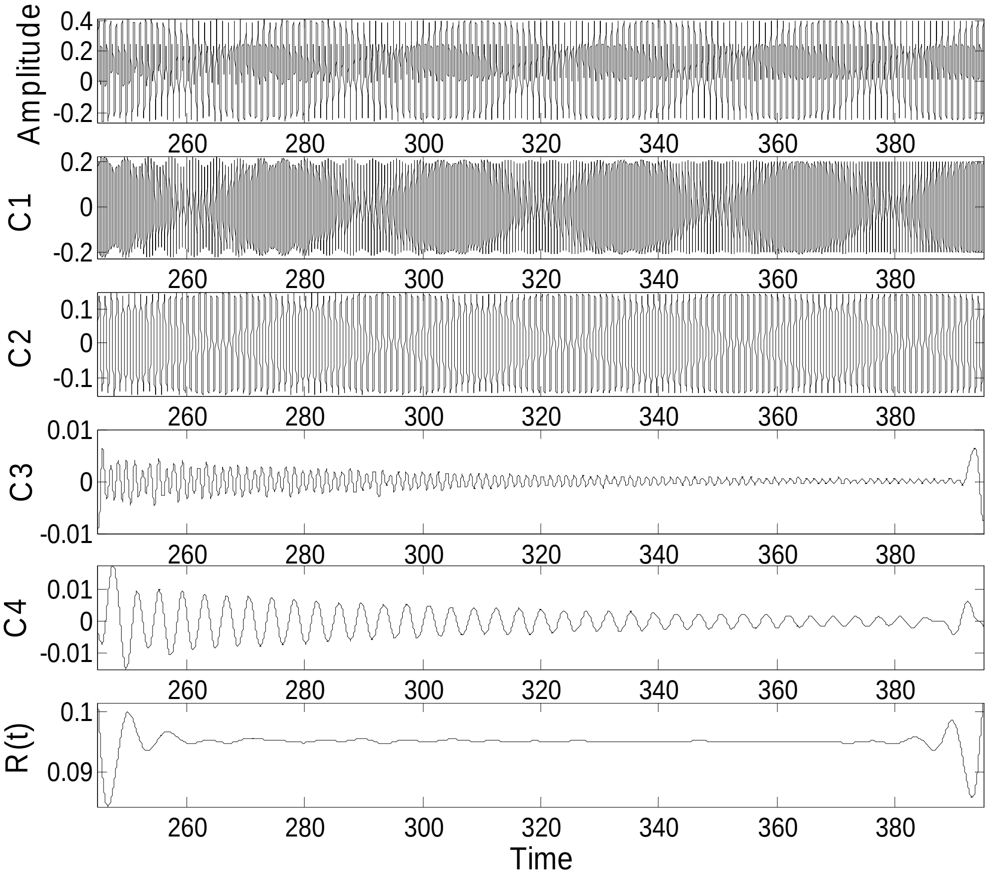

(a)

Figure 7.12 (a) Time waveform and its IMFs, (b) Instantaneous frequencies, and (c) Marginal spectrum for $\omega = 100\pi$ and $h_r = 0.16$ to 0.205

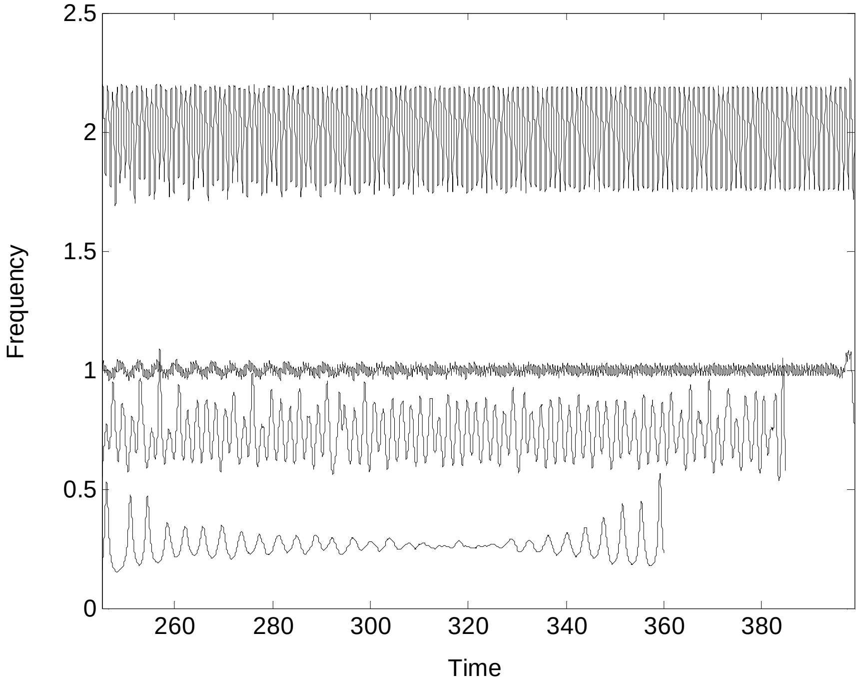

(b)

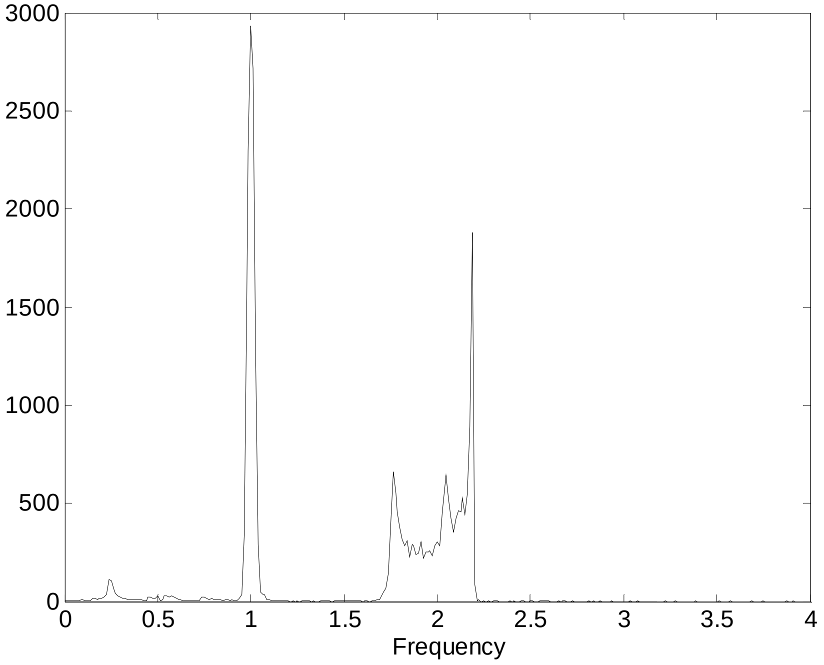

(c)

Figure 7.12 Continued

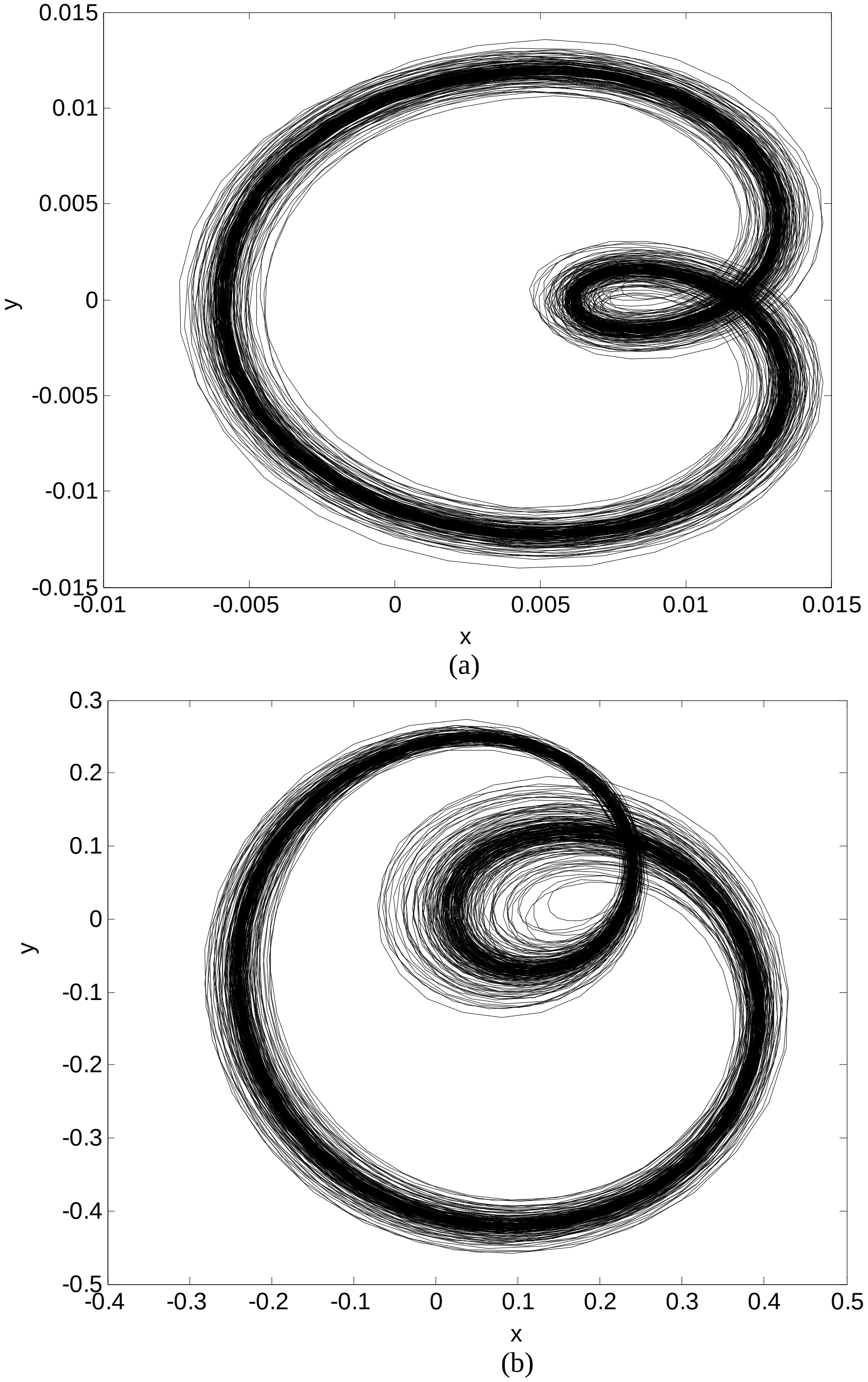

Figure 7.13 (a) Orbit of journal center at ω = 100π and h_r = 0.005. (b) Orbit of journal center at ω = 100π and h_r =0.205

response corresponding to the case when $\omega = 100\pi$ and $h_r = 0.0003$ to 0.001, along with the three decomposed intrinsic modes. The C1 mode of frequency 2 represents the characteristic mode of crack development as previously discussed before, the C2 mode of frequency 1 is the driving frequency mode, and the mode of frequency 0.5 resulted from period doubling is seen gradually disappearing with further crack development. Thus, all the resolved intrinsic modes have their respective definitive physical meaning. It is important to note that the IMFs and their corresponding instantaneous frequencies given in Figures 7.11 (a) and (b) all show some aberrations in the transient process, suggesting that they are not periodic functions of time within this time span. After the transient, all these IMFs and instantaneous frequencies would gradually become regular over time. When the surface crack develops, the frequency components of the response do not change much, however, the vibration amplitude of the journal center becomes quite large. The transient signal at $\omega = 100\pi$ and $h_r = 0.16$ to 0.205 along with its four intrinsic modes is plotted in Figure 7.12. The C1 mode of frequency 2 is the mode corresponding to the crack-induced dissimilar flexibility and the mode of frequency 1 carries the driving frequency. The vibration amplitude does not vary much while h_r is being increased from 0.16 to 0.205. However, this amplitude is about ten times that of the amplitude when h_r was kept constant at 0.001. The C3 and C4 modes clearly show that more period-doubling bifurcations happened in the transient. The C3 mode is of frequency 0.75 while C4 is of frequency 0.25. One of the universal properties for period doubling bifurcation in nonlinear systems is the Feigembaum number [37, 112]. With a cascade of period doublings, the (frequency) order of the newborn modes appears in the spectrum is 1, ½ and its harmonics, ¼ and its harmonics, and so on. The C3 and C4 modes resulted from two period-doublings are readily present; however, it is noted also that the ½ mode that was previously present is no longer in sight. Again, Figures 7.11 (c) and 7.12 (c) show the corresponding marginal spectra. All plots found in Figure 7.13 in which the case when $\omega = 100\pi$ and $h_r = 0.005$ and 0.205 is considered indicate that the system has becomes chaotic and, if h_r is allowed to go beyond 0.205, the system would fail.

When the rotating speed is increased to 3600 rpm (at 120π rad/sec), the overall dynamics does not see many changes as shown in Figures 7.14-7.16. Nevertheless, there are changes in the transient. Before the crack develops in the rotating shaft, the system is still in the period-2 motion from period-doubling bifurcation (Figure 7.16 (a)). With the crack setting in, system dynamics starts changing. The transient vibration history acquired at $h_r = 0.0001$ and 0.0005, along with the three intrinsic modes is given and its associated instantaneous frequencies are given in Figure 7.14 (a) and Fig 7.14 (b), respectively. Similar to the previous cases, the C1 mode of frequency 2 is used to characterize crack-induced frequency, C2 is the driving frequency mode, and C3 is from period doubling bifurcation. Again, the C3 mode would gradually disappear as the crack is allowed to open further in time. The C1 and C3 modes are seen to demonstrate beating during the transient. These beatings are registered as sudden broadband instantaneous frequency and eventually disappear as the transient runs out. Figure 7.14 (c) gives the probability of which modes would show up at a particular frequency. With the progression of crack opening, the system becomes more and more unstable and has larger vibration amplitudes. Figures 7.16(a-d) show this progression in response to $h_r = 0.00$, 0.01, 0.10 and 0.136. With increasing h_r, the subharmonic mode borne out of the period doubling bifurcation is seen disappearing and the driving frequency and the super-harmonic mode corresponding to the crack-induced dissimilar flexibility dominate the dynamics of the rotor system. As is readily indicated in Figure 7.16 (d), modes (or frequencies) other than those discussed are contributing to the broadened spectrum indicative of imminent chaos. In this process, the vibration amplitude increases continuously. To detect the frequencies indicating the initiation of instability, Figure 7.15(a) gives, along with its four resolved intrinsic modes, the

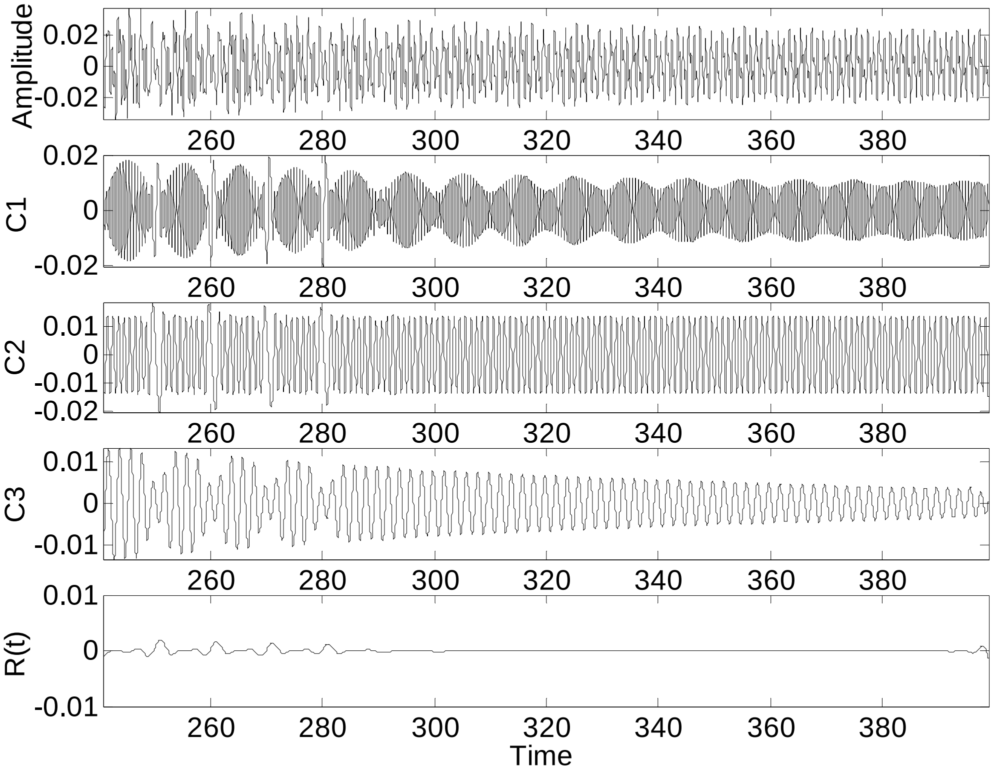

(a)

Figure 7.14 (a) Time waveform and its IMFs, (b) Instantaneous frequencies, and (c) Marginal spectrum for $\omega = 120\pi$ and h_r =0.0001 to 0.0005

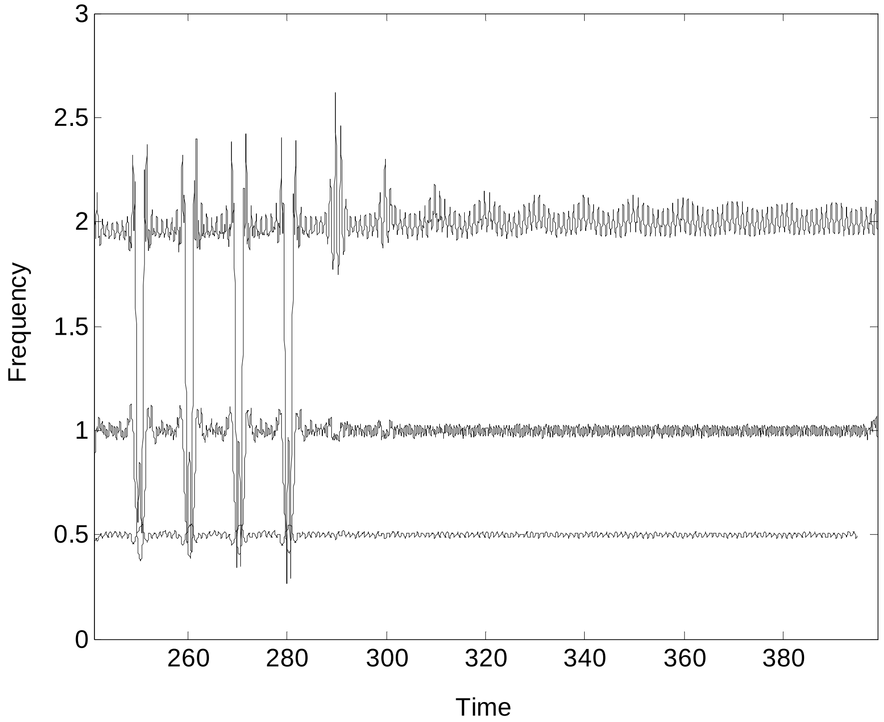

(b)

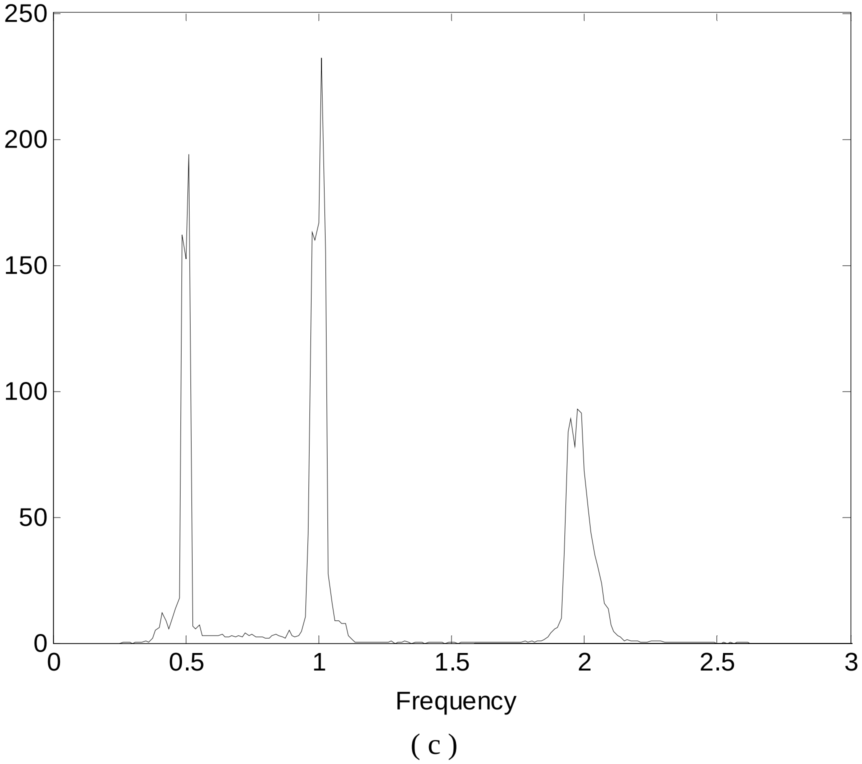

(c)

Figure 7.14 Continued

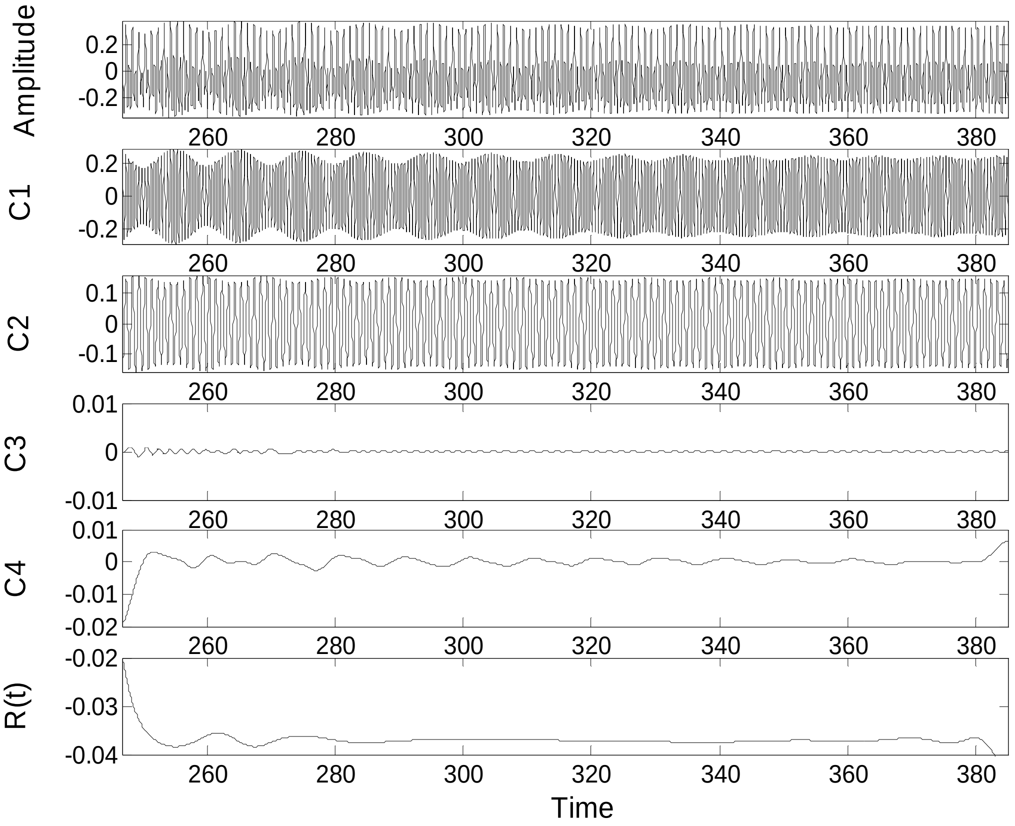

(a)

Figure 7.15 (a) Time waveform and its IMFs, (b) Instantaneous frequencies, and (c) Marginal spectrum for $\omega = 120\pi$ and h_r =0.10 to 0.136

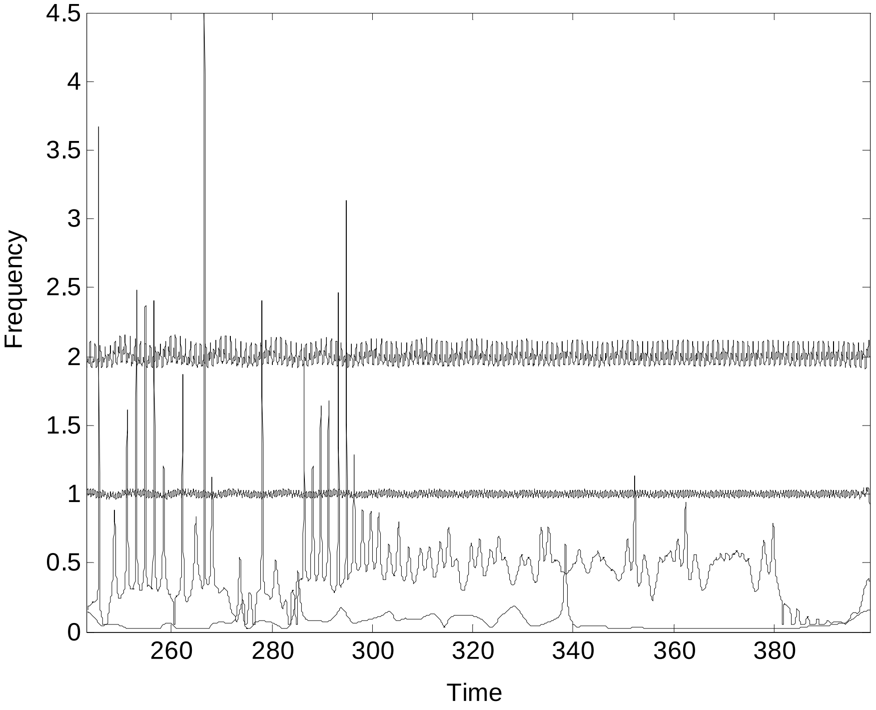

(b)

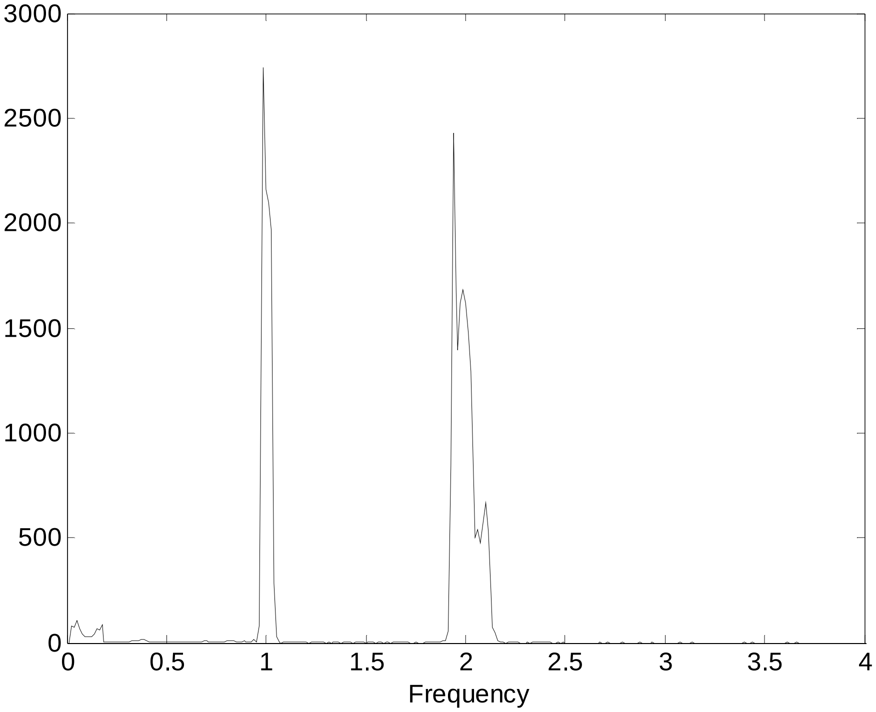

(c)

Figure 7.15 Continued

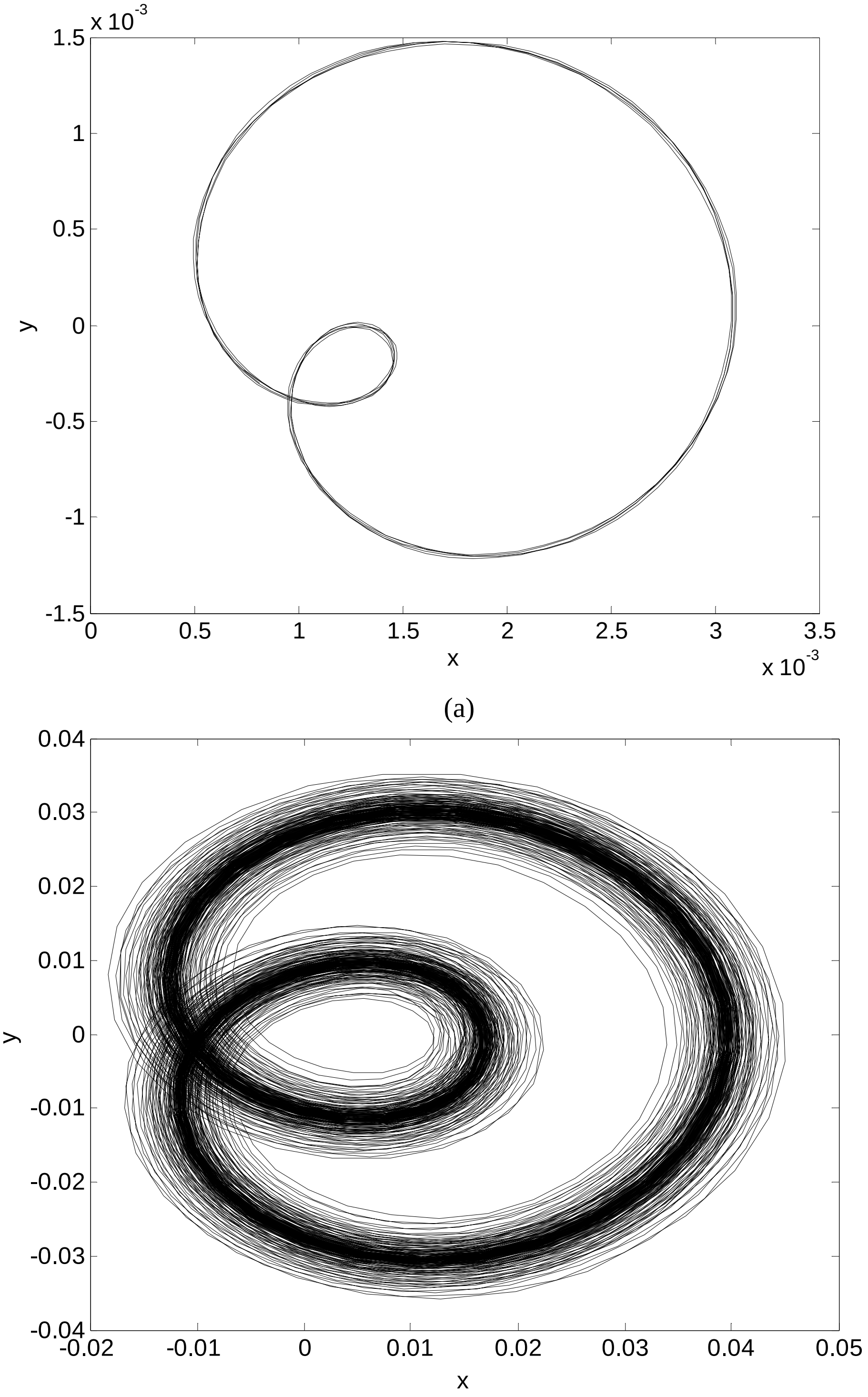

(a)

(b)

Figure 7.16 Orbit of journal center at $\omega = 120\pi$ and (a) h_r =0.00. (b) h_r = 0.01. (c) h_r =0.10. (d) h_r =0.136

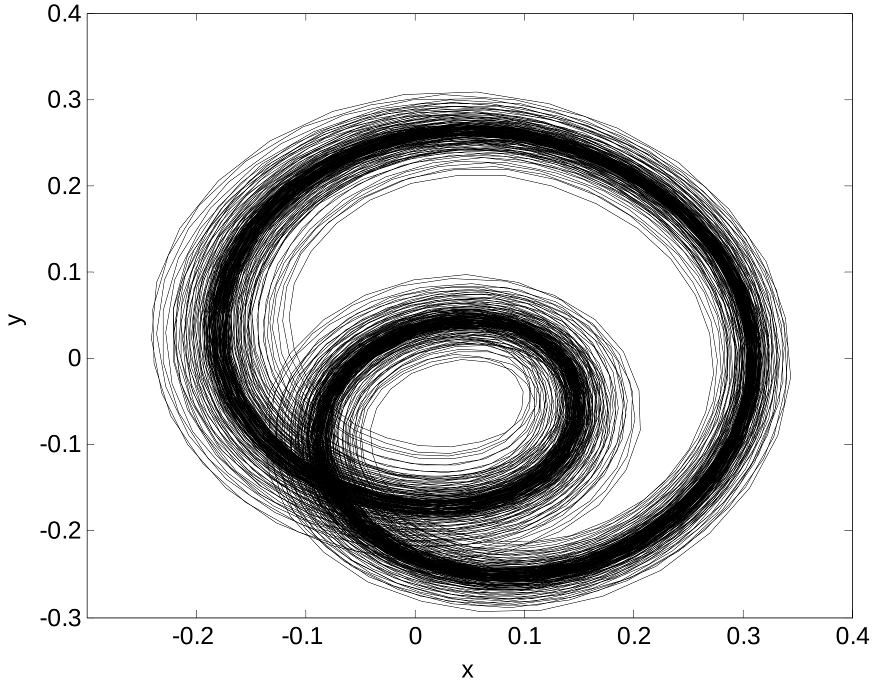

(c)

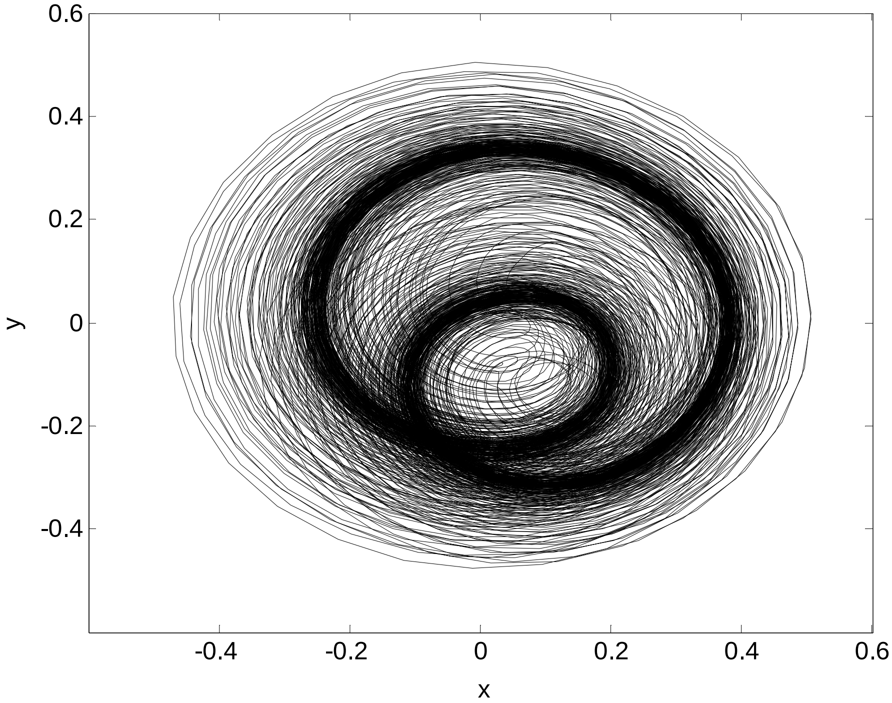

(d)

Figure 7.16 Continued

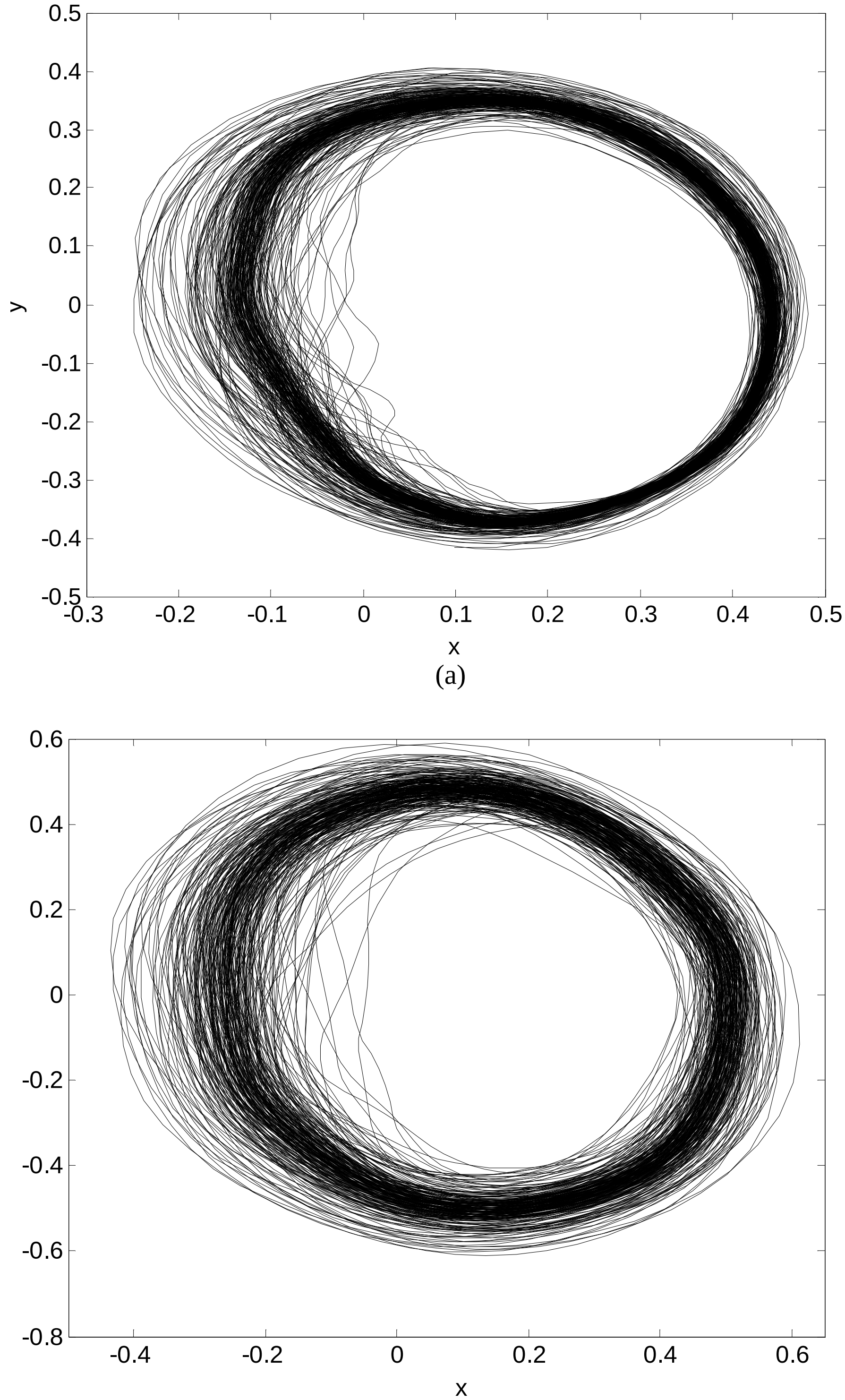

(a)

(b)

Figure 7.17 Orbit of journal center at (a) $\omega = 150\pi$ and $h_r = 0.39$. (b) $\omega = 180\pi$ and $h_r = 0.49$

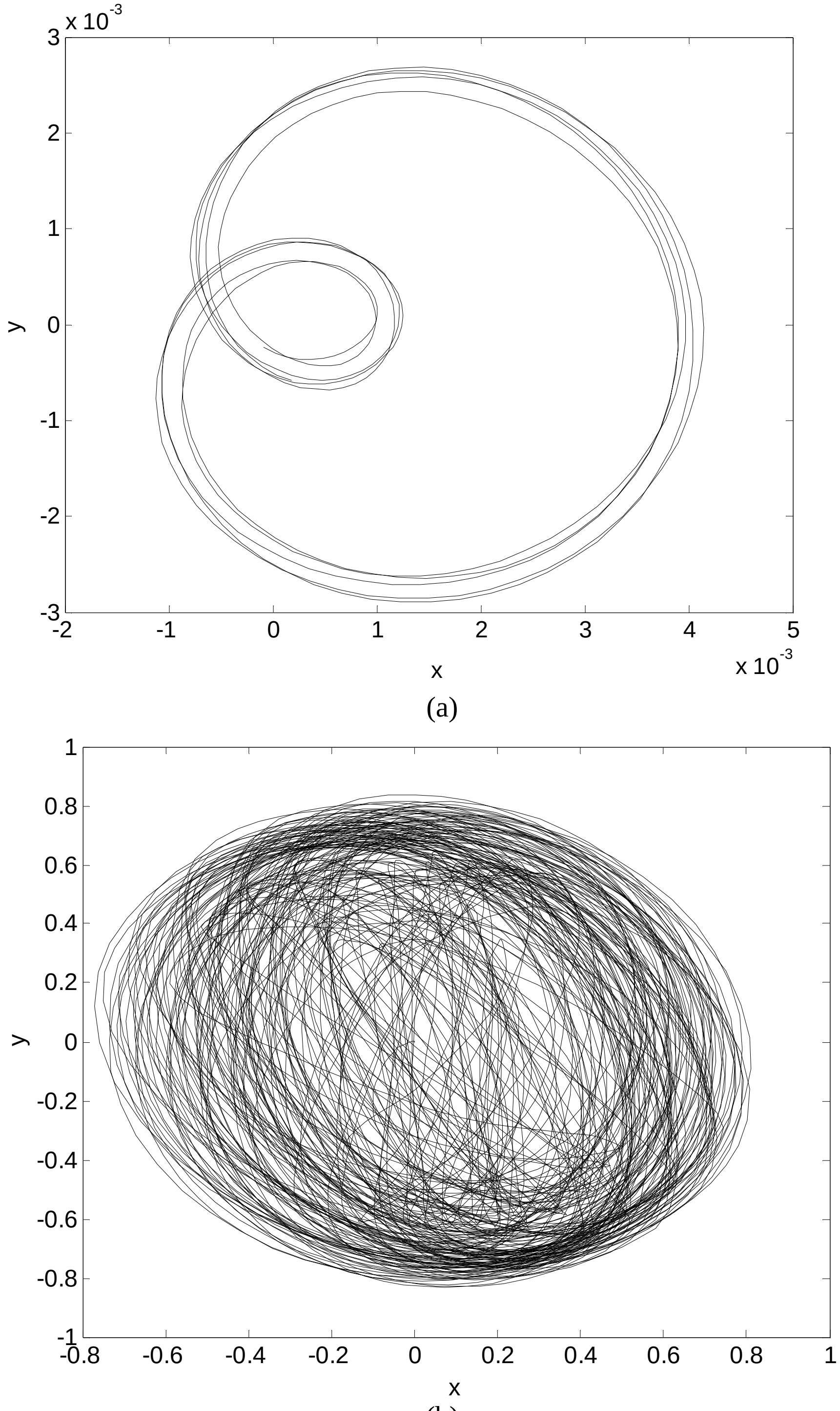

(a)

(b)

Figure 7.18 Orbit of journal center at ω =200π and (a) h_r =0.00. (b) h_r =0.39

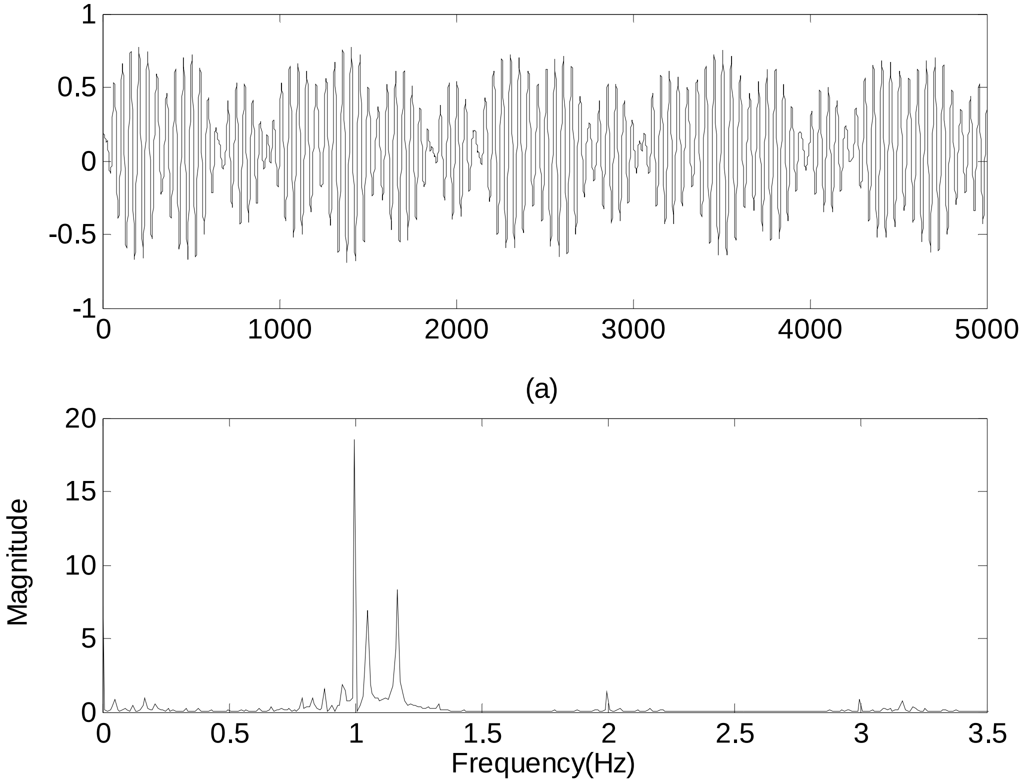

(a)

(b)

Figure 7.19 (a) Vibration signal of journal center at ω=200π and h_r =0.39. (b) The associated FFT transient vibration time history at $\omega = 120\pi$ and $h_r = 0.10$ to 0.136. Again, C1 of frequency 2 and C2 of frequency 1 are, respectively, the crack-induced mode and the excitation mode. IMF C4 has very low frequency and disappear eventually once the steady-state is reached. The C3 mode is of particular interest as its corresponding instantaneous frequency (Figure 7.15(b)) oscillates noticeably in the transient and leads the way to an unstable state of motion. Even after the transient, the mode does not demonstrate any periodic changes as the system rotates. Therefore, it is concluded that it is this newborn mode that is most responsible for the chaotic response that is ready to take place. Also, the broadband marginal spectrum shown in Figure 7.15 (c) implies the same that non-periodic chaotic motion is imminent.

When higher rotating speeds are applied to the rotor system, dynamic responses including weakly chaotic motion and eventual dynamic failure that are similar to those obtained for the case when $\omega = 120\pi$ rad/sec would be observed. Figure 7.17 (a-b) show the orbits of the journal center at $\omega = 150\pi$ rad/sec and 180π rad/sec, in which total failures were preceded with features indicative of chaotic response. However, when the speed is increased to 200π rad/sec, the dynamics of the rotor system is totally changed. Without crack opening, the system experiences several period-doubling bifurcations. Figure 7.18 (a) plots the center orbit at $\omega = 200\pi$ rad/sec and $h_r = 0.00$, in which more than one period doubling bifurcation is indicated, while the orbit in Figure 7.18 (b) corresponding to $\omega = 200\pi$ rad/sec and $h_r = 0.39$ shows that the system is experiencing chaotic motion. However, examining its spectrum in Figure 7.19 shows that the frequency 2 component due to crack breathing doesn’t remain dominant as always. In Figure 7.19 (a-b) the orbit and its associated spectrum for the case when $\omega = 200\pi$ rad/sec and $h_r = 0.39$ are considered. The waveform in Fig 7.19 (a) indicates that beating is occurring. The FFT plots show that dominant frequency components are all very close to frequency 1 and that the broadband spectrum also necessarily implies the extent of prominent chaotic state. This chaotic motion is the direct result of the coupled effect contributed by the fluid-film bearing force and crack breathing.

When the rotor is run at speeds exceeding 200π rad/sec, even with no cracks present, the system is seen to bifurcate subject to the sole action of the fluid film bearing forces, as was also reported the same by Noah [5] and Zheng [34]. Within the speed range, the system would experience nonlinear resonant zone, which is similar to the resonant zone defined in linear analysis. In the zone, very high vibration amplitudes and jump phenomena [11] would be observed, thus signifying high level of instability. After running through the zone, chaotic responses would be induced either by the nonlinear excitation of the (plain journal) bearing oil-film forces alone or by the coupling of the forces with crack breathing. As a contrast, it is noted that linearized dynamic analysis methods predict that a rotor system would experience low amplitude vibration after the resonance zone is passed. From Figure 7.20, in which the steady-state center orbit corresponding to $\omega = 900\pi$ rad/sec and $h_r = 0.10$ are plotted, it can be seen the system is in a very strong chaotic state. It can also be seen that from Figure 7.21 (a-b) that only the C1 mode of instantaneous frequency oscillating about 1 shows some periodic features. The C2 mode of frequency around 0.3 and C3 of frequency 0.1 do not show any periodic behaviors. All these, together, they indicate a strong chaotic state of motion. Again, using the accumulative spectrum found in Figure 7.21 (c), the low frequency components can be monitored to detect the nonlinear response.

When all these data are available, a dynamic failure chart can be generated to provide some tentative rules for maintaining the safe operation of rotary machinery and avoiding unexpected accidents. All parameter ranges selected for studying the dynamics of the model system are seen to induce various nonlinear responses demonstrating different levels of bifurcation. For example, even at $\omega = 50\pi$ rad/sec (1500 rpm), the system has already

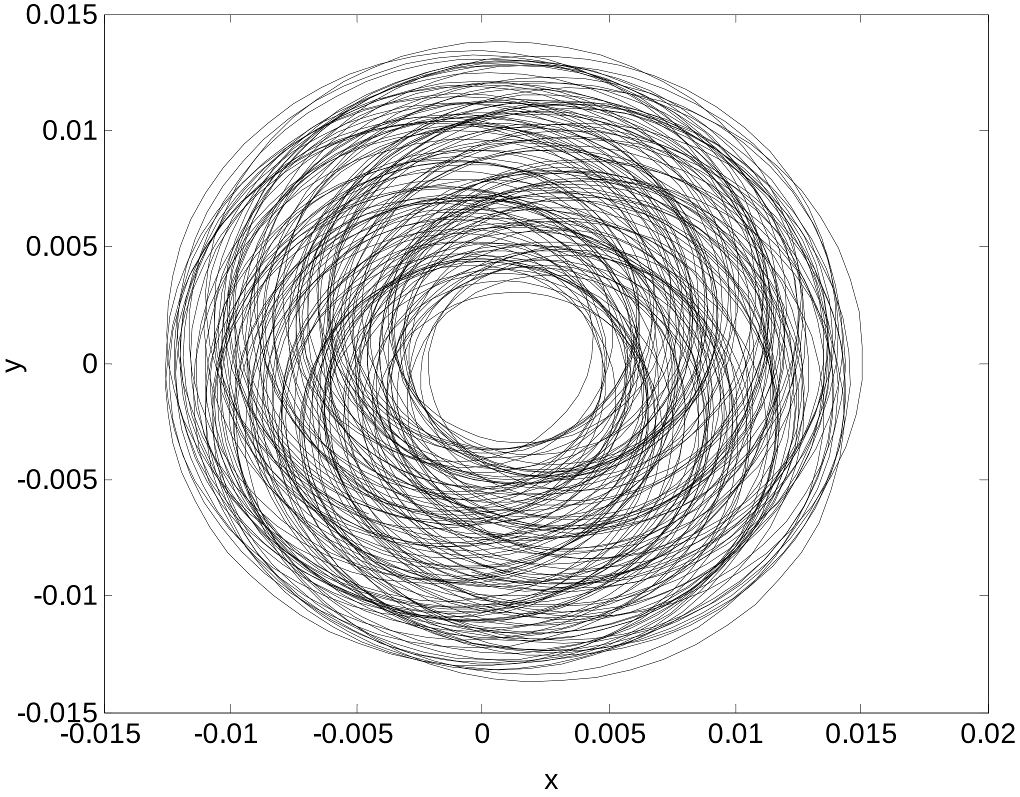

Figure 7.20 Orbit of journal center at ω=900π and h_r =0.10

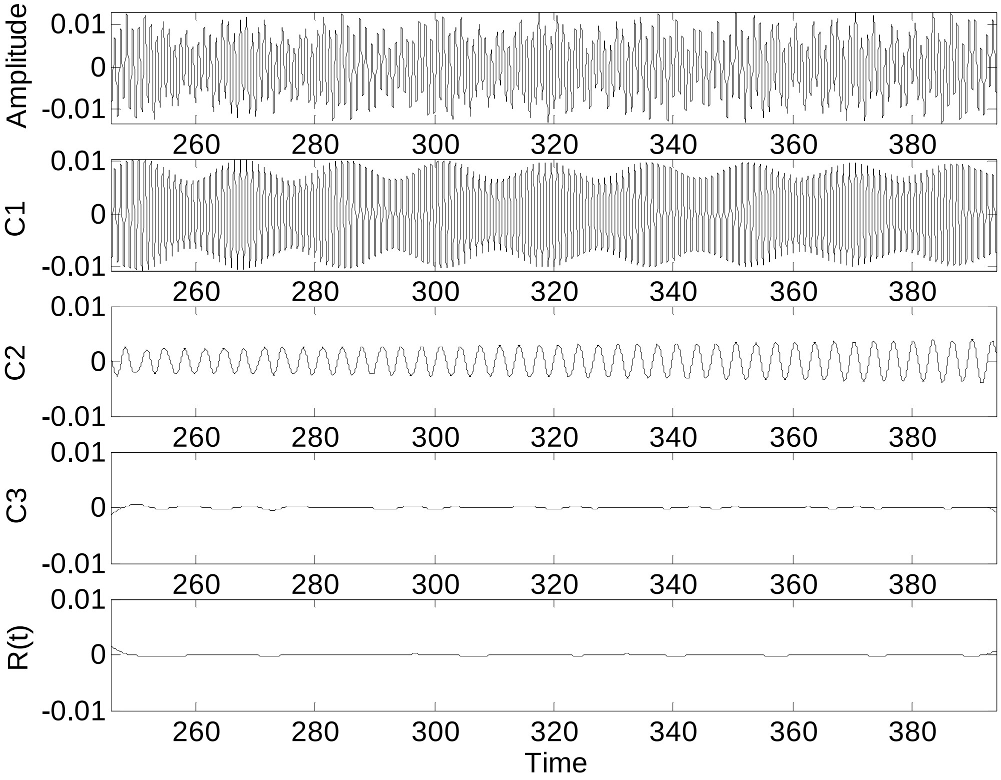

(a)

Figure 7.21 (a) Time waveform and its IMFs, (b) Instantaneous frequencies, and (c) Marginal spectrum for $\omega = 900\pi$ and $h_r = 0.10$

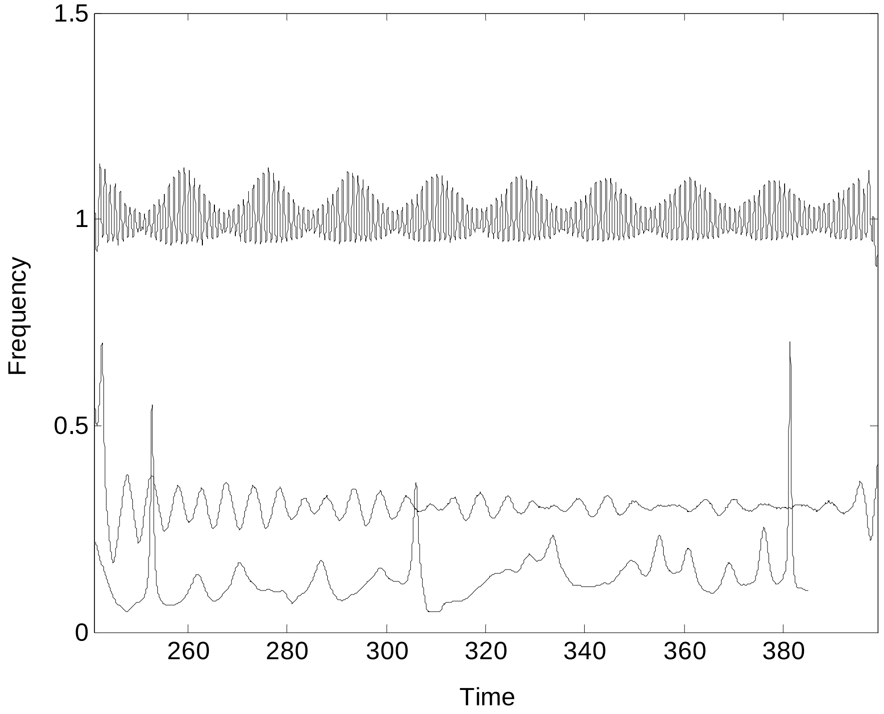

(b)

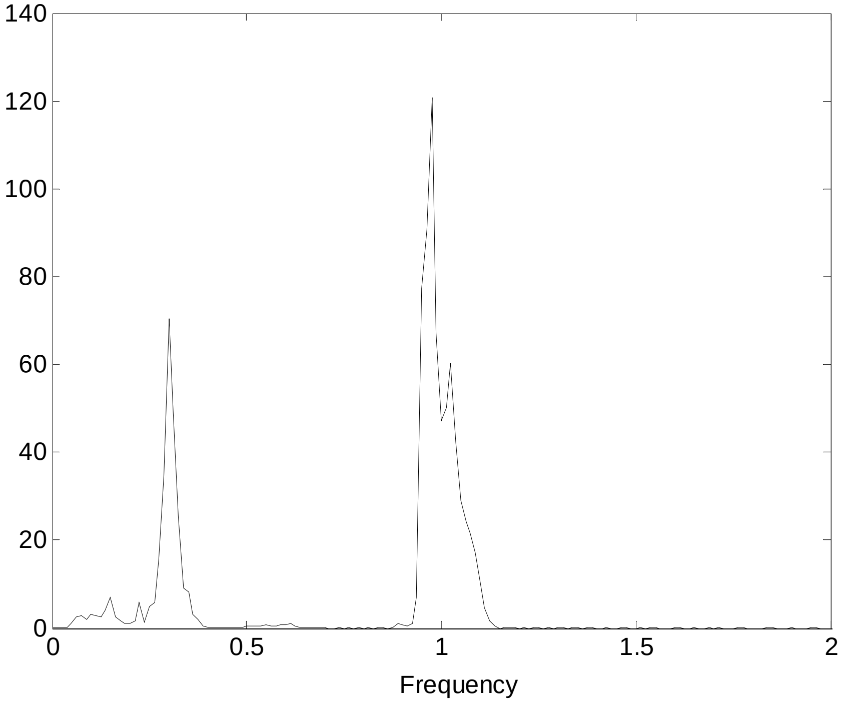

(c)

Figure 7.21 Continued

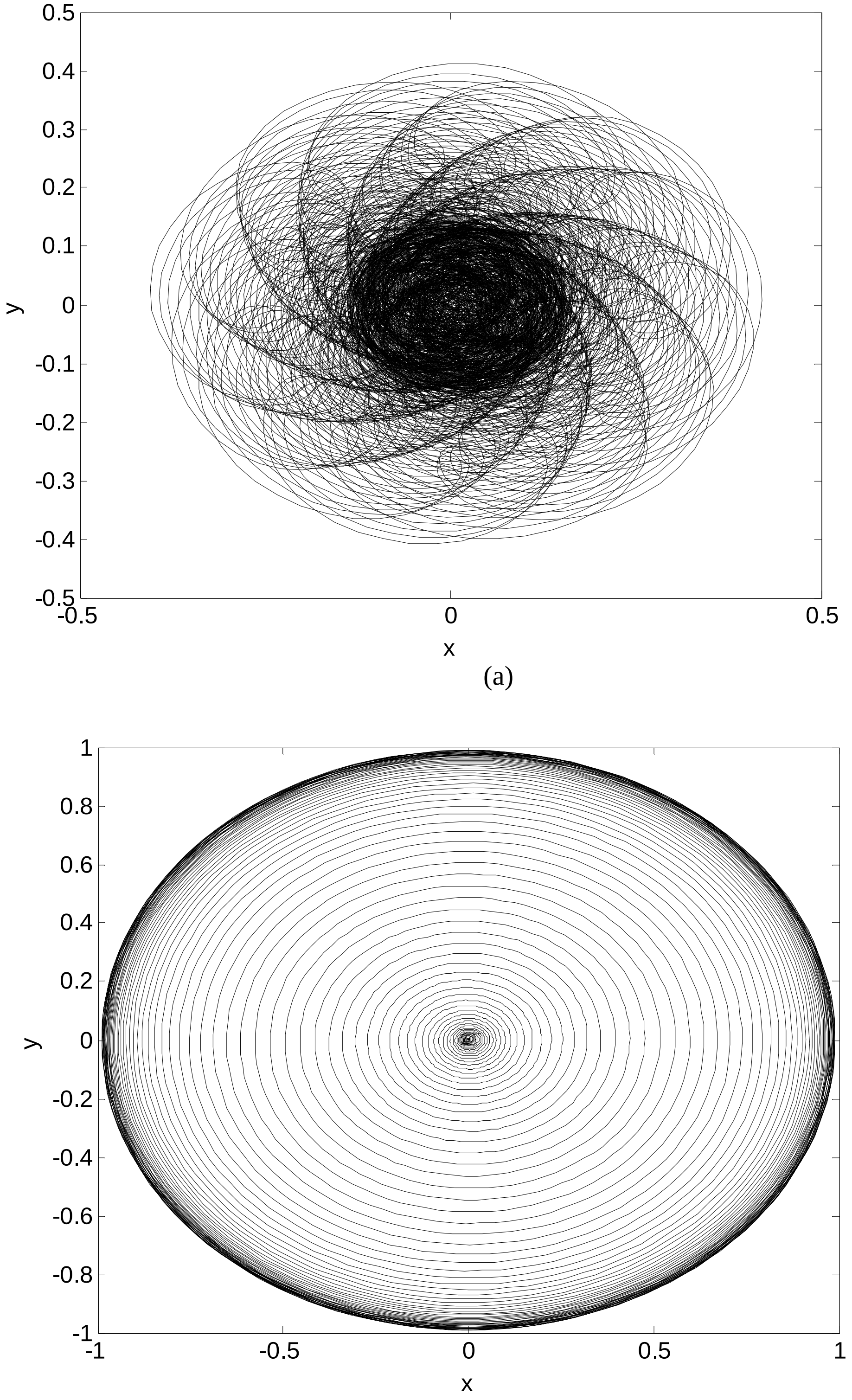

(a)

(b)

Figure 7.22 Orbit of journal center at (a) ω=700π and h_r =0.10. (b) ω=500π and h_r =0.00

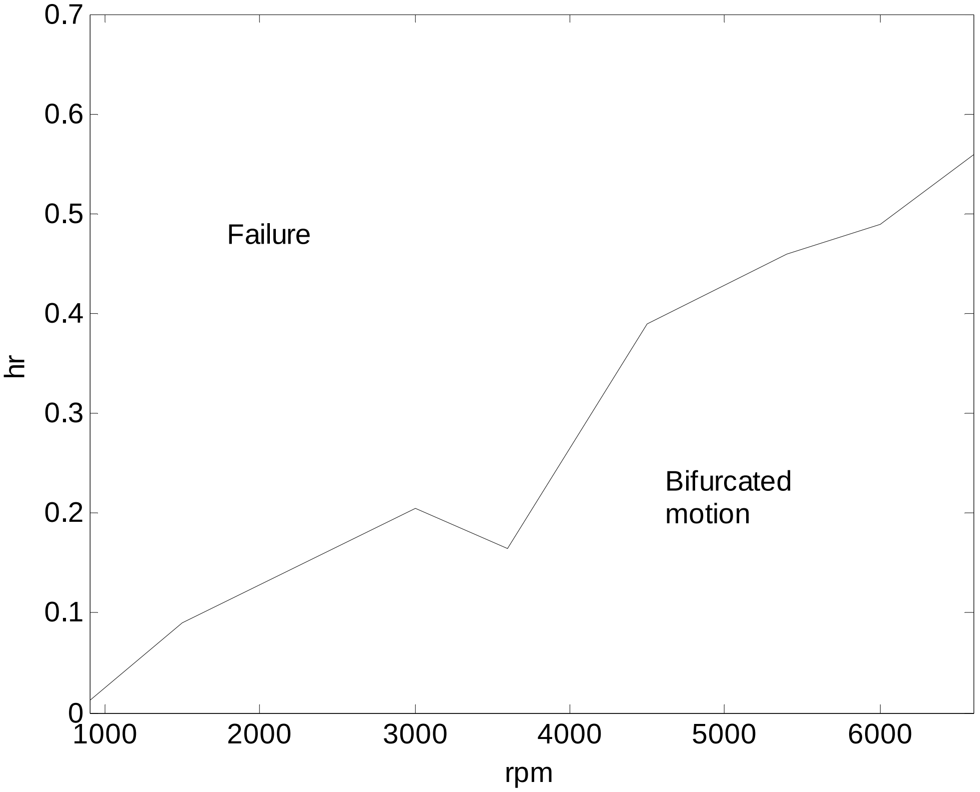

Figure 7.23 Tentative dynamic failure chart for the studied rotor-journal bearings system

experienced period-doubling bifurcation. Hence, only the ranges of parameters that contribute to total system failure are considered in the following. By total failure it means that beyond a certain threshold value, the rotating system loses its functionality. This corresponds to a physical scenario when a finite clearance is no longer maintained and thus the rotor rolls around the inner surface of the journal bearings. Figure 7.22 gives two such cases. As the system response is seen to diverge from the very beginning in time, Figure 7.22 (b) presents the case in which the plain journal bearings cannot support the operation of the whole rotor system at that particular speed considered. The case shown in Figure 7.22 (a) is one that the coupled action of the two different sources of nonlinearity is the reason to which system stability is lost. For both cases, the journal would eventually roll around the bearings and the clearance between the journal and the bearing would become almost zero. As in these cases the film thickness reduces down to the point where the Reynolds equation breaks down and is no longer valid, other theories governing the generation and profiling of (thin) film pressure would need to be applied, if not developed first. The journal would contact and scrub the surfaces of the bearings if the clearance is too small, thus jeopardizing the integrity of the rotor-bearing system with thermal damages. Figure 7.23 provides a tentative dynamic failure chart for the studied model rotor system supported by two plain journal bearings. The curve in the figure is obtained by numerical integration. The curve itself is the border separating the zone representing bifurcated motions from the one in which total failure would occur. Correct interpretation of the chart is that the systems will become dangerously unstable when its parameters are located close to this border curve. Beyond this limiting border, the system will fail from either modes of dynamic instability including chaos or overheating.

From Figure 7.23, it can be seen that crack-induced nonlinearity has a larger effect on the rotor dynamics when the rotating speed is low. It has very little effect on the vibration amplitude of the system when the rotating speed is over 7500 rpm, a conclusion identical to that reported by Gasch [108]. However, crack-induced nonlinearity does affect the type and occurrence of system bifurcation. The reason is that the effect of crack breathing on shaft stiffness is a function of the crack depth, rotating angle and crack opening condition only, thus meaning that when the fixed-depth crack is open, its effect on the rotor system is independent of the rotating speed and imbalance. But the load capacity provided by the journal bearings is increased with increasing rotating speed. This is why the system with rotor surface cracking would fail at low running speed. However, there is one exception at $\omega = 120\pi$ rad/sec (3600 rpm), the crack-induced nonlinearity has larger impact on the dynamics than the case when ω $=100\pi$ rad/sec (3000 rpm). The observed discrepancy is still under investigation. However, one of the speculated, whiles also highly likely, explanation is as followings. Because crack opening and closing effectively lowers the shaft stiffness locally, and if the change of shaft stiffness is also accompanied by the contribution from the nonlinear bearing film pressure, system instability would possibly occur much faster than scenarios that only one source of nonlinearity is involved or dominant. Numerical studies show that the system subject to such an excitation configuration goes out of bearing bounds at the speed.

7.2 Discussion

In the chapter, the concept of instantaneous frequency has been applied to resolve the true physical characteristics of the model system displaying non-stationary, nonlinear responses and undergoing bifurcation. The rotor model developed in chapter V was employed to demonstrate the effectiveness of the method in detecting the inception and progression of various bifurcated states of motion. The model is a comprehensive finite element model that incorporates translational and rotational inertia, bending stiffness, gyroscopic moments, and shear deformation. It was subjected to the breathing and slow growth of a transverse crack and, also, the support of two plain journal bearings. The journal bearing forces were theoretically shown to be strong nonlinear functions of journal displacement and velocity. The model rotor system was first studied by designating the rotor speed and the relative flexibility embodying the extent of crack development as the two controlled parameters. Because it is a rotor model of practicality having two sources of nonlinearity included, many interesting nonlinear phenomena have been obtained, observed, and investigated. The disappearing of sub-harmonics attributable to the oil-film force was first observed when crack opening was suppressed. At different rotating speeds, the ways by which the system fails were different. The model system was seen to fail from one of the three possible scenarios of significant practical importance: super-harmonic bifurcation, prolonged chaotic response, and large vibration amplitudes accompanied by no bifurcation. IMFs along with their associated instantaneous frequencies were demonstrated to be effective in identifying all these system changes. For example, in one of the presented cases a chaotic motion was detected as the instantaneous frequencies displaying broadband and aperiodic characteristics. It was also demonstrated that, by monitoring the energy content of each instantaneous frequency component, the marginal spectra can also be used to quantify the accumulative effect of different frequencies and to detect the bifurcated and changing state of dynamics.

Where more than one source of nonlinearity were present, the induced system responses were very different from those subject to only one nonlinear source. It is noted that investigations on multi-degree of freedom systems involving only one source nonlinearity are both rare and not readily available. The dissertation thus represents the first report of its own kind on the results and conclusions associated with the multi-DOF rotor-bearing system subject to two sources of nonlinearity of significant engineering interests. The responses subject to more than two sources of nonlinearity could therefore be even more complex. Extensive research in this regard is therefore anticipated.

Presence of cracks could impact and alter the dynamics of a rotor-journal bearing system to a significant extent. Thus the stability criterion need to be re-evaluated and redefined based on the results realized using nonlinear analysis approach. It was shown that if nonlinearity within the system is very strong, linear stability analysis would yield erratic results even at low rotating speeds.

There have been two cracked rotor models presented over the years. The first is the small crack model by Gasch [107], in which an opening crack affects the rotor local stiffness in half cycle. The second is the improved deep crack model by Mayes [77], in which crack induced dissimilar flexibility decreases the local stiffness in the whole cycle. The second one was largely followed for the doctoral study. Both crack models are only functions of the rotating angle and crack opening condition. They are independent of the rotating speed and imbalance response. As discussed, these models enable prominent effects at low speeds and obscure the true rotor-dynamic characteristics at high rotating speeds if the rotating system is also supported by fluid-film bearings. If a rotor system is elastically supported, the displaying dynamics at low speeds is physically and fundamentally different from that of being supported using fluid-film bearings. As was reported the same in [108], the crack would have little effect on swaying the response of the system at low speeds if elastic supports were employed.

Because the dynamics of a rotor system is much affected by the local flexibility imparted by crack opening and closing, the exact location and configuration of a surface crack could be determined from its response of nonlinearity. Nonlinear response induced by cracks of different configurations and locations are characteristically different. For example, a crack near the center of the rotor shaft affects the stiffness much more than the crack located near the bearings. And this nonlinearity is fully registered and carried by the intrinsic modes of the nonlinear response. Conceptually it is possible as well as viable that relevant information regarding the configuration and location of the crack be fully extracted from the instantaneous time-frequency domain. As pointed out by Dimarogonas [105], a uniform vibration theory feasible for cracked beams and multi-DOF systems are still being sought. With the demonstrated capability and sensitivity, the method of instantaneous frequency should prove a useful characterization tool for developing such a theory.

CHAPTER VIII

RESULTS OF CRACKED ROTOR MODEL SUPPORTED BY JOURNAL BEARINGS WITH VARIOUS CLEARANCES

8.1 Description of Results

In Chapters VI and VII, the dynamical responses of one elastically supported rotor and one journal bearing supported rotor were investigated using the concept of instantaneous frequency and amplitude. Both rotor models were subjected to the slow development of a transverse surface crack. These rotor models demonstrated the effectiveness of the method in detecting the inception and progression of various bifurcated states of motion. In this chapter, the same finite element rotor model employed in Chapter VII is used. The model is, again, supported by journal bearings and subjected to the opening and closing of a surface crack. Because varying the clearance of journal bearings can greatly impact the dynamics, and thus stability, of the rotor-bearing system, the effect of varying clearance at different rotating speeds is investigated in the current chapter. Figures 8.1-8.10 present the dynamical responses of the model of several different clearances at speed $\omega = 100\pi$, while Figures 8.11-8.20 give the various dynamical responses of the same model at $\omega = 200\pi$.

For a specific journal bearing, its clearance is designated to guarantee its loading capacity. As such, journal-bearing clearance is kept constant in the following study. Several values are considered to enable a quantitative understanding of the rotor dynamical behavior in response to different clearances. Again, a normalized time step $\Delta t = 0.02$ is used to integrate the rotor vibration response from $t = 0$. For the sake of visualization, only the portion of data registered between $t = 140$ and $t = 300$ (8000 time steps) are analyzed and presented. The (normalized) Y-direction response components of the left bearing are considered in the following

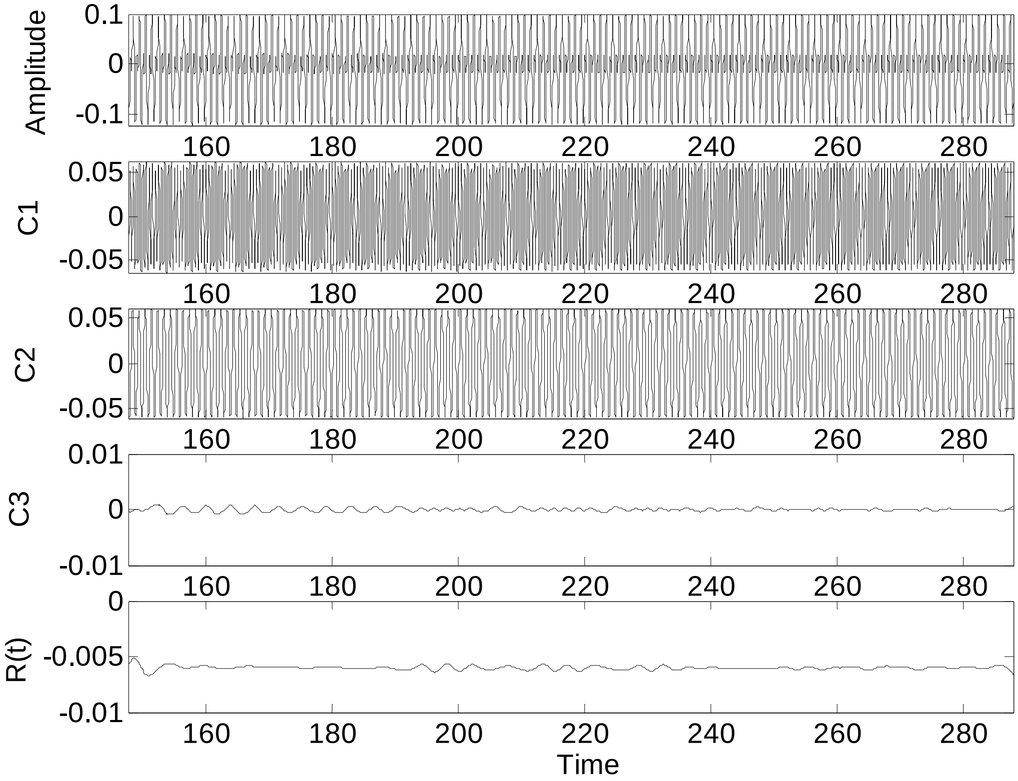

(a)

Figure 8.1 (a) Time waveform and its IMFs, (b) Instantaneous frequencies, and (c) Marginal spectrum for $\omega = 100\pi$, Cr=0.0025r and h_r =0.05

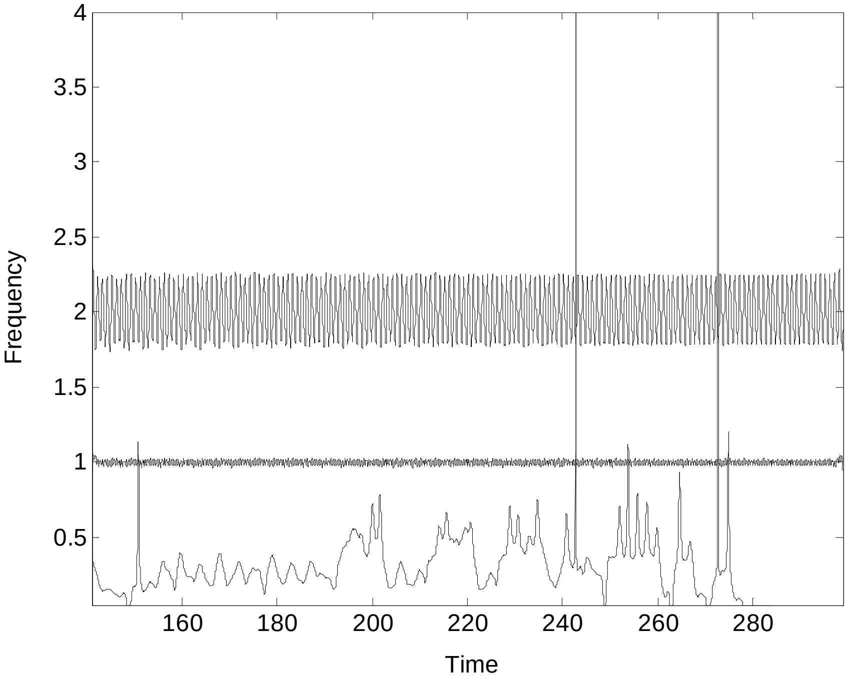

(b)

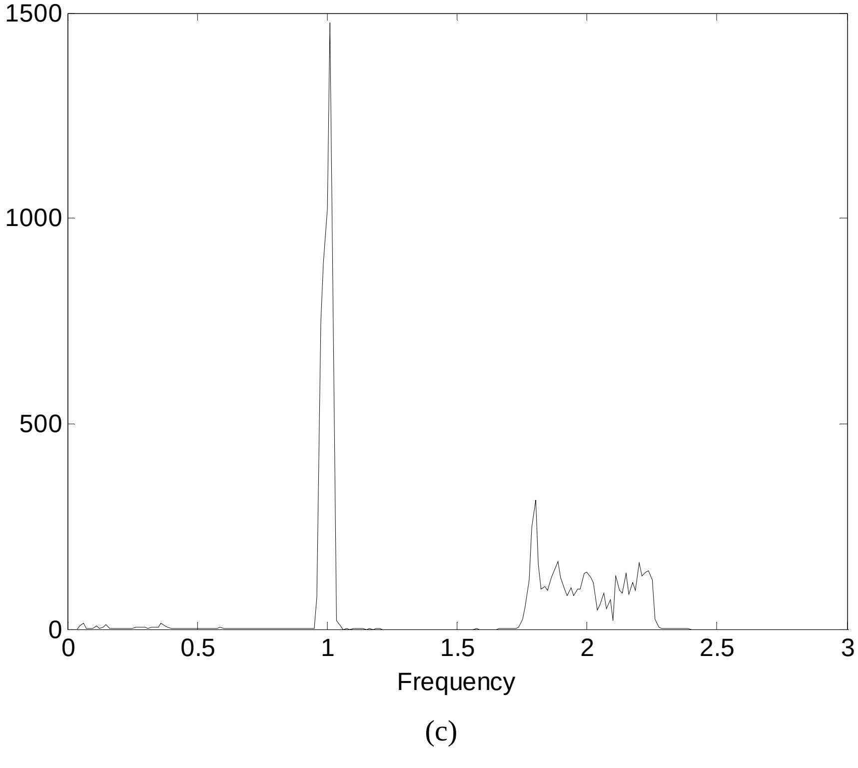

(c)

Figure 8.1 Continued

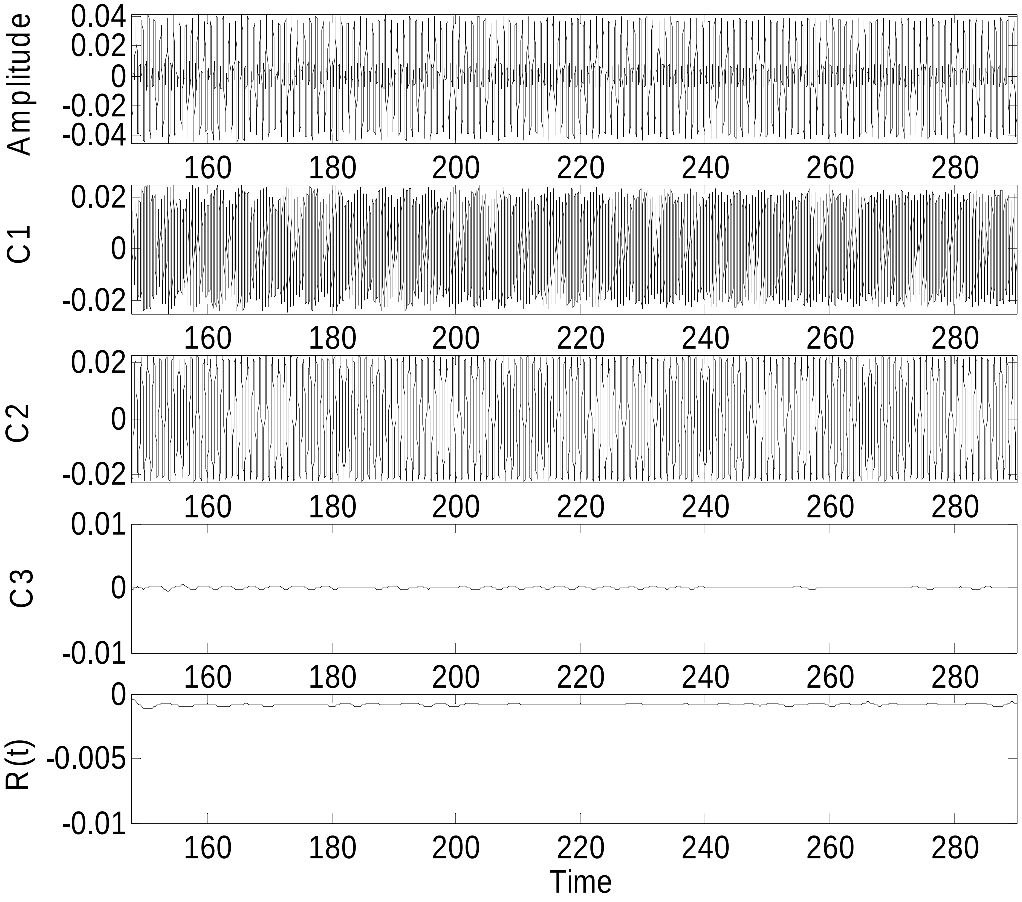

(a)

Figure 8.2 (a) Time waveform and its IMFs, (b) Instantaneous frequencies, and (c) Marginal spectrum for $\omega = 100\pi$, Cr=0.002r and h_r =0.05

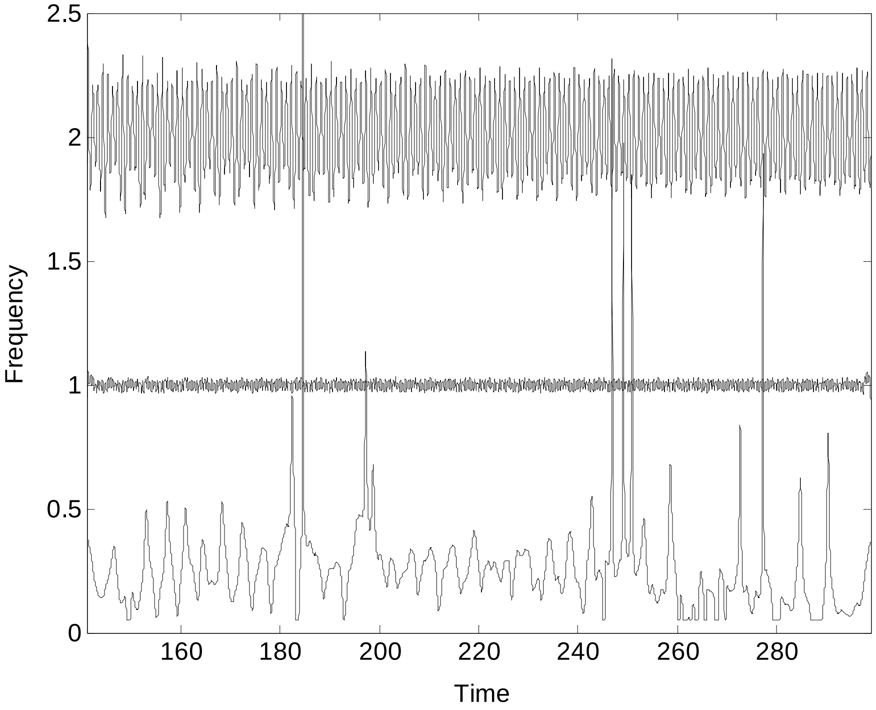

(b)

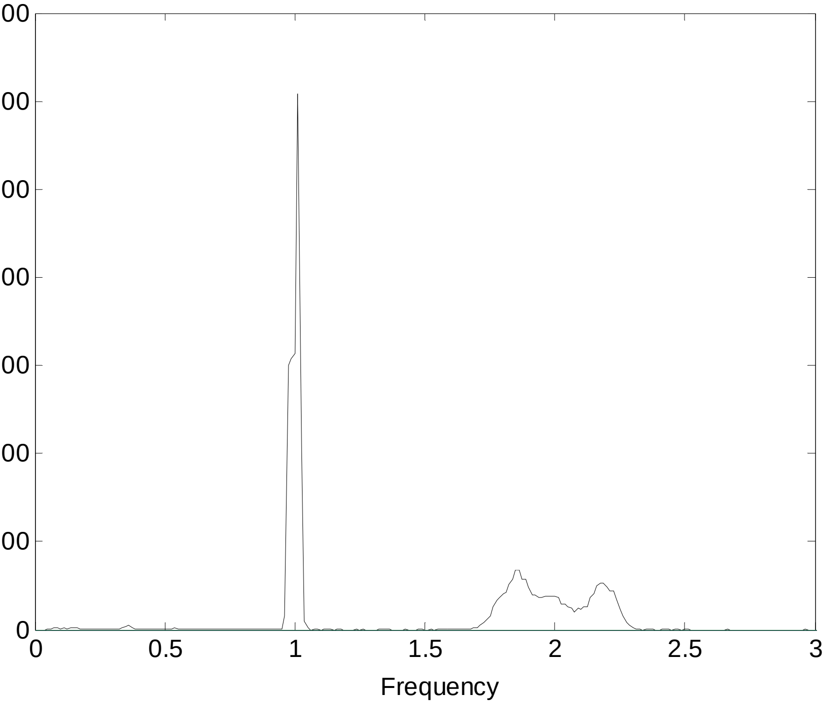

(c)

Figure 8.2 Continued

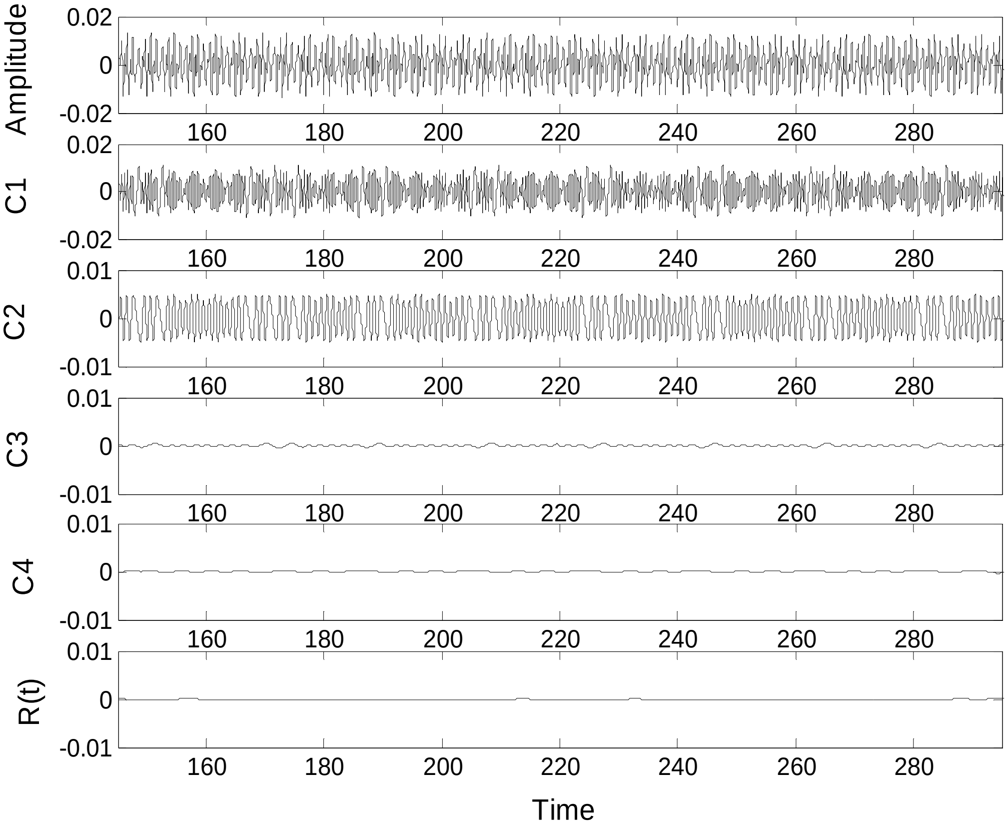

(a)

Figure 8.3 (a) Time waveform and its IMFs, (b) Instantaneous frequencies, and (c) Marginal spectrum for $\omega = 100\pi$, Cr=0.001r and h_r =0.05

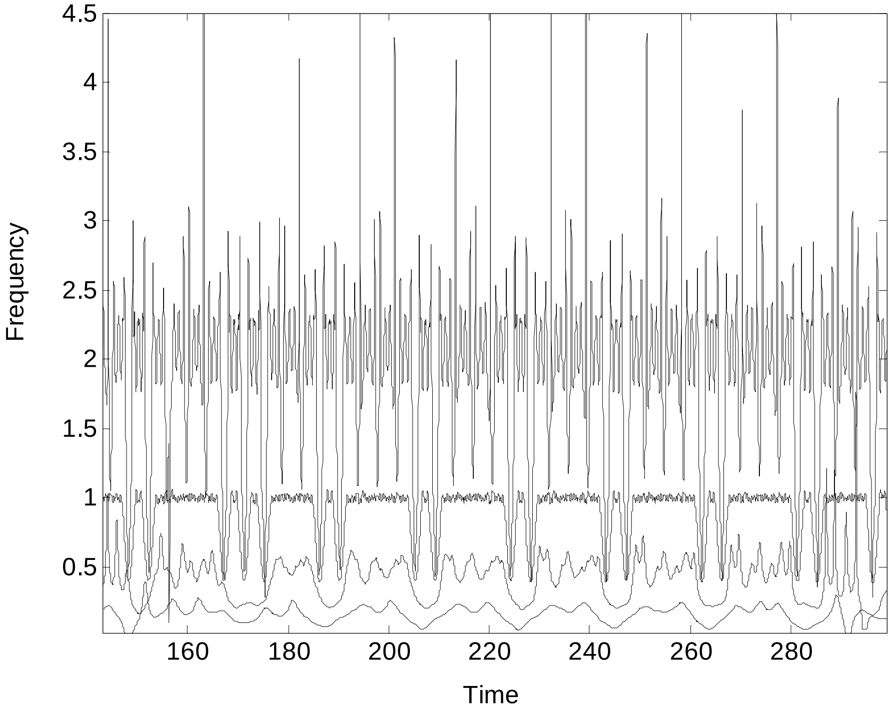

(b)

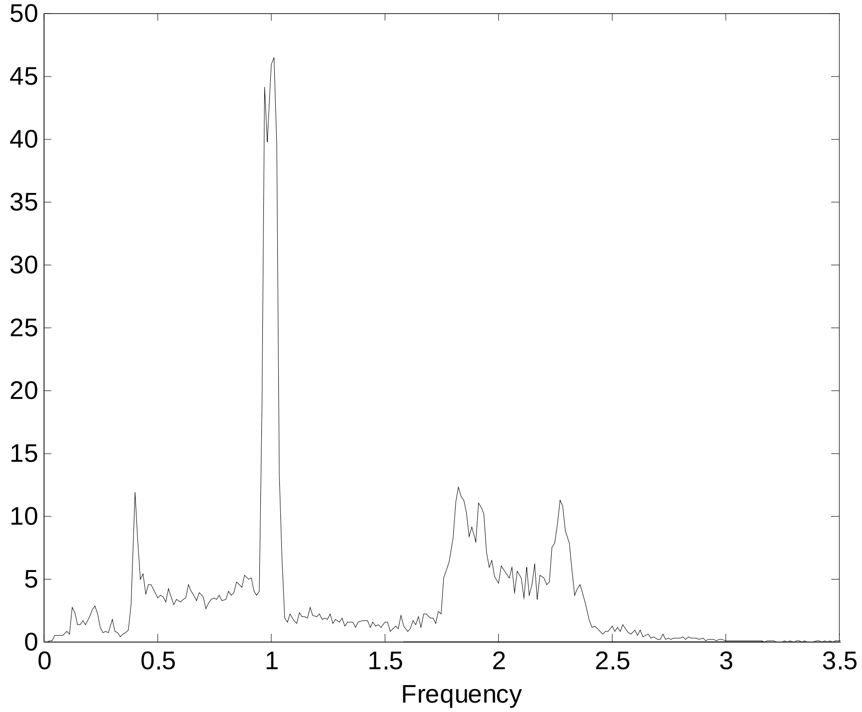

(c)

Figure 8.3 Continued

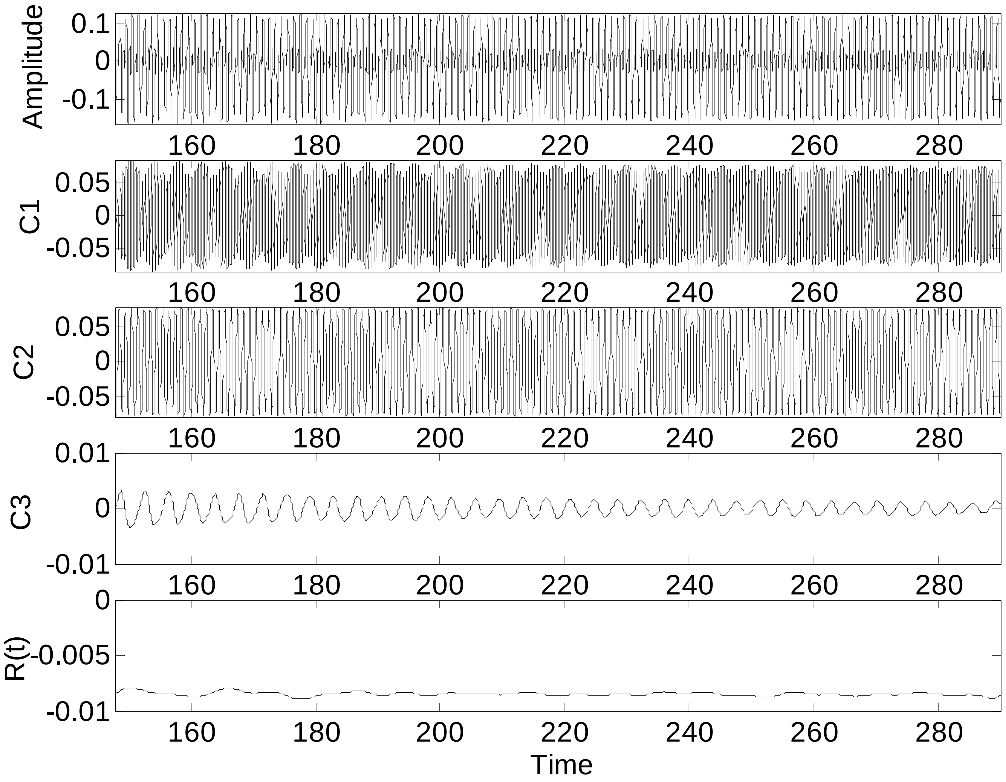

(a)

Figure 8.4 (a) Time waveform and its IMFs, (b) Instantaneous frequencies, and (c) Marginal spectrum for $\omega = 100\pi$, Cr=0.002r and h_r =0.10

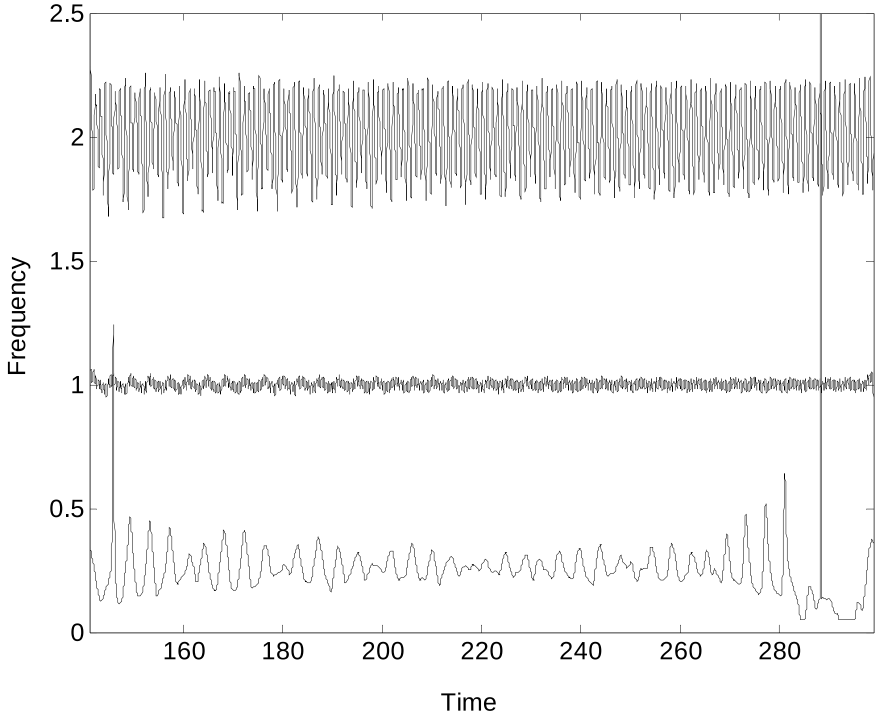

(b)

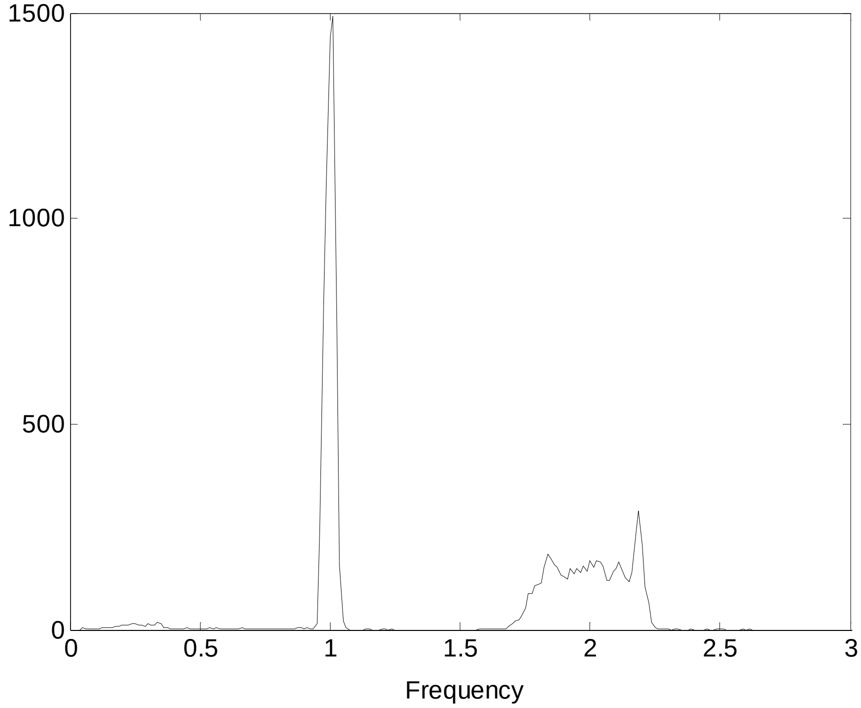

(c)

Figure 8.4 Continued

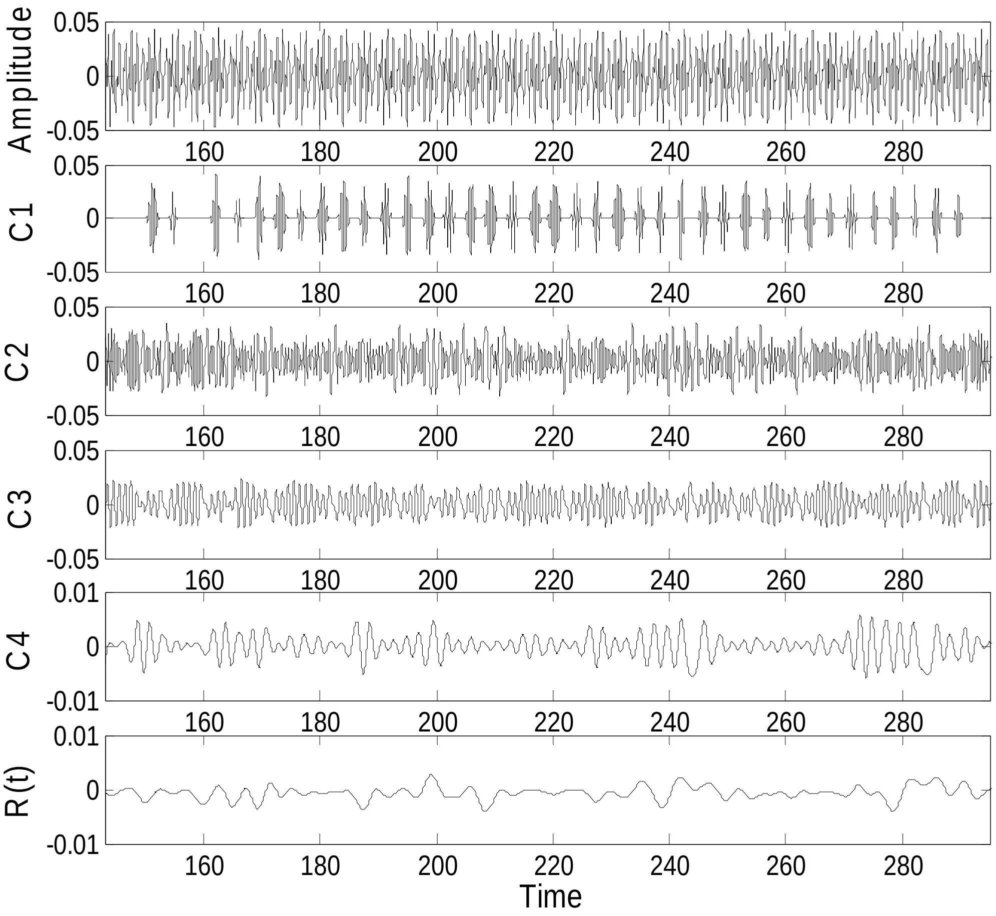

(a)

Figure 8.5 (a) Time waveform and its IMFs, (b) Instantaneous frequencies, and (c) Marginal spectrum for $\omega = 100\pi$, Cr=0.001r and h_r =0.10

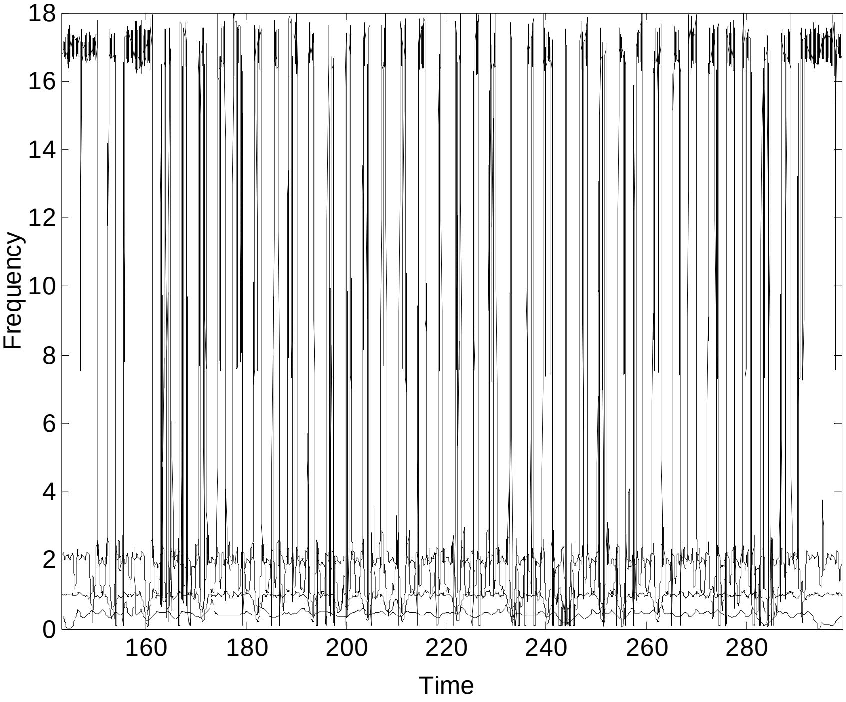

(b)

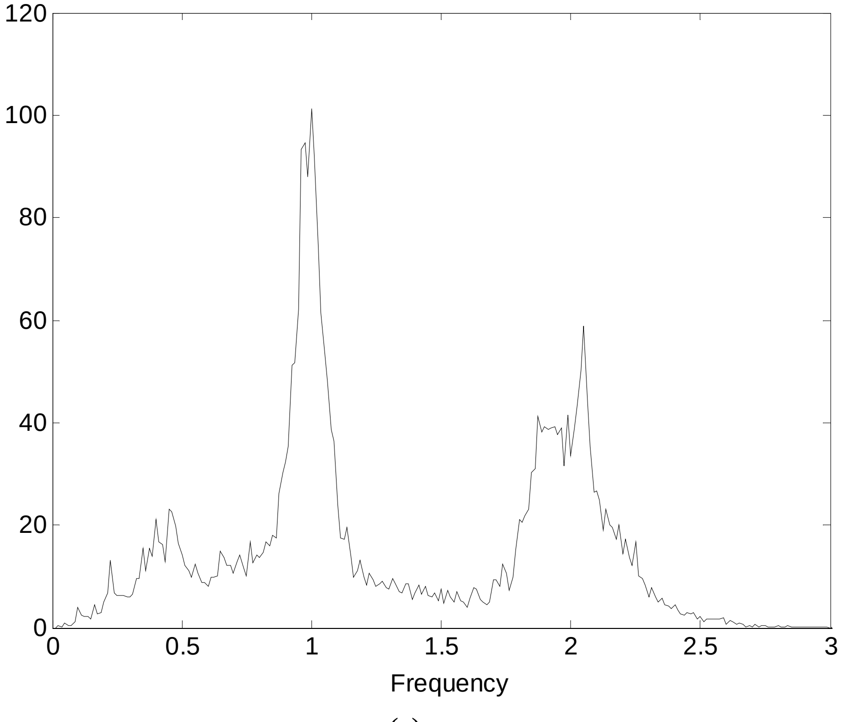

(c)

Figure 8.5 Continued

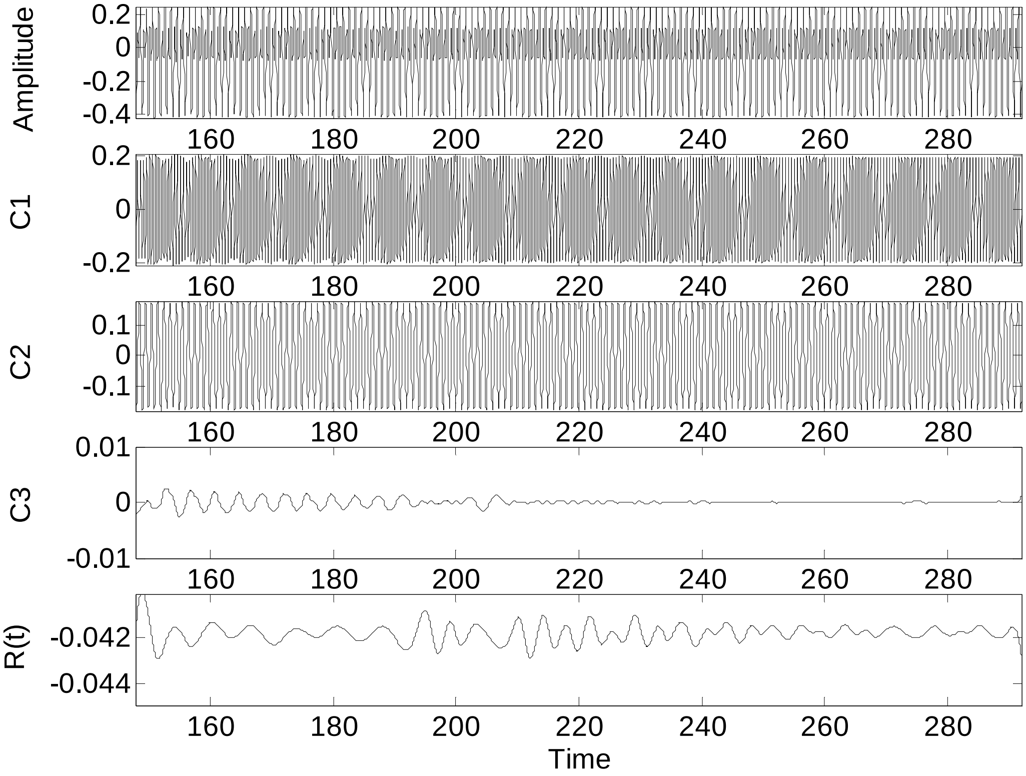

(a)

Figure 8.6 (a) Time waveform and its IMFs, (b) Instantaneous frequencies, and (c) Marginal spectrum for $\omega = 100\pi$, Cr=0.0025r and h_r =0.20

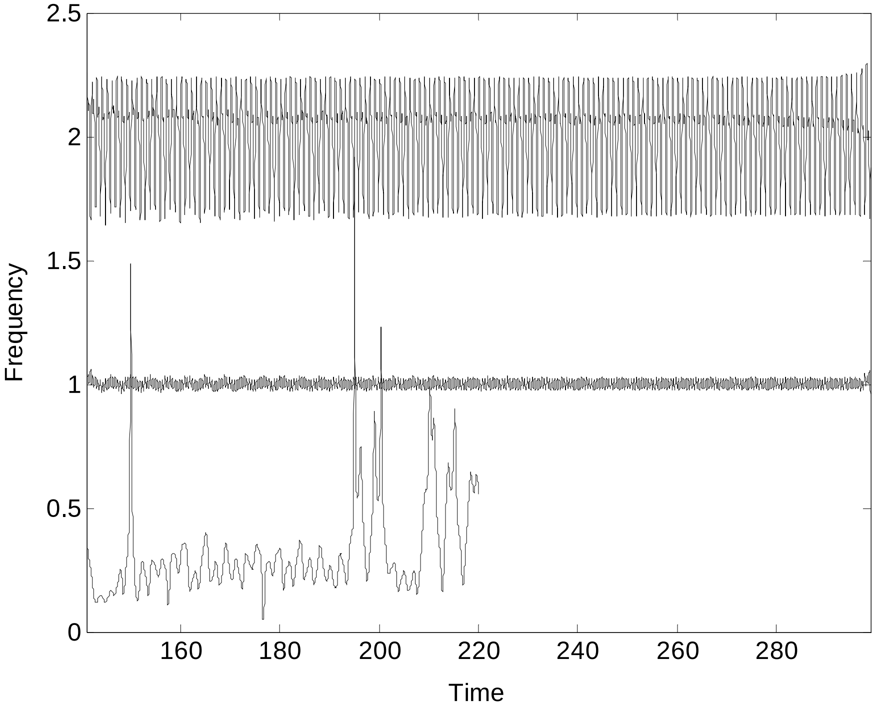

(b)

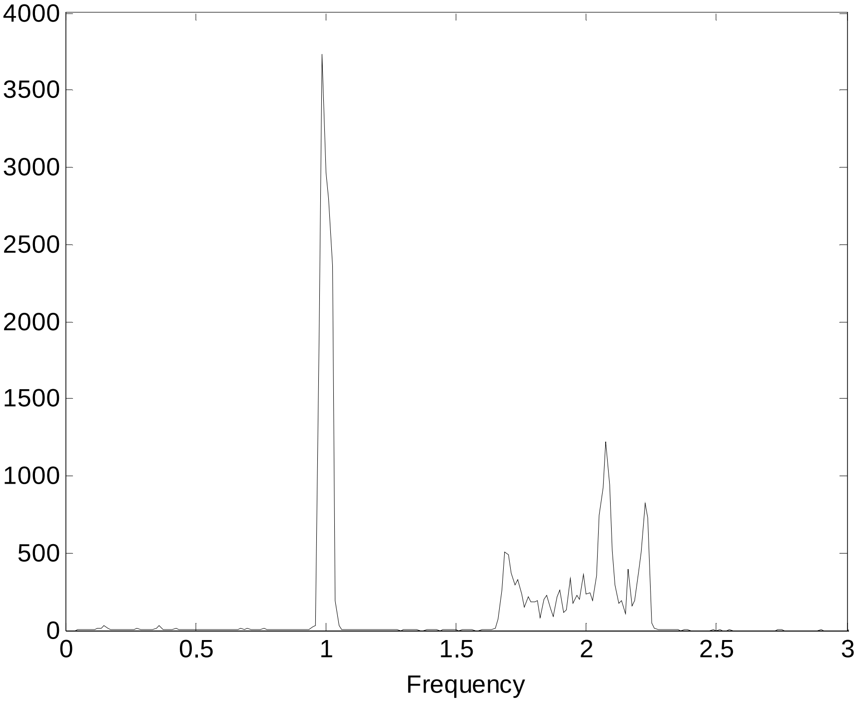

(c)

Figure 8.6 Continued

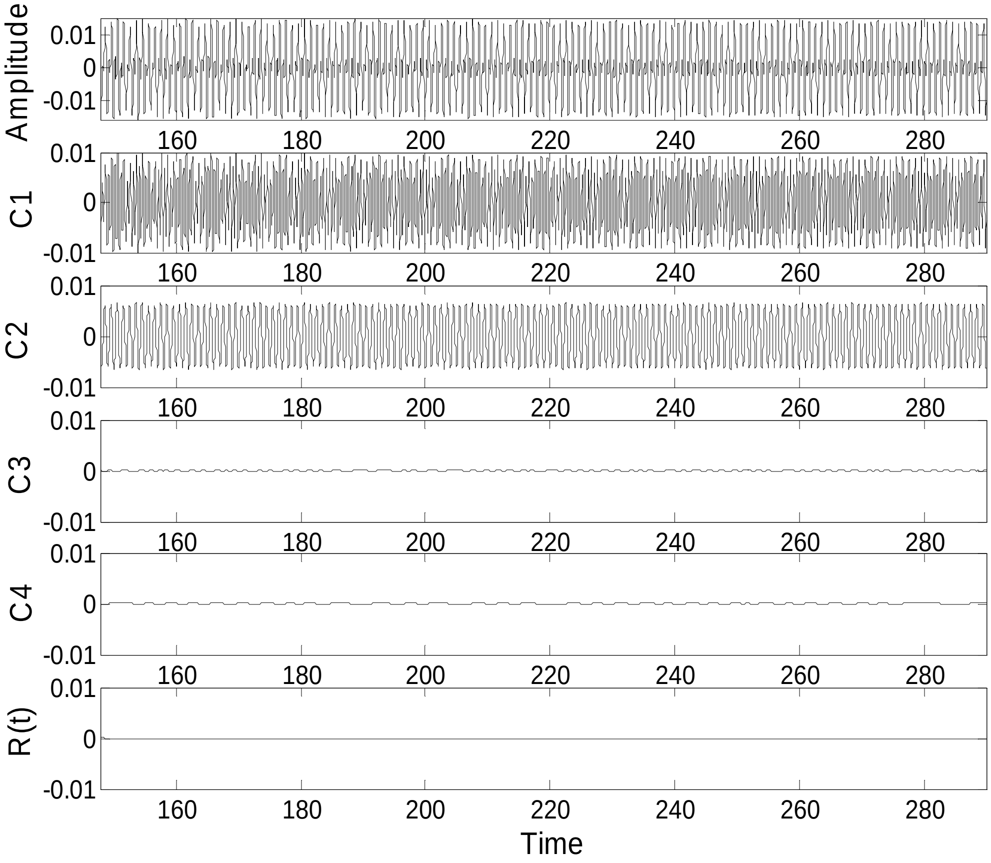

(a)

Figure 8.7 (a) Time waveform and its IMFs, (b) Instantaneous frequencies, and (c) Marginal spectrum for $\omega = 100\pi$, Cr=0.002r and h_r =0.20

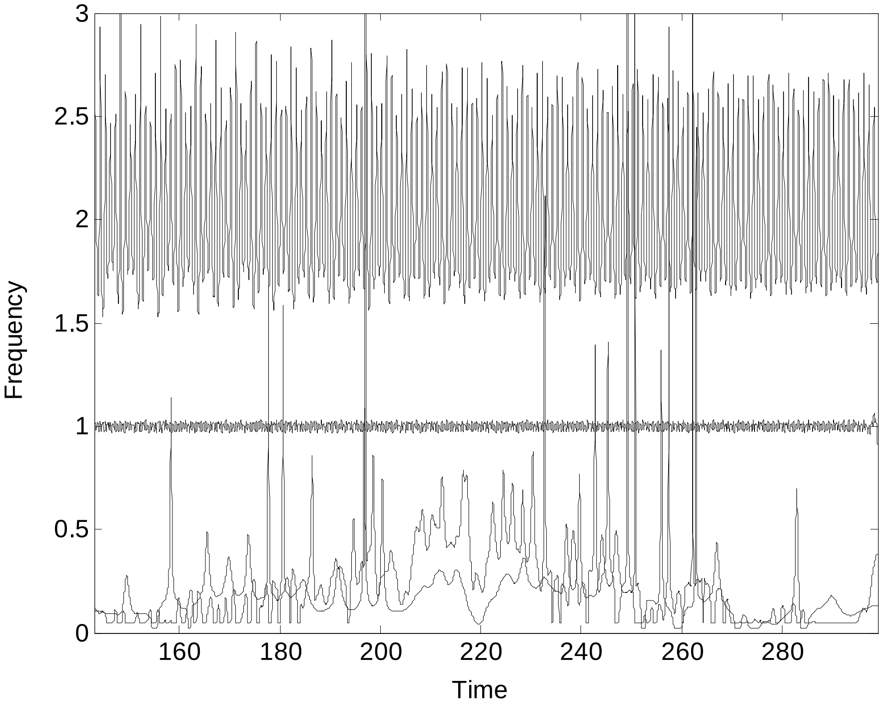

(b)

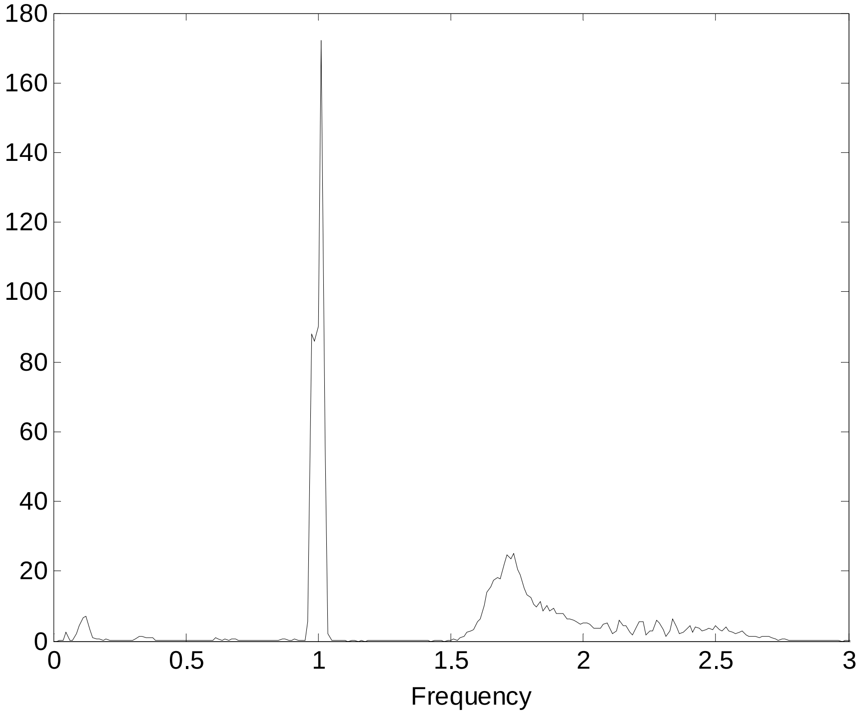

(c)

Figure 8.7 Continued

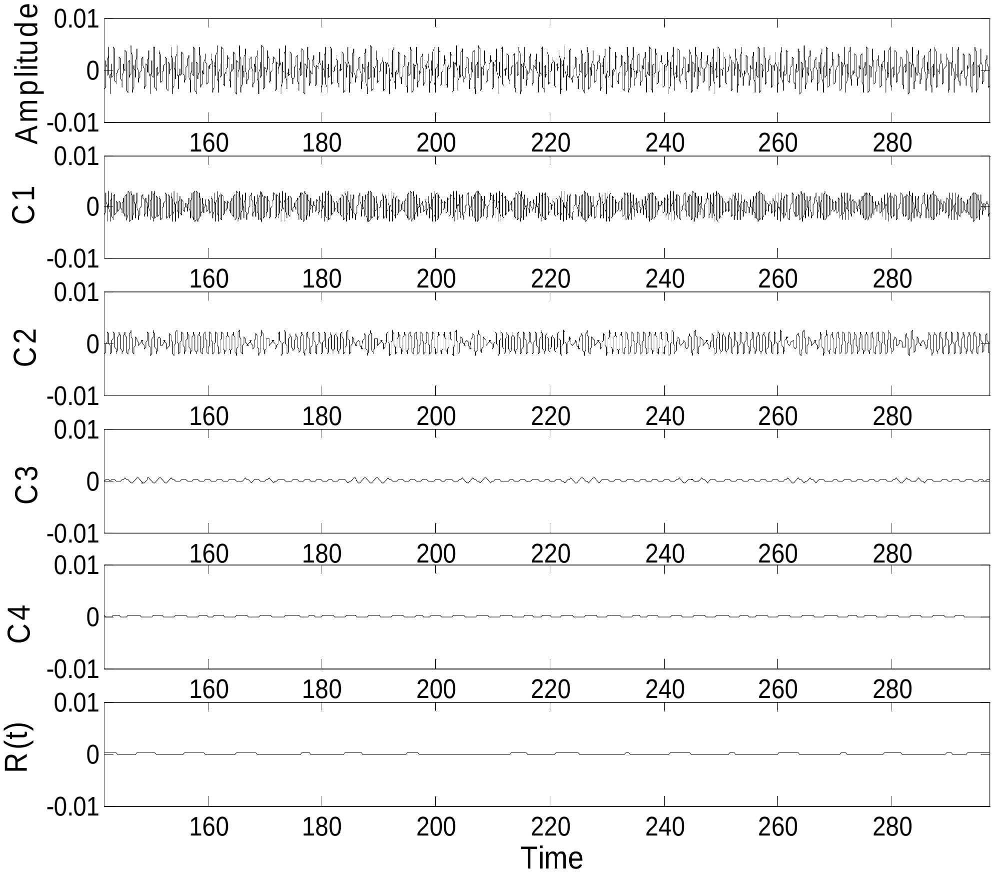

(a)

Figure 8.8 (a) Time waveform and its IMFs, (b) Instantaneous frequencies, and (c) Marginal spectrum for $\omega = 100\pi$, Cr=0.001r and h_r =0.20

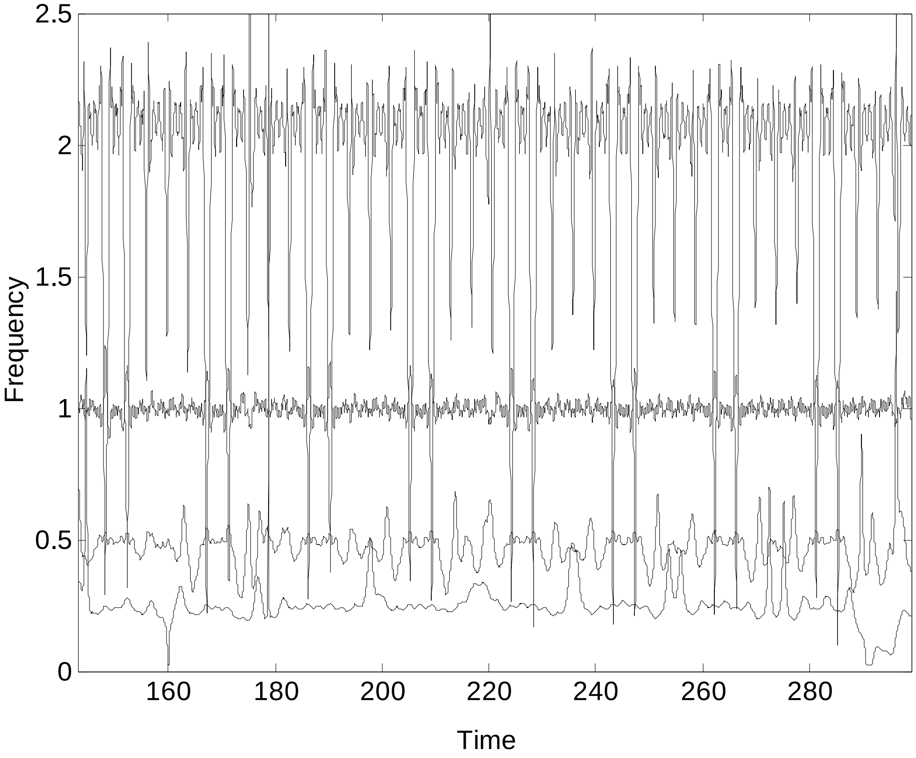

(b)

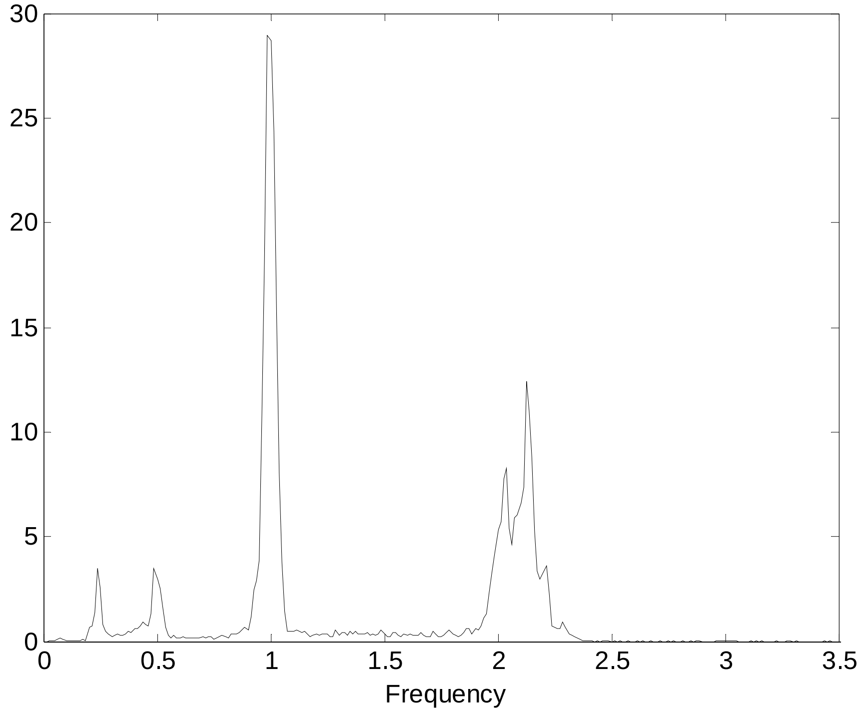

(c)

Figure 8.8 Continued

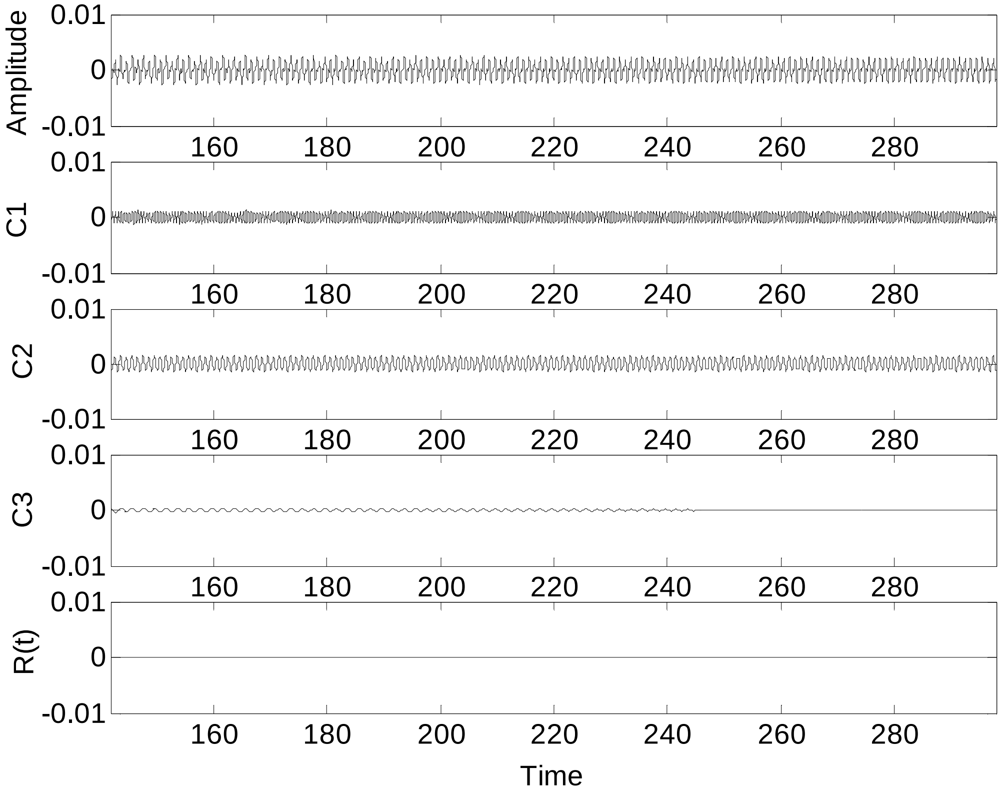

(a)

Figure 8.9 (a) Time waveform and its IMFs, (b) Instantaneous frequencies, and (c) Marginal spectrum for $\omega = 100\pi$, Cr=0.002r and h_r =0.30

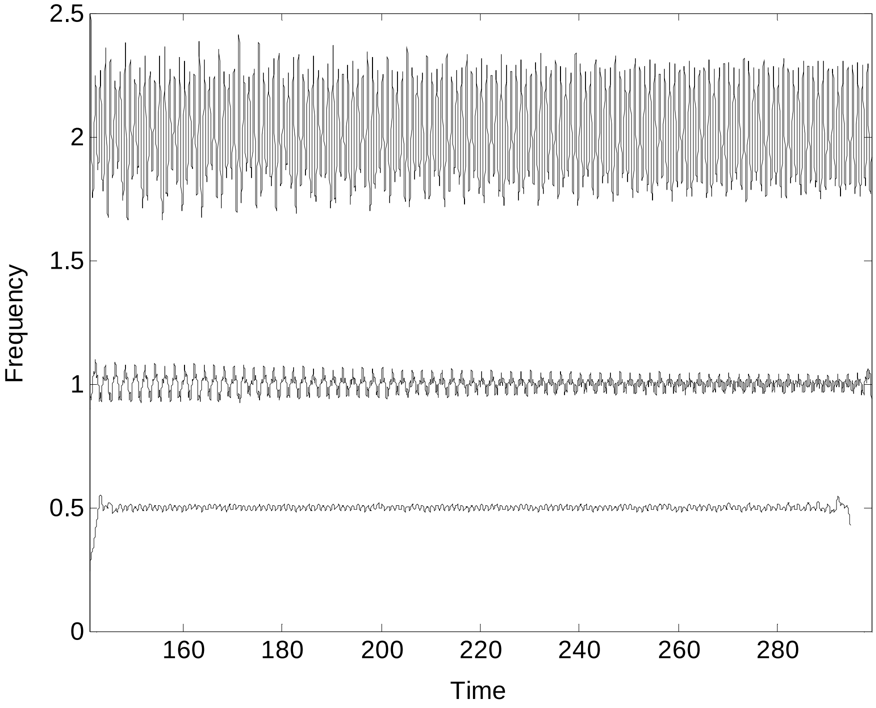

(b)

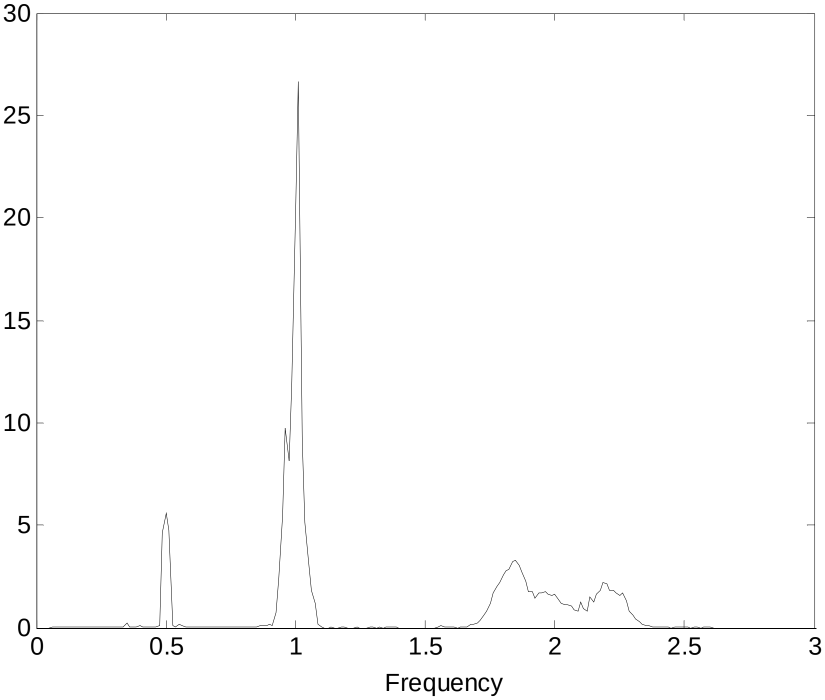

(c)

Figure 8.9 Continued

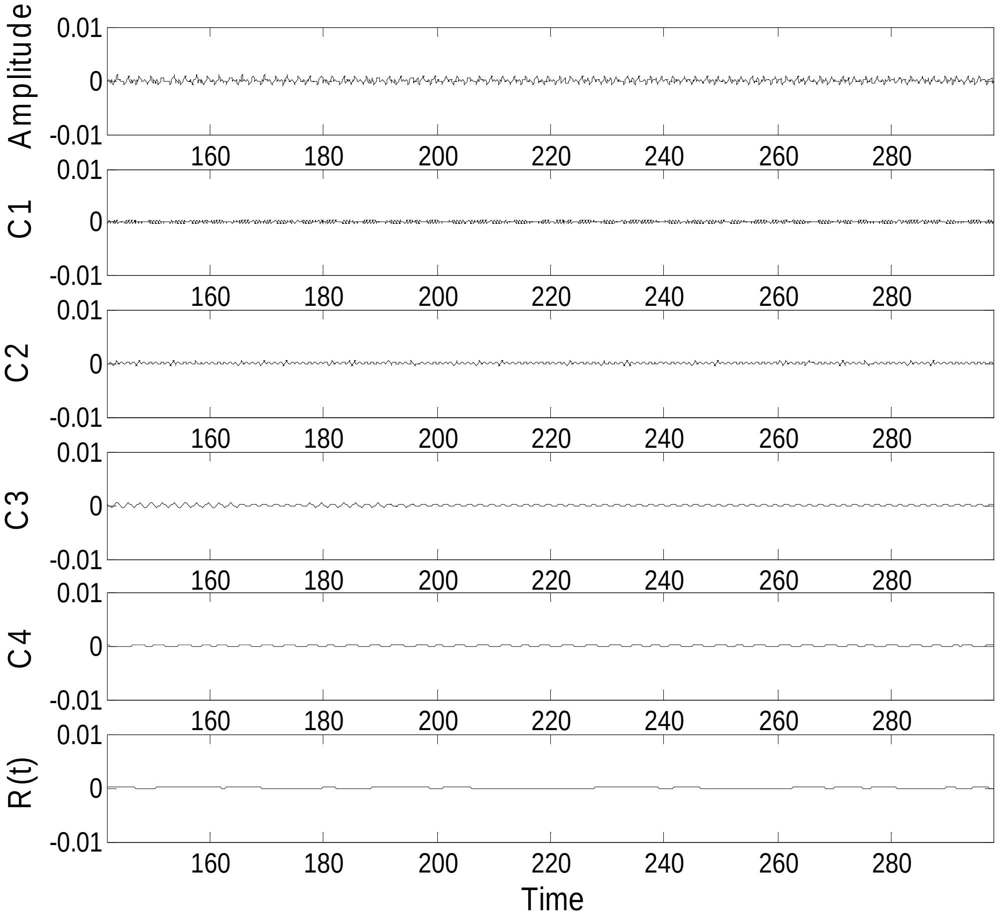

(a)

Figure 8.10 (a) Time waveform and its IMFs, (b) Instantaneous frequencies, and (c) Marginal spectrum for $\omega = 100\pi$, Cr=0.001r and h_r =0.30

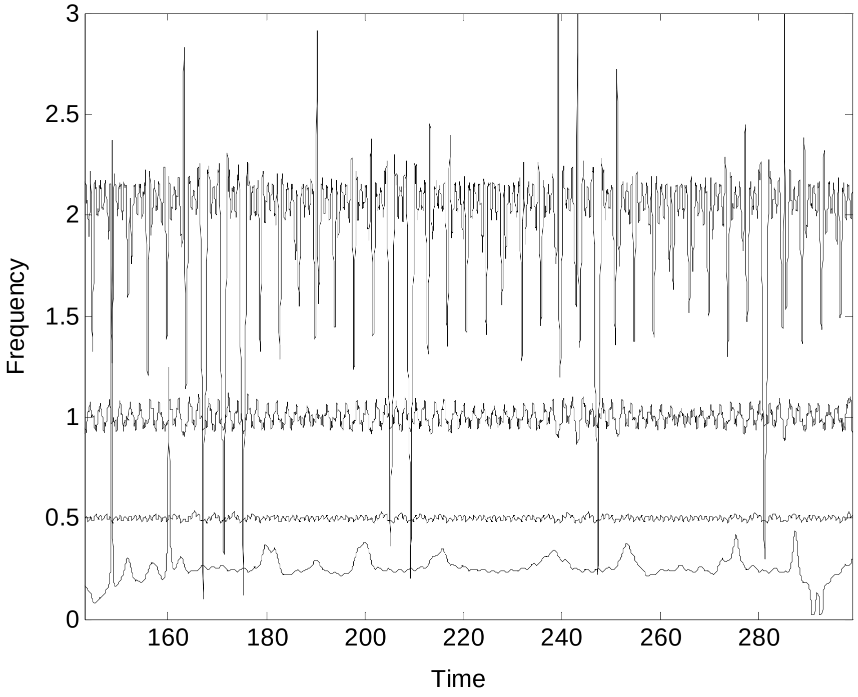

(b)

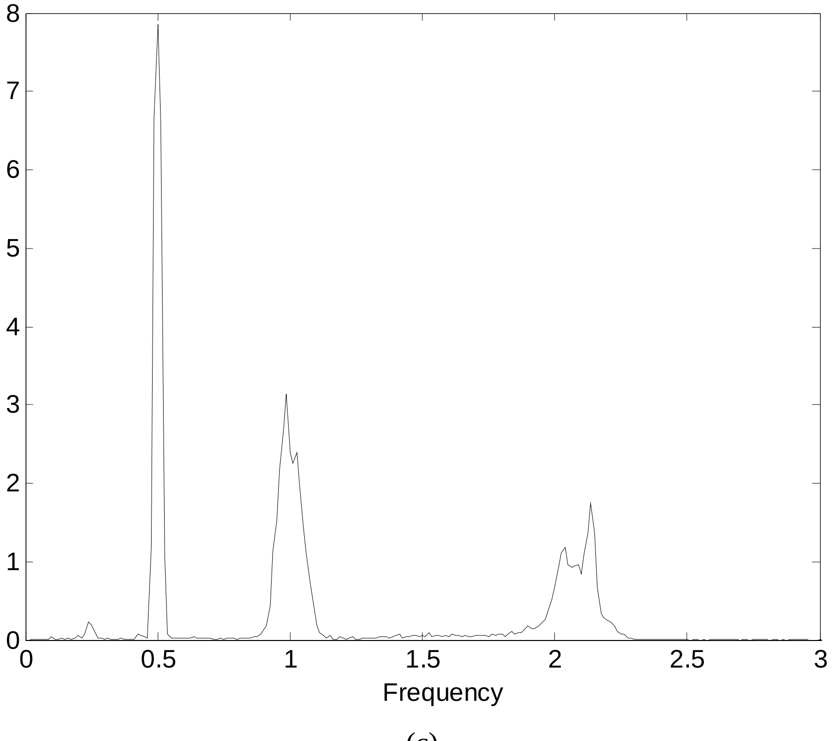

(c)

Figure 8.10 Continued

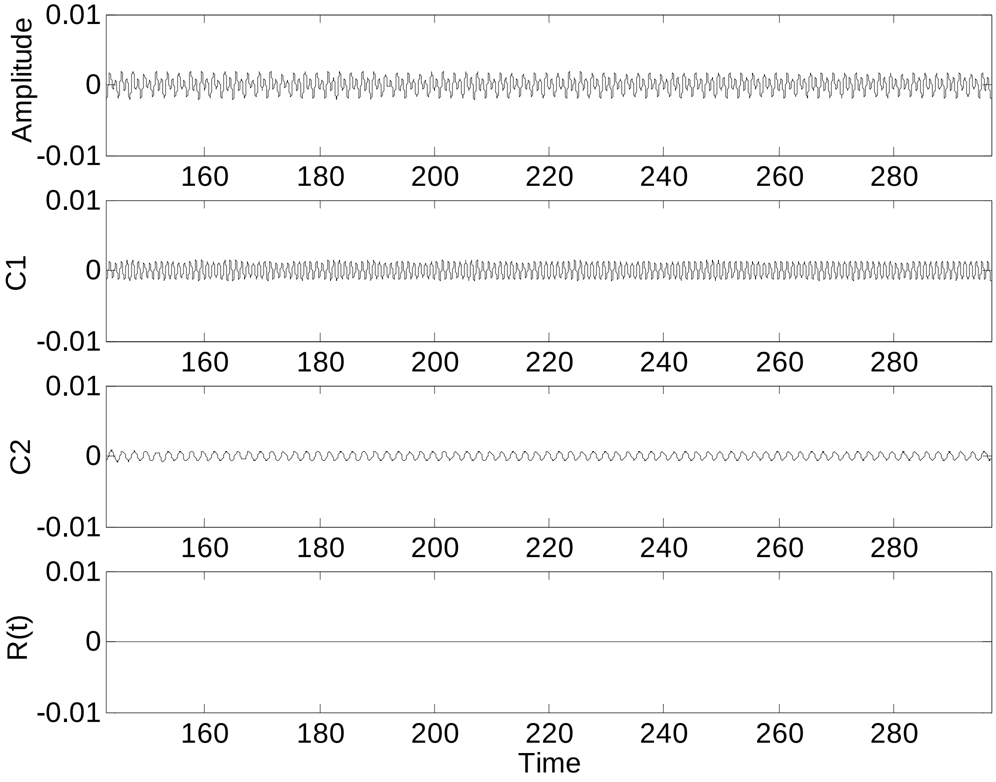

(a)

Figure 8.11 (a) Time waveform and its IMFs, (b) Instantaneous frequencies, and (c) Marginal spectrum for $\omega = 200\pi$, Cr=0.002r and h_r =0.05

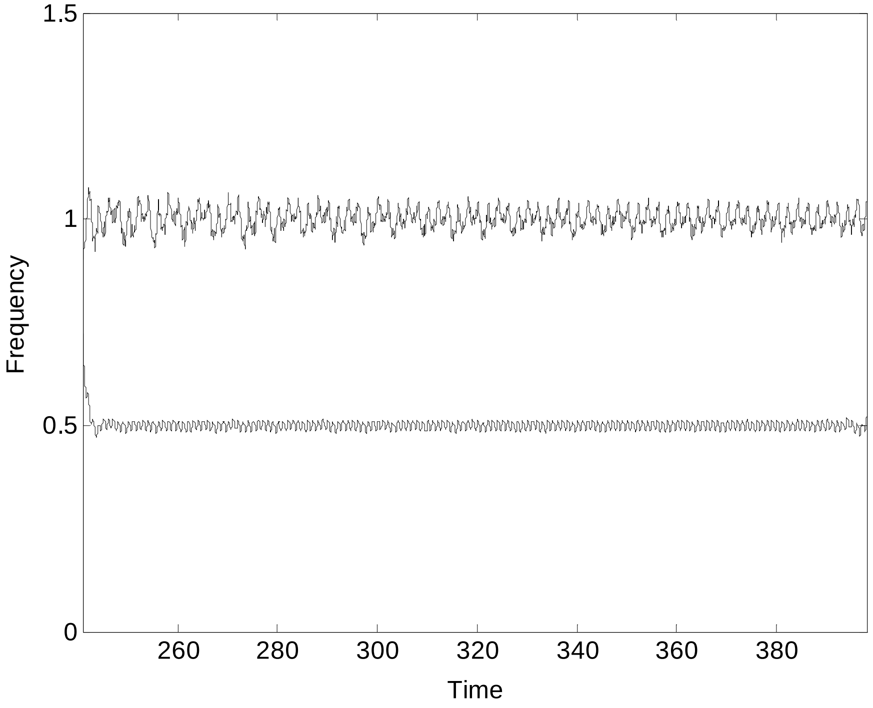

(b)

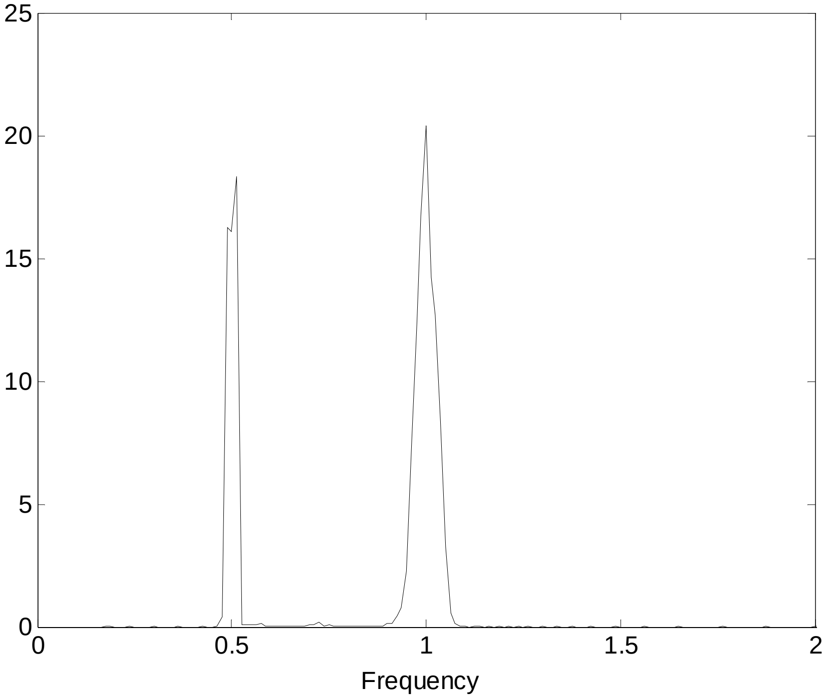

(c)

Figure 8.11 Continued

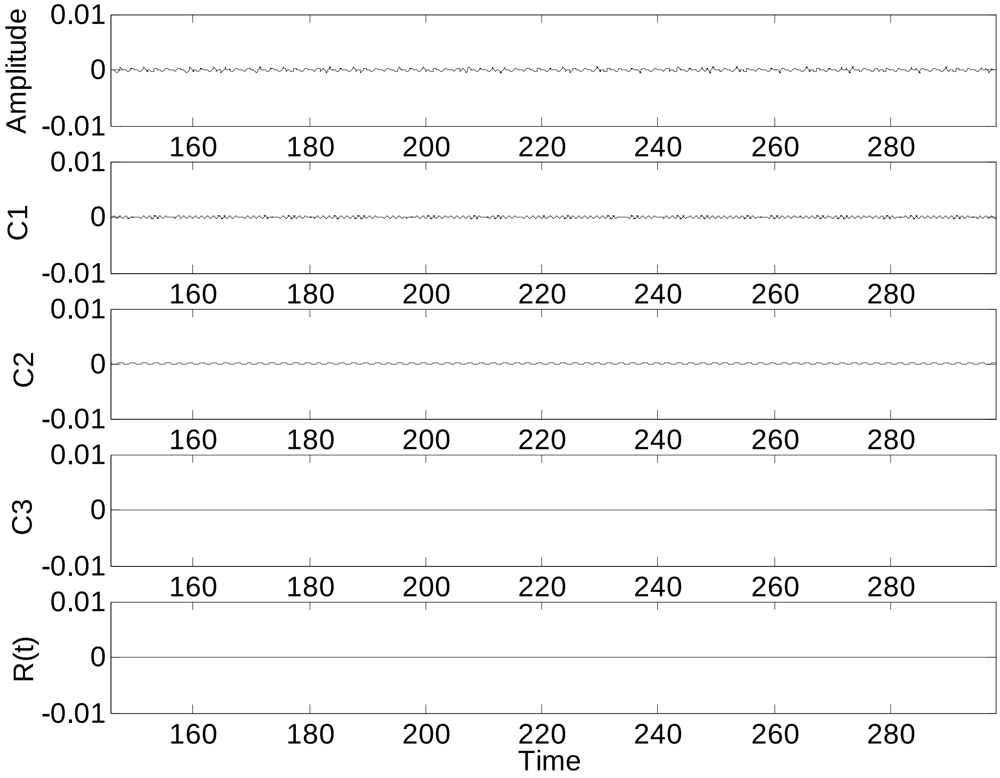

(a)

Figure 8.12 (a) Time waveform and its IMFs, (b) Instantaneous frequencies, and (c) Marginal spectrum for $\omega = 200\pi$, Cr=0.001r and h_r =0.05

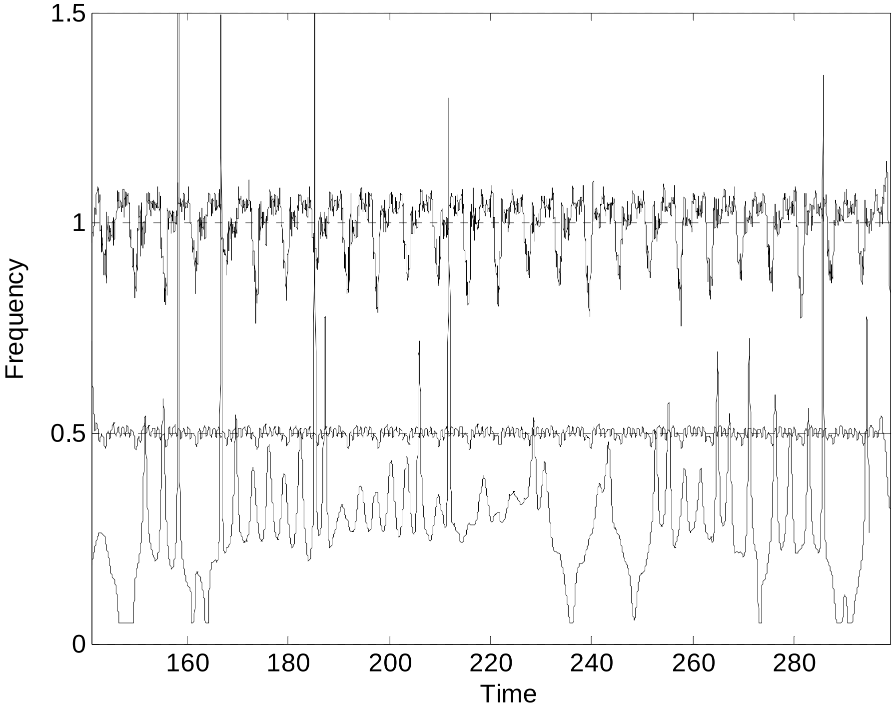

(b)

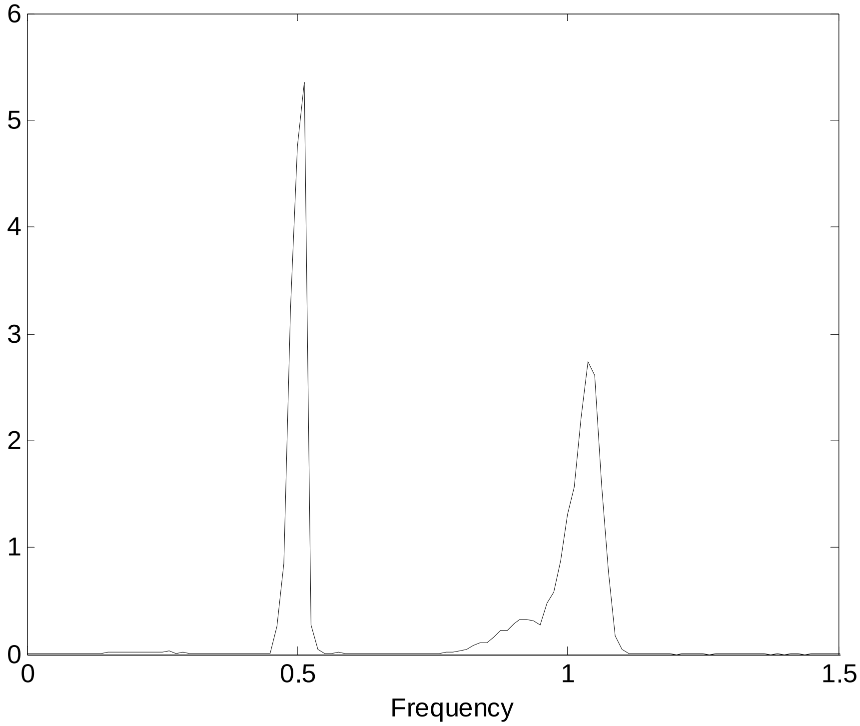

(c)

Figure 8.12 Continued

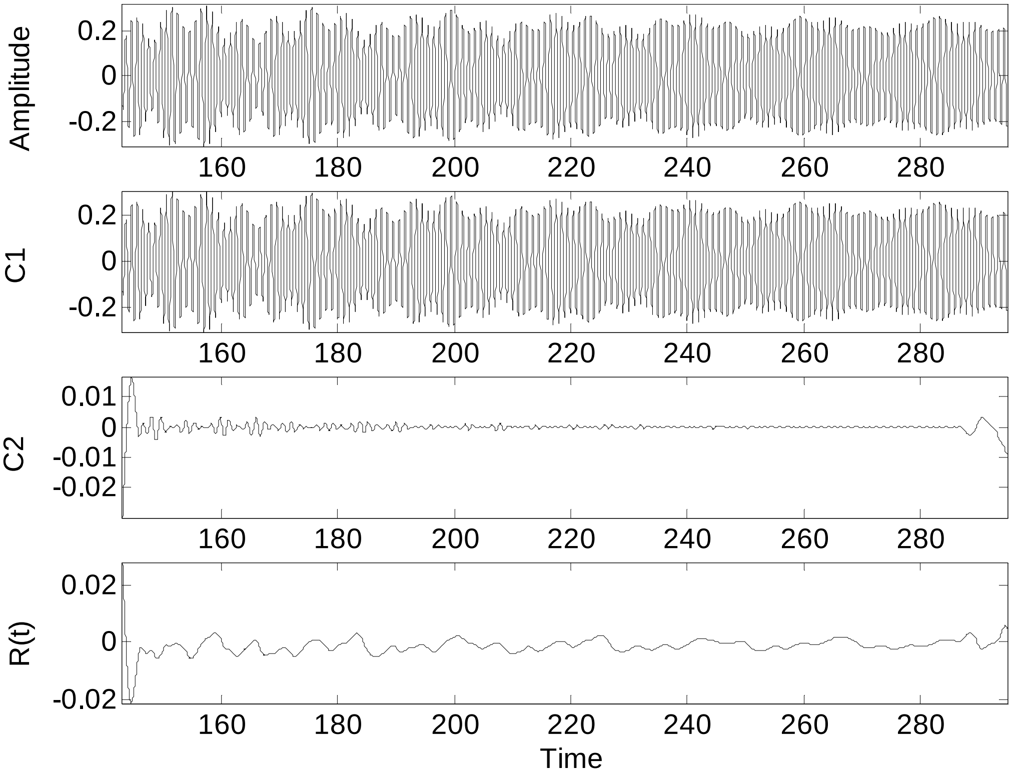

(a)

Figure 8.13 (a) Time waveform and its IMFs, (b) Instantaneous frequencies, and (c) Marginal spectrum for $\omega = 200\pi$, Cr=0.0025r and h_r =0.10

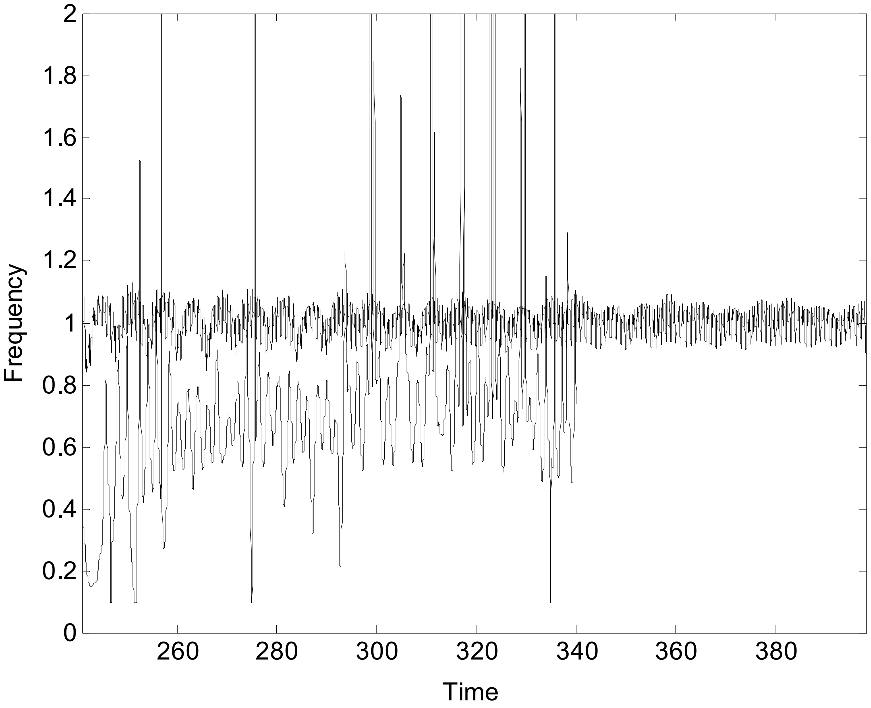

(b)

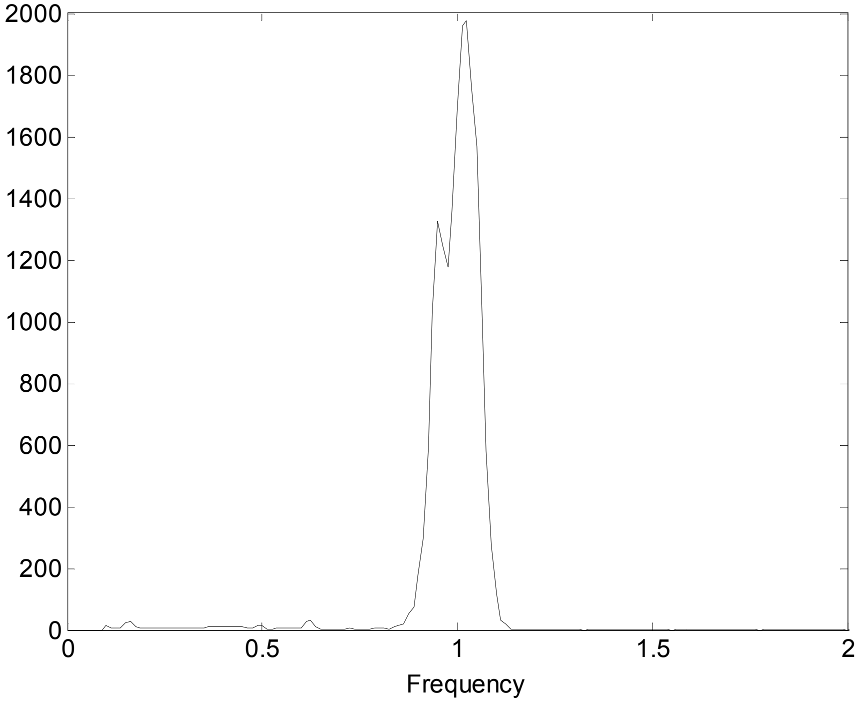

(c)

Figure 8.13 Continued

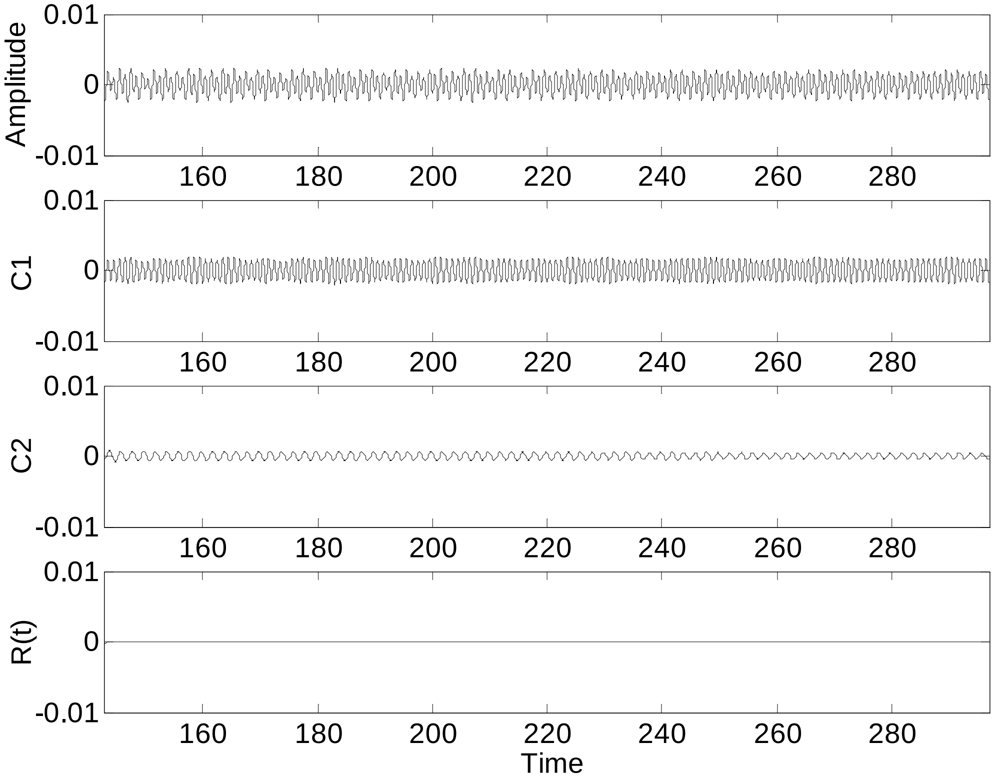

(a)

Figure 8.14 (a) Time waveform and its IMFs, (b) Instantaneous frequencies, and (c) Marginal spectrum for $\omega = 200\pi$, Cr=0.002r and h_r =0.10

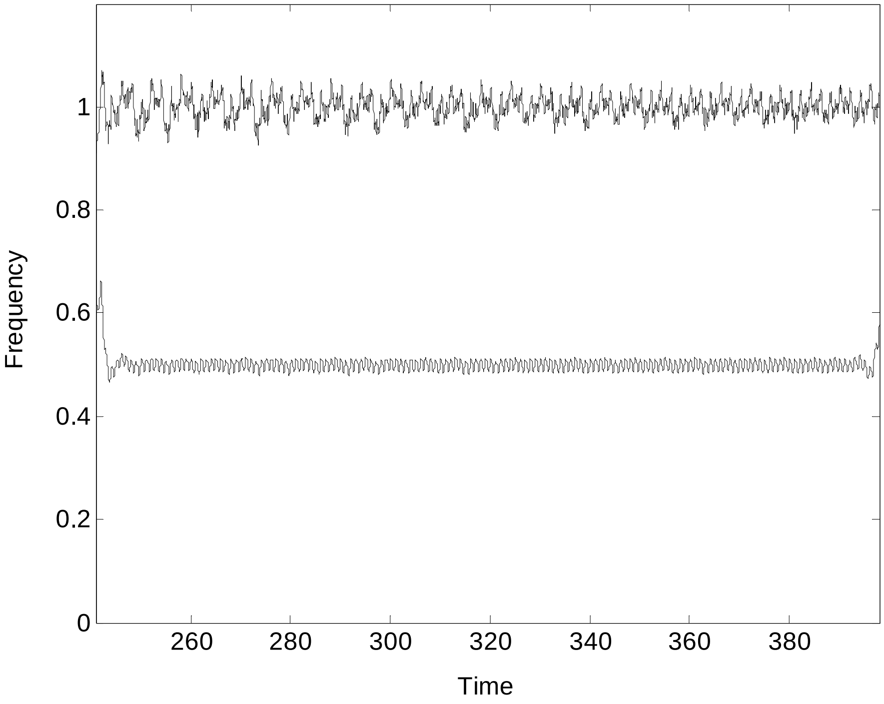

(b)

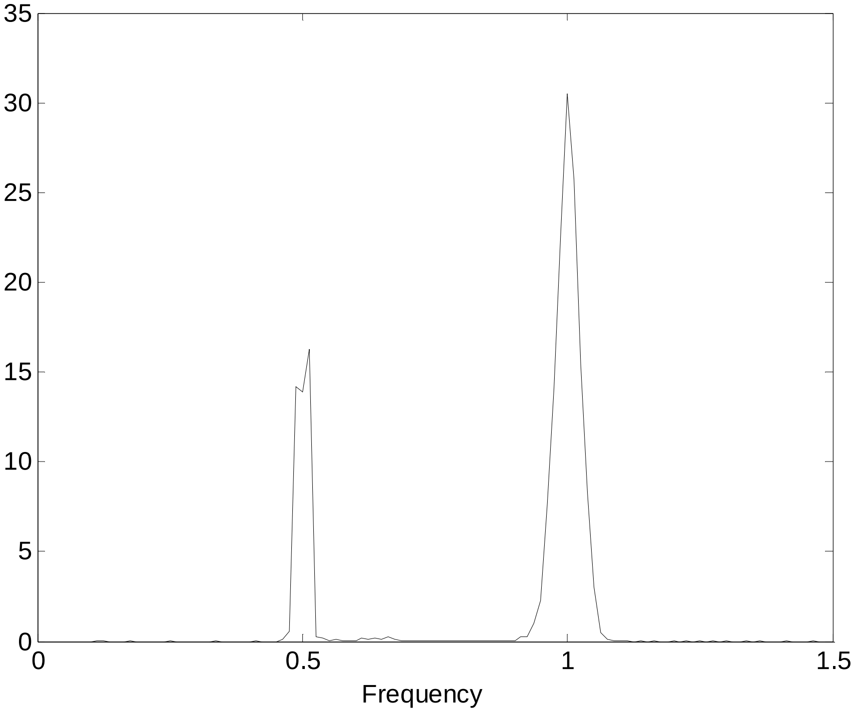

(c)

Figure 8.14 Continued

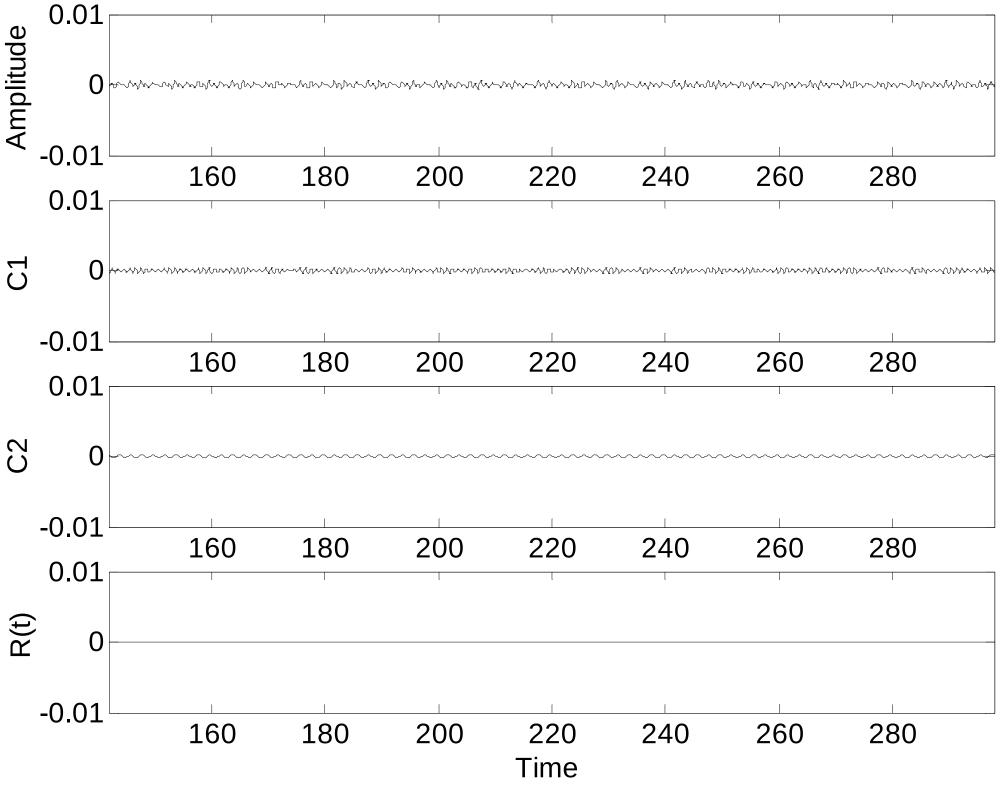

(a)

Figure 8.15 (a) Time waveform and its IMFs, (b) Instantaneous frequencies, and (c) Marginal spectrum for $\omega = 200\pi$, Cr=0.001r and h_r =0.10

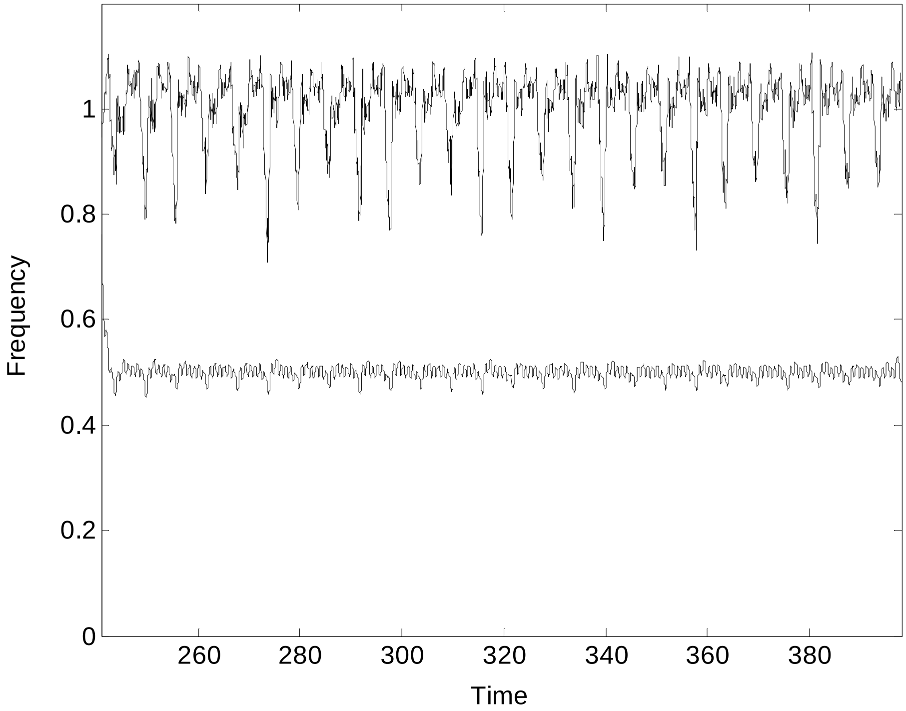

(b)

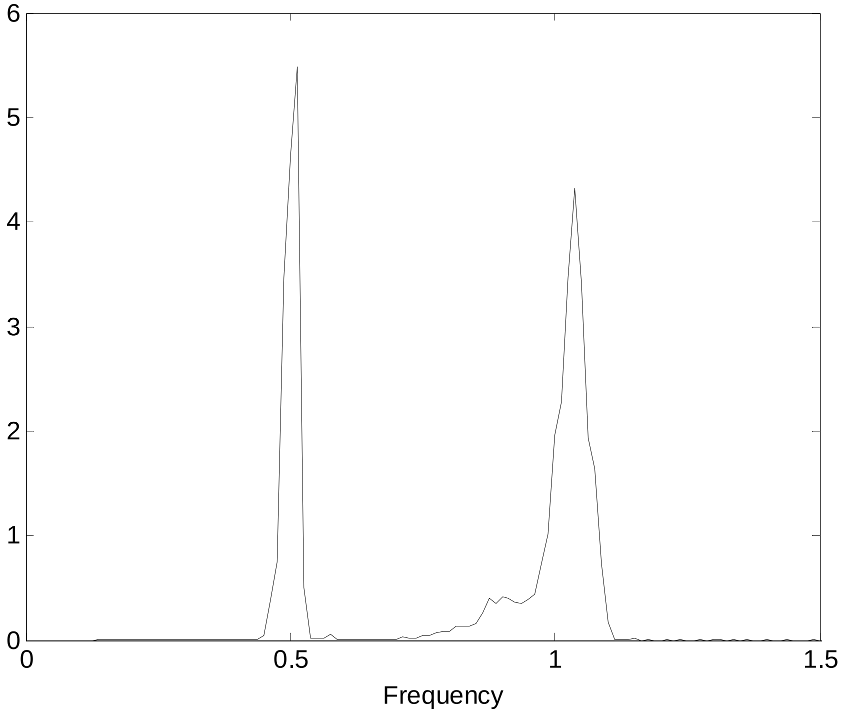

(c)

Figure 8.15 Continued

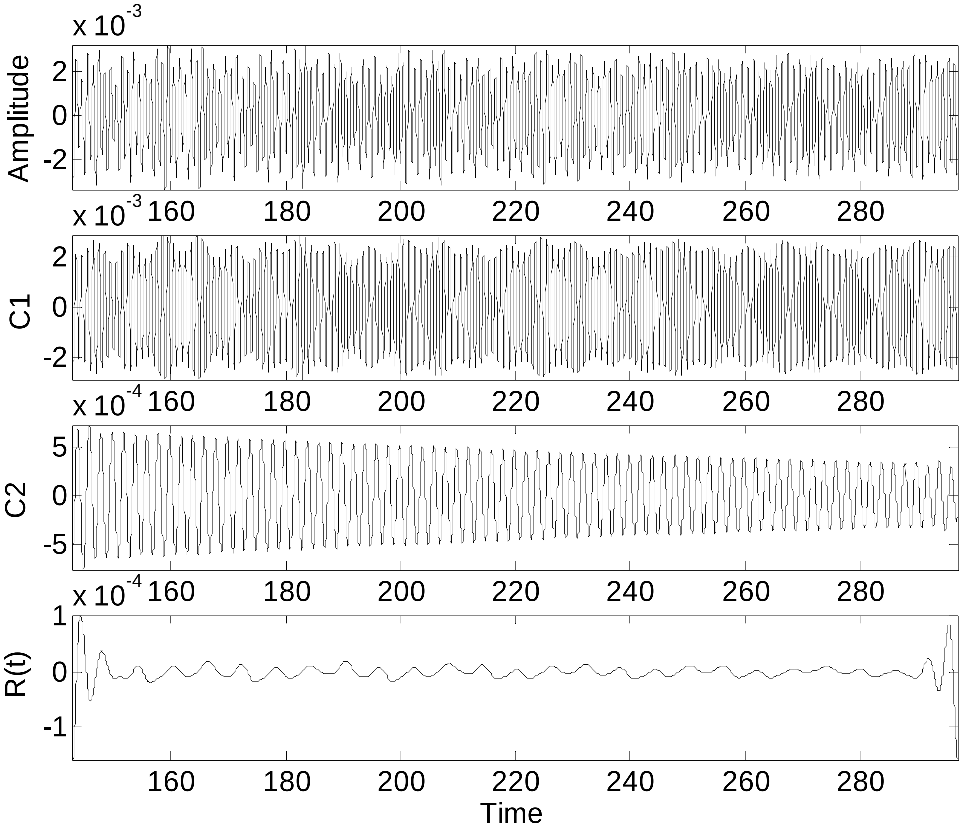

(a)

Figure 8.16 (a) Time waveform and its IMFs, (b) Instantaneous frequencies, and (c) Marginal spectrum for $\omega = 200\pi$, Cr=0.002r and h_r =0.20

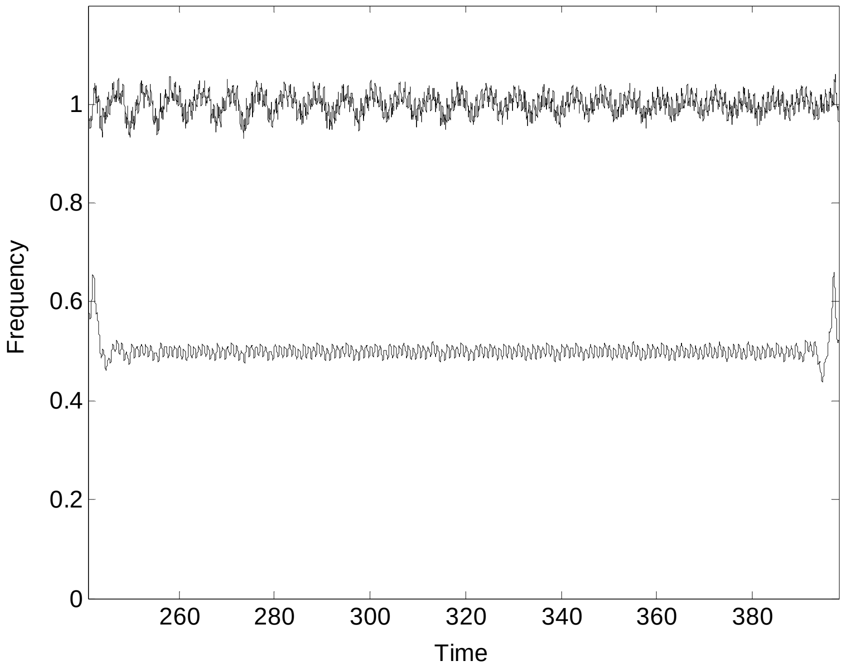

(b)

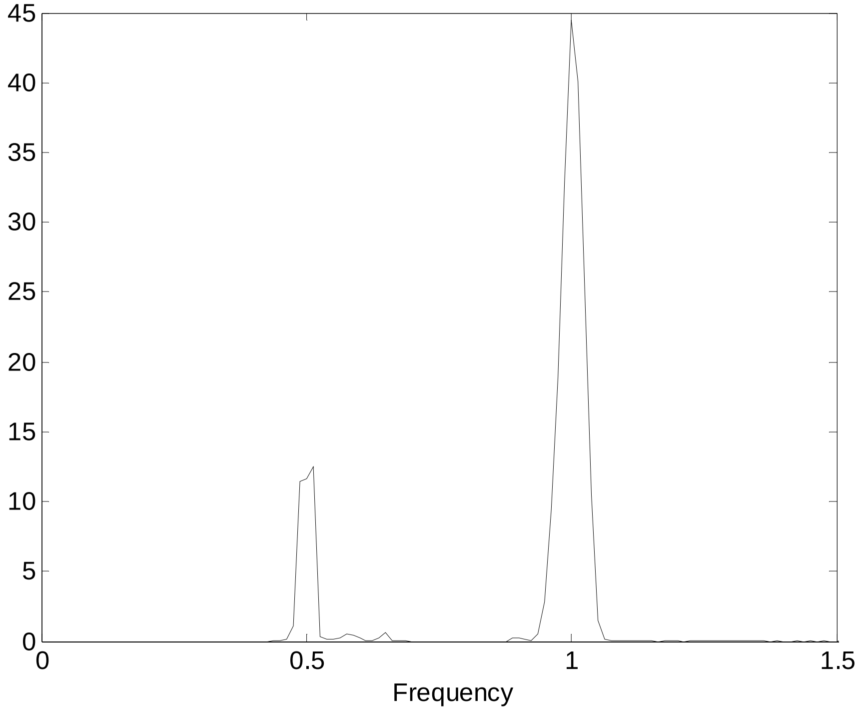

(c)

Figure 8.16 Continued

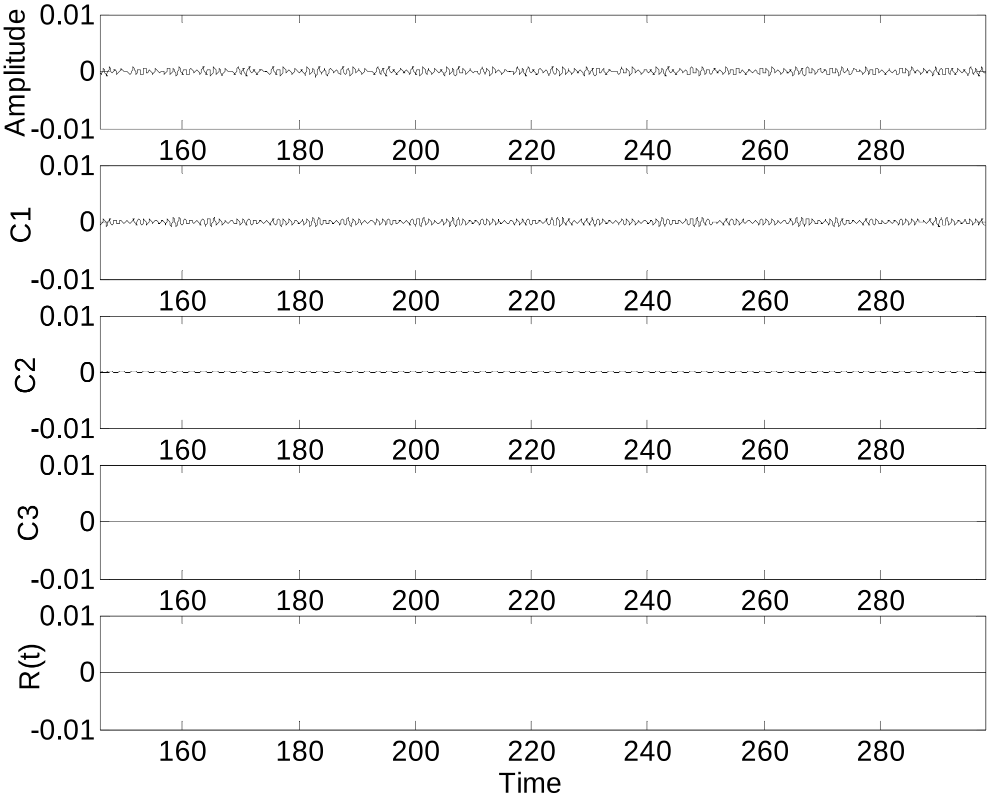

(a)

Figure 8.17 (a) Time waveform and its IMFs, (b) Instantaneous frequencies, and (c) Marginal spectrum for $\omega = 200\pi$, Cr=0.001r and h_r =0.20

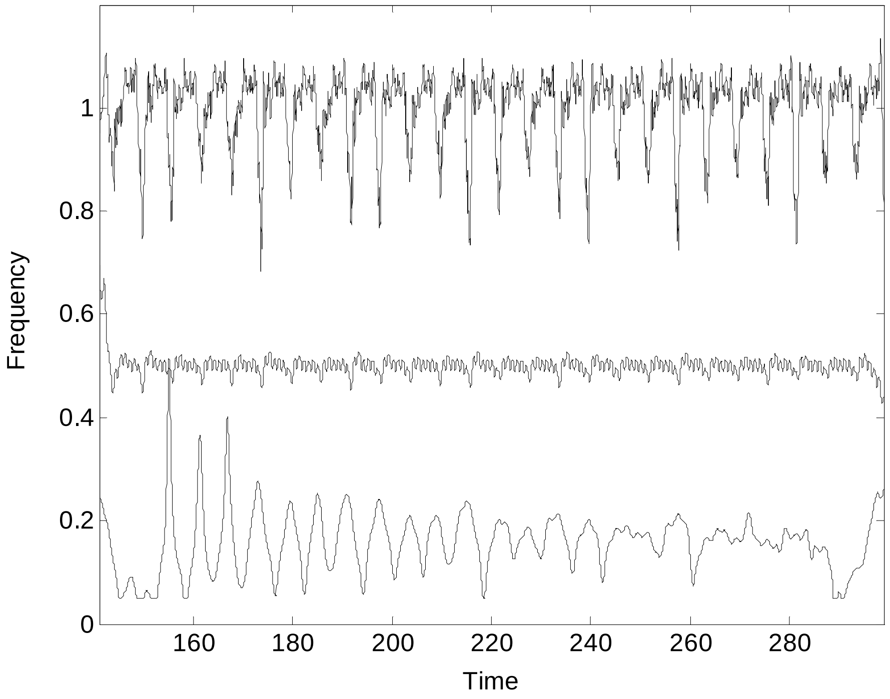

(b)

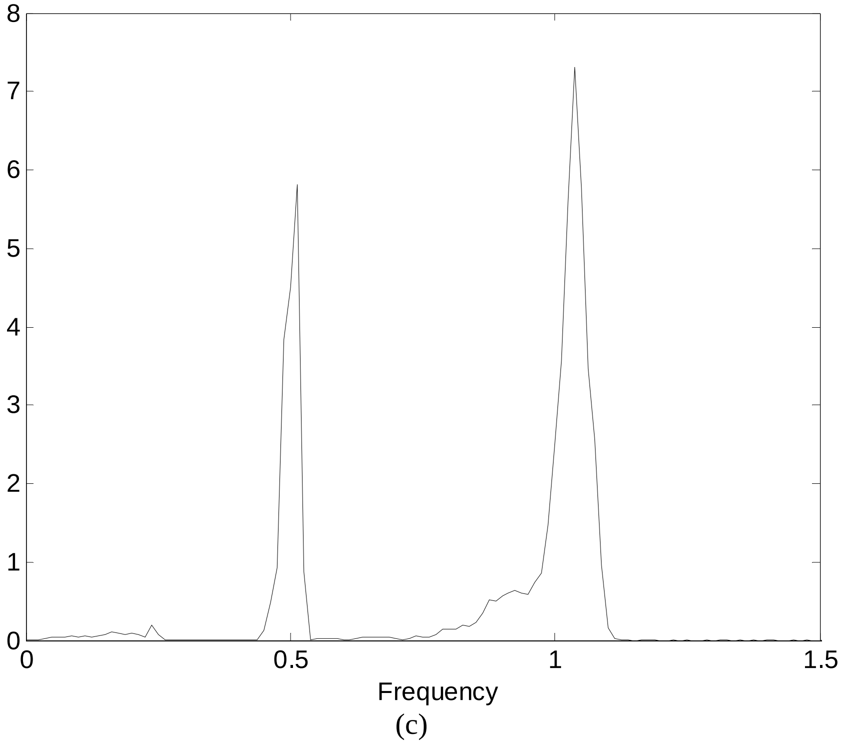

(c)

Figure 8.17 Continued

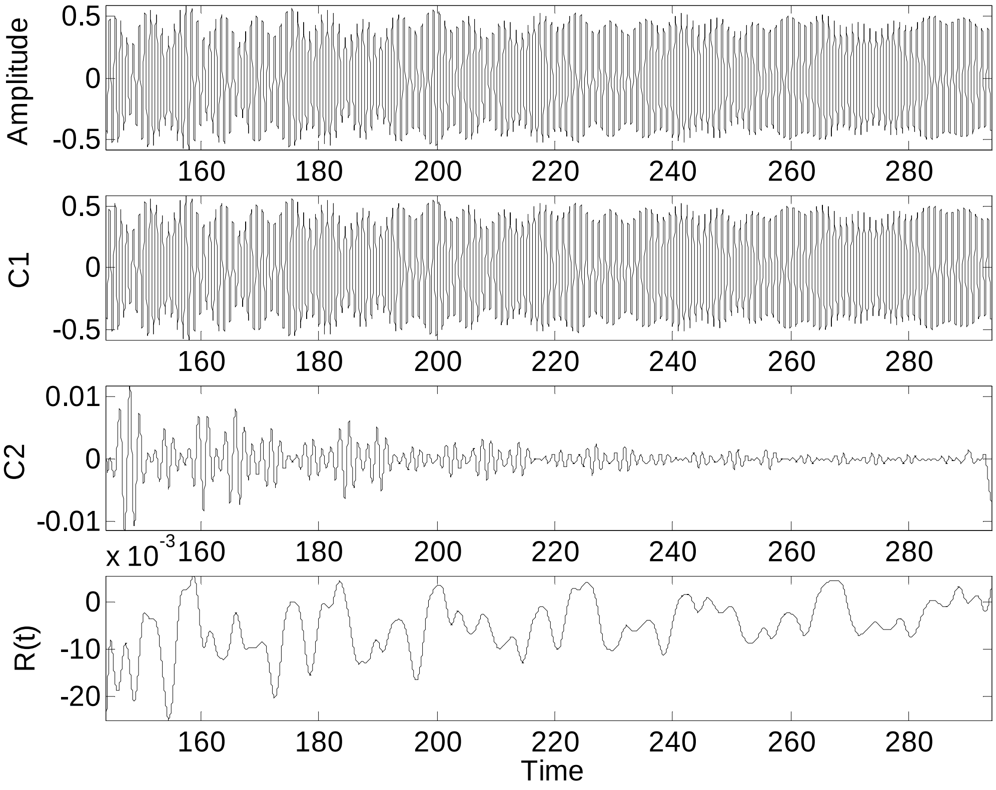

(a)

Figure 8.18 (a) Time waveform and its IMFs, (b) Instantaneous frequencies, and (c) Marginal spectrum for $\omega = 200\pi$, Cr=0.0025r and h_r =0.25

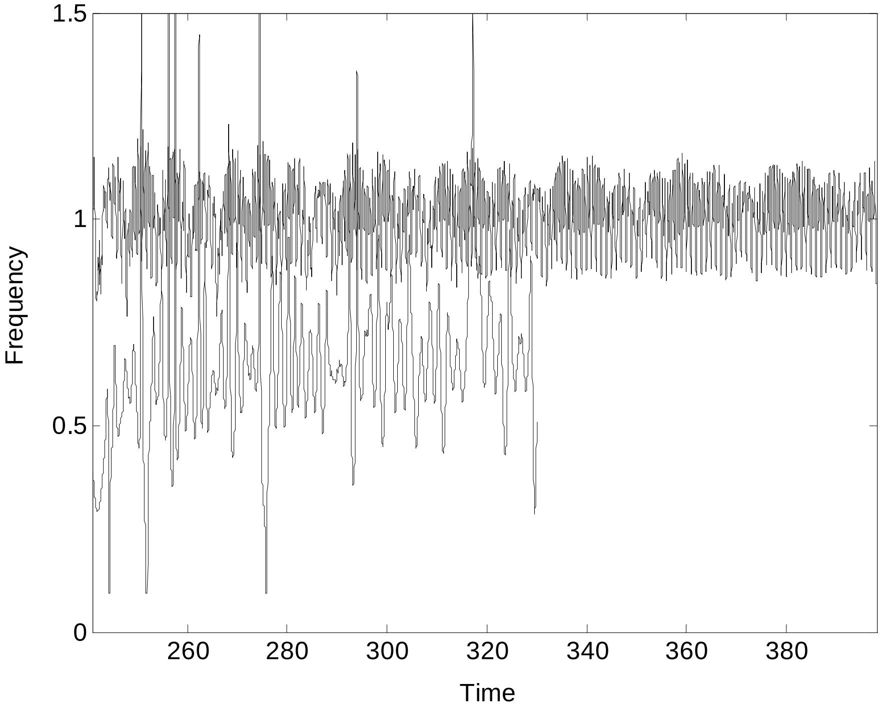

(b)

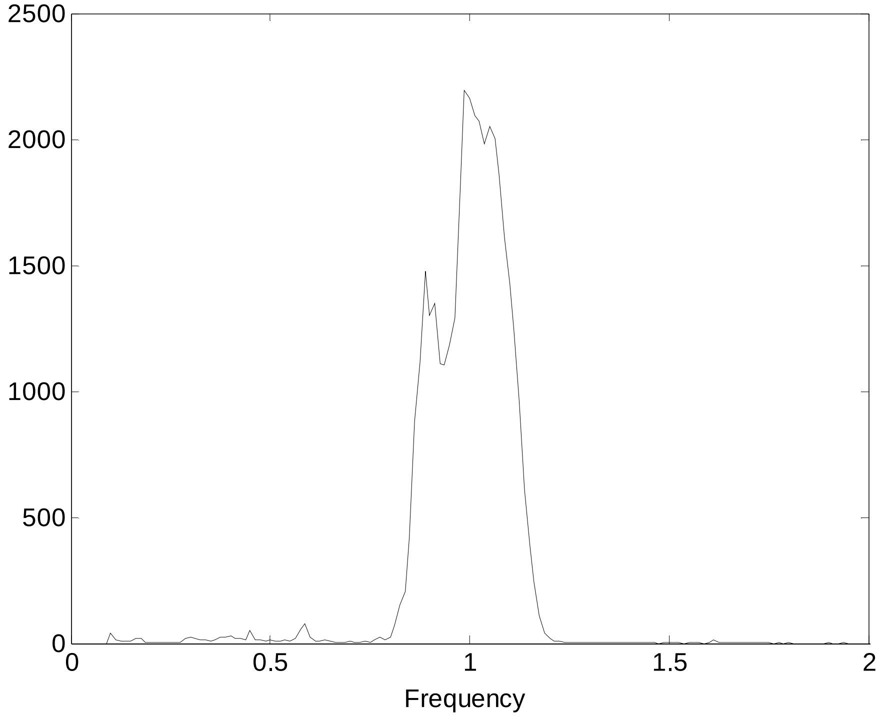

(c)

Figure 8.18 Continued

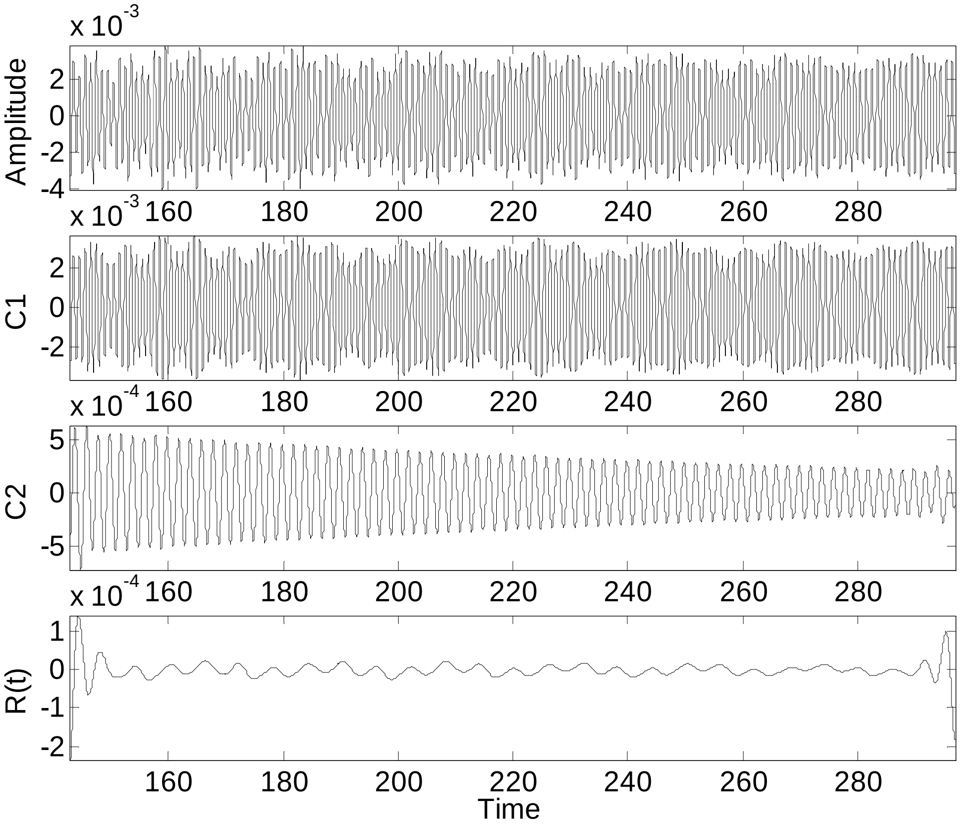

(a)

Figure 8.19 (a) Time waveform and its IMFs, (b) Instantaneous frequencies, and (c) Marginal spectrum for $\omega = 200\pi$, Cr=0.002r and h_r =0.30

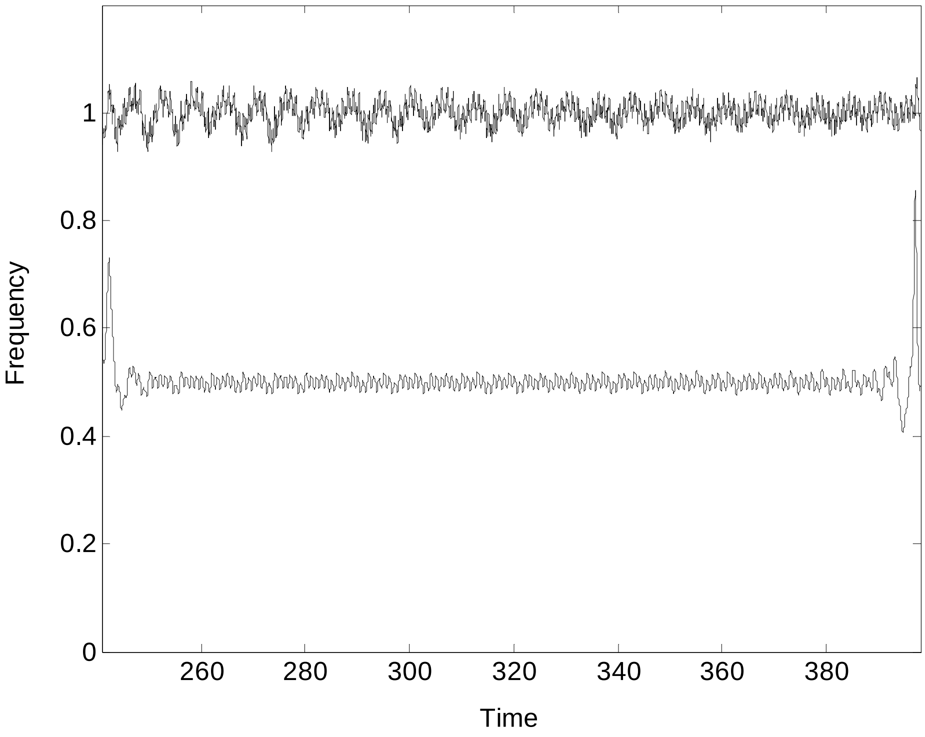

(b)

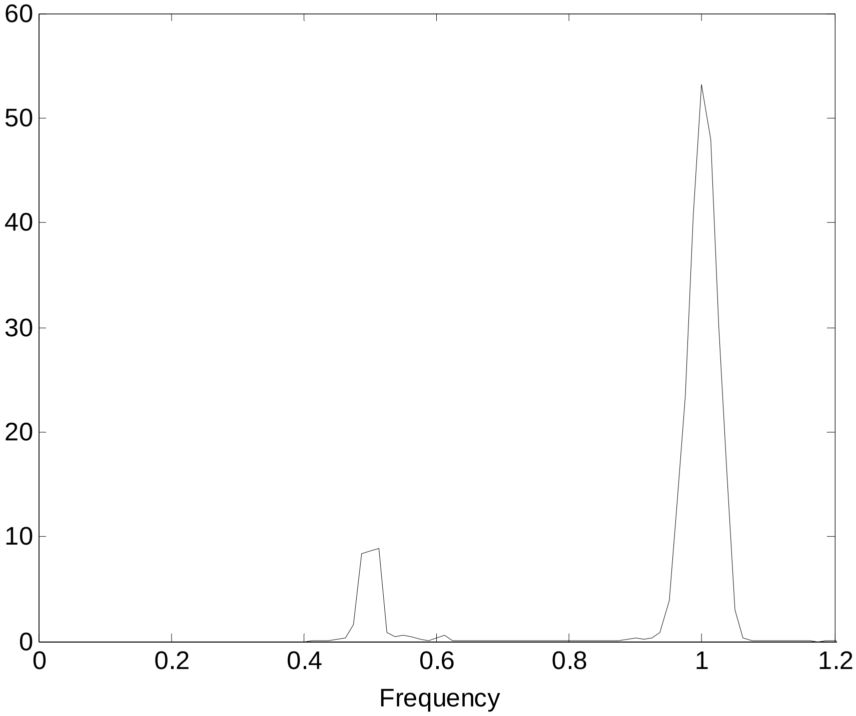

(c)

Figure 8.19 Continued

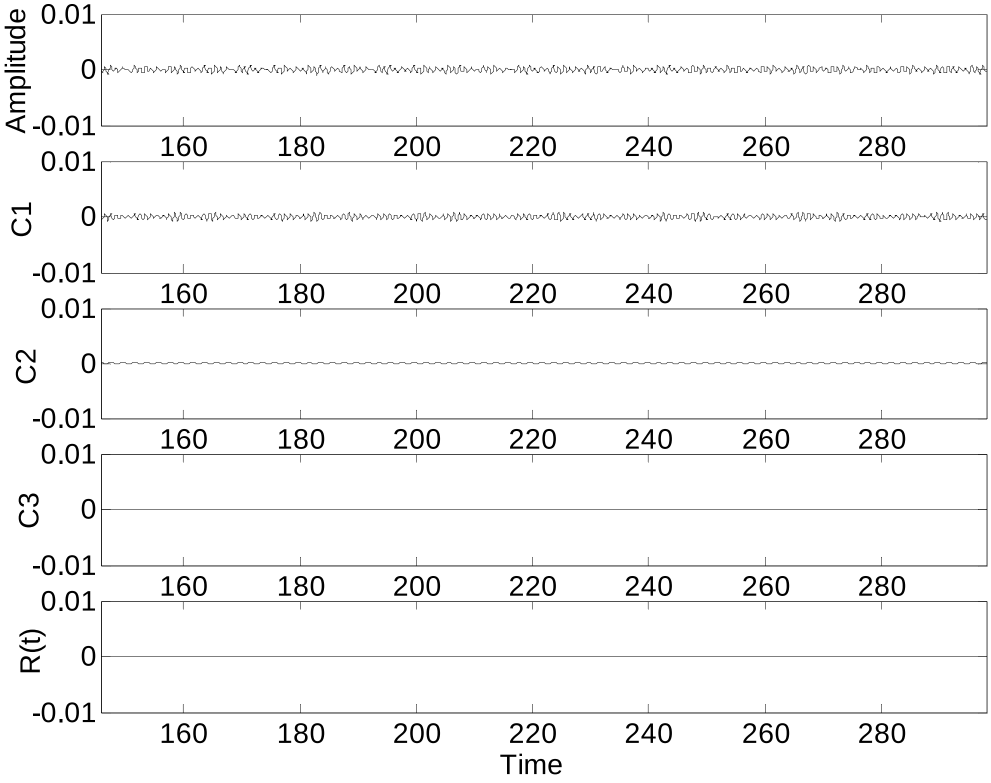

(a)

Figure 8.20 (a) Time waveform and its IMFs, (b) Instantaneous frequencies, and (c) Marginal spectrum for $\omega = 200\pi$, Cr=0.001r and h_r =0.30

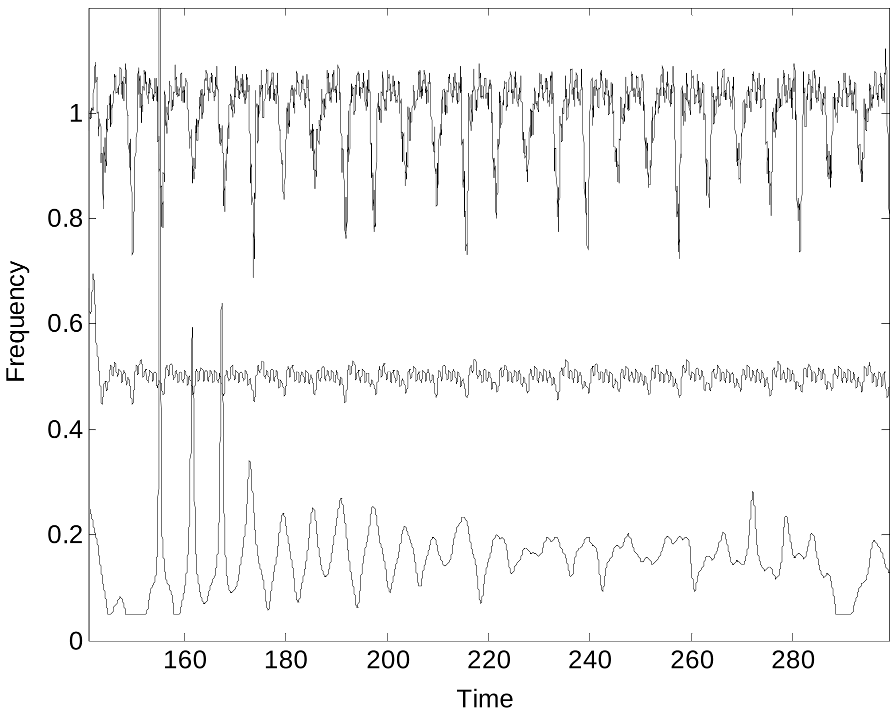

(b)

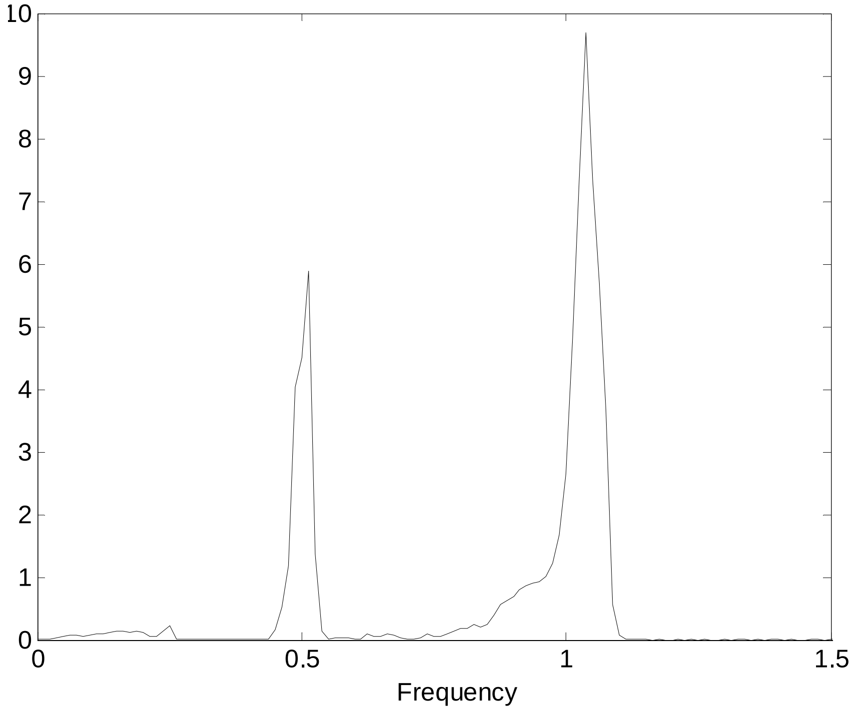

(c)

Figure 8.20 Continued

analysis.

First consider the cases corresponding to $\omega = 100\pi$, and $h_r = 0.05$. Figures 8.1-8.3 show, respectively, the dynamical responses of the rotor with clearance Cr = 0.0025r, 0.002r and 0.001r, in which r is the shaft radius. As seen in Figures 8.1(a)-8.3(a), when the clearance is decreased, the induced bearing force increases (see Eqs. 5.9 and 5.11), and the corresponding vibration amplitude is also decreased. In addition, when Cr = 0.001r, the rotor response has one additional intrinsic mode. From their associated instantaneous frequencies given in Figures 8.1(b)-8.3(b), one can discern that the intrinsic mode C1 of frequency 2 is due to the crack-induced local dissimilarity in shaft flexibility and that the C2 mode of frequency 1 is the driving frequency. The C3 mode of low frequency as seen in Figures 8.1 and 8.2 disappears eventually when steady state is reached. However, the C3 mode of frequency 0.5 and C4 mode of frequency 0.25 in Figure 8.3 do not disappear. These two modes indicate that period-doubling bifurcation had happened twice in the process. The system is seen to lose stability over decreasing bearing clearances. None of the instantaneous frequencies of these four modes shown in Figure 8.3 (b) displays periodic-modal structure in the instantaneous time-frequency plane, thus indicating the dynamical state of deteriorating stability. Figures 8.1(c)-8.3(c) each shows the probabilistic cumulative effect of the instantaneous frequency components. Also, the broadband marginal spectrum in Figure 8.3(c) highlights that the low frequency components are becoming significant as the bearing clearance is being decreased.

The dynamical responses, along with their intrinsic modes, in response to clearances of 0.002r and 0.001r, and subject to $h_r = 0.10$ and $\omega = 100\pi$, are given in Figures 8.4(a) and 8.5(a). It is seen through comparing with Figures 8.2 and 8.3 that the vibration amplitude becomes larger with the growth of surface crack and that the crack induced mode of frequency 2 becomes more significant as is evident in the associated marginal spectra, Figures 8.4 (c) and 8.5 (c).

Figure 8.4 shows a case similar to Figures 8.1 and 8.2 where the C1 mode of frequency 2 and C2 mode of frequency 1 represent, respectively, the modes from crack breathing and excitation frequency. The C3 mode of frequency 0.25 is associated with the period-doubling bifurcation that is going to eventually disappear in the steady state. The instantaneous frequencies of the C1 and C2 modes both demonstrate periodic structure in the instantaneous time frequency plane. However, Figure 8.5 shows a very different phenomenon in which the C1 mode exhibits intermittency at frequency 17. The C2 mode of frequency 2 is due to crack breathing, the C3 mode of frequency 1 is the driving frequency and the C4 mode of frequency 0.5 is associated with the period doubling bifurcation. All these modes are not periodic in time; nor do their instantaneous frequencies displaying periodic-modal structure in the instantaneous time frequency domain. The motion depicted in Figure 8.5 shows chaotic characteristics and thus is unstable. The marginal spectrum shown in Figure 8.4 (c) reveals two dominant frequencies at 1 and 2, and the one found in Figure 8.5 (c) indicates a broadband frequency distribution.

In the following cases, the crack is further opened to $h_r = 0.20$ and the rotating speed is again kept at 100π rad/s. From Figures 8.6(a)-8.8(a) in which the vibration time waveforms and their associated intrinsic modes at Cr = 0.0025r, 0.002r and 0.001r are considered it can be observed that the vibration amplitudes are becoming smaller with decreasing bearing clearances. By comparing Figure 8.4(a) with Figure 8.7 (a), the rotor vibration amplitude at $h_r = 0.20$ is smaller than that at $h_r = 0.10$, thus indicating that crack growth is able to suppress vibration amplitude. As the opening-closing behavior of the crack alters the local stiffness of the shaft and thus the natural frequency of the rotor system, one speculated while equally probable explanation would be that crack breathing effectively separates the resonance zone from the running speed $\omega = 100\pi$, thus rendering lower vibration amplitudes. As a contrast, the two cases considered in Figures 8.6(a) and 8.8(a) demonstrate the events when vibration amplitudes increase along with increased crack growth. The low frequency C3 mode corresponds to the large clearance case in Figure 8.6 is seen to fast disappearing, leaving the mode from crack breathing and still another from excitation the two predominant modes. There are four intrinsic modes for the case of intermediate clearance found in Figure 8.7 in which the low amplitudes of the C3 and C4 modes of low frequency and the persistence of the two modes indicate the occurrence of bifurcation. On the other hand, two period-doubling bifurcations are clearly observed for the small clearance case. The C3 and C4 modes found in Figure 8.8 (a-b) are modes of period-doubling bifurcation both having significant effects on the dynamics of the system. From the marginal spectra shown in Figures 8.6(c)-8.8(c) it can be seen that the low frequency components have increasingly important influence as the bearing clearance decreases.

If crack is allowed to further grow to $h_r = 0.30$, the modes from bifurcation would take dominate the response of the system with more energy. Figure 8.9 shows that in the case when Cr = 0.002r, the C3 mode of frequency 0.5 commands much more energy than all previously considered cases (Figures 8.4 and 8.7). Figure 8.10 shows when Cr = 0.001r there are four modes, with the C3 of frequency 0.5 and C4 of frequency 0.25 both modes of period-doubling bifurcation. It should be noted from the marginal spectrum given Figure 8.10 (c) that the C3 mode from bifurcation has more prominent effect than the C2 mode of driving frequency. In addition, all these modes and their associated instantaneous frequencies do not show structures indicative of periodicity. The system is experiencing a chaotic motion is therefore noticed.

When the rotor runs at higher speed at $\omega = 200\pi$, the system responds quite differently than it was at lower speed $\omega = 100\pi$. Figures 8.11-8.20 reveal that the crack-induced mode of frequency 2 is suppressed. The reason is as follows. Because the presented crack model is independent of imbalance response and rotating speed, the crack-induced effects only depend on the crack configuration (direction and depth), thus, the model enables prominent effects at low speeds and obscures the true rotor-dynamic characteristics at high speeds as discussed already in Chapter VI. These observations are still valid for cases of high-speed, though. For example, the vibration amplitudes decrease with decreasing bearing clearances and the vibration amplitudes increase with increasing crack depth. Most importantly, the system would become unstable should the clearance become small. Figure 8.18 shows the scenario that when $\omega = 200\pi$, $h_r = 0.25$ and Cr = 0.025r there is only one dominant mode of frequency 1. The case considering $\omega = 200\pi$, $h_r = 0.30$, and Cr = 0.002r is presented in Figure 8.19, in which the mode of bifurcation of frequency 0.5 is increasingly significant in affecting the overall system dynamics. As seen in Figure 8.20 where $\omega = 200\pi$, $h_r = 0.30$, and Cr = 0.001r are considered, the mode of frequency 0.5 is one of the dominant modes in the marginal spectrum and the low frequency mode C3 is with the sub-harmonic bifurcation. Together they imply that the rotor system stability is further deteriorating at this relatively small clearance.

8.2 Discussion

In this chapter, the effects of varying bearing clearance on the rotor-dynamic responses of the model system were investigated as functions of rotating speed and relative crack depth. The existence of crack induced various prominent effects at low speeds and dominated to a large extent the rotor-dynamics at high speeds. This was explained as that the bearing force plays a predominant role and exerts significant influence on the dynamic stability of the system at high speeds and that the crack model is independent of the rotating speed and imbalance response.

It was observed that when the clearance was decreased, the loading capacity of the journal bearings increased accordingly and the observed vibration amplitudes decreased. However, when the rotating speed and crack configuration, ω and h_r, were fixed, smaller bearing clearances produced larger bearing forces and thus served to be the destabilizing mechanism impacting the rotor-dynamic stability. In addition, the rotor-bearing system of smaller clearance was seen to experience more bifurcations indicative of increasingly unstable states. Normally, the crack-induced dissimilarity of local flexibility would excite vibration modes of large amplitude at twice the driving frequency. However, abnormal cases did occur at $\omega = 100\pi$, and Cr = 0.002r.

At low speeds, the forcing frequency 1 and crack-induced frequency 2 were the two dominant frequencies seen in the marginal spectra. When bearing clearances were kept small, the rotor system experienced complex motions of bifurcation including chaos, as shown in Figures 8.5 and 8.8. At high rotating speed (e.g. $\omega = 200\pi$ rad/sec), the mode due to crack-induced dissimilarity of local flexibility was suppressed and the frequency 2 component was not readily visible in the marginal spectrum. This result is consistent with those reported in [108]. However, crack existence did affect the rotor dynamic characteristics at high speeds. As was considered in Figures 8.17 and 8.20, when bearing clearances were small, the rotor system demonstrated more bifurcations and motions of instability.

CHAPTER IX

CONCLUSIONS AND RECOMMENDATIONS

9.1 Conclusions

The objectives of this research are to study various rotor-dynamic instabilities induced by two sources of nonlinearity using a model rotor-bearings system and to investigate the applicability of the fundamental concept of instantaneous frequency to the full characterization of rotor-dynamic nonlinear responses. The need for correlating nonlinear responses with system parameters and the mode and range of rotor-dynamic instability motivated the work. By incorporating many factors of engineering significance that affect rotor-dynamics, a comprehensive rotor-bearing model was developed using the finite element method. The Runge-Kutta and Newmark numerical integration schemes were employed to obtain different nonlinear time histories as responses subjected to the actions of crack breathing and bearing fluid film force. The intrinsic modes and their instantaneous frequencies were applied to these nonlinear rotor-dynamic responses to characterize the inception and progression of bifurcations indicative of changing rotor-dynamic state and impending instability. The dissertation has presented and demonstrated an effective approach that integrates nonlinear rotor-dynamics, instantaneous time-frequency analysis, advanced notions of dynamic system diagnostics and numerical modeling to the detection and identification of sensitive variations indicative of bifurcated state dynamic instability. In particular, the wide applicability of the concept of instantaneous frequency to nonlinear time series analysis was also demonstrated.

The study comparing nonlinear analytical methods with linear methods using a simple rigid rotor asserts that linear stability analysis can misinterpret a bifurcated response as stable and an almost stable motion as unstable. The study also shows that linear approach is unable to resolve delicate while important nonlinear phenomena such as, for example, the return of a dynamic system to stable periodic motion after experiencing chaos. Thus the improper use of linear methods would risk missing out on important stability information and misinterpreting nonlinear phenomena signifying imminent instability. Due to these reasons, many nonlinear methods were introduced into the analysis of nonlinear dynamic system and response. Among them, the Fast Fourier transform and Fourier-based time-frequency distributions are commonly employed, respectively, to detect the change of system behaviors in the frequency domain and to resolve system transitions in the time-frequency domain, thus providing a probable direction for the study and understanding of nonlinear phenomena. However, their inherent low resolution and linear nature, together, prevent their wide applications in the nonlinear dynamic analysis.

The fundamental concepts of instantaneous frequency and amplitude were developed and applied to the analysis of nonlinear rotor-dynamic responses displayed by the model rotor-bearing system. Ville's definition of instantaneous frequency is widely accepted, but when it is applied to signals of multi-component, the fact that the obtained instantaneous frequency could occasionally be of infinite and negative amplitude unfortunately and inevitably hinders its wide applications. After reviewing the problems with the definition, it was found that the root cause is simply the misuse of the powerful concept. Because a multi-component signal has several instantaneous frequencies, instead of one, at any given moment, the key to resolve the plaguing problems is to separate the multi-component signal into its several monocomponent subsets (modes). Meaningful instantaneous frequency would result only when the Ville's definition is applied to signals of monocomponent. An effective decomposition method named as the EMD was employed to decompose multi-component signals into their respective orthogonal monocomponent modes, in which the amplitude modulation and frequency modulation are fully decoupled. The feasibility and effectiveness of instantaneous frequency in resolving a nonlinear, non-stationary signal in both the time and frequency domain was also demonstrated.

To obtain system transient response as a result of changing system parameters, a finite element rotor-bearing model capable of incorporating nonlinear forces was developed. The model (thus the equations of motion) was solved using direct integration schemes including the Runge-Kutta and Newmark methods. Difficulties associated with solving the nonlinear equations of motion and integrating response time history were discussed and strategies for effectively overcoming these difficulties were also presented. Simulated system time responses reflect the physical nature of the nonlinear dynamic system subject to various initial and boundary conditions, thus helping to understand the dynamics in response to the actions of the sources of nonlinearity considered in the study.

The EMD algorithm and the concepts of instantaneous frequency and amplitude have been applied to simultaneously analyze system evolution in the time domain and examine frequency domain representations. This scheme was shown to be able to characterize and detect the birth and disappearance of modes necessarily indicative of bifurcation in progress and the development of system instability in the model rotor system. The marginal spectrum was shown to be a powerful tool for quantifying nonlinearities and detecting the occurrence of bifurcation and instability. The effectiveness and applicability to nonlinear time series analysis of the instantaneous frequency have been demonstrated using several examples. The presented approach resolves the difficulties commonly experienced in applying the definition of instantaneous frequency and enables the interpretation of instantaneous frequency to have concrete physical meanings and practical values. In addition, the employment of instantaneous frequencies in this research has enabled a new insightful way of interpreting and understanding nonlinear rotor-dynamic phenomena.

All studies presented in the dissertation on rotor system responses subject to various system configurations and ranges of parameters showed good agreement with published results. The validation is further enhanced by the ability of being able to investigate the evolution of the system intrinsic modes and the variation of instantaneous frequency in the instantaneous time-frequency domain. The adequacy of the rotor-bearing finite model in predicting system behaviors subject to one or more source of nonlinearity were demonstrated. Under the influence of one nonlinear source, the model system was shown to display transition behavior typical of a nonlinear dynamic system, going from periodic to (a series of) period-doubling to chaotic to eventual failure. When two sources of nonlinearity were considered, the model system conducted very different behaviors and failed from different set and ranges of control parameters. This has very important practical implications on the maintenance and operation of rotary machinery. It was concluded from these studies that rotor-dynamic behaviors could become more complicated if more causes of nonlinearity were considered.

In summary, this dissertation has presented a new approach effective for understanding the nonlinear dynamic systems and for characterizing nonlinear responses. The comprehensive rotor-bearing finite element model developed for the research has allowed rotor-dynamic nonlinearities and responses to be accurately modeled. Insightful interpretations of rotor-dynamic system responses were obtained by applying the EMD and the notions of instantaneous frequency. Wide applications of the presented approach to the characterization, trouble-shooting and design of high speed rotary systems are thus expected.

9.2 Contributions

The contributions of this dissertation are listed as follow:

1. Introduced a new characterization tool to the analysis of nonlinear rotor-dynamic response and provided new understandings and interpretations of nonlinear

phenomena. This new technique provides simultaneous qualitative and quantitative measure for nonlinear analysis through representing a time domain response in the joint time-frequency domain. As oppose to all currently available tools for nonlinear analysis, the interpretation of the new approach of a rotor-dynamic response is physically accurate, comprehensive and complete.

2. Provided knowledge about nonlinear rotor-dynamics that is not previously available. This includes establishing the correlation correlating system configuration and parameters with the induced nonlinear responses and rotor-dynamic instability. The availability of the knowledge would thus positively impact the operating safety of rotary machinery.
3. Provided guidelines for better or instability-free rotary machine concept development and configuration design.

9.3 Concepts and Design Guidelines for Instability-Free Rotary Machines

It was found and established in the course of this research that nonlinear analysis is essential and necessary for the design of rotor-dynamic mechanical systems. Linear stability analysis employing critical speeds, resonance chart and eigenvalue analysis, is not enough to guarantee the operating safety of a rotary system when the rotating speed is high or the nonlinearity within is prominent. Because every machine design has its own requirements and considerations, it is hard to give specifics applicable to the design of ultra-stable machines in general. However, considering the nonlinear characteristics and instability problems commonly observed of a rotor system, some general rules for consideration and observation are provided as follow:

1. Rotor system configuration. Rotor configuration, including the structure of the rotor, the arrangement of disks and bearing supports, the clearance and type of the bearings and seals used,

is the most critical factor impacting many types of rotary instability. These instability problems could be due to the nonlinear source(s) in the configuration, the intrinsic instability mechanism(s) of the rotor structure or simply the internal damping. For example, certain types of self-excited vibration are extremely difficult to avoid by changing the running speed simply because they occur in a wide range of rotating speed. To suppress self-excited vibrations, the mechanism of charging energy into facilitating these vibrations has to be eliminated [2]. Modifying configurational dimensions may not be enough and the configuration of the rotary system would have to be completely altered. Among the self-excited vibrations, oil whip, vibrations from seals, steam whirl from steam flow and vibration of a rotor partially filled with liquid are commonly seen. These kinds of vibration can induce serious nonlinear responses in the rotor system. To avoid these vibrations, the bearing support or rotor configuration will need to be modified.

2. Bearing supports. The instability problems from bearings and seals are very commonly encountered. Several scenarios ought to be considered:

i) Though fluid-film bearings, especially the plain journal bearings, are widely used in industry to support the load, reduce the friction and provide damping, they should be avoided for middle and high rotating speed. Because of the intrinsic nonlinear instability mechanism that exists in the supporting forces of this kind of bearings, when the rotating speed is increased beyond certain levels, instability and nonlinear responses always occur. This is supported by the second example discussed in Chapter VI, where the rotor system already experienced period doubling bifurcation at a low speed of 1500 rpm. Ball bearings, rolling element bearings and magnetic bearings are good alternative choices. If fluid-film bearings have to be used, then Multi-lobe bearings, tilting pad bearings, and Squeeze Film Dampers should be considered as alternatives because they can provide larger loading capacity and eliminate certain disabling mechanisms commonly found in the plain journal bearings. Nevertheless, nonlinear analysis has to be performed to avoid possible nonlinear instability induced by the coupled interaction of the supports and other sources of nonlinearity in the desired or design speed range. In addition, however, if the rotating speed is increased continuously, it needs be kept in mind that a rotor system could return to stable periodic motion after it experienced chaotic motion.

ii) Bearing clearance. Bearing clearance is a very critical parameter, whose effect as shown in the previous chapters is realized as the bearing film forces of very high nonlinearity. In Chapter V, the film-induced bearing force is inversely proportional to the cubic power of the bearing clearance. Thus, a small variation in the bearing clearance can bring about very large while undesirable effects on the bearing load capacity and thus also the induced rotor response. On the other hand, if the clearance is large, the bearing supporting forces would therefore be smaller. A possible scenario would be that the forces are too small to be able to support the rotor. Hence, choosing the right type of bearing with the right clearances is thus essential. As some auxiliary bearings of large clearances are commonly used for supporting bearings in places where large capacity is required, it worths noting that this physical configuration is prone to inducing nonlinear responses [22-24, 113-114].

iii) Increase bearing load capacity. Bearing load capacity is a function of bearing clearance, bearing length, bearing radius, rotating speed, viscosity and preload, to name a few. Should the bearing load capacity be large, the bearing can support heavier system, suppress the amplitude of vibration and prevent the occurrence of instability.

3. Capture the presence and development of surface crack as early as possible. A transverse fatigue crack is a very common and dangerous cause for serious accident in the operation of rotating machinery [115]. The existence of a crack can greatly change the dynamics of a rotor system and increase the vibration amplitude. The crack-induced nonlinear responses have to be investigated thoroughly. Using the technique presented in the dissertation, the crack-induced bifurcations and nonlinear responses can be detected and identified at early stage.

4. Avoid nonlinearity, especially presence of multiple nonlinearities. As few as one source of nonlinearity is capable of inducing complicated nonlinear responses and instability problems in a simple rotor system. If sources of nonlinearity can be avoided, understanding of system dynamic response can then be easily established and strategies for dealing with stability and instability issues can be quickly formulated. Unfortunately, nonlinearity cannot be avoided with the continual increasing of the rotating speed. Furthermore, as shown in Chapters VI-VIII, multiple nonlinear sources would generate sophisticated nonlinear responses that are different from those acquired when only one source is at work. Thus elements, causes or sources of nonlinearity should be avoided.

5. Avoid external perturbation, especially the combined or coupled action of several external perturbations. For a rotor system running in the stable range, if the external perturbation is large enough, the system still can produce nonlinear responses and dynamic instability. Multiple external perturbations would certainly make the situation worse. Therefore, whenever possible, avoid external perturbations such as decreasing or eliminating base excitations in machine design and in installation.

6. Perform nonlinear analysis. Methods of linearization could misinterpret nonlinear rotor-dynamics and thus wrongly predict the induced response. Therefore, nonlinear stability analysis is definitely needed if rotary safety at high speeds is to be concerned.

REFERENCES

1. Lund, J., 1968, “Calculation of Stiffness and Damping Properties of Gas Bearings,” Journal of Lubrication Technology, Ser. F, **90**, pp. 793-803.

2. Yamamoto, T., Ishida, Y., 2001, *Linear and Nonlinear Rotordynamics*, John Wiley & Sons, New York.

3. Sundararajan, P., 1996, “Response and Stability of Nonlinear Rotor Bearing Systems,” Ph.D. Dissertation, Texas A&M University, College Station, TX.

4. Yang, B., Suh, C. S. and Chan, A. K., 2002, “Characterization and Detection of Crack-Induced Rotary Instability,” ASME Journal of Vibration and Acoustics, **124**, No. 1, pp. 40-48.

5. Sundararajan, P., Noah, S. T., 1997, “Dynamics of Forced Nonlinear Systems Using Shooting/Arc-Length Continuation Method—Application to Rotor Systems,” ASME Journal of Vibration and Acoustics, **119**, No. 1, pp. 9-20.

6. Seydel, R., 1994, *Practical Bifurcation and Stability Analysis*, Springer-Verlag, New York.

7. Nayfeh, A.H. and Balachandran, B., 1994, *Applied Nonlinear Dynamics*, John Wiley & Sons, New York.

8. Yang, B., Suh, C. S., 2002, “On the Characteristics and Interpretation of Bifurcation and Nonlinear Dynamic Response,” ASME Journal of Vibration and Acoustics, Under Review.

9. Suh, C. S., 1997, “Numerical Modeling of Laser Acoustic Waves Using Finite Element Method and Fast Integral Wavelet Transform,” Ph.D. Dissertation, Texas A&M University, College Station, TX.

10. Yang, B., Suh, C. S., 2003, “Interpretation of Crack-Induced Rotor Nonlinear Response Using Instantaneous Frequency,” Mechanical Systems and Signal Processing, in press.

11. Ehrich, F. F., 1966, “Subharmonic Vibrations of Rotors in Bearing Clearance,” ASME paper No. 66-MD-1, ASME, New York.

12. Bently, D., 1974, “Forced Subrotative Speed Dynamic Action of Rotating Machinery,” ASME paper No. 74-PET-16, ASME, New York.

13. Lund, J. W., 1987, “Review of the Concept of Dynamic Coefficients for Fluid-Film Bearings,” ASME Journal of Tribology, **109**, pp. 38-41.

14. Barret, L. E., Akers, A., Gunter, E. J., 1976, "Effect of Unbalance on a Journal Bearing Undergoing Oil Whirl," *Proceedings of Institute of Mechanical Engineers*, **190**, pp. 525-543.

15. Sundararajan, P., Noah, S. T., 1998, "An Algorithm for Response and Stability of Large Order Nonlinear Systems—Application to Rotor Systems," Journal of Sound and Vibration, **214**, No. 4, pp. 695-723.

16. Noah, S. T., Sundararajan, P., 1995, "Significance of Considering Nonlinear Effects in Predicting the Dynamics Behavior of Rotating Machinery," Journal of Vibration and Control, **1**, pp. 431-458.

17. Childs, D. W., 1982, "Fractional-Frequency Rotor Motion due to Nonsymmetric Clearance Effects," ASME Journal of Energy and Power, **104**, pp. 533-541.

18. Myers, C. J., 1984, "Bifurcation Theory Applied to Oil Whirl in Plain Cylindrical Journal Bearings," ASME Journal of Applied Mechanics, **51**, pp. 244-250.

19. Zhao, J. Y., Linnett, I. W., McLean, L., J., 1994, "Stability and Bifurcation of Unbalanced Response of a Squeeze Film Damped Flexible Rotor," ASME Journal of Vibration and Acoustics, **116**, No. 2, pp. 361-368.

20. Choi, Y. S., Noah, S. T., 1987, "Nonlinear Steady-State Response of a Rotor-Support System," ASME Journal of Vibration, Acoustics, Stress, and Reliability in Design, **109**, pp. 255-261.

21. Choi, Y. S., Noah, S. T., 1988, "Forced Periodic Vibration of Unsymmetrical Piecewise-linear Systems," Journal of Sound and Vibration, **121**, No. 1, pp. 117-126.

22. Choi, Y. S., Noah, S. T., 1989, "Periodic Response of a Link Coupling with Clearance," ASME Journal of Vibration, Acoustics, Stress, and Reliability in Design, **111**, pp. 253-259.

23. Kim, Y. B., Noah, S. T., 1990, "Bifurcation Analysis for a Modified Jeffcott Rotor with Bearing Clearances," Nonlinear Dynamics, **1**, pp. 221-241.

24. Kim, Y. B., Noah, S. T., 1991, "Response and Bifurcation Analysis of a MDOF Rotor System with A Strong Nonlinearity," Nonlinear Dynamics, **2**, pp. 215-234.

25. Kim, Y. B., Noah, S. T., 1991, "Stability and bifurcation Analysis of Oscillators with Piecewise-Linear Characteristics: A General Approach," ASME Journal of Applied Mechanics, **58**, pp. 545-553.

26. Choi, S. K., Noah, S. T., 1994, "Mode-Locking and Chaos in a Jeffcott Rotor with Bearing Clearances," ASME Journal of Applied Mechanics, **61**, pp. 131-138.

27. Chancellor, R. S., Alexander, R.M., and Noah, S.T., 1996, "Detecting Parameter Changes Using Experimental Nonlinear Dynamics and Chaos," ASME Journal of Vibration and Acoustics, **118**, pp. 375-383.

28. Sankaravelu, A., 1994, "The Effect of Bifurcation and Chaos on the Functioning of Mechanical Systems with Clearance," Ph.D. Dissertation, Texas A&M University, College Station, TX.

29. Soffker, D., Bajkowski, J., Muller, P.C., 1993, "Detection of Cracks in Turborotors-A New Observer Based Method," ASME Journal of Dynamic System, Measurement, and Control, **115**, pp. 518-524.

30. Childs, D. W., 1993, *Turbomachinery Rotordynamics: Phenomena, Modeling and Analysis*, John Wiley and Sons, New York.

31. Glasgow, D. A., Nelson, H. D., 1980, "Stability Analysis of Rotor Bearing Systems Using Component Mode Synthesis," ASME Journal of Mechanical Design, **102**, pp. 352-359.

32. Nelson, H. D., Meacham, W. L., Fleming, Kascak, A. F., 1983, "Nonlinear Analysis of Rotor-Bearing Systems Using Component Mode Synthesis," ASME Journal of Engineering for Power, **105**, pp. 606-614.

33. Li, D. F., Gunter, E. J., 1982, "Component Mode Synthesis of Large Rotor Systems," ASME Journal of Engineering for Power, **104**, pp. 552-560.

34. Zheng, T., Hasebe, N., 2000, "Nonlinear Dynamics Behavior of a Complex Rotor-Bearing System," ASME Journal of Applied Mechanics, **67**, No. 3, pp. 485-495.

35. Zheng, T., Hasebe, N., 1999, "An Effective Analysis of High-Order Dynamical System with Local Nonlinearity," ASME Journal of Vibration and Acoustics, **121**, No. 2, pp. 408-416.

36. Huang, N.E., Shen, Z., Long, S. R., Wu, M. C., Shih, H. H., et al., 1998, "The Empirical Mode Decomposition and Hilbert Spectrum for Nonlinear and Nonstationary Time Series Analysis," Proceedings of Royal Society, London Series A, **454**, pp. 903-995.

37. Hilborn, R.C., 2000, *Chaos and Nonlinear Dynamics*, Oxford University Press, New York.

38. Frarey, J. L., 2002, "Pitfalls in the Analysis of Machinery Vibration Measurements," Sound and Vibration, **2002**, pp. 18-25.

39. Yoshihiro, K., 1998, "Identification of Nonlinear Structural Dynamic Systems Using Wavelets," Journal of Engineering Mechanics, **124**, No. 10, pp. 1059-1066.

40. Lind, R., Snyder, K., Brenner, M., 2001, "Wavelet Analysis to Characterize Nonlinearities and Predict Limit Cycles of an Aeroelastic System," Mechanical Systems and Signal Processing, **15**, No. 2, pp. 337-356.

41. Mastroddi, F., Bettoli, A., 1999, "Wavelet Analysis for Hopf Bifurcations with Aeroelastic Applications," Journal of Sound and Vibration, **225**, No. 5, pp. 887-913.

42. Ghanem, R., Romeo, F., 2001, "A Wavelet-Based Approach for Model and Parameter Identification of Nonlinear Systems," International Journal of Non-linear Mechanics, **36**, pp. 835-859.

43. Newland, N.E., 1994, "Wavelet Analysis of Vibration: Theory and Wavelet Maps," ASME Journal of Vibration and Acoustics, **116**, pp. 409-425.

44. Gaberson, H. A., 2002, "The Use of Wavelets for Analyzing Transient Machinery Vibration," Sound and Vibration, **2002**, pp. 12-17.

45. Dalpiaz, G., Rivola, A., 1997, "Condition Monitoring and Diagnostics in Automatic Machines: Comparison of Vibration Analysis Techniques," Mechanical Systems and Signal Processing, **11**, No. 1, pp. 53-73.

46. Staszewski, W. J., 1998, "Structural and Mechanical Damage Detection Using Wavelets," Shock and Vibration Digest, **30**, No. 6, pp. 457-472.

47. Liu, B., and Ling, S.-F., 1999, "On the Selection of Informative Wavelets for Machinery Diagnosis," Mechanical Systems and Signal Processing, **13**, No. 1, pp. 145-162.

48. Gaul, L., Hurlebaus S., 1997, "Identification of the Impact Location on a Plate Using Wavelets," Mechanical Systems and Signal Processing, **12**, No. 6, pp. 783-795.

49. Spina, D., Valente, C., Tomlinson, G. R., 1996, "A New Procedure for Detecting from Transient Data Using the Gabor Transform," Nonlinear Dynamics, **11**, pp. 235-254.

50. Staszewski, W.J., 1998, "Identification of Nonlinear System Using Multiscale Ridges and Skeletons of Wavelet Transform," Journal of Sound and Vibration, **214**, No. 4, pp. 639-658.

51. Boulahbal, D., Farid Golnaraghi, M., and Ismail, F., 1999, "Amplitude and Phase Wavelet Maps for the Detection of Cracks in Geared Systems," Mechanical Systems and Signal Processing, **13**, No. 3, pp. 423-436.

52. Yang, B., Suh, C. S., Chan, A. K., 2003, "Wavelet Based Algorithm for Crack Detection in Rotor-Machinery," International Journal of COMADEM, **6**, No. 1, pp. 31-40.

53. Suh, C. S., Khurjekar, P. P., Yang, B., 2002, "Characterisation and Identification of Dynamic Instability in Milling Operation," Mechanical Systems and Signal Processing, **15**, No. 5, pp. 829-848.

54. Goswami, J.C., and Chan, A.K., 1999, *Fundamentals of Wavelets*, John Wiley and Sons, New York.

55. Chui, C. K., 1997, *Wavelets: A Mathematical Tool for Signal Analysis*, SIAM, Philadelphia.

56. Rioul, O., Vetterli, M., 1991, "Wavelet and Signal Processing," IEEE Signal Processing Magazine, pp. 14-38.

57. Gottlieb, O., Feldman, M., Yim, S.C.S., 1996, "Parameter Identification of Nonlinear Ocean Mooring Systems Using the Hilbert Transform," ASME Journal of Offshore Mechanics and Arctic Engineering, **118**, pp. 29-36.

58. Gottlieb, O., Feldman, M., 1997, "Application of a Hilbert Transform-Based Algorithm for Parameter Estimation of a Nonlinear Ocean Systems Roll Model," ASME Journal of Offshore Mechanics and Arctic Engineering, **119**, pp. 239-243.

59. Feldman, M., 1997, "Nonlinear Free Vibration Identification via the Hilbert Transform," Journal of Sound and Vibration, **208**, No. 3, pp. 475-489.

60. Brandon, J., 2000, "Nonlinear Vibration of Cracked Structures: Perspectives and Horizons," Shock and Vibration Digest, **32**, No. 4, pp. 273-280.

61. Wowk, V., 1991, *Machinery Vibration Measurement and Analysis*, McGraw-Hill, New York.

62. Vance, J. M., 1988, *Rotordynamics of Turbomachinery*, John Wiley and Sons, New York.

63. Shiau, T. N., Jean, A. N., 1990, "Prediction of Steady State Response of Flexible Rotor System with Nonlinear Supports: A New Technique," ASME Journal of Vibration and Acoustics, **112**, pp. 501-507.

64. Fey, R. H. B., van Campen, D. H., de Kraker, A., 1996, "Long Term Structural Dynamics of Mechanical System with Local Nonlinearities," ASME Journal of Vibration and Acoustics, **118**, pp. 147-153.

65. Nelson, H. D., McVaugh, J. M., 1976, "The Dynamics of Rotor-Bearing Systems Using Finite Elements," ASME Journal of Engineering for Industry, **98**, No. 2, pp. 593-600.

66. Zorzi, E. S., Nelson, H. D., 1977, "Finite Element Simulation of Rotor-Bearing Systems with Internal Damping," ASME Journal of Engineering for Power, **99**, No. 1, pp. 71-76.

67. Nelson, H. D., 1980, "A Finite Rotating Shaft Element Using Timoshenko Beam Theory," ASME Journal of Mechanical Design, **102**, No. 4, pp. 793-803.

68. Childs, D.W., Moes, H., van Leeuwen, H., 1977, "Journal Bearing Impedence Descriptions for Rotordynamic Applications," Journal of Lubrication Technology, **99**, pp. 198-219.

69. Lund, J., 1964, "Spring and Damping Coefficients for the Tilting Pad Journal Bearing," ASLE Transactions, **7**, pp. 342-352.

70. Lund, J., 1965, "The Stability of an Elastic Rotor in Journal Bearings with Flexible, Damped Support," ASME Journal of Applied Mechanics, **32,** pp. 911-920.

71. Lund, J., 1966, "Self-Excited, Stationary Whirl Orbits of a Journal in a Sleeve Bearing," Ph.D. Dissertation, Rensselaer Polytechnic Institute, Troy, NY.

72. Lund, J., 1974, "Stability and Damped Critical Speed of a Flexible Rotor in Fluid Film Bearings," ASME Journal of Engineering for Industry, **96**, pp. 509-517.

73. Zhu, C., 2002, "Experimental Investigation into the Instability of an Over-Hung Rigid Centrifuge Rotor Partially Filled with Fluid," ASME Journal of Vibration and Acoustics, **124**, pp. 483-491.

74. Guran, A., Bajaj, A., Ishida, Y., Perkins, N., D'Eleuterio, G., et al., 1999, *Stability of Gyroscopic Systems*, World Scientific, River Edge, NJ.

75. Ehrich, F. F., 1991, "High Order Subharmonic Response of High Speed Rotors in Bearing Clearance," ASME Journal of Vibration and Acoustics, **113**, pp. 50-56.

76. Ehrich, F. F., 1993, *Handbook of Rotordynamics*, McGraw-Hill, New York.

77. Mayes, I. W., and Davies, W. G. R., 1984, "Analysis of the Response of a Multi-Rotor-Bearing System Containing a Transverse Crack in a Rotor" Journal of Vibration, Acoustics, Stress and Reliability in Design, **106**, No. 1, pp.139-145.

78. Thompson, J.M.T., Stewart, H.B., 2001, *Nonlinear Dynamics and Chaos*, John Wiley and Sons, New York.

79. Moon, F. C., 1987, *Chaotic Vibration: An Introduction for Applied Scientists and Engineers*, John Wiley and Sons, New York.

80. Suh, C. S., Yang, B., 2003, "On the Nonlinear Features of Time-delayed Feedback Oscillators," Communications in Nonlinear Science and Numerical Simulation, in press.

81. Moon, F. C., 1992, *Chaotic and Fractal Dynamics*, John Wiley and Sons, New York.

82. Cohen, L., 1995, *Time-Frequency Analysis*, Prentice Hall, Upper Saddle River, NJ.

83. Qian, S., Chen, D., 1996, *Joint Time-Frequency Analysis*, Prentice Hall, Upper Saddle River, NJ.

84. Harms, K. D., Suh, C. S., 2002, “Laser-Optic Evaluation for Bond Quality of Polymeric Medical Tubing,” ASME Journal of Pressure Vessel Technology, **124**, No. 3, pp. 283-292.

85. Chui, C.K., 1992, *An Introduction to Wavelets*, Academic Press, San Diego, CA.

86. Kishmoto, K., Inoue, H., Hamada, M., Shibuya, T., 1995, “Time Frequency Analysis of Dispersive Wave by Means of Wavelet Transform,” Journal of Applied Mechanics, **62**, pp. 841-846.

87. Boashash, B., 1992, “Estimating and Interpreting the Instantaneous Frequency” Proceedings of IEEE, **80**, pp. 520-568.

88. Gabor, D., 1946, “Theory of Communications,” IEEE Journal of Communication Engineering, **93**, pp. 429-457.

89. Ville, J., 1958, *Theory and Applications of the Notion of Complex Signals*, Translated by I. Seline in RAND Tech. Rept. T-92, RAND Corp., Santa Monica, CA.

90. Mandel, L., 1974, “Interoperation of Instantaneous Frequency,” American Journal of Physics, **42**, pp. 840-846.

91. Oliveira, P. M., Barroso, V., 2000, “Definitions of Instantaneous Frequency under Physical Constraints,” Journal of Franklin Institute, **337**, pp. 303-316.

92. Cohen, L., 2000, “Instantaneous Frequency and Group Delay of a Filtered Signal,” Journal of Franklin Institute, **337**, pp. 329-346.

93. Cohen, L., Loughlin, P., Vakman, O., 1999, “On an Ambiguity in the Definition of the Amplitude and Phase of a Signal,” Signal Processing, **79**, pp. 301-307.

94. Loughlin, P. J., Tacer, B., 1996, “On the Amplitude- and Frequency-Modulation Decomposition of Signals,” Journal of Acoustic Society of America, **100**, pp. 1594-1601.

95. Barkat, B., 2001, “Instantaneous Frequency Estimation of Nonlinear Frequency-Modulated Signals in the Presence of Multiplicative and Additive Noise,” IEEE Trans. Signal Processing, **49**, pp. 2214-2222.

96. Barkat, B., Boashash, B., 2001, “A High-Resolution Quadratic Time–Frequency Distribution for Multicomponent Signal Analysis,” IEEE Trans. Signal Processing, **49**, pp. 2232-2239.

97. Oliveira, P.M., Barroso, V., 1999, “Instantaneous Frequency of Multicomponent Signals” IEEE Signal Processing Letters, **6**, pp. 81-83.

98. Loughlin, P. J., Tacer, B., 1997, “Comments on the Interpretation of Instantaneous Frequency,” IEEE Signal Processing Letters, **4**, pp. 123-125.

99. Nho, W., Loughlin, P. J., 1999, "When is Instantaneous Frequency the Average Frequency at Each Time?" IEEE Signal Processing Letters, **6**, pp. 78-80.

100. Wei, D., Bovick, A. C., 1998, "On the Instantaneous Frequencies of Multicomponent AM-FM Signals," IEEE Signal Processing Letters, **5**, pp. 84-86.

101. L. Cohen, 1996, "Generalized Phase-Space Distribution," Journal of Mathematical Physics, **7**, pp. 781-786.

102. Childs, D., 1978, "The Space Shuttle Main Engine High Pressure Fuel Turbopump Rotordynamic Instability Problem," ASME Journal of Engineering for Industry, **100**, pp. 48-57.

103. Ruhl, R. L., Booker, J. F., 1972, "A Finite Element Model for Distributed Parameter Turborotor Systems," ASME Journal of Engineering for Industry, **94**, pp. 128-132.

104. Gasch, R., 1976, "Vibration of Large Turbo-Rotors in Fluid-Film Bearings on an Elastic Foundation," Journal of Sound and Vibration, **47**, pp. 53-73.

105. Dimarogonas, A. D., 1996, "Vibration of Cracked Structures: A State of the Art Review," Engineering Fracture Mechanics, **55**, No. 5, pp. 831-857.

106. Wauer, J., 1990, "On the Dynamics of Cracked Rotors: A Literature Survey," Applied Mechanics Review, **43**, pp. 13-17.

107. Gasch, R., 1976, "Dynamics Behavior of A Simple Rotor with a Cross-Sectional Crack," *Vibrations in Rotating Machinery*, Institution of Mechanical Engineers, London, pp. 123-128.

108. Gasch, R., 1993, "A Survey of the Dynamic Behavior of a Simple Rotating Shaft with a Transverse Crack," Journal of Sound and Vibration, **160**, No. 2, pp. 313-332.

109. Muller, P.C., Bajkowski, J., and Soffker, D., 1994, "Chaotic Motions and Fault Detection in a Cracked Rotor," Nonlinear Dynamics, **5**, pp. 233-254.

110. Bathe, K. J., 1996, *Finite Element Procedures*, Prentice Hall, Upper Saddle River, NJ.

111. Reddy, J. N., 1993, *An Introduction to the Finite Element Method*, McGraw-Hill, New York, NY.

112. Feigenbaum, M. J., 1980, "Universal Behavior in Nonlinear Systems," Los Alamos Science, **1**, pp. 4-27.

113. Xie, H., Flowers, G.T., Feng, L., Lawrence, C., 1999, "Steady-State Dynamics of a Flexible Rotor with Auxiliary Support from a Clearance Bearing," ASME Journal of Vibration and Acoustics, **121**, No. 1, pp. 78-83.

114. Lawen, J. L., Flowers, G.T., 1999, "Interaction Dynamics between a Flexible Rotor and an Auxiliary Clearance Bearing," ASME Journal of Vibration and Acoustics, **121**, No. 2, pp. 183-189.

115. Grabowski, B., 1980, "The Vibrational Behavior of a Turbine Rotor Containing a Transverse Crack," ASME Journal of Mechanical Design, **102**, No. 1, pp. 140-146.

VITA

Baozhong Yang was born on April 1974, in Shandong Province, People's Republic of China. He received his B.S. degree from Xi'an University of Technology, China in 1995 and M.S. degree from Shanghai Jiao Tong University, China in 1998, both in mechanical engineering. He received his Ph.D. degree in mechanical engineering in August 2003 from Texas A&M University. His research interests include dynamical mechanical system analysis, mechanical fault detection, system condition monitoring, time-frequency analysis, wavelets, Hilbert analysis and their applications in mechanical system diagnostics and condition evaluation. Mr. Yang's permanent address is:

Guanxian Sangezhen Xiaozhangzhuang
Shandong, 252500
China
Email: yangbaozhong@yahoo.com